On the objective occlusion effect induced by in-ear devices under bone-conducted stimulation: A theoretical investigation of the influence of the earcanal wall vibration and its spatial distribution

by

Kévin CARILLO

MANUSCRIPT-BASED THESIS PRESENTED TO ÉCOLE DE TECHNOLOGIE SUPÉRIEURE IN PARTIAL FULFILLMENT FOR THE DEGREE OF DOCTOR OF PHILOSOPHY
Ph.D.

MONTREAL, JULY 28, 2021

ÉCOLE DE TECHNOLOGIE SUPÉRIEURE
UNIVERSITÉ DU QUÉBEC

BOARD OF EXAMINERS

THIS THESIS HAS BEEN EVALUATED

BY THE FOLLOWING BOARD OF EXAMINERS

Mr. Olivier Doutres, Thesis Supervisor
Department of Mechanical Engineering, École de technologie supérieure

Mr. Franck Sgard, Thesis Co-supervisor
Scientific Division
Institut de recherche Robert-Sauvé en santé et en sécurité du travail

Mrs. Claudiane Ouellet-Plamondon, President of the board of examiners
Department of Construction Engineering, École de technologie supérieure

Mr. Thomas Dupont, Member of the jury
Department of Mechanical Engineering, École de technologie supérieure

Mr. Elliott Berger, Member of the jury
President
Berger Acoustical Consulting

Mr. Stefan Stenfelt, External examiner
Department of Biomedical and Clinical Sciences, Linköping University

THIS THESIS WAS PRESENTED AND DEFENDED

IN THE PRESENCE OF A BOARD OF EXAMINERS AND THE PUBLIC

ON JUNE 8, 2021

AT ÉCOLE DE TECHNOLOGIE SUPÉRIEURE

REMERCIEMENTS

Il est entendu que si une seule page de ce manuscrit devait être lue, que ce soit par hasard, inadvertance, erreur ou contrainte, ce serait à coup sûr celle des remerciements. Elle possède en effet la force d'attraction du voyeurisme et confère à ce document un visage humain. J'espère donc que le lecteur trouvera ici ce qu'il y cherche, son prénom, un peu d'amour ou bien quelques minutes de divertissement.

On ne sait peut-être pas toujours exactement pourquoi on entame un doctorat, certes. Mais que ce soit par hasard, inadvertance, erreur ou contrainte, on sait toujours pourquoi il se termine : l'arrêt du financement. Entre ce début un peu flou et cette fin brutale, de nombreuses personnes ont contribué à rendre cette expérience inoubliable. À toutes ces personnes, veuillez accepter les hommages qui suivent.

On me demande souvent : « c'est une bonne situation ça doctorant? » Ce à quoi je réponds toujours : « Vous savez, je ne crois pas qu'il y ait de bonne ou de mauvaise situation » (Otis, 2002). Je crois cependant que mon doctorat n'aurait pu mieux se passer qu'avec mes directeurs Olivier Doutres et Franck Sgard, un duo hors pair. Merci infiniment Olivier pour ta pédagogie, ton soutien, ta vision, ta bonne humeur et ta disponibilité de chaque jour comme en témoignent nos nombreuses rencontres improvisées dans les couloirs de l'ÉTS. À toi Franck, merci infiniment pour ton exigence, ta rigueur, ton humour (si si), tes encouragements à me dépasser et ton sens du détail : « 0.2 dB d'écart, ça compte ». Finalement, par-delà notre relation hiérarchique s'est tissée au fil des années une sincère amitié. Merci à vous, du fond du cœur. Vous avez été les meilleurs encadrants que j'ai eus durant mon doctorat.

Un immense merci à Thomas Dupont, all my gratitude to Elliott Berger and stort tack till Stefan Stenfelt de faire partie du jury de ma thèse, it is a great honor to defend my thesis in front of you.

Comme dirait Thomas Padois, une thèse n'avance jamais autant qu'au bar. Merci donc à toi et Simon Benacchio, promoteurs malgré vous, pour les soirées de dégustation de breuvages, dans un sens ou dans l'autre. Si toutes n'ont pu être mémorisées, certaines ne seront jamais oubliées.

À tous mes collègues du lab, j'ai nommé Bastien, Simon, Hugo, Yu, Huiyang, Saber, Louis, Valentin, Solène, Maxime, Marc-Olivier, Alexis, merci pour la bonne ambiance, les sorties, les fous rires!

Merci aux membres de CRITIAS, je pense en particulier à Jérémie Voix, Rachelle, Guilhem, Fabien, Antoine et Vincent ; notre road trip à Orlando reste mémorable.

À toutes les personnes croisées durant les rencontres GRAM et au détour des couloirs labyrinthiques de l'ÉTS, ce fut un plaisir.

À ma gang montréalaise – Dydy, Adri, Moises, Phed, Tina – et aux amis de France – Kokoach, Krstic, Flo – much love.

À mes collocs Nick et Violaine, vous m'avez nourri pendant ces derniers mois de rédaction, un grand merci. À toi Jacko, notre colloc félin, un miaou de reconnaissance.

À mes parents et mes sœurs pour votre amour indéfectible, votre soutien et votre présence, même à 5829.451 km de distance. Je vous aime.

À ma cerise sur le gâteau, ma chérie d'amour, soleil de mes nuits, première fan et plus grande source de distraction, merci Karole pour tout, tu es parfaite. À Fridoune, notre premier enfant canin.

Finalement, il est entendu que si un prénom a été omis dans les remerciements qui précède, c'est assurément par hasard, inadvertance, erreur ou. . .

Étude théorique de l'effet d'occlusion objectif associé aux dispositifs intra-auriculaires: focus sur l'influence de la vibration pariétale du conduit auditif et de sa distribution spatiale

Kévin CARILLO

RÉSUMÉ

L'effet d'occlusion est généralement ressenti comme la perception accrue de ses propres bruits physiologiques lorsque le conduit auditif est occlus. En diminuant le confort acoustique des utilisateurs de protecteurs auditifs et d'aides auditives, l'effet d'occlusion réduit leur temps de port. Dans cette thèse, l'effet d'occlusion objectif induit par le port de dispositifs intra-auriculaires est investigué dans le but de réduire ce phénomène à terme. Cette thèse se concentre ainsi sur (i) l'explication et l'interprétation du mécanisme fondamental de l'effet d'occlusion, (ii) l'influence de la vibration pariétale du conduit auditif et de sa distribution spatiale, ainsi que (iii) le(s) mécanisme(s) de contribution des dispositifs intra-auriculaires à l'effet d'occlusion. Dans une première partie, le comportement vibro-acoustique du conduit auditif ouvert et occlus par une impédance infinie et soumis à une stimulation solidienne est minutieusement analysé, illustré et interprété à l'aide d'un modèle éléments finis 3D d'une oreille externe réaliste et en conjonction avec un modèle électro-acoustique qui lui est associé. Les deux modèles se révèlent être très complémentaires afin de détailler les phénomènes physiques mis en jeu dans le conduit auditif. Cette approche permet également de mettre en évidence et d'interpréter l'influence de la distribution spatiale de la vibration normale du conduit auditif sur le comportement vibro-acoustique de ce dernier lorsqu'il est ouvert. Cette distribution vibratoire est ici caractérisée par la position de son barycentre le long de l'axe curviligne du conduit. En particulier, il est démontré que cette position correspond à la localisation de la source équivalente de débit acoustique représentant la vibration normale de la paroi du conduit au sein du modèle électro-acoustique. Enfin, il est montré que les interprétations courantes de l'effet d'occlusion en termes de « fuites » et de « piège » ne décrivent pas adéquatement le mécanisme fondamental du phénomène lié à l'augmentation de l'impédance du conduit auditif vue par sa paroi dans le cas occlus. Dans une seconde partie, une théorie largement répandue de l'effet d'occlusion objectif proposée par Tonndorf en 1964 est revisitée dans le but de clarifier certains points ambigus desquels certaines interprétations du phénomène ont pu être tirées. L'investigation du modèle électro-acoustique associé à cette théorie met en évidence l'existence d'un filtre passe-haut du second ordre entre le débit acoustique imposé par la paroi du conduit et celui transféré au tympan. Ce filtre persiste dans le cas d'une occlusion partielle du conduit mais disparait dans le cas d'une occlusion parfaite, devenant constant avec la fréquence. Dans ce dernier cas, le débit acoustique transféré entre la paroi du conduit et le tympan augmente considérablement, ce qui explique la prédominance du chemin de transmission par conduction osseuse de l'oreille externe occluse en basses fréquences. Dans une troisième partie, le principe d'une méthode indirecte d'estimation de la position du barycentre de la vitesse normale du conduit auditif est présenté. Cette méthode consiste à mesurer la fonction de transfert de pression acoustique au tympan entre le conduit ouvert et occlus par un tube fermé à son autre extrémité. La stimulation du conduit est réalisée par conduction osseuse. La position du barycentre de

vitesse normale est ensuite estimée à la fréquence d'antirésonance la plus basse du système couplé à l'aide d'un modèle électro-acoustique associé à ce dernier. Cette méthode indirecte est évaluée et étudiée à l'aide d'un modèle éléments finis 3D de l'oreille externe. Dans une dernière partie, les mécanismes de contribution des bouchons d'oreille à l'effet d'occlusion sont étudiés à l'aide d'un modèle 2D axi-symétrique par éléments finis de l'oreille externe en conjonction avec un modèle électro-acoustique associé. Deux mécanismes sont mis en évidence: (i) un effet de Poisson induit par la composante normale de la vibration pariétale du conduit auditif et (ii) un mouvement longitudinal provoqué par la composante tangentielle de cette vibration. En faisant varier la géométrie des tissus biologiques entourant le conduit auditif, il est montré que la distribution spatiale de sa vibration pariétale, dans les directions normale et tangentielle, influence la contribution des bouchons d'oreille à l'effet d'occlusion. Aussi, il est montré que la contribution du bouchon d'oreille à l'effet d'occlusion domine celle de la paroi du conduit non-couverte par le bouchon à partir d'une profondeur d'insertion moyenne. Dans son ensemble, cette thèse constitue un effort supplémentaire dans la compréhension de l'effet d'occlusion induit par les dispositifs intra-auriculaires et s'achève aux balbutiements du développement de nouveaux concepts passifs atténuant ce phénomène par le moyen de leur propre comportement vibro-acoustique.

Mots-clés: effet d'occlusion, modélisation par éléments finis, analogie electro-acoustique, vibration pariétale du conduit auditif, contribution des dispositifs intra-auriculaires

On the objective occlusion effect induced by in-ear devices under bone-conducted stimulation: A theoretical investigation of the influence of the earcanal wall vibration and its spatial distribution

Kévin CARILLO

ABSTRACT

The occlusion effect is commonly experienced as the altered perception of one's own physiological noise when the earcanal entrance is blocked. By affecting the acoustic comfort of hearing protectors and hearing aids' users, the occlusion effect participates to their inconsistent or incorrect use. In this thesis, the objective occlusion effect caused by in-ear devices under bone-conducted stimulation is investigated in order to ultimately mitigate the phenomenon. For this purpose, this thesis focuses on (i) the explanation of the fundamental mechanism of the objective occlusion effect and its multiple interpretations, (ii) the influence of the earcanal wall vibration and its spatial distribution, and (iii) the mechanism(s) of contribution of in-ear devices to the occlusion effect. In a first part, the vibro-acoustic behavior of the earcanal open and occluded by an infinite impedance and submitted to a bone-conducted stimulation is thoroughly analyzed, illustrated and interpreted using a 3D finite element model of a realistic outer ear in conjunction with an associated electro-acoustic model. The two models are very complementary to dissect physical phenomena and to highlight the influence of the earcanal wall normal vibration distribution on the vibro-acoustic behavior of the open earcanal. This distribution is here characterized by its centroid position along the earcanal curvilinear axis. In particular, it is shown that this centroid position corresponds to the location of an equivalent source representing the normal vibration of the earcanal wall in electro-acoustic model. In addition, common interpretations of the occlusion effect in terms of "leak" and "trap" are shown to misrepresent the fundamental mechanism of the phenomenon related to the earcanal impedance increase. In a second part, a widespread theory of the objective occlusion effect provided by Tonndorf in 1964 is revisited to clarify its ambiguous points from which several misinterpretations of the phenomenon could have been derived. Investigating the electro-acoustic model associated with the theory, a second order high-pass filter effect for the volume velocity transferred between the earcanal wall and the eardrum is highlighted. This filter remains for partial occlusion but vanishes for perfect occlusion. In the latter case, the volume velocity transferred from the earcanal cavity to the middle ear through the eardrum drastically increases, which explains the predominance of the occluded outer ear pathway on the hearing by bone-conduction at low frequencies. In a third part, the principle of an indirect method to estimate the centroid position of the earcanal wall normal velocity is presented. This method consists in measuring the acoustic pressure transfer function between the earcanal open and occluded by an external capped duct coupled to the earcanal entrance under bone-conducted stimulation. The centroid position is then estimated at the lowest antiresonance frequency of the earcanal coupled to the external duct using an electro-acoustic model associated to the coupled system. This indirect method is evaluated and investigated using a 3D outer ear finite element model. In a last part, the mechanism(s) of contribution of earplugs to the occlusion effect is investigated using a 2D axi-symmetric finite element model of the outer ear in conjunction with an associated electro-acoustic model.

Two mechanisms are highlighted: (i) a Poisson effect induced by the normal component of the earcanal wall vibration and (ii) a longitudinal motion caused by the tangential component of the earcanal wall vibration. By varying the geometry of the earcanal surrounding tissues, the spatial distribution of the earcanal wall vibration, in both normal and tangential directions, is shown to influence the contribution of earplugs to the occlusion effect. Also, it is shown that the contribution of earplugs to the occlusion effect dominates that of the earcanal wall which is not covered by them from medium to deep insertion depth. Overall, this thesis constitutes an additional effort in the understanding of the occlusion effect induced by in-ear devices and ends at the beginning of the development of new concepts mitigating the phenomenon using their own passive vibro-acoustic behavior.

Keywords: occlusion effect, finite element modeling, electro-acoustic analogy, earcanal wall vibration, in-ear devices contribution

TABLE OF CONTENTS

LIST OF TABLES

LIST OF FIGURES

LIST OF ABBREVIATIONS

2D	Two-Dimensionsional
3D	Three-Dimensionsional
EA	Electro-Acoustic
FE	Finite Element
NSERC	Natural Sciences and Engineering Research Council of Canada
OE	Occlusion Effect
SPL	Sound Pressure Level
WHO	World Health Organization

LIST OF SYMBOLS AND UNITS OF MEASUREMENTS

s	second
Hz	hertz (with prefix k for *kilo-*)
m	meter (with prefix c for *centi-* or m for *milli-*)
°	arc degree
kg	kilogram
N	newton
Pa	pascal (with prefix M for *mega-*)
J	joule
W	watt
K	kelvin
°C	degree Celsius
dB	decibel

INTRODUCTION

0.1 Context

Intense sound impulse and prolonged noise exposure are responsible for irreversible hearing loss. According to the World Health Organization (WHO), over 5% of the world's population presents disabling hearing loss (WHO, 2020). The WHO estimates that this proportion could reach 10% by 2050. Among the many causes of hearing loss, occupational noise represents an important risk factor (Nelson, Kohnert, Sabur & Shaw, 2005). In Quebec, despite the legislation of occupational noise exposure (Légis-Québec, 2020), hearing loss is the most recorded occupational disease and costs hundreds of millions of dollars in compensation and indirect costs (Lebeau, 2014). In addition to auditory effect, noise exposure induces non-auditory health effects such as stress, disturbs sleep, and also increases the risk of hypertension and cardiovascular disease (Basner, Babisch, Davis, Brink, Clark, Janssen & Stansfeld, 2014). Hearing protection devices such as earplugs and earmuffs are commonly used to protect workers from noise-induced hearing loss. Their performance comes from the sound attenuation they provide. To be efficient, however, hearing protectors require to be consistently and correctly worn during the exposure time (Berger, 2003). The lack of comfort associated with wearing hearing protectors is a strong factor influencing their use (Doutres, Sgard, Terroir, Perrin, Jolly, Gauvin & Negrini, 2019). The comfort perception depends on the environment of use, the user and the hearing protection device used (Doutres, Sgard, Terroir, Perrin, Jolly, Gauvin & Negrini, 2020). A recent definition of hearing protector comfort underlined the multidimensionality of this construct and proposes to focus on the following four dimensions of comfort: (i) physical, (ii) functional, (iii) acoustical and (iv) psychological (Doutres *et al.*, 2019). The acoustical dimension is of particular interest in this thesis. This dimension refers to the alteration of the hearing of external sounds (*e.g.*, noise but also oral communication between workers or alarm signals) and internal sounds (*e.g.*, physiological noise such as one's own voice, chewing or

heartbeat). The increased auditory perception of physiological noise is known as the occlusion effect (OE) and is deemed to be a notable source of discomfort (Berger, 2003; Suter, 2002; Doutres *et al.*, 2019). This phenomenon occurs when the earcanal entrance is covered or blocked and amplifies the hearing sensation of bone-conducted sounds (Berger, 2003). The OE is most prominent in the case of earplug compared to earmuff (Berger, 2003). The OE also affects the acoustic comfort of hearing aids' users (Kochkin, 2010). Comfort issues could contribute to the 83% gap in hearing aid need and use estimated by the WHO (2020). In both hearing protection and hearing aid fields, solutions have been proposed to mitigate the OE. They can be, however, associated with drawbacks and provide a compromise between different comfort dimensions. New solutions are thus still sought to optimize the wearers' comfort. This thesis is an additional effort in this direction and focuses on the OE caused by in-ear devices.

0.2 Research problem

The OE is intrinsically related to the hearing by bone-conduction and depends on the occlusion device and its fit. Therefore, Sec. 0.2.1 first describes the ear anatomy and details the bone-conduction mechanisms. Then, Sec. 0.2.2 presents the OE, its descriptions and interpretations. Finally, Sec. 0.2.3 focuses on the influence of in-ear devices and the strategies already proposed to mitigate the OE.

0.2.1 Ear anatomy and bone-conduction mechanisms

The human ear, illustrated in Fig. 0.1, is commonly divided into the outer, the middle and the inner components. The outer ear includes the pinna and the earcanal. In conjunction with the head, pinnae play an important role on the spatial location of air-conducted sounds from the surrounding environment (Makous & Middlebrooks, 1990). Also, the geometry of the pinna and the earcanal determines the free field-to-eardrum acoustic pressure transfer function, which is maximum around the quarter-wavelength acoustic resonance of the open earcanal around 3 kHz

(Wightman & Kistler, 1989). The curvature and the cross-section of the earcanal generally vary along its length and depend on each human subject (Stinson & Lawton, 1989). Pinna and earcanal are covered by skin tissue. Between one-third (Alvord & Farmer, 1997; Oliveira & Hoeker, 2003) and one-half (Ballachanda, 2013) of the earcanal is backed by cartilage that also fills the pinna. The remaining portion of the earcanal towards the eardrum is backed by the temporal bone. The tympanic membrane marks the medial end of the earcanal and couples the outer ear to the middle ear. The middle ear acts as a transducer that transforms acoustic signals into vibratory signals transmitted to the inner ear. This transfer is ensured by the auditory ossicles including the malleus, the incus and the stapes. These ossicles are supported by stabilizing ligaments (not detailed in Fig. 0.1) connected to the wall of the tympanic cavity surrounding the auditory ossicles. The stapes is connected to the oval window of the cochlea. The cochlea constitutes the hearing organ of the inner ear and transforms vibratory signals into nerve impulses transmitted to the brain where they are interpreted as hearing sensation (Gelfand, 2009). The outer, middle and inner ears contribute together to the bandwidth of hearing (Ruggero & Temchin, 2002). The previous description of the human hearing assumed an intact and functional ear.

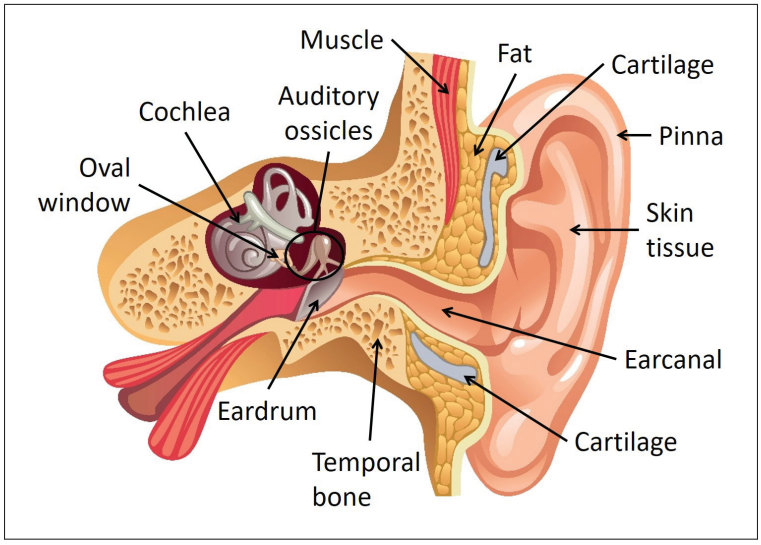

Figure 0.1 Anatomy of the human ear

The hearing by bone-conduction has been the subject of many studies (Bàràny, 1938; Békésy, 1948, 1949, 1960; Huizing, 1960; Tonndorf, 1964; Goldstein & Hayes, 1965; Khanna, Tonndorf & Queller, 1976; Berger & Kerivan, 1983; Stenfelt, Wild, Hato & Goode, 2003; Stenfelt & Goode, 2005; Dobrev, Sim, Stenfelt, Ihrle, Gerig, Pfiffner, Eiber, Huber & Röösli, 2017; Sohmer, 2017; Chordekar, Perez, Adelman, Sohmer & Kishon-Rabin, 2018; Dobrev, Farahmandi, Sim, Pfiffner, Huber & Röösli, 2020). Bone-conducted sounds, or body-conducted sounds (Homma, Du & Puria, 2009), originate from (i) internal body sources referred to as physiological noise (*e.g.*, bone-conduction part of one's own voice, breathing, heartbeat, chewing), (ii) external mechanical stimulation of the body (*e.g.*, bone-transducer applied to the head), or (iii) external acoustical stimulation. In the latter case, the bone-conduction pathway is known to limit the sound attenuation that a hearing protection device can achieve by blocking the air-conduction pathway (Berger, Kieper & Gauger, 2003; Homma, Shimizu, Kim, Du & Puria, 2010). Bone-conducted sounds propagates up to the cochlea through the outer, middle and inner ears via different mechanisms (Tonndorf, Greenfield & Kaufman, 1966; Stenfelt & Goode, 2005). In the outer ear, the bone-conducted propagation induces the vibration of the earcanal wall, which generates an acoustic pressure. The latter excites the tympanic membrane similarly to air-conducted sounds. In the middle ear, the bone-conducted propagation sets into vibration the auditory ossicles through their ligaments. It is interesting to note that the ossicular resonance mode of the middle ear below 2 kHz (not detailed here) differs between air-conducted and bone-conducted propagation (Homma *et al.*, 2009). In the inner ear, the bone-conducted propagation induces vibrational distortions of the bone enclosing the cochlea fluid. The relative contribution of each mechanism on the hearing by bone-conduction is frequency-dependent (Stenfelt, 2016). At low frequencies, the contribution of the outer ear mechanism is not of primary importance when the earcanal is open but it becomes predominant when the earcanal is occluded (Stenfelt *et al.*, 2003). This change of contribution to the hearing by bone-conduction corresponds to the OE.

0.2.2 Occlusion effect

According to Huizing (1960), Wheatstone (1827) and Tortual (1827) independently reported, in 1827, the first known experiments highlighting the phenomenon now referred to as the OE. Using a tuning fork held against the head of a human subject, Wheatstone noted that a louder sound was perceived by the occluded ear compared to the open one (Wheatstone, 1827). Tortual observed the same phenomenon using the ticking sound of a mechanical watch clamped between the teeth (Tortual, 1827). Nowadays, the OE is commonly encountered by in-ear devices' wearers. This phenomenon is usually perceived as the increased sensation of bone-conducted part of one's own physiological noise (Berger, 2003). This amplification is most significant for low frequencies, typically below 1 kHz. In the case of speech production, the OE is usually described as one's own voice perceived as "hollow" or "talking into a barrel" (Mueller, Bright & Northern, 1996). This perception is the conjunction of both the bone-conducted transmission increase and the air-conducted transmission decrease due to the presence of the occlusion device (Stenfelt & Reinfeldt, 2007).

The name "OE" encompasses three descriptions of the phenomenon. Firstly, the perceptive OE is related to the discomfort induced by the phenomenon and commonly quantified using questionnaires (Brown-Rothwell, 1986; Conrad & Rout, 2013). Secondly, the subjective OE is defined as the difference between the open and occluded hearing thresholds (Huizing, 1960; Berger & Kerivan, 1983; Stenfelt & Reinfeldt, 2007; Reinfeldt, Stenfelt & Håkansson, 2013). Thirdly, the objective OE is defined as the sound pressure level (SPL) difference between occluded and open configurations (Bàràny, 1938; Huizing, 1960; Stenfelt & Reinfeldt, 2007; Reinfeldt *et al.*, 2013; Brummund, Sgard, Petit, Laville & Nélisse, 2015). The perceptive OE is probably the most important to reduce since it is directly related to the acoustical comfort dimension. The perceptive OE is, however, also the most intricate to relate to physical variables compared to subjective and objective OEs. At low frequencies, the objective OE is generally

greater than the subjective OE (Huizing, 1960; Stenfelt & Reinfeldt, 2007; Saint-Gaudens, Nélisse, Sgard, Laville & Doutres, 2019) due to the difference in bone-conduction pathways accounted for between both OEs. Indeed, the objective OE only accounts for the outer ear pathway, contrary to the subjective OE which includes all bone-conduction pathways. When the earcanal is open, the outer ear pathway is negligible in the hearing by bone conduction. The acoustic pressure generated in the earcanal, therefore, is not responsible for the hearing sensation in the open case compared to the occluded case. The difference in hearing thresholds between occluded and open configurations is thus smaller than the corresponding difference in earcanal acoustic pressure levels. The SPL in open and occluded earcanals is not expected to be significantly influenced by the acoustic radiation of the tympanic membrane induced by the vibration of the middle ear ossicles excited via their ligaments by the bone-conducted propagation at least at low frequencies below the middle ear resonance (Schroeter & Poesselt, 1986; Stenfelt, Hato & Goode, 2002). This phenomenon, however, influences the vibration transmitted to the cochlea and therefore influences the perception of the OE (Schroeter & Poesselt, 1986; Stenfelt *et al.*, 2003). In this thesis, the focus is put on the objective OE, easier to study, assuming that a reduction of the objective OE is also associated with a reduction of the perceived OE.

Several explanations of the fundamental mechanism of the objective OE coexist in the literature[1]. The first one was proposed by Tonndorf (1964) and has been widely quoted in the literature (Khanna *et al.*, 1976; Berger & Kerivan, 1983; Schroeter & Poesselt, 1986; Howell, Williams & Dix, 1988; Kuk, 1991; Fagelson & Martin, 1998; Stenfelt *et al.*, 2002, 2003; Stenfelt & Goode, 2005; Vasil & Cienkowski, 2006; Stenfelt & Reinfeldt, 2007; Reinfeldt, Stenfelt, Good & Håkansson, 2007; Lee, 2011; Small & Hu, 2011; Brummund, Sgard, Petit & Laville, 2014; Brummund *et al.*, 2015). Based on a simple electro-acoustic (EA) model of the open and

[1] Alternative explanations of the OE than those presented here such as the "masking theory" (Guild, 1936) and the "outflow theory" (Mach, 1863) are not included since they have been invalidated (Huizing, 1960; Stenfelt & Goode, 2005). In addition, the explanation of the OE provided by Huizing (1960) and related to the change in resonance properties of the earcanal when it is occluded is not presented since this explanation does not apply at low frequencies (Tonndorf, 1964; Stenfelt *et al.*, 2003).

occluded earcanal, Tonndorf's theory explained the objective OE as the removal of the open earcanal high-pass filter effect due to the occlusion of the earcanal entrance. Characteristics of this filter, however, have never been clearly defined. In a second explanation of the objective OE, the increase of acoustic pressure generated by the vibrating earcanal wall has been explained by the augmentation of the earcanal acoustic reactance (imaginary part of the acoustic impedance), seen by the earcanal wall, due to the occlusion (Berger & Kerivan, 1983; Schroeter & Poesselt, 1986; Hansen, 1998; Stenfelt & Reinfeldt, 2007; Zurbrügg, Stirnemannn, Kuster & Lissek, 2014). This explanation has been supported by several analytical models of the OE (Schroeter & Poesselt, 1986; Hansen, 1998; Stenfelt & Reinfeldt, 2007; Zurbrügg *et al.*, 2014). Thirdly, Brummund *et al.* (2014) have alternatively proposed to explain the objective OE as the increase of the acoustic power (time-averaged over one period) injected by the vibrating earcanal wall to the earcanal cavity due to the augmentation of the earcanal acoustic resistance (real part of the acoustic impedance), seen by the earcanal wall, when the earcanal is occluded. Finally, one may wonder how these different explanations are consistent with each other.

In addition, the OE has been commonly interpreted as follows: the bone-conducted sound generated by the earcanal wall "escapes" through the earcanal opening, whereas it is "trapped" when the earcanal entrance is occluded (Carle, Laugesen & Nielsen, 2002; Kiessling, Brenner, Jespersen, Groth & Jensen, 2005; Keidser, Carter, Chalupper & Dillon, 2007). Sometimes, the "bone-conducted sound" has been replaced by the "sound pressure" (Staab, 1996; Nielsen & Darkner, 2011) or the "sound vibration" (Winkler, Latzel & Holube, 2016). In many cases, the earcanal opening has been interpreted as a "leak" for the sound energy which has been assumed to be "trapped" in the occluded earcanal (Kuk, 1991; Mueller, 1994; Mueller *et al.*, 1996; Chung, 2004; Borges, Costa, Naylor & Ferreira, 2014). Sound waves generated by the earcanal wall are assumed to be mainly transmitted in the surrounding environment in the open case and mainly reflected back by the occlusion device towards the tympanic membrane, therefore increasing the acoustic pressure in the occluded earcanal (Hansen & Stinson, 1998). These multiple interpreta-

tions can seem “logical” but are ambiguous in the author’s opinion because they describe the OE using several physical variables, concepts and sometimes an instinctive vocabulary. Therefore, one may wonder if these interpretations are consistent with the fundamental mechanism of the OE.

0.2.3 Influence of in-ear devices and their fit

Several factors are known to influence the OE: (i) the ear anatomy (Stenfelt *et al.*, 2003; Zurbrügg *et al.*, 2014), (ii) the bone-conducted stimulation (Hansen, 1998; Reinfeldt *et al.*, 2013; Saint-Gaudens *et al.*, 2019) and (iii) the occlusion device and its fit (Watson & Gales, 1943; Schroeter & Poesselt, 1986; Hansen, 1998; Stenfelt & Reinfeldt, 2007; Lee, 2011; Brummund *et al.*, 2015). Unlike the two first factors which are intrinsic to the wearer, the third factor (*i.e.*, the influence of the occlusion device) is of great interest in order to reduce the OE. Hundreds of passive earplug models exist in the market and vary in terms of geometry and material properties. A foam earplug is known to cause an OE lower than a silicone earplug (Hansen, 1998; Lee, 2011; Brummund *et al.*, 2015). However, none is known to significantly reduce the OE. The deep insertion principle has been proposed for this purpose and also used with hearing aids (Mueller, 1994; Staab, 1996; Nielsen & Darkner, 2011; Branda, 2012). This principle is based on the reduction of the vibrating earcanal wall area generating acoustic pressure in the occluded earcanal. The deep insertion, however, is often associated with a mechanical discomfort due to the sensitivity of the earcanal bony part. In the hearing aid field, the use of vent (Kuk, 1991; Carle *et al.*, 2002; Kiessling *et al.*, 2005; Keidser *et al.*, 2007) or open-fittings (MacKenzie, 2006; Blau, Sankowsky, Stirnemann, Oberdanner & Schmitt, 2008) can significantly reduce the OE but are associated with feedback issue (Chung, 2004; Borges *et al.*, 2014; Winkler *et al.*, 2016). More recently, the development of active earplugs (Bernier, 2013) and hearing aids (Ryan, Rule & Armstrong, 2006; Sunohara, Osawa, Hashiura & Tateno, 2015) has opened an interesting way to mitigate the OE. Active solutions are based on the principle of destructive

interference and require an electronic system to do so. The development of new passive solutions, on the other hand, could be interesting to avoid the use of electronic system. In this case, the reduction of the OE would rather only rely on the mechanical properties of the occlusion device.

0.3 Research objectives

This research aims at improving the understanding of the OE caused by in-ear devices in order to ultimately develop new concepts that mitigate the phenomenon using their own passive vibro-acoustic behavior. For this purpose, three specific objectives are identified:

1. First of all, the way the OE is explained and interpreted certainly influences the solutions sought to reduce it. Therefore, the fundamental mechanism of the OE will be revisited and its multiple interpretations will be investigated.
2. Secondly, since the OE originates from the vibration of the earcanal wall, the influence of its spatial distribution in terms of amplitude, phase and direction, on the OE will be investigated in open and occluded earcanals.
3. Thirdly, in order to mitigate the OE using occlusion devices them-selves, their mechanism(s) of contribution must be known and thus will be studied.

0.4 Thesis overview

The structure of the thesis is organized as follows. Chapter 1 is dedicated to a literature review related to the thesis objectives. Scientific developments are presented from Chapter 2 to Chapter 5 and correspond to four papers published in or submitted to peer-reviewed journals. Finally, Chapter 6 ends this thesis with a general conclusion on this work. The remainder of this section provides summaries of the six chapters of this thesis.

0.4.1 Chapter 1: Literature review

Chapter 1 is dedicated to a comprehensive literature review related to the three specific objectives of this thesis. Therefore, this literature review focuses on (i) the fundamental mechanism of the objective OE, (ii) the influence of the earcanal wall vibration, its modeling and measurement, and (iii) the contribution of in-ear devices to the OE. Both experimental and modeling works available in the literature are included. Finally, the usefulness of OE models to deepen the understanding of aforementioned aspects is demonstrated and a mixed investigation approach including both EA and FE models is presented.

0.4.2 Chapter 2: Fundamental mechanism of the occlusion effect and its interpretations

Chapter 2 is a paper published in the *Journal of the Acoustical Society of America* in May 2020. This paper is entitled "Theoretical investigation of the low-frequency fundamental mechanism of the objective occlusion effect induced by bone-conducted stimulation" (Carillo, Doutres & Sgard, 2020). This chapter mainly answers to the first and, to a lesser extent, to the second specific objectives. Indeed, this chapter aims at revisiting the fundamental mechanism of the objective OE in order to clarify the multiple interpretations of the phenomenon. For this purpose, the vibro-acoustic behavior of the earcanal open and occluded by an infinite impedance is thoroughly analyzed and illustrated using a 3D FE model of a realistic outer ear adapted from Brummund *et al.* (2014). An associated EA model is proposed to help interpretation. Inputs of the EA model are all derived from the 3D FE model. In particular, the parameters of the volume velocity source used in the EA model are directly related to the earcanal wall normal vibration pattern predicted by the 3D FE model. The two models are complementary to dissect physical phenomena involved in the fundamental mechanism of the OE. In addition, the influence of the earcanal wall normal vibration spatial distribution on the vibro-acoustic behavior of the open earcanal is highlighted. This spatial distribution is characterized by its centroid position which

is shown to correspond to the position of the equivalent volume velocity source representing the earcanal wall normal vibration in the EA model. The multiple interpretations of the OE are finally discussed to clarify the existing ambiguities.

0.4.3 Chapter 3: Clarification of a widespread theory of the occlusion effect

Chapter 3 is a paper submitted to *Acta Acustica* in March 2021 and currently in revision (first revision submitted in July 2021). This paper is entitled "On the removal of the open earcanal high-pass filter effect due to its occlusion: A bone-conduction occlusion effect theory." In complement to Chapter 2, this chapter focuses on the clarification of a widespread theory of the OE proposed by Tonndorf (1964). This theory relies on a simplified EA model and describes the OE as the removal of the open earcanal high-pass filter effect due to a perfect or partial occlusion. This filter, however, has not been clearly defined and several ambiguities are highlighted in this chapter. Tonndorf's theory is then revisited in detail in order to clarify the open earcanal high-pass filter effect and how perfect and partial occlusions affect it. This chapter contributes to the first specific objective.

0.4.4 Chapter 4: A method to assess the centroid of the earcanal wall normal vibration

Chapter 4 is a paper published in *Applied Acoustics* in June 2021. This paper is entitled "Principle of an acoustical method for estimating the centroid position of the earcanal wall normal velocity induced by bone-conducted stimulation: Numerical evaluation." By proposing a method to assess the centroid position of the earcanal wall normal vibration, this chapter is related to the second specific objective. The centroid position can be used as an indicator of the earcanal wall normal vibration distribution to study the influence of the type of bone-conduction stimulation on the outer ear pathway and on the OE. In addition, the knowledge of the centroid position could be used to validate the earcanal wall vibration patterns exhibited by FE models, to guide the insertion depth of in-ear devices and ultimately to mitigate the OE induced by in-ear devices. The

principle of this method rests on the measurement of the OE caused by an external capped duct coupled to the earcanal entrance of a subject submitted to a bone-conducted stimulation. This produces an acoustic antiresonance in the coupled system where a minimum acoustic pressure occurs at the centroid position of the earcanal wall normal vibration. The centroid position is then estimated by minimizing the difference between the measured antiresonance frequency and the antiresonance frequency computed using an associated EA model of the coupled system. The EA model requires the knowledge of the earcanal shape and the geometrical dimension of the coupling duct. The method is investigated numerically using the 3D FE model of a realistic outer ear developed by Brummund *et al.* (2014) and adapted to account for the coupling duct. A comparison between FE simulation and existing experimental data is also provided. The accuracy of the method is assessed numerically and the influence of several parameters related to the coupled system is investigated.

0.4.5 Chapter 5: Mechanisms of contribution of earplugs to the occlusion effect

Chapter 5 is a paper submitted to the *Journal of the Acoustical Society of America* in December 2020 and currently in revision (second revision submitted in July 2021). This paper is entitled "Numerical investigation of the earplug contribution to the low-frequency occlusion effect induced by a bone-conducted stimulation" and contributes to the second and third specific objectives. Among the several factors influencing the OE such as the ear anatomy or the bone-conducted stimulation, this chapter focuses on the contribution of earplugs in order to ultimately reduce the phenomenon using their own vibro-acoustic behavior. For this purpose, a 2D axi-symmetric FE model of the outer ear originally developed by Brummund *et al.* (2015) is improved. In order to assess the validity of the 2D FE model, simulation results are compared with measurement data taken from the literature. To help the interpretation of FE simulations, an associated EA model of the open and occluded earcanal is proposed. Compared to past analytical models, the earplug is introduced as an ideal source of volume velocity which is distinct from

the source representing the vibration of the earcanal wall. This distinction is facilitated by the fact that all EA model inputs are derived from the 2D FE model. Two mechanisms of contribution of earplugs are highlighted: (i) a Poisson's effect of the earplug induced by the normal component of the earcanal wall vibration and (ii) a longitudinal motion of the earplug caused by the tangential component of the earcanal wall vibration. By varying the geometry of the earcanal surrounding tissues, the spatial distribution of the earcanal wall vibration is shown to influence the contribution of earplugs to the OE.

0.4.6 Chapter 6: Conclusion

Chapter 6 concludes this thesis by a synthesis of the scientific developments made during this doctoral project, a discussion of the main limitations of this work and finally a presentation of perspectives for future work. In particular, the experimental assessment of the earcanal wall vibration pattern and the development of new concepts of in-ear devices mitigating the OE are the main future avenues proposed from this work. Finally Appx. I summarizes the academic achievements that I obtained during my doctorate.

CHAPTER 1

LITERATURE REVIEW

The literature review is related to the three specific objectives of this thesis (see Sec. 0.3). Section 1.1 focuses on the explanation of the fundamental mechanism of the objective occlusion effect (OE). Then, Sec. 1.2 puts the light on the earcanal wall vibration – the source of the OE – and particularly on its measurement, modeling and parameters of influence. In Sec. 1.3, the focus is rather put on the contribution of in-ear devices to the OE, the modeling of these devices and the mechanism(s) explaining their contribution. Finally, Sec. 1.4 provides a synthesis on the use of OE models to explore aforementioned aspects of this phenomenon and emphasizes the benefit of using electro-acoustic (EA) and finite element (FE) models together.

1.1 Fundamental mechanism of the objective occlusion effect

At low frequencies, the objective OE induced by a bone-conducted stimulation is characterized by a sound pressure level (SPL) increase in the occluded earcanal compared to the open earcanal (Huizing, 1960; Tonndorf, 1964; Hansen, 1998; Stenfelt & Reinfeldt, 2007; Brummund *et al.*, 2015). As mentioned in introduction (see Sec. 0.2.2), several explanations of this phenomenon have been proposed in the literature. Tonndorf (1964) provided the first model of the OE based on EA analogy of the open and occluded earcanal. In the open case, the air within the earcanal cavity was accounted for using an acoustic mass representing its inertia effect towards the earcanal opening and an acoustic compliance representing its compressibility effect towards the eardrum. In the occluded case, the inertia effect of the open earcanal vanished due to the occlusion device blocking the earcanal entrance and only the compressibility effect remained. Tonndorf described the earcanal opening as a "leak" related to the acoustic energy "dissipated" in the surrounding environment. No acoustic resistance was, however, accounted for in Tonndorf's model to take into account this phenomenon. Then, Tonndorf explained the OE as the removal of the open earcanal high-pass filter effect due to the occlusion of the earcanal entrance (Tonndorf, 1964; Tonndorf *et al.*, 1966; Tonndorf, 1972). The transfer function associated to the open

earcanal high-pass filter was, however, not defined (*i.e.*, physical nature of the input and output signals, order of the filter) and the filter resulting from the occlusion was not explicated either. In fact, the nature of the source representing the earcanal wall vibration was not mentioned and the model was only put forward to illustrate the theory. Since then, Tonndorf's theory has been the most quoted explanation of the objective OE in the literature (see Sec. 0.2.2). Therefore, it is possible that the ambiguities associated to this theory, in particular the description of the earcanal entrance as a "leak", could have contributed to the multiple interpretations of the low-frequency OE found in the literature and expressed in terms of "leak" and "trap" (see Sec. 0.2.2). The question of the meaning of Tonndorf's theory is therefore raised.

In analytical models subsequent to Tonndorf's model, the fundamental mechanism of the low-frequency OE has been attributed to the increase of the earcanal acoustic reactance (imaginary part of the impedance) seen by the vibrating earcanal wall when the earcanal entrance was occluded by an infinite impedance (Schroeter & Poesselt, 1986; Hansen, 1998; Stenfelt & Reinfeldt, 2007; Zurbrügg *et al.*, 2014). In these models, the 1D wave propagation in open and occluded earcanals was modeled using transfer matrix method (Schroeter & Poesselt, 1986; Hansen, 1998; Zurbrügg *et al.*, 2014) or EA analogy (Stenfelt & Reinfeldt, 2007). Furthermore, the spatial distribution of the earcanal wall normal vibration was considered as one (Schroeter & Poesselt, 1986; Hansen, 1998; Zurbrügg *et al.*, 2014) or two (Stenfelt & Reinfeldt, 2007) ideal volume velocity source(s) concentrated at given position(s) along the earcanal axis. Amplitude and position of these sources were generally assumed (Hansen, 1998; Stenfelt & Reinfeldt, 2007; Zurbrügg *et al.*, 2014) or adjusted based on SPL measurements (Schroeter & Poesselt, 1986). The use of ideal volume velocity source(s) was based on the assumption that the normal vibration of the earcanal wall would not be significantly influenced by the acoustic load. In the open case, Zurbrügg *et al.* (2014) showed that the level in dB (factor 20) of the earcanal acoustic reactance seen by the source increased with frequency by 20 dB/decade. In the occluded case, the earcanal acoustic reactance was significantly higher but decreased with frequency by 20 dB/decade. These slopes indicate that the acoustic reactance of the earcanal seen by the source is governed by an inertia effect in the open case and by a compressibility effect in the occluded case. This

ties in with Tonndorf's idea that the acoustic mass of the open earcanal would vanish when the earcanal entrance is occluded (Tonndorf, 1964). By definition, an acoustic mass is associated with an acoustic pressure difference across it (Bruneau, 2013). Therefore, the acoustic pressure generated by the source in the open earcanal would not be uniform along the earcanal axis, even at low frequencies. In consequence, the acoustic reactance seen by the source should depend on the source position when the earcanal is open but this dependence has not been investigated. In the occluded case, Zurbrügg *et al.* (2014) showed that the position of the source along the earcanal axis had no influence on the SPL computed at the tympanic membrane at low frequencies. Above 4 kHz, however, significant difference in SPL (up to 30 dB) were observed but not explained. A possible explanation of Zurbrügg *et al.*'s findings follows. At low frequencies, the occluded earcanal is governed by its compressibility effect (Berger & Kerivan, 1983) so the acoustic pressure should be uniform. Therefore, the source would see the same acoustic reactance whatever its position along the occluded earcanal. Above 4 kHz, however, the acoustic pressure could not be uniform due to the half-wavelength acoustic resonance (around 6 kHz for a shallow occlusion). In consequence, the acoustic reactance seen by the source would vary depending on its position (*e.g.*, close to a node or an anti-node) in the occluded earcanal, explaining the SPL variation at the tympanic membrane. Since the source is supposed to represent the normal vibration of the earcanal wall, the question of the meaning of its position along the earcanal axis is therefore raised (see more detail in Sec. 1.2).

More recently, Brummund *et al.* (2014) investigated the fundamental mechanism of the low-frequency objective OE using a 3D FE model of an outer ear open and occluded by an infinite impedance defined at the earcanal entrance. They showed that the surface averaged earcanal wall normal velocity was little reduced (<1 dB) by the change in acoustic load between the open and occluded earcanal, as assumed in analytical models. Then, by adopting an acoustic power balance approach, Brummund *et al.* showed that a significant proportion of the acoustic power injected by the earcanal wall in the open earcanal is radiated through the earcanal entrance. They related this phenomenon to the open earcanal high-pass filter effect mentioned by Tonndorf (1964), despite the absence of acoustic resistance in Tonndorf's model. However, Brummund *et*

al. explained that the removal of the earcanal opening acoustic radiation, due to the occlusion, could not explain the OE. Therefore, they rather explained the OE as the increase of the acoustic power injected by the earcanal wall due to the augmentation of the surface averaged acoustic resistance (real part of the acoustic impedance) seen by the earcanal wall in the occluded case compared to the open case. However, they neglected to take into account visco-thermal losses in the earcanal volume. This could influence the acoustic power balance in both open and occluded cases and could thus affect Brummund *et al.*'s conclusion. By calculating the surface averaged acoustic impedance seen by the earcanal wall, Brummund *et al.* used the acoustic impedance of the earcanal cavity seen from a transverse direction (*i.e.*, the normal direction of the earcanal wall) whereas the earcanal cavity acoustic impedance computed by analytical models was necessarily seen from a longitudinal direction (*i.e.*, the earcanal middle axis). In consequence, these two impedances are fundamentally different and could have different values if the acoustic pressure field were not uniform along the earcanal axis, in the open case for example. In this case, the acoustic impedance seen by the source could differ from the surface averaged acoustic impedance seen by the earcanal wall even though the source represents it. This raises the question about the relation between the source and the spatially distributed earcanal wall normal vibration.

1.2 Vibration of the earcanal wall

The vibration of the earcanal wall is known to vary along and probably around the circumference of the earcanal. While the earcanal wall vibration has never been directly measured due to experimental difficulty, indirect findings indicate the reduction of the earcanal wall normal vibration amplitude from the earcanal entrance to the eardrum. The reduction of the OE with insertion depth of the occlusion device is generally explained by the reduction of both the earcanal wall surface not covered by the occlusion device and the amplitude of its vibration (Tonndorf *et al.*, 1966; Berger & Kerivan, 1983; Schroeter & Poesselt, 1986; Stenfelt & Reinfeldt, 2007; Brummund *et al.*, 2015). Also, Stenfelt *et al.* (2003) showed that the SPL generated by the earcanal wall vibration induced by a bone-conducted stimulation in an intact earcanal was about

10 dB greater than when the earcanal cartilaginous part was removed. The greater vibration of the cartilaginous part of the earcanal compared to the bony part was explained by the lower stiffness of earcanal surrounding tissues in the former than in the latter (Stenfelt *et al.*, 2003; Berger & Kerivan, 1983).

In analytical models, the earcanal wall vibration has been accounted for using ideal volume velocity source(s). In most cases, the source represented the vibration of the earcanal cartilaginous part whereas the contribution of the earcanal bony part was neglected (Schroeter & Poesselt, 1986; Hansen, 1998; Zurbrügg *et al.*, 2014). Stenfelt & Reinfeldt (2007), however, accounted for the vibration of both parts using two distinct volume velocity sources. In any case, these sources were located at a chosen position assumed in their corresponding portion of the earcanal. Also, the amplitude of these sources was maximum in the open earcanal and diminished as a function of the insertion depth in the occluded earcanal. The function governing the amplitude decrease was assumed (Stenfelt & Reinfeldt, 2007; Zurbrügg *et al.*, 2014) or adjusted from SPL measurements (Schroeter & Poesselt, 1986). In Hansen's model, the decrease of the source amplitude was governed by the change in mechanical impedance of the earcanal surrounding tissues from the cartilaginous part to the bony part (Hansen, 1998). In all models, the amplitude of these sources was a function of the in-ear device insertion depth and accounted for a given spatial distribution of the earcanal wall normal vibration. In addition, these sources were always located in the portion of the earcanal that they represent but their exact positions were assumed. The question of whether the exact position of sources is related to a characteristic of the spatial distribution of the earcanal wall normal vibration is therefore raised. This distribution, however, is still unknown and would be intricate to measure in the human earcanal.

Brummund *et al.* have been the first to introduce the use of FE models of the human outer ear to study the objective OE induced by bone-conducted stimulation (Brummund *et al.*, 2014, 2015). These models account for the spatial distribution of the earcanal wall vibration by including the earcanal surrounding tissues (*e.g.*, skin, cartilage, bone) as isotropic linear elastic solid domains. In their 3D FE model, Brummund *et al.* (2014) obtained the anatomical geometry from cross-sectional cryosection images of a female cadaver head available in the Visible Human

Project®. In their 2D axi-symmetric FE model (Brummund *et al.*, 2015), geometrical data were rather taken from literature. To limit the computation cost of their models, Brummund *et al.* used a truncated portion of the head including the earcanal cavity and its surrounding tissues only. Due to the truncation, bone-conducted stimulations were introduced in a simplified way and both models required the imposition of a set of boundary conditions which were adjusted to obtain OE simulations comparable with experimental data taken from the literature. Brummund *et al.* did not detail the spatial distribution exhibited by their FE models but it is sure that the geometry, material properties, boundary conditions and loading influence it. Due to models' truncation, the last two are intricate to adjust in a realistic way. On the other hand, full head FE models (Chang, Kim & Stenfelt, 2016; Xu, Sgard, Wagnac & De Guise, 2019) could be useful to exhibit realistic earcanal wall vibration pattern since they overcome the limitations of truncated models. The former, however, require considerably more computational resources than the latter. In any case, FE models, truncated or not, are still simplification of reality. The spatial distribution that they highlight should be confronted to real earcanal vibration pattern.

As mentioned previously, the earcanal wall vibration pattern would be difficult to assess experimentally. Indeed, the small size of the earcanal and its tortuosity make it difficult, if not impossible, to perform Doppler laser vibrometer or accelerometer measurements. Hansen & Stinson (1998) proposed an indirect method to estimate the surface averaged normal vibration amplitude of the earcanal wall based on the measure of the SPL in the occluded earcanal cavity and the knowledge of its acoustic impedance. However, the normal vibration of the earcanal wall could be influenced by the presence of the occlusion device. In addition, the latter could contribute to the SPL generated in the occluded earcanal therefore influencing the estimation of the earcanal wall normal vibration amplitude. Hansen (1998) also proposed another indirect method to estimate the normal vibration of the earcanal wall. This method used a microphone in a cavity created in a rubber made occlusion device. The cavity was open on the vibrating earcanal wall. From the knowledge of the cavity volume and the measured acoustic pressure, Hansen estimated the vibration of the earcanal wall at the aperture of this cavity. This method, however, suffers from the same limitations as the previous one. The development of an indirect

method characterizing the spatial distribution of the earcanal wall normal vibration without influencing it would be of great interest.

1.3 Contribution of in-ear devices

In-ear devices are known to influence the OE depending on their fit in the earcanal and their mechanical properties. The fit includes the insertion depth and the type of fitting (*e.g.*, open, vented or closed) and has already been discussed in introduction (see Sec. 0.2.3). Here, the focus is rather put on the influence of the in-ear device mechanical properties. Several experimental work have highlighted that a silicone earplug produces a 5 to 10 dB greater objective OE than a foam earplug at medium insertion (Hansen, 1998; Brummund *et al.*, 2015) and that this difference increases around 15 dB at deep insertion (Lee, 2011). This raises the questions of the mechanism(s) explaining the contribution of earplugs to the OE and their dependence with insertion depth.

According to Hansen (1998), earplugs could contribute to the OE in three ways: (i) the acoustic impedance of their medial surface influences the SPL generated by the active portion of the vibrating earcanal wall, (ii) the medial earplug surface is set into vibration due to its coupling with the earcanal wall and thus contributes to the SPL in the occluded earcanal and/or (iii) the presence of the earplug influences the normal vibration of the active portion of the earcanal wall. Hansen demonstrated that the acoustic impedance of the medial earplug surface seen from inside the earcanal could not explain the experimental difference in objective OE found between silicone and foam earplugs. Therefore, Hansen focused on mechanisms (ii) and (iii) to explain this difference. In mechanism (ii), Hansen assumed a rigid body motion of the earplug excited by the surrounding skin tissue in the direction of the earcanal axis. By this mechanism, the medial earplug surface imposed a volume velocity to the occluded earcanal cavity. To account for this mechanism, Hansen modeled the earcanal surrounding tissues using their mechanical impedance. This mechanism predicted that a heavy earplug would induce a lower OE than a light earplug while the contrary was observed experimentally (the heavier silicone earplug produced a greater OE than the lighter foam earplug). Therefore, Hansen proposed mechanism (iii) in

which the earplug did not impose a volume velocity to the earcanal cavity but rather influenced the volume velocity imposed by the portion of the earcanal wall which was not covered by the earplug. For this purpose, Hansen assumed that the whole earcanal wall vibration (covered and not covered by the earplug) acted as an ideal volume velocity source and that the mass of the earplug decreased the vibration of the covered portion of the earcanal, and therefore, increased the vibration of the not covered earcanal wall portion. Since this mechanism predicted the experimental difference in OE between a silicone and a foam earplug, Hansen concluded that the earplug mass governs the earplug contribution to the OE. This conclusion is, however, in contradiction with an experimental work provided by Watson & Gales (1943) who showed that there is no relation between the earplug mass and the resulting OE. Also, the assumption that the whole earcanal wall vibration acts as an ideal volume velocity source is debatable and one could rather expect that the earplug decreases the vibration of both covered and, to a lesser extent, not covered earcanal wall portions due to the earcanal surrounding tissues continuity. Since the mass cannot explain the contribution of earplugs to the OE, this raises the question of the influence of other mechanical properties of earplugs.

In order to investigate the contribution of earplugs to the OE, Brummund *et al.* modeled earplugs as isotropic linear elastic solid domains in their 3D and 2D axi-symmetrical FE models (Brummund *et al.*, 2014, 2015). They assumed earplugs to perfectly adapt to the surrounding earcanal wall without deforming the latter. A foam and a silicone earplug were used, and three insertion depths were included (shallow, medium and deep insertion). Material properties of earplugs were taken from the literature. Brummund *et al.* observed the experimental difference in OE between foam and silicone earplugs using their FE models and used an acoustic power balance approach for interpreting their simulations. They observed that the proportion of acoustic power injected in the occluded earcanal by the medial earplug surface was significantly higher for the silicone earplug compared to the foam earplug. However, they did not relate the earplug contribution to its material properties. At medium and deep insertion, Brummund *et al.* also highlighted that the contribution of the medial earplug surface in terms of acoustic power injected to the earcanal cavity was significantly higher than that of the uncovered earcanal wall.

This indicates that the earplug could be the primary source of SPL generated in the occluded earcanal at medium and deep insertion. However, acoustic power exchange can be intricate to interpret the contribution of the uncovered earcanal wall and the medial earplug surface on the acoustic pressure generated in the earcanal. Therefore, Brummund *et al.*'s findings should be further investigated. Accordingly, the mechanism(s) of contribution of earplugs remains unknown, as well as the influence of earplugs on the earcanal wall vibration, and the influence of the earcanal wall vibration, in both normal and tangential directions, on the vibration of earplugs. The question of the influence of the earcanal wall vibration spatial distribution on the earplug contribution is also raised.

1.4 Synthesis and research approach

Several questions have been raised previously regarding (i) the fundamental mechanism of the objective OE and in particular the relation between the equivalent source and the spatial distribution of the earcanal wall normal vibration that it represents, (ii) the vibration of the earcanal wall and the influence of its spatial distribution on the OE, and (iii) the mechanism(s) of contribution of in-ear devices to the OE, in relation to the earcanal wall vibration. In order to provide answers to these questions and achieve the specific objectives of this thesis, EA and FE models will be jointly used. On one hand, localized constants associated with EA analogy can be given a physical interpretation which facilitates the understanding of vibro-acoustic phenomena. However, the way the earcanal wall normal vibration is accounted for in EA models by a volume velocity source prevents any analysis of the influence of this vibration on the OE. In fact, the physical meaning, if it exists, of the source position is unknown. In addition, mechanical properties of in-ear devices and their mechanical and vibro-acoustical couplings to the surrounding earcanal wall and the earcanal cavity respectively, are intricate to take into account using EA models. On the other hand, FE models are practical for this purpose since they are able to account for precise geometry, material properties, boundary conditions and loading. These parameters, however, can be difficult to assess experimentally or to adjust from experimental data. This constitutes a major limitation of this approach which is still a

simplification of reality. Furthermore, due to their complexity, the vibro-acoustic behavior exhibited by FE models can be difficult to interpret, contrary to EA models. Therefore, the conjunction of both EA and FE models makes it possible to combine their respective pros whereas part of their cons could be compensated by each other.

CHAPTER 2

THEORETICAL INVESTIGATION OF THE LOW-FREQUENCY FUNDAMENTAL MECHANISM OF THE OBJECTIVE OCCLUSION EFFECT INDUCED BY BONE-CONDUCTED STIMULATION

Kévin Carillo[a] , Olivier Doutres[a] , Franck Sgard[b]

[a] Department of Mechanical Engineering, École de technologie supérieure,
1100 Notre-Dame Ouest, Montréal, Québec, Canada H3C 1K3
[b] Direction Scientifique, Institut de recherche Robert-Sauvé en santé et en sécurité du travail,
505 Boulevard de Maisonneuve Ouest, Montréal, Québec, Canada H3A 3C2

Paper published in *Journal of the Acoustical Society of America*, May 2020.

2.1 Abstract

The objective occlusion effect induced by bone-conducted stimulation refers to the low-frequency acoustic pressure increase that results from occluding the earcanal opening. This phenomenon is commonly interpreted as follows: the bone-conducted sound "leaks" through the earcanal opening and is "trapped" by the occlusion device. This instinctive interpretation misrepresents the fundamental mechanism of the occlusion effect related to the earcanal impedance increase and already highlighted by existing electro-acoustic models. However, these models simplify the earcanal wall vibration (*i.e.*, the origin of the phenomenon) to a volume velocity source which, in the authors' opinion, (i) hinders an exhaustive comprehension of the vibro-acoustic behavior of the system, (ii) hides the influence of the earcanal wall vibration distribution, and (iii) could blur the interpretation of the occlusion effect. This paper analyzes, illustrates and interprets the vibro-acoustic behavior of the open and occluded earcanal using an improved finite element model of an outer ear in conjunction with an associated electro-acoustic model developed in this work. The two models are complementary to dissect physical phenomena and to highlight the influence of the earcanal wall vibration distribution, characterized here by its curvilinear centroid position, on the occlusion effect.

2.2 Introduction

The term occlusion effect (OE) is commonly used to describe an increase in the auditory perception of bone-conducted sound that results from occluding the earcanal opening. In everyday life, the OE is often perceived as the increased sensation of the bone-conducted part of one's own physiological noises (*e.g.*, one's own voice, breathing, chewing, heartbeat) (Berger, 2003) which is most significant for low frequencies (<1 kHz). The OE is deemed to be a notable source of discomfort to workers wearing shallowly inserted passive occlusion devices such as earplugs (Doutres *et al.*, 2019). The OE also affects the hearing aid users' comfort (Kochkin, 2010) but can be greatly reduced using open-fittings (Winkler *et al.*, 2016). The deep-fitting of the occlusion device in the bony part of the earcanal is also known to reduce the OE (Killion, Wilber & Gudmundsen, 1988) but seems associated with wearers' discomfort (Kiessling *et al.*, 2005; Nielsen & Darkner, 2011). The bone-conducted sound travels to the cochlea through different pathways (Stenfelt & Goode, 2005; Dobrev *et al.*, 2017; Sohmer, 2017; Chordekar *et al.*, 2018). The outer ear pathway corresponds to the sound pressure generated in the earcanal cavity due to the vibration of the earcanal wall, which constitutes the source of the OE. At low frequencies, the outer ear pathway is negligible when the earcanal is open (Stenfelt *et al.*, 2003; Stenfelt, 2016) but dominates when it is occluded (Stenfelt *et al.*, 2003). The OE is thus objectively characterized by an acoustic pressure increase in the occluded earcanal at low frequencies (Huizing, 1960; Schroeter & Poesselt, 1986; Stenfelt & Reinfeldt, 2007). This objective description of the OE is the one used in this paper.

In the literature, the OE is commonly interpreted as follows: the bone-conducted sound generated by the earcanal wall "escapes" through the earcanal opening (*i.e.*, open earcanal entrance), whereas it is "trapped" in the occluded case (Carle *et al.*, 2002; Kiessling *et al.*, 2005; Keidser *et al.*, 2007). The bone-conducted sound is expected to take the path of least "resistance" (Staab, Dennis, Schweitzer & Weber, 2004). Sometimes, authors refer to the sound pressure generated by the earcanal wall (Staab, 1996; Nielsen & Darkner, 2011) or to the "sound vibration" imposed by the earcanal wall (Winkler *et al.*, 2016). In many cases, the earcanal opening is interpreted as a "leak" for the sound energy which is presumed to be "trapped" in the occluded earcanal (Kuk,

1991; Mueller, 1994; Mueller *et al.*, 1996; Chung, 2004; Borges *et al.*, 2014). Therefore, sound waves generated by the earcanal wall are assumed to be mainly transmitted in the surrounding environment in the open case. On the contrary, they are expected to be mainly reflected by the occlusion device towards the tympanic membrane, leading to an enhanced acoustic pressure in the occluded earcanal (Hansen & Stinson, 1998). These multiple interpretations, found either in experimental or modeling studies in both hearing aid and hearing protection fields, are ambiguous because they describe the OE using several physical variables, concepts and an instinctive vocabulary. Furthermore, the way the phenomenon is interpreted could influence the solutions sought to reduce it. These interpretations thus must be clarified and OE models can be helpful for this purpose.

In order to investigate the OE, different models have been elaborated in the past (Tonndorf *et al.*, 1966; Schroeter & Poesselt, 1986; Hansen, 1998; Stenfelt & Reinfeldt, 2007; Zurbrügg *et al.*, 2014; Brummund *et al.*, 2014, 2015; Sgard, Carillo & Doutres, 2019). Lumped elements models based on electro-acoustic (EA) analogy (Tonndorf *et al.*, 1966; Schroeter & Poesselt, 1986; Hansen, 1998; Stenfelt & Reinfeldt, 2007) were historically the first OE models. These models account for the air within the earcanal cavity as acoustic masses, compliances and resistances and have highlighted the fundamental mechanism of the OE as the increase of the earcanal cavity acoustic impedance seen by the cavities' vibrating walls due to the occlusion. However, the spatially distributed earcanal wall vibration (*i.e.*, the source of the OE) is idealized as one (Schroeter & Poesselt, 1986; Hansen, 1998; Zurbrügg *et al.*, 2014) or two (Stenfelt & Reinfeldt, 2007) volume velocity source(s) concentrated at a chosen position in the earcanal. Due to the cramped and tortuous aspects of the human earcanal, amplitude and position of the source(s) are difficult to assess experimentally and are generally assumed or adjusted based on sound pressure measurements in open and occluded earcanal. This prevents any analysis of the influence of the earcanal wall vibration amplitude and, in particular, distribution, though it is the source of the OE. In addition, the earcanal cavity is commonly simplified to one (Schroeter & Poesselt, 1986; Hansen, 1998; Zurbrügg *et al.*, 2014) or two (Stenfelt & Reinfeldt, 2007) uniform cylindrical duct(s), considering that the acoustic wavelength is much larger than the earcanal dimensions at

low frequencies. To overcome these limitations, finite element (FE) models (Brummund *et al.*, 2014, 2015; Sgard *et al.*, 2019) of the OE can be used since they make it possible to account for a precise geometry, material properties, boundary conditions and stimulation. However, FE models are limited by the knowledge of the corresponding inputs which can be difficult to characterize experimentally.

Recently, Brummund *et al.* (2014) developed a three-dimensional (3D) FE model of a "realistic" outer ear in which the set of equivalent loading and boundary conditions is questionable. Indeed, in order to mimic the placement of a standard bone transducer, a normal force was applied directly on the mastoid process while the remaining surface of the truncated geometry was fixed (Brummund *et al.*, 2014). This set induces a compression motion in the temporal bone which is rather expected to behave as a rigid body at low frequencies (Stenfelt *et al.*, 2003). In addition, this set forces the vibration to travel from the bony tissue to the soft and skin tissues while the latter should be rather primarily excited by the bone transducer. Despite these limitations, this model has been shown to provide the slope of the OE at shallow/medium insertion (Brummund *et al.*, 2014) measured on 20 subjects by Stenfelt & Reinfeldt (2007). Based on this model, Brummund *et al.* (2014) investigated the fundamental mechanism of the OE using an acoustic power balance approach. They pointed out that an acoustically rigid occlusion of the earcanal entrance increases the resistance (real part) of the earcanal cavity acoustic impedance seen by its wall compared to the open case (Brummund *et al.*, 2014). This resistance governs the acoustic power injected into the earcanal cavity by its wall (Brummund *et al.*, 2014). However, Brummund *et al.* (2014) assumed no visco-thermal dissipation within the earcanal cavity, although it is higher than the acoustic power radiated at the open earcanal entrance at low frequencies (Keefe, Bulen, Campbell & Burns, 1994), and could have underestimated the resistance of the open earcanal. In addition, the acoustic power balance approach only describes the acoustic energy transfer but does not detail the vibro-acoustic (*i.e.*, acoustic pressures and particle velocities) behavior that explains this transfer. The use and limits of this approach are thus revisited in this work.

Both EA and FE models are useful to explain the fundamental mechanism of the OE. However, the source of the OE, namely the vibration of the earcanal wall, is overly simplified in EA models and too intricate in FE models. The influence of the earcanal wall vibration is thus hidden in both models. In addition, these models have not been used to fully detail physical phenomena occurring in both open and occluded earcanal under a bone-conducted stimulation. In the authors' opinion, taking these steps (*i.e.*, investigating the influence of the earcanal wall vibration and detail physical phenomena in the earcanal cavity) is necessary to accurately revisit our understanding of the OE and the role of its source, to clarify the ambiguity that surrounds the interpretation of the OE and to ultimately open new ways to mitigate this phenomenon. For this purpose, the FE model of a "realistic" outer ear proposed by Brummund *et al.* (2014) is revisited, improved and used in conjunction with an associated EA model developed in this work. In the current work, the occlusion is simplified to an infinite impedance defined at the earcanal entrance to focus on the fundamental mechanism of the OE. The intricate influence of the occlusion device (Lee & Casali, 2011; Lee, 2011; Brummund *et al.*, 2014, 2015; Sgard *et al.*, 2019), therefore, is not taken into account.

The originality of the current work is threefold. Firstly, the FE model is used to thoroughly analyze and illustrate the vibro-acoustic behavior of both open and occluded earcanal at low frequencies from 100 Hz to 1 kHz. Secondly, all inputs of the EA model presented here are derived from the FE model. In particular, the volume velocity source characteristics are here directly related to the earcanal wall vibration field. The EA model is thus useful to clarify and interpret in a simplified way physical phenomena involved in the earcanal as well as the influence of the earcanal wall vibration distribution on the OE. Results computed using both FE and EA models are presented, compared and discussed. Thirdly, common interpretations of the OE are discussed in the light of the results presented here in open and occluded cases.

2.3 Models of the occlusion effect

An implicit harmonic temporal dependency is taken into account by the term $e^{j\omega t}$ where j is the complex number such as $j^2 = -1$, ω is the circular frequency such that $\omega = 2\pi f$, f denotes the

frequency, and t the time. An arbitrary space and time dependent physical variable $h\left(\underline{x},\, t\right)$ is written in the complex form such that

$$h\left(\underline{x},\, t\right) = \Re\left[\hat{h}\left(\underline{x}\right)\, e^{j\omega t}\right], \tag{2.1}$$

where $\underline{x} = (x_1,\, x_2,\, x_3)$ denotes the position vector of the point of interest in the 3D space, $\hat{h}$ is the complex amplitude and $\Re\,[.]$ takes the real part of its argument. Solving for $\hat{h}$ is equivalent to solving for h. In addition, $\hat{h}^*$ is the complex conjugate, $\left|\hat{h}\right|$ is the modulus and $\left\langle\hat{h}\right\rangle$ is the surface averaged value. In the EA model, all vibro-acoustic variables are spatial averages and $\hat{h} = \left\langle\hat{h}\right\rangle$.

2.3.1 Finite element model of the outer ear

2.3.1.1 Geometry and materials

The FE model of the outer ear developed by Brummund *et al.* (2014) and used in this study is illustrated in Fig. 2.1(a). The geometry was obtained from cross-sectional cryosection images of a female cadaver from the Visible Human Project®. Figure 2.1(b) presents a sectional view in the horizontal plane of the FE model superimposed on the corresponding cryosection image. In the FE model, the earcanal cavity is embedded into a circular cross section cylinder (medial-lateral axis) with a diameter of 27 mm (see the pink and green regions of Fig. 2.1(a)). This reduces the computation time compared to an entire head model (Chang *et al.*, 2016). This model distinguishes the skin (including the fat) from other soft tissues (including cartilage and muscle) and it includes the entire temporal bone (see the gray part of Fig. 2.1(a)). More recent studies rather separate cartilage from soft tissues (including skin, fat and muscle) (Chang *et al.*, 2016; Benacchio, Doutres, Le Troter, Varoquaux, Wagnac, Callot & Sgard, 2018).

In the current model, the pinna and the middle and inner ears are not fully modeled but are accounted for by estimates of the acoustic impedance associated with sound flow through these structures (see Sec. 2.3.1.2). A complete view of the earcanal cavity from the tympanic

membrane to the earcanal entrance is presented in Fig. 2.1(c). The earcanal curvilinear axis z (see Fig. 2.1(c)), also called middle or center axis in the literature, is computed using an iterative method developed by Stinson & Lawton (1989). In this work, the earcanal entrance plane is defined normal to the earcanal curvilinear axis rather than in a sagittal plane (Brummund *et al.*, 2014). The earcanal shape represented as a radius function $r_{EC}(z)$ (assuming circular cross-sections) is displayed in Fig. 2.2. Compared to 15 radius functions presented by Hudde & Engel (1998b), the current model includes a constriction close to the earcanal entrance. In addition, the current earcanal curvilinear length (l_{EC} = 34.7 mm) is higher than the average earcanal length (known to be around 27 mm) while the eardrum coupling region length (close to 8 mm) is similar (Hudde & Engel, 1998b).

Solid domains are considered isotropic linear elastic solids under the small deformations' assumption. Their mechanical properties come from literature data (except structural loss factors which have been assumed (Brummund *et al.*, 2014)) and are summarized in Table-A II-1 (see Appx. II). While the air within the earcanal cavity was considered a perfect compressible fluid by Brummund *et al.* (2014), it is here rather modeled as a Navier-Stokes-Fourier compressible fluid to account for visco-thermal dissipation (Pierce, 1994; Kampinga, Wijnant & de Boer, 2010). Classic values of ambient air properties are used and given in Table-A II-2 (see Appx. II).

2.3.1.2 Boundary conditions and model limitations

In the authors' opinion, the main limitation of the current FE model developed by Brummund *et al.* (2014) comes from its truncated geometry (see Fig. 2.1(a)). As exposed in Sec. 2.2, this model requires the imposition of a set of equivalent loading and boundary conditions which are particularly tricky to define since the truncated geometry is supposed to be surrounded by biological tissues (see Fig. 2.1(b)). The set chosen by Brummund *et al.* (2014) results in a vibration pattern concentrated approximately at the earcanal mid-length (see Appx. III) near the transition between soft and bony tissues while this vibration is rather expected to be concentrated in the earcanal cartilaginous part close to the earcanal entrance (Stenfelt *et al.*, 2003; Stenfelt & Reinfeldt, 2007). In this paper, another set is chosen in order to be more consistent

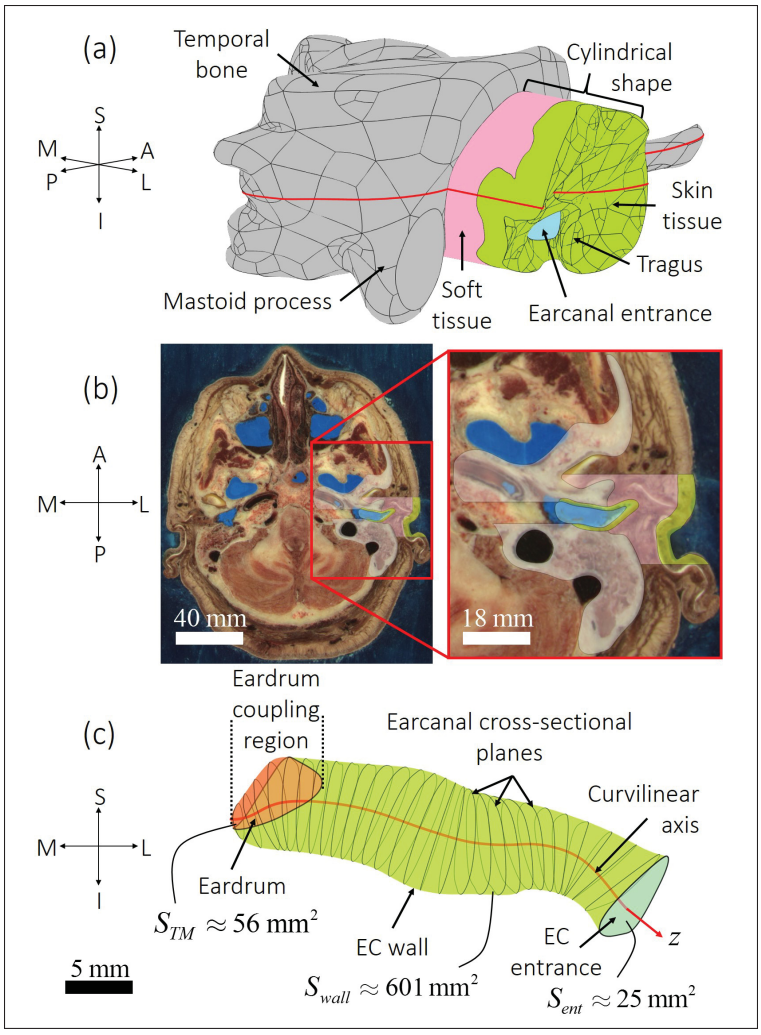

Figure 2.1 (a) 3D FE model of an outer ear (Brummund *et al.*, 2014), (b) sectional view in the horizontal plane (specified by a red line in (a)) superimposed on the corresponding cryosection image from the Visible Human Project® and (c) earcanal cavity alone. The coordinate system refers to superior (S), inferior (I), posterior (P), anterior (A), medial (M) and lateral (L)

with realistic loading and boundary conditions and to reproduce a “plausible” vibration pattern (see Sec. 2.4.1), even though the latter has never been directly measured due to experimental limitations nor studied numerically. A bone transducer stimulation applied on the mastoid process is expected to induce a compression motion in the skin and soft tissues which then

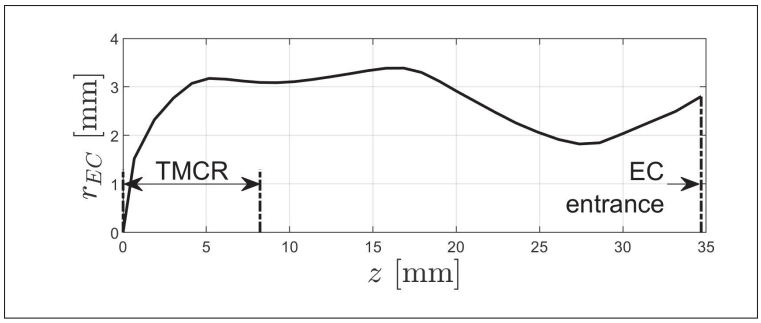

Figure 2.2 Earcanal radius $r_{EC}(z)$ (assuming circular cross-sections) as a function of the curvilinear axis z

stimulate the temporal bone. Therefore, skin and soft tissues are here excited in a simplified way by a uniform normal velocity field $V_n\left(\underline{x},\, t\right) = \Re\left[A(\underline{x})e^{j\omega t}\right]$ applied to their circumferential surface. The amplitude $A(\underline{x}) = 10^{-5}$ m s^{-1} is chosen to produce realistic sound pressure levels in both open and occluded earcanal (see Sec. 2.4.4). The temporal bone external boundary and the skin in contact with the surrounding environment (not modeled (Brummund *et al.*, 2014)) are free. Continuity of stress vectors and displacements is assumed between solid domains. Since the earcanal wall vibration distribution depends on the chosen set of loading and boundary conditions, the influence of various sets (summarized in Appx. III) on the OE is studied (see Sec. 2.4.6). Due to its truncation, the current model is not used to study the bone-conducted sound transmission through the head or the outer ear for a specific individual but rather to detail general physical phenomena in the earcanal cavity.

Acoustic boundary conditions applied to the earcanal cavity are similar to those used by Brummund *et al.* (2014). A locally reacting acoustic impedance boundary condition is specified on the tympanic membrane of surface S_{TM} (see Fig. 2.1(c)). The impedance associated with sound-induced motion of the tympanic membrane is referred to as $\hat{Z}_{TM}$ and defined by the model of Shaw & Stinson (1981) (see Appx. IV), which compares well to measurement data at low frequencies (Hudde & Engel, 1998a). An acoustic impedance $\hat{Z}^k_{ent}$, where $k \in \{open,\, occl\}$, is also defined at the earcanal entrance of surface S_{ent} (see Fig. 2.1(c)). In the open case, this impedance is equal to the radiation impedance $\hat{Z}_{rad}$ of a baffled circular piston of the same

surface (see Appx. V). At low frequencies, this impedance is a reasonable approximation of that measured if the earcanal entrance plane is chosen not too “inside” the earcanal (portion of the earcanal included) nor too “outside” (acoustic wave no longer plane) (Hudde & Engel, 1998b). In the occluded case considered here, the earcanal entrance has an infinite impedance instead of a real physical occlusion device (Brummund *et al.*, 2014).

2.3.1.3 Finite element modeling

In the coupled elasto-acoustic (visco-thermal) model, the coupling at the earcanal wall/cavity boundary implies the continuity of velocity vectors and stress vectors. The earcanal wall is assumed isothermal since the human body is considered at constant temperature. Adiabatic thermal couplings are assumed at the earcanal entrance and the tympanic membrane since negligible heat transfers are expected. The visco-thermal acoustics model requires lots of computational resources due to the number of variables and the refinement of the mesh at the earcanal wall boundary. This model is thus only used to accurately illustrate physical phenomena in the 3D earcanal cavity at 100 Hz (see Fig. 2.4). Vibro-acoustic indicators presented in Sec. 2.3.1.4 are computed over the whole frequency range of interest using a low reduced frequency model (Kampinga, 2010) applied to the earcanal cavity (see Appx. VI). In the low reduced frequency model, viscous and thermal losses are distributed in the bulk of the fluid through a complex wavenumber (Kampinga, 2010; Kampinga *et al.*, 2010). The coupling at the earcanal wall boundary is thus simplified to the continuity of normal component velocity vectors and normal component stress vectors (Atalla & Sgard, 2015). The radius used for the low reduced frequency model corresponds to the equivalent earcanal radius function $r_{EC}(z)$ (see Fig. 2.2). Both coupled elasto-acoustic models are meshed according to a criterion of at least six 10-noded tetrahedral elements per wavelength at 1 kHz and solved using COMSOL Multiphysics 5.5 (COMSOL®, Sweden). The meshes of the low reduced frequency and the visco-thermal FE models consist of 613 452 and 1 331 740 elements respectively and achieve convergence.

2.3.1.4 Vibro-acoustic indicators

When submitted to the chosen mechanical excitation (see Sec. 2.3.1.1), the earcanal wall vibrates and imposes to the earcanal cavity a volume velocity defined by $\hat{q}_{wall} = \langle \hat{v}_{n,wall} \rangle S_{wall}$ with $\langle \hat{v}_{n,wall} \rangle$ the surface averaged earcanal wall normal velocity and S_{wall} the earcanal wall surface. According to Brummund *et al.* (2014), $\langle \hat{v}_{n,wall} \rangle$ is only slightly reduced (<1 dB) at low frequencies by the earcanal cavity acoustic load change between open and occluded cases (confirmed but not shown here). Since the occlusion is defined at the earcanal entrance, $\hat{q}_{wall}$ is thus approximately equal in both open and occluded cases. Volume velocities passing through the tympanic membrane and the earcanal entrance (zero in the occluded case due to the acoustically rigid occlusion) are referred to as $\hat{q}^k_{TM}$ and $\hat{q}^k_{ent}$ respectively and computed similarly to $\hat{q}_{wall}$. The earcanal wall vibration is not expected to be homogeneous but rather non-uniformly distributed over the earcanal wall surface. This distribution is here characterized by the centroid position $\underline{x}_c$ of the earcanal wall normal velocity in the 3D space such that

$$\underline{x}_c = \frac{\int_{S_{wall}} \underline{x} \left| \hat{v}_{n,wall}(\underline{x}) \right| \mathrm{d}S}{\int_{S_{wall}} \left| \hat{v}_{n,wall}(\underline{x}) \right| \mathrm{d}S}. \tag{2.2}$$

The normal projection of the centroid position $\underline{x}_c$ on the earcanal curvilinear axis z defines the centroid curvilinear position l_c of the earcanal wall normal velocity from the tympanic membrane.

The surface averaged acoustic pressure $\langle \hat{p}^k_{wall} \rangle$ generated by the earcanal wall is governed by the earcanal acoustic impedance $\hat{Z}^k_{EC/wall}$ seen by the earcanal wall and defined by

$$\hat{Z}^k_{EC/wall} = \frac{\langle \hat{p}^k_{wall} \rangle}{\hat{q}_{wall}}. \tag{2.3}$$

The OE is then computed using the surface averaged tympanic membrane acoustic pressure $\langle \hat{p}^k_{TM} \rangle$ such that

$$OE = 20\log_{10}\left(\left|\frac{\langle \hat{p}^{occl}_{TM} \rangle}{\langle \hat{p}^{open}_{TM} \rangle}\right|\right). \tag{2.4}$$

The OE is commonly interpreted in terms of acoustic energy (see Sec. 2.2). The transfer of acoustic energy per unit time in the earcanal cavity is studied here as time-averaged over one period $T = 1/f$ and is referred to as the time-averaged acoustic power. The time-averaged acoustic power flowing through the earcanal wall ($\bar{W}^k_{wall}$), the tympanic membrane ($\bar{W}^k_{TM}$) and the earcanal entrance ($\bar{W}^k_{ent}$, zero in the occluded case due to the acoustically rigid occlusion) is defined by

$$\bar{W}^k_m = \left|\int_{S_m} \underline{\bar{I}}_k \cdot \underline{n}_m \, \mathrm{d}S\right|, \tag{2.5}$$

with $\underline{\bar{I}}_k = \frac{1}{2}\Re\left[\hat{p}_k \times \underline{\hat{v}}^*_k\right]$ the active acoustic intensity vector (Bruneau, 2013), $\hat{p}_k$ the complex acoustic pressure, $\underline{\hat{v}}_k$ the complex acoustic particle velocity vector, $\underline{n}_m$ the inward normal vector and $m \in \{wall, TM, ent\}$. The acoustic power $\bar{W}^k_{diss}$ dissipated by visco-thermal effects in the earcanal cavity is then obtained from the acoustic power balance such as $\bar{W}^k_{diss} = \bar{W}^k_{wall} - \bar{W}^k_{TM} - \bar{W}^k_{ent}$.

2.3.2 Electro-acoustic model of the earcanal

2.3.2.1 Electro-acoustic model

The present EA model illustrated in Fig. 2.3(a) is associated with the 3D FE model from which its inputs are derived (see Sec. 2.3.2.3). The earcanal is considered as a circular cross-sectional duct of length l_{EC} and varying radius $r_{EC}(z)$. The vibration of the earcanal wall is accounted for as an ideal source Q of volume velocity $\hat{q}_{wall}$ concentrated at a distance l_c from the tympanic membrane. The earcanal is schematically divided into two sections: (i) the downstream section defined from the tympanic membrane to the source and (ii) the upstream section defined from the source to the earcanal entrance. In both open (see Fig. 2.3(b)) and occluded (see Fig. 2.3(c)) cases, the model of Shaw & Stinson (1981) is used to define the tympanic membrane

acoustic impedance $\hat{Z}_{TM}$ (see Appx. IV). Furthermore, the downstream section is governed at low frequencies by its compressibility effect of acoustic compliance C_d in parallel with an acoustic resistance $R_{d,th}$ representing thermal losses so that its acoustic impedance is equal to $\hat{Z}_d^{occl} = \left[R_{d,th}^{-1} + j\omega C_d\right]^{-1}$. In the open case, the earcanal upstream section is controlled at low frequencies by its inertia effect represented by an acoustic mass L_u in series with an acoustic resistance $R_{u,vi}$ representing viscous losses so that its acoustic impedance is equal to $\hat{Z}_u^{open} = R_{u,vi} + j\omega L_u$. The earcanal opening is characterized by the acoustic impedance $\hat{Z}_{rad} = R_{rad} + j\omega L_{rad}$ of a baffled circular piston of radius r_{ent}. R_{rad} is the acoustic radiation resistance representing the dissipation in the surrounding environment while L_{rad} is the acoustic radiation mass representing the inertia effect of the surrounding environment. In the occluded case, the acoustic impedance $\hat{Z}_u^{occl} = \left[R_{u,th}^{-1} + j\omega C_u\right]^{-1}$ of the earcanal upstream section is governed at low frequencies by its compressibility effect similarly to $\hat{Z}_d^{occl}$. Table 2.1 summarizes the calculation of aforementioned acoustic masses, compliances and resistances (Bruneau, 2013).

Table 2.1 Calculation of the EA model localized constants (C_u and $R_{u,th}$ are computed similarly to C_d and $R_{d,th}$ respectively, replacing the interval $[0,\ l_c]$ by $[l_c,\ l_{EC}]$)

$C_d = \int_0^{l_c} \frac{\pi r_{EC}^2}{\rho_0 c_0^2} \mathrm{d}z$	$R_{d,th} = \left[\int_0^{l_c} (\gamma - 1)\frac{\pi r_{EC}}{\rho_0 c_0^2}\sqrt{\frac{2\lambda\omega}{\rho_0 C_p}} \mathrm{d}z\right]^{-1}$
$L_u = \int_{l_c}^{l_{EC}} \frac{\rho_0}{\pi r_{EC}^2} \mathrm{d}z$	$R_{u,vi} = \int_{l_c}^{l_{EC}} \frac{\sqrt{2\rho_0\omega\mu}}{\pi r_{EC}^3} \mathrm{d}z$
$L_{rad} = \frac{8\rho_0}{3\pi^2 r_{ent}}$	$R_{rad} = \frac{\omega^2 \rho_0}{2\pi c_0}$

2.3.2.2 Computation of vibro-acoustic indicators

The EA model is used to provide explicit expression of some vibro-acoustic indicators computed using the FE model. The acoustic impedance $\hat{Z}_{EC/Q}^k$ of the earcanal seen by the source Q is computed as the downstream and upstream sections in parallel (see Fig. 2.3(b) and (c)). The acoustic impedance of the earcanal downstream section is defined in both open and occluded

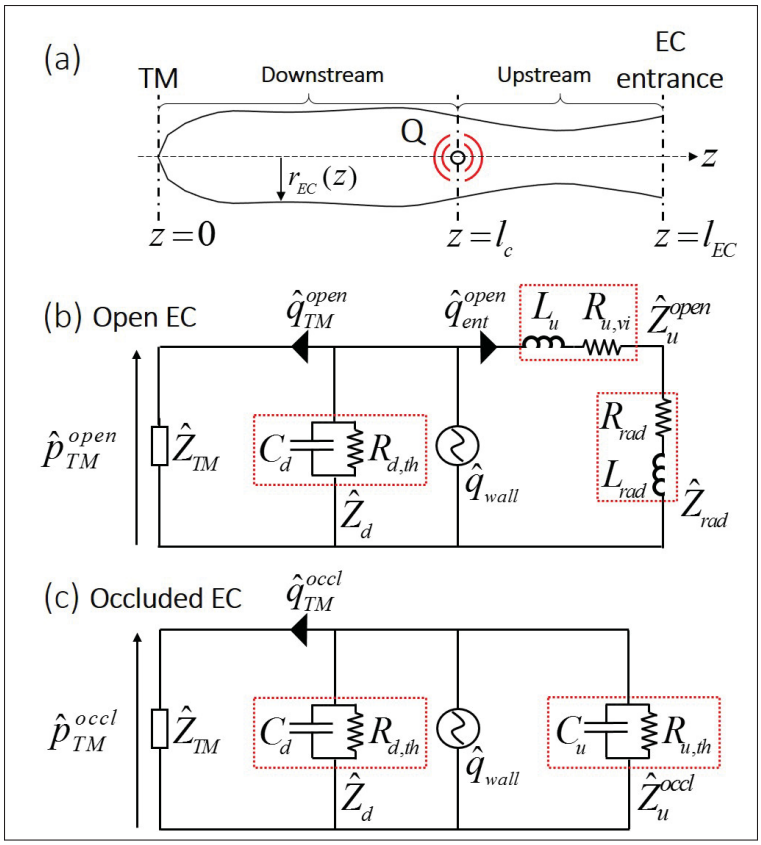

Figure 2.3 (a) earcanal geometry of the EA model (b) open and (c) occluded by an infinite impedance defined at the earcanal entrance

cases by $\hat{Z}_{EC/Q,d} = \left[\hat{Z}_d^{-1} + \hat{Z}_{TM}^{-1}\right]^{-1}$. The earcanal upstream section acoustic impedance is given in the open case by $\hat{Z}_{EC/Q,u}^{open} = \hat{Z}_u^{open} + \hat{Z}_{rad}$ and in the occluded case by $\hat{Z}_{EC/Q,u}^{occl} = \hat{Z}_u^{occl}$. In the low-frequency range of interest (*i.e.*, 100 Hz to 1 kHz), $\hat{Z}_d$ is dominated by C_d, $\hat{Z}_u^{open}$ by L_u, $\hat{Z}_{rad}$ by L_{rad} and $\hat{Z}_u^{occl}$ by C_u (not shown here for the sake of conciseness). In addition, below approximately 500 Hz, the tympanic membrane acoustic impedance is dominated by the compliance C_{TM} of the tympanic cavity volume (approximately 0.78 cm^3) (Stepp & Voss, 2005; Zurbrügg *et al.*, 2014). Therefore, the earcanal acoustic impedance can be approximated at low frequencies (see Sec. 2.4.3) in the open case to

$$\hat{Z}_{EC/Q}^{open} \approx j\omega \left(L_{rad} + L_u\right), \tag{2.6}$$

and in the occluded case to

$$\hat{Z}_{EC/Q}^{occl} \approx [j\omega(C_u + C_d + C_{TM})]^{-1}. \tag{2.7}$$

The tympanic membrane acoustic pressure $\hat{p}_{TM}^{k}$ is equal to that generated by the source (see Fig. 2.3(b) and (c)) so that

$$\hat{p}_{TM}^{k} = \hat{Z}_{EC/Q}^{k} \times \hat{q}_{wall}. \tag{2.8}$$

Substituting Eq. (2.8) in Eq. (2.4), the OE is written as

$$OE = 20\log_{10}\left(\left|\frac{\hat{Z}_{EC/Q}^{occl}}{\hat{Z}_{EC/Q}^{open}}\right|\right). \tag{2.9}$$

At low frequencies, substituting Eqs. (2.6) and (2.7) in Eq. (2.9), the OE can be approximated (see Sec. 2.4.6) to

$$OE \approx 20\log_{10}\left(\left[\omega^2 \times (L_{rad} + L_u) \times (C_u + C_d + C_{TM})\right]^{-1}\right). \tag{2.10}$$

The equivalent of the acoustic power $\bar{W}_{wall}^{k}$ passing through the earcanal wall in the FE model is the acoustic power flowing from the source Q to the earcanal defined in the EA model by

$$\bar{W}_{Q}^{k} = \frac{1}{2}\Re[\hat{Z}_{EC/Q}^{k}] \times |\hat{q}_{wall}|^2. \tag{2.11}$$

The earcanal cavity acoustic resistance $\Re[\hat{Z}_{EC/Q}^{k}]$ represents the capability of the earcanal cavity (including the entrance and the tympanic membrane) to dissipate/transmit acoustic energy. Equations (2.6) and (2.7) thus cannot be used in Eq. (2.11) since they neglect acoustic resistances.

2.3.2.3 Inputs from the finite element model

In the EA model, the earcanal has the same radius function (*i.e.*, l_{EC}, $r_{EC}(z)$ and $r_{ent} = r_{EC}(l_{EC})$) as in the 3D FE model (see Table 2.1). The ideal volume velocity source Q is assumed to be concentrated at the curvilinear position l_c of the earcanal wall normal velocity centroid

computed using the FE model (see Sec. 2.3.1.4). This assumption has been proposed by the authors (Carillo, Doutres & Sgard, 2019) and is evaluated in Sec. 2.4.6 for several earcanal wall vibration patterns induced by various mechanical loading and boundary conditions imposed to the FE model (see Appx. III). Using the set of loading and boundary conditions described in Sec. 2.3.1.2, the position l_c computed using the FE model does not significantly vary at low frequencies (see Sec. 2.4.1). The value of l_c at 100 Hz is thus used in the EA model for the whole frequency range. The volume velocity $\hat{q}_{wall}$ is computed using the FE model (see Sec. 2.3.1.4).

2.4 Results and discussions

2.4.1 Earcanal wall velocity

The normal component of the earcanal wall velocity is of great interest since it is transferred to "acoustic particles" in its vicinity. The curvilinear centroid position l_c and the amplitude of the earcanal wall normal velocity computed at 100 Hz using the FE model are illustrated in Fig. 2.4(a). The centroid position characterizes the distribution of normal velocity over the earcanal wall (see Sec. 2.3.1.4). This distribution is here concentrated at 100 Hz at a curvilinear distance $l_c = 23.6$ mm from the tympanic membrane (see Fig. 2.4(a), left side) which corresponds to the earcanal cartilaginous part. The location of l_c varies by less than 1 mm as frequency increases from 100 Hz to 1 kHz. Thus, Fig. 2.4(a) (right side) is representative of the FE model earcanal wall vibration pattern up to 1 kHz. As mentioned in Sec. 2.3.1.2, this vibration pattern depends on the set of loading and boundary conditions applied to the FE model and has been chosen in order to exhibit a vibration pattern in qualitative agreement with experimental findings (Stenfelt *et al.*, 2003; Stenfelt & Reinfeldt, 2007). The chosen set is a simplification imposed by the truncated nature of the current model. In particular, the uniform normal velocity field applied on the circumferential boundary of soft and skin tissues is likely to be non-uniform in amplitude, phase and direction. The lack of quantitative experimental data does not make it possible yet to precisely compare the FE model vibration distribution to that induced by a bone transducer in an in-vivo earcanal. However, by applying various sets of

loading and boundary conditions (see Appx. III), the current model is useful to highlight how the earcanal wall vibration distribution could influence the OE (see Sec. 2.4.6).

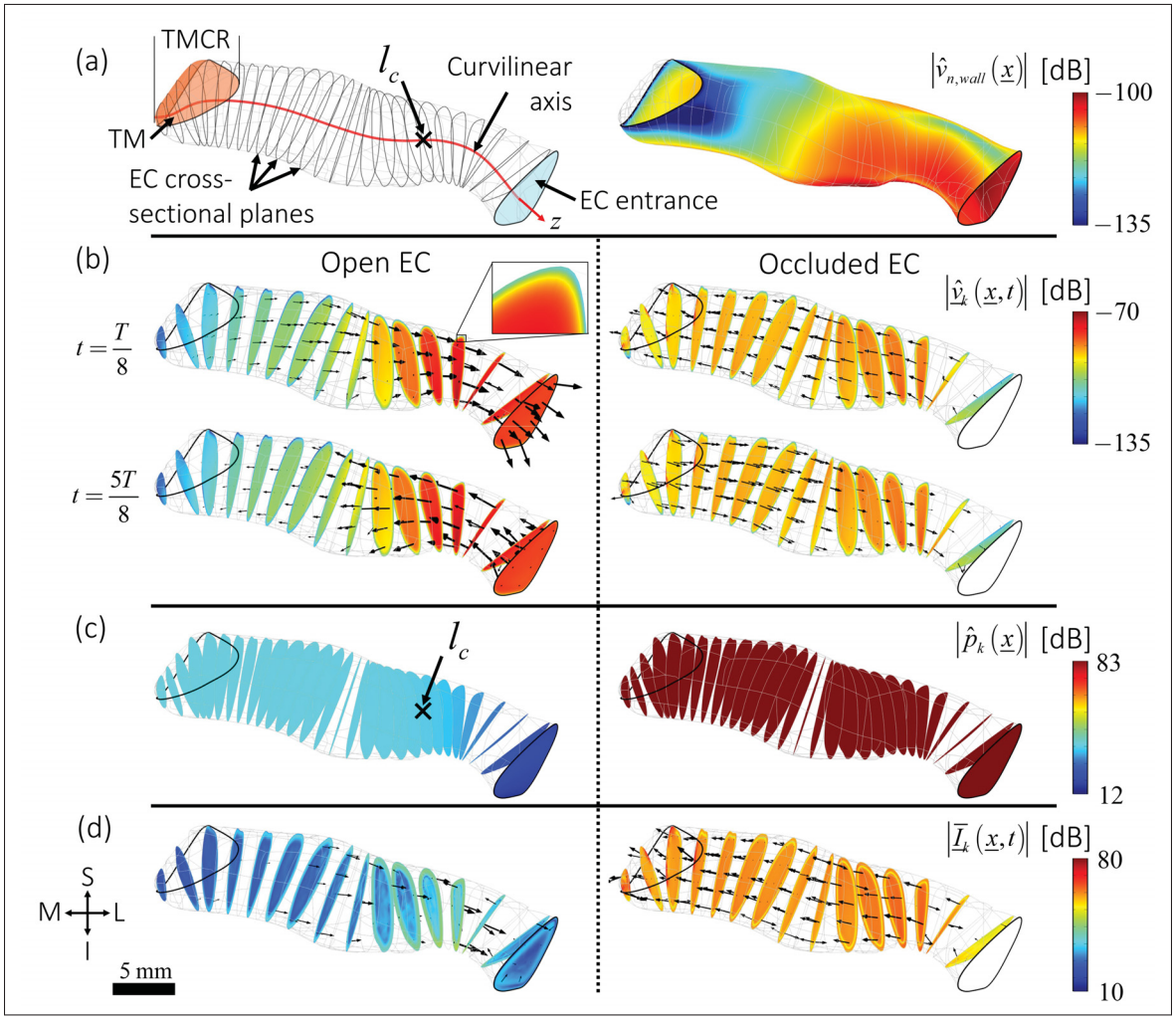

Figure 2.4 (a) earcanal wall normal velocity centroid position l_c (left) and amplitude $\left|\hat{v}_{n,wall}(\underline{x})\right|$ (right) in dB (factor 20, ref. 1 m s^{-1}), (b) instantaneous acoustic particle velocity vectors $\underline{v}_k(\underline{x}, t)$ (black arrows) and amplitude $\left|\underline{v}_k(\underline{x}, t)\right|$ in dB (colormaps), (c) acoustic pressure level in dB (factor 20, ref. 2×10^{-5} Pa) and (d) active acoustic intensity vectors $\overline{\underline{I}}_k(\underline{x})$ (black arrows) and amplitude $\left|\overline{\underline{I}}_k(\underline{x}|\right)$ (colormaps) in dB (factor 10, ref. 10^{-12} W m^{-2}) computed at 100 Hz using the coupled elasto-acoustic (visco-thermal) FE model. The white earcanal entrance surface in (b) and (d) corresponds to zero value

2.4.2 Acoustic particle velocity and volume velocity transfer in the earcanal cavity

The transfer of the earcanal wall velocity in the earcanal cavity is illustrated in Fig. 2.4(b) which displays the instantaneous (at $t \in \{T/8,\, 5T/8\}$) acoustic particle velocity vectors and amplitude computed in both open and occluded cases at 100 Hz using the FE model. The Eulerian specification of the acoustic field is used here. This means that vector fields represent the velocity of "acoustic particles" passing through a position $\underline{x}$ at a time t. At $t = T/8$, the acoustic particle velocity is mainly oriented towards the earcanal entrance in the open case (left side) and towards the tympanic membrane in the occluded case (right side) due to the compression motion of the earcanal wall. In the half-period that follows (at $t = 5T/8$), the acoustic particle velocity behaves in the exact opposite direction since $h(\underline{x},\, t + T/2) = -h(\underline{x},\, t)$ in harmonic regime (see Eq. (2.1)). In the open case, the amplitude of the acoustic particle velocity is maximum in the constriction part of the current earcanal close to the opening and minimum in the eardrum coupling region. The gradient of acoustic particle velocity tangential to the earcanal wall is thus maximum in the region of this constriction. In the occluded case, the acoustic particle velocity amplitude is rather homogeneous except at the earcanal entrance where it is zero due to the acoustically rigid occlusion considered here. Note that a real occlusion device would impose a non-zero volume velocity to the occluded earcanal cavity.

The transfer of acoustic particle velocity in the earcanal cavity is now investigated by computing the volume velocity passing through the earcanal entrance and tympanic membrane surfaces using both FE and EA models in Fig. 2.5. Results computed by both models are in good agreement. In the open case, the volume velocity passing through the earcanal entrance is 16 to 52 dB higher than that passing through the tympanic membrane. The volume velocity passing through the earcanal opening is almost equal to that imposed by the earcanal wall (not shown here). This corroborates the observation made in Fig. 2.4(b) for the open case (left side). In the occluded case, the volume velocity passing through the tympanic membrane is 6 to 45 dB larger than in the open case: the occlusion drastically increases the volume velocity transferred between the earcanal wall and the tympanic membrane. This volume velocity is however approximately

7 dB lower than that passing through the open earcanal entrance due to the local volume changes that result from the compression of the air within the occluded earcanal.

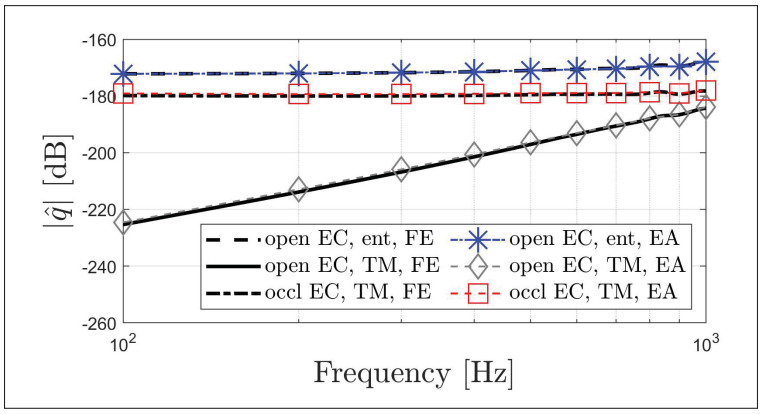

Figure 2.5 Level in dB (factor 20, ref. 1 $m^3\ s^{-1}$) of the volume velocity passing through the earcanal entrance (zero in the occluded case) and the tympanic membrane computed using both FE and EA models

2.4.3 Acoustic impedance of the earcanal cavity

The earcanal cavity acoustic impedance governs the acoustic pressure generated in reaction to the vibration of the earcanal wall. Based on EA analogy, the earcanal cavity acoustic impedance represents the "opposition" of the earcanal cavity to the transfer of the volume velocity imposed by its wall. This "opposition" is manifested in terms of acoustic pressure. Figure 2.6(a) displays the level in dB of the earcanal cavity acoustic impedance in open and occluded earcanal computed using both FE and EA models. The occlusion is seen to drastically increase (by 8 to 47 dB) the earcanal cavity acoustic impedance (Hansen, 1998; Zurbrügg *et al.*, 2014). It should be noted that the earcanal cavity acoustic impedance computed using FE and EA models are not strictly equal. Indeed, the former uses the surface averaged earcanal wall acoustic pressure (see Eq. (2.3)) while the latter rather considers the acoustic pressure at the position l_c of the volume velocity source Q (see Sec. 2.3.2.2). This has no influence in the occluded case since the acoustic pressure is homogenous at low frequencies but explains the difference of approximately

2 dB in the open case between FE and EA simulations (see Fig. 2.6(a)) due to the open earcanal acoustic pressure gradient (see Fig. 2.4(c), left side, and Sec. 2.4.4).

According to Fig. 2.6(a), the level of the earcanal cavity acoustic impedance increases with frequency by approximately +20 dB/decade in the open case while it decreases with frequency by approximately -20 dB/decade in the occluded case (Zurbrügg *et al.*, 2014). From Eq. (2.6), the EA model indicates that, at low frequencies, the open earcanal cavity acoustic impedance is approximately mass-controlled (L_u + L_{rad}) which is proportional to ω (+20 dB/decade). This means that the air in the open earcanal upstream section is being mainly accelerated at low frequencies. The acoustic mass L_u of the open earcanal upstream section depends on the location of the source Q which is assumed equal to the curvilinear position l_c of the earcanal wall normal velocity centroid computed using the FE model. The evaluation of this assumption as well as the influence of the distribution of the earcanal wall vibration on the OE is presented in Sec. 2.4.6. From Eq. (2.7), the EA model indicates that, at low frequencies, the occluded earcanal cavity acoustic impedance is approximately governed by its whole acoustic compliance which is proportional to ω^{-1} (-20 dB/decade). This means that the air in the occluded earcanal is being mainly compressed at low frequencies. According to Fig. 2.6(a), neglecting the influence of the downstream section, including the tympanic membrane, in the open case (dash-dotted purple curve with crosses) or simplifying the tympanic membrane to an equivalent compliance C_{TM} in the occluded case (dashed blue curve with stars) leads to an underestimation of 2 to 4 dB at 1 kHz.

The EA model is now used to provide simple interpretations of the volume velocity transfer in the earcanal cavity (see Sec. 2.4.2). The source Q representing the earcanal wall schematically divides the earcanal cavity into the upstream and downstream sections towards the earcanal entrance and the tympanic membrane respectively (see Fig. 2.3(a)). Acoustic impedance levels of these sections are displayed in Fig. 2.6(b). In the open case, the earcanal upstream section has an impedance 11 to 47 dB lower than the downstream section which is almost seen as infinite. The volume velocity is transferred through the “path” of least “opposition” thus between the earcanal wall and the opening. The mass-controlled open earcanal upstream section acts as

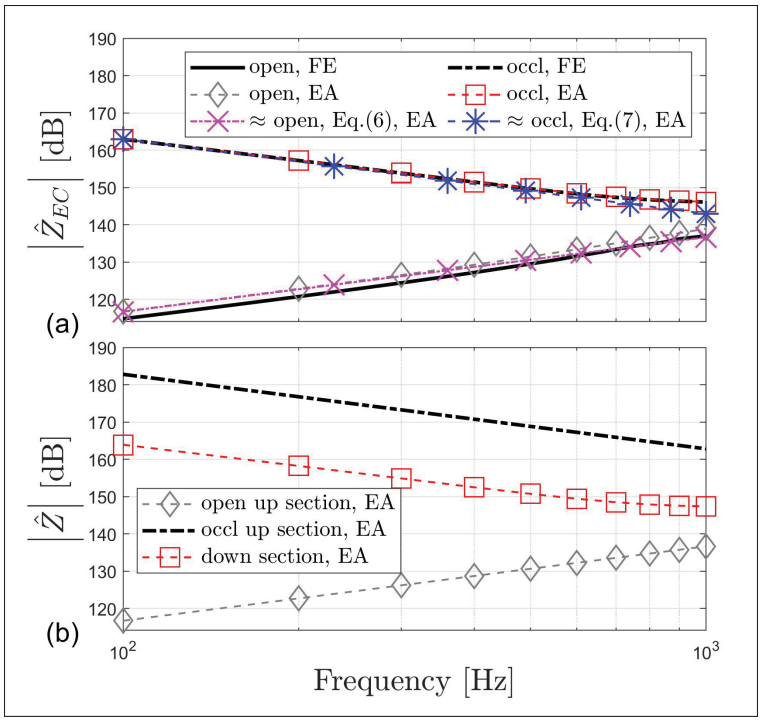

Figure 2.6 Acoustic impedance levels in dB (factor 20, ref. 1 N s m^{-5}) of (a) the earcanal cavity seen by its wall (FE model) or the source Q (EA model) and of (b) the upstream and downstream earcanal sections seen by the source Q (EA model) in both open and occluded cases

a shunt (Tonndorf *et al.*, 1966) for the volume velocity imposed by the earcanal wall. In the occluded case, the earcanal upstream section has an impedance rather 15 to 19 dB higher than the downstream section due to the acoustically rigid occlusion. The volume velocity is thus mainly transferred between the earcanal wall and the tympanic membrane.

2.4.4 Acoustic pressure in the earcanal cavity

The level in dB of the acoustic pressure generated by the earcanal wall in both open and occluded cases computed at 100 Hz using the FE model is illustrated in Fig. 2.4(c). In the open case (left side), an acoustic pressure gradient is observed between the earcanal opening and approximately the curvilinear position l_c of the earcanal wall normal velocity centroid while the acoustic

pressure level is then almost homogeneous up to the tympanic membrane. According to the EA model, the acoustic pressure level gradient is explained by the acoustic mass L_u of the earcanal upstream section while the acoustic compliance of the earcanal downstream section is responsible for the acoustic pressure level homogeneity. The distribution of the earcanal wall vibration as well as the earcanal shape thus govern the acoustic pressure field induced by bone-conducted stimulation in the open earcanal. To the authors' knowledge, the acoustic pressure distribution in the open earcanal has only been studied for acoustic excitations from the surrounding environment (Stinson & Daigle, 2005; Hudde & Schmidt, 2009) or for a reverse mechanical stimulation of the tympanic membrane from the ossicles (Ravicz, Cheng & Rosowski, 2019). In the occluded earcanal, the acoustic pressure level is homogeneous at low frequencies (see Fig. 2.4(c), right side) since it is controlled by its acoustic compliance. In addition, the acoustic pressure level is higher in the occluded earcanal compared to the open earcanal. This observation is corroborated by Fig. 2.7 which displays the tympanic membrane acoustic pressure level computed in both open and occluded cases using FE and EA models. In both cases, the slope of the tympanic membrane acoustic pressure level is the conjunction of the earcanal cavity acoustic impedance level and of the volume velocity level imposed by the earcanal wall. Since the occlusion increases the earcanal cavity acoustic impedance (see Sec. 2.4.3), the acoustic pressure generated by the earcanal wall is also increased (Hansen, 1998; Stenfelt & Reinfeldt, 2007; Zurbrügg *et al.*, 2014). The tympanic membrane acoustic pressure is the force per unit surface responsible for the motion of the tympanic membrane. The increase of acoustic pressure at low frequencies leads to the increase of volume velocity at the tympanic membrane in the occluded case (see Fig. 2.5).

2.4.5 Acoustic intensity and power flow in the earcanal cavity

The propagation of acoustic waves in the earcanal is associated with an acoustic power flow. Figure 2.8 displays the level in dB of the acoustic power injected into the earcanal cavity by its wall, computed in open and occluded cases using both FE (low reduced frequency) and EA models. Note that the FE (low reduced frequency) model compares well to the visco-thermal

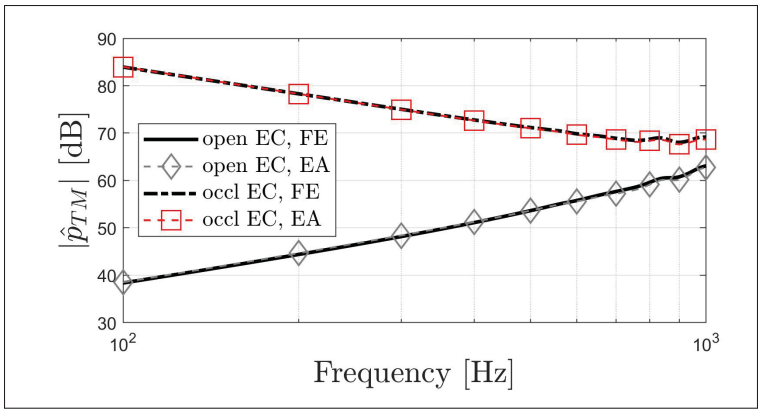

Figure 2.7 Level in dB (factor 20, ref. 2×10^{-5} Pa) of tympanic membrane acoustic pressure computed in open and occluded cases using both FE and EA models

model computed at 100 Hz, 500 Hz and 1 kHz, except that it underestimates by approximately 1 dB the acoustic power dissipated by visco-thermal effects in the open earcanal cavity. According to Fig. 2.8, the acoustic power injected by the earcanal wall is significantly higher in the occluded case compared to the open one (Brummund *et al.*, 2014). For a given volume velocity imposed to the earcanal cavity, Eq. (2.11) of the EA model explicitly indicates that the injected acoustic power is governed by the acoustic resistance of the earcanal cavity seen by the source Q representing the earcanal wall. Using the current FE model, an expression similar to Eq. (2.11) has been proposed by Brummund *et al.* (2014) but is only equivalent to Eq. (2.5) if at least the acoustic pressure field or the earcanal wall normal velocity field is homogeneous over the earcanal wall surface. The first condition is only valid in the occluded case at low frequencies (see Sec. 2.4.4) while the second condition cannot be expected in any case (see Sec. 2.4.1). In the open case, the acoustic pressure gradient thus explains the difference (<2 dB) seen in Fig. 2.8 between FE and EA simulations while results in the occluded case are in good agreement. Brummund *et al.* have shown that the earcanal cavity acoustic resistance drastically increases due to the occlusion (Brummund *et al.*, 2014) but have not accounted for visco-thermal dissipation in the earcanal cavity. The increase of the earcanal cavity acoustic resistance due to the occlusion is also found in this work (not shown here). This is coherent with the increase of the acoustic power

injected to the occluded earcanal cavity (see Fig. 2.8). However, neglecting the visco-thermal dissipation underestimates the open earcanal cavity acoustic resistance by approximately 42 dB at 100 Hz (and approximately 1 dB at 1 kHz) which consequently underestimates the acoustic power injected in the open earcanal by approximately 21 dB at 100 Hz (and approximately 0.5 dB at 1 kHz).

In the occluded case, neglecting the visco-thermal losses slightly underestimates the occluded earcanal acoustic resistance (<1.5 dB) and the acoustic power injected (<1 dB) because the dissipation at the tympanic membrane dominates (see Appx. VII). Accounting for visco-thermal losses in the earcanal cavity is thus necessary to study the acoustic power flow illustrated in Fig. 2.4(d) and to accurately compute the acoustic power balance, in particular in the open case (Keefe *et al.*, 1994), detailed in Appx. VII. However, visco-thermal losses do not significantly influence the acoustic pressure nor the volume velocity transfer in the earcanal cavity at low frequencies. Indeed, as shown in Sec. 2.4.3 using the EA model, the vibro-acoustic behavior of the earcanal cavity can be well approximated at low frequencies using acoustic reactances only. The use of the acoustic power balance approach to analyze and interpret the OE (Brummund *et al.*, 2014) is thus debatable (see Sec. 2.5). The increase of acoustic power dissipated at the tympanic membrane due to the occlusion (Brummund *et al.*, 2014) (not shown here) is simply explained by the increased volume velocity transferred through the tympanic membrane (see Sec. 2.4.2).

2.4.6 Occlusion effect

Figure 2.9 displays the OE computed using both FE (solid black curve) and EA (dashed gray curve with diamonds) models. The OE begins at approximately 45 dB at 100 Hz and decreases with frequency by approximately -40 dB/decade. Similar slopes are observed with other models at low frequencies (Hansen, 1998; Stenfelt & Reinfeldt, 2007; Brummund *et al.*, 2015; Sgard *et al.*, 2019) while the amplitude obtained here corresponds to an extreme case of shallow insertion due to the occlusion at the earcanal entrance (Berger, 2003; Stenfelt & Reinfeldt, 2007). Experimentally, at frequencies less than approximately 300 Hz, the OE is often less than that

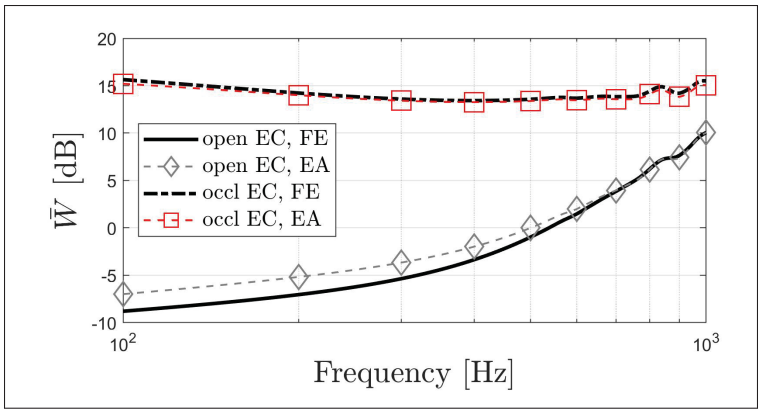

Figure 2.8 Level in dB (factor 10, ref. 10^{-12} W) of the time-averaged acoustic power injected per unit time into the earcanal cavity by its wall (FE model) and the source Q (EA model) computed in open and occluded cases

predicted by Fig. 2.9, possibly due to an incomplete seal between the occlusion device and the earcanal wall (Hansen, 1998; Brummund *et al.*, 2014).

Figure 2.9 also displays the low-frequency approximation of the OE (dashed red curve with squares) computed from Eq. (2.10) of the EA model. From Eq. (2.10), the slope of -40 dB/decade of the OE is completely described by the dependence on ω^{-2}. This dependence is explained by the change in the character of the impedance between the mass-controlled ($L_{rad} + L_u$) open earcanal state and the compliance-controlled ($C_u + C_d + C_{TM}$) occluded earcanal state. As shown in Fig. 2.6(a), neglecting the influence of the earcanal downstream section, including the tympanic membrane, in the open case or simplifying the tympanic membrane to an equivalent compliance C_{TM} in the occluded case, leads to inaccuracies in the computation of the earcanal cavity acoustic impedance as the frequency increases. In the OE computed using Eq. (2.10), these inaccuracies approximately compensate.

In the EA model, the acoustic mass L_u of the open earcanal depends on the position of the volume velocity source Q. This position is generally assumed or adjusted based on sound pressure measurements in the earcanal cavity. In this work, the source is presumed to be concentrated at the curvilinear position l_c (defined from the tympanic membrane) of the earcanal wall normal

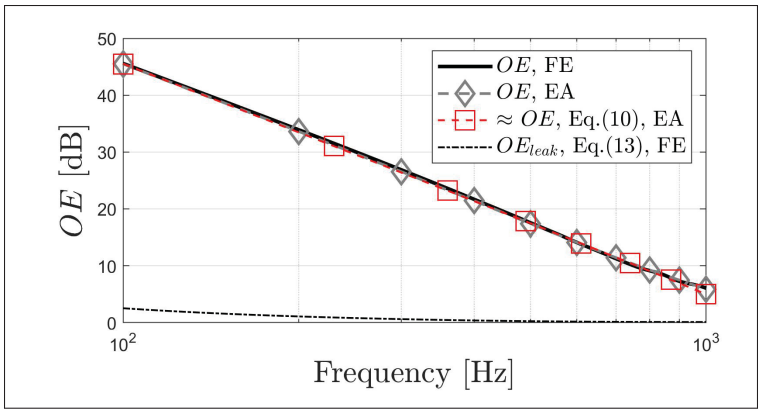

Figure 2.9 OE computed using FE and EA models. OE_{leak} refers to a hypothetical OE detailed in Sec. 2.5

velocity computed using the FE model. This assumption and the influence of the earcanal wall vibration distribution on the OE are now evaluated. OE induced by a volume velocity source while the source position l_c varies from the eardrum coupling region to the earcanal entrance (following the earcanal curvilinear axis) in both FE (earcanal cavity only) and EA models are computed at 100 Hz and displayed in Fig. 2.10. The OE increases with the curvilinear position l_c because the acoustic mass L_u of the open earcanal decreases "proportionally" (depending on the earcanal shape). The whole acoustic compliance ($C_u + C_d + C_{TM}$) of the occluded earcanal remains constant when l_c varies. EA simulation is in good agreement with FE one because both models share the same earcanal shape. Indeed, note that using a uniform earcanal cylindrical duct of same volume and earcanal wall surface leads to significant discrepancies (up to approximately 6 dB in the constriction region, not shown here). Figure 2.10 also displays the OE computed at 100 Hz using the coupled FE model for several earcanal wall vibration distributions induced by various sets of loading and boundary conditions presented in Appx. III and characterized by the curvilinear centroid position l_c. Results show an accurate correspondence between the OE induced by various earcanal wall vibration distributions characterized by their centroid position l_c (red crosses) and by an equivalent volume velocity source located at the same position l_c. Differences of approximately 0.5 and 1 dB are respectively observed around 17 and 29 mm

possibly due to an influence of the shape of the earcanal wall vibration distribution which is only characterized here in a simplified way by the centroid position.

According to Fig. 2.10, the influence of the earcanal wall vibration distribution on the OE is mainly observed in the earcanal cartilaginous part close to the earcanal entrance where the OE increases by approximately 20 dB from 20 to 35 mm. This distribution would be expected to vary with different stimulus types and locations. Such variation might explain the variation in OE with stimulator position (Reinfeldt *et al.*, 2013) and could also contribute to the OE inter-individual difference (Stenfelt & Reinfeldt, 2007). Furthermore, this distribution could be frequency-dependent possibly due to earcanal structural modes which are not observed using the current truncated FE model (see Sec. 2.4.1) but could appear in an entire head model. Such dependence might explain that experimental OE does not precisely follow the decrease with frequency by approximately -40 dB/decade since L_u would be frequency-dependent in Eq. (2.10).

Finally, it should be emphasized that the earcanal wall vibration distribution only influences the open earcanal here. However, this distribution is also expected to influence the vibro-acoustic behavior of the earcanal occluded by a real physical occlusion device rather than the current infinite impedance. In the authors' opinion, the decrease of the OE with the insertion depth is underestimated by the FE model of Brummund *et al.* (2014) (approximately 7 dB lower from 7 to 22 mm at 100 Hz) compared to measurement data (Stenfelt & Reinfeldt, 2007) (median values approximately 15 dB lower from 7 to 22 mm around 160 Hz) because the contribution of the earcanal bony part on the acoustic pressure generated in the earcanal cavity is overestimated since the earcanal wall vibration distribution is concentrated at the mid-length of the earcanal cavity (see Appx. III) rather than in the cartilaginous part.

2.5 Interpretations of the occlusion effect

As mentioned in Sec. 2.2, the OE is commonly interpreted as follows: the "sound pressure, vibration, energy or wave" is presumed to "leak" through the earcanal opening and to be "trapped"

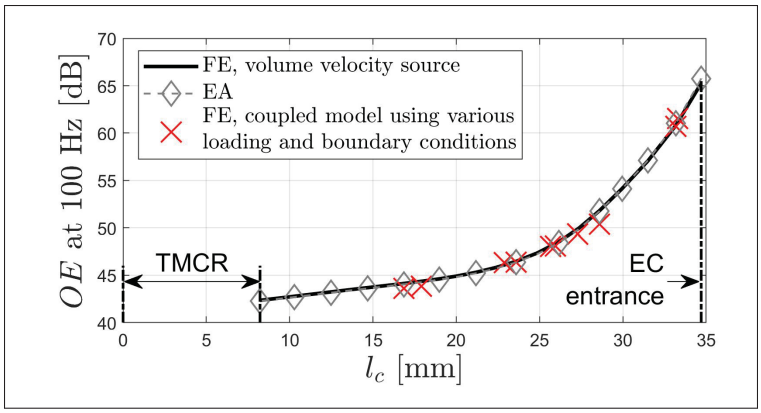

Figure 2.10 OE computed at 100 Hz as a function of the curvilinear position l_c of the volume velocity source (FE with the earcanal cavity only and EA models) and of the earcanal wall normal velocity centroid position (coupled FE model using various loading and boundary conditions summarized in Appx. III)

in the occluded earcanal. A common definition of the verb "leak" states that something (matter or energy) comes out of a container through a hole, *i.e.*, the leak (Macmillan-Dictionary, 2020). These interpretations are now discussed.

The earcanal wall acts as an ideal source of volume velocity (see Sec. 2.4.1). This volume velocity is mainly transferred between the earcanal wall and the earcanal entrance in the open case or between the earcanal wall and the tympanic membrane in the occluded one (see Sec. 2.4.2). In harmonic regime, the volume velocity is transferred back and forth and alternatively changes sign. The volume velocity cannot literally "leak" (even through the earcanal opening) since it comes in and out. Qualifying the volume velocity transfer between the wall and the entrance as a "leak" and that between the wall and the tympanic membrane as a "trap" may provide a "mental image" (Stenfelt & Reinfeldt, 2007) of these transfers. However, in the authors' opinion, the terms "leak" and "trap" do not accurately represent the physics. In both open and occluded cases, the volume velocity is mainly transferred through the "path" of least "opposition" (see Sec. 2.4.3). The term "opposition" is here preferred instead of "resistance" (Staab *et al.*, 2004) because the latter rather refers to the real part of the acoustic impedance.

The acoustic impedance of the earcanal cavity represents its "opposition" to the volume velocity transfer and governs its reaction in terms of acoustic pressure. The acoustic pressure does not "leak" nor is it "trapped." It simply increases because the "opposition" increases due to the occlusion (see Sec. 2.4.4).

From a vibro-acoustic point of view, acoustic pressure and acoustic particle velocity are physical variables that describe at every position and anytime, the continuum acoustic field made of "acoustic particles" which oscillate around their rest position (see Sec. 2.4.2). In this way, only acoustic waves travel and could literally "leak." A "leak" could be interpreted as acoustic waves not being or being little reflected while a "trap" would mean a high or perfect reflection. Assuming acoustic plane wave propagation in the earcanal cavity at low frequencies, the normal incidence pressure reflection coefficient $\hat{R}_i^k$ is defined (Bruneau, 2013) by

$$\hat{R}_i^k = \frac{\hat{Z}_i^k - \rho_0 c_0 / S_i}{\hat{Z}_i^k + \rho_0 c_0 / S_i}, \tag{2.12}$$

with $\hat{Z}_i^k$, where $i \in \{ent, TM\}$, the acoustic impedance of the earcanal entrance or the tympanic membrane seen from the earcanal cavity and $\rho_0 c_0$ the characteristic impedance of the air. Figure 2.11 displays $\hat{R}_i^k$ in (a) modulus and (b) phase. In the low-frequency regime, the modulus of the earcanal opening reflection coefficient is close to the acoustically rigid occluded earcanal entrance and higher than the tympanic membrane. The earcanal opening is thus rather a "trap" than a "leak" for acoustic waves at low frequencies which are almost entirely reflected due to the impedance mismatch between the open earcanal cavity and the surrounding environment just like in the occluded case due to the acoustically rigid termination. However, the change of phase between open and occluded cases (see Fig. 2.11(b)) influences the way how acoustic waves are reflected at the earcanal entrance and thus governs the multiple acoustic wave reflections pattern inside the earcanal cavity. At low frequencies, the occlusion does not "trap" acoustic waves since they are already mainly "trapped" in the open earcanal cavity but rather influences the way how acoustic waves are "trapped."

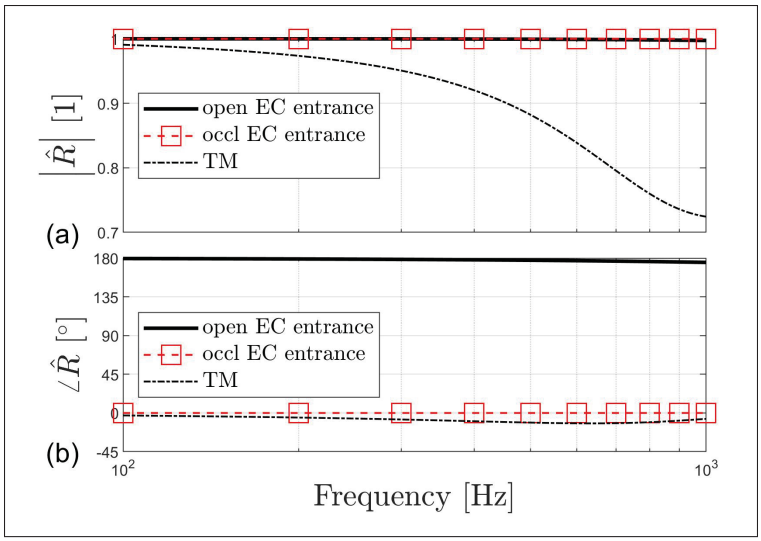

Figure 2.11 Reflection coefficient of the earcanal entrance (open and occluded) and the tympanic membrane in (a) modulus and (b) phase

However, the reflection coefficient of the earcanal entrance is not exactly equal to unity in the open case. In harmonic regime, a fraction of time-averaged injected acoustic power is radiated through the earcanal opening in the surrounding environment (see Sec. 2.4.5). In the case of a rigid occlusion, no acoustic power is radiated through the earcanal entrance. The question then arises: does the reduction, from $\bar{W}_{ent}^{open}$ to 0, of the acoustic power radiated at the earcanal entrance (*i.e.*, the seal of the acoustic power "leak") could explain the OE ? To answer this question, the following hypothetical situation is considered: the occlusion only implies that the acoustic power radiated at the open earcanal entrance is now dissipated at the tympanic membrane assuming an equal injected acoustic power in both open and occluded configurations. The resulting OE is denoted OE_{leak}. At low frequencies, the OE can be expressed in terms of acoustic power dissipated at the tympanic membrane because the acoustic pressure field is homogeneous over the tympanic membrane surface (see Appx. VIII). Based on the open earcanal cavity acoustic power balance, OE_{leak} is defined by (see Appx. VIII)

$$OE_{leak} = 10\log_{10}\left(1 + \bar{W}_{ent}^{open} \big/ \bar{W}_{TM}^{open}\right). \tag{2.13}$$

According to Fig. 2.9, OE_{leak} (dash-dotted curve) is negligible which means that the reduction of the acoustic power radiated at the earcanal entrance cannot cause the OE, as suggested by Brummund *et al.* (2014). Indeed, the acoustic power radiated at the earcanal opening is significantly lower than the increase of acoustic power dissipated at the tympanic membrane due to the occlusion because the earcanal wall is not an ideal source of acoustic power (see Sec. 2.4.5). An interpretation in terms of acoustic power "leak" could be better adapted in the case of constant input acoustic power in open and occluded cases (*e.g.*, insertion loss induced by an earplug for an external acoustic excitation). Moreover, the OE is well explained without accounting for acoustic losses at low frequencies (see Sec. 2.4.6). Interpreting the OE in terms of acoustic power thus departs from its fundamental mechanism.

In the authors' opinion, the aforementioned common interpretations of the OE misrepresent the underlying physical phenomena. Since the role of the earcanal cavity acoustic impedance is useful to explain the fundamental mechanism of the OE (Hansen, 1998; Stenfelt & Reinfeldt, 2007; Zurbrügg *et al.*, 2014), an interpretation based on this concept is found more accurate. For example, the occlusion increases the "opposition" of the earcanal cavity to the volume velocity imposed by its wall and increases the amplitude of the acoustic pressure that is generated in reaction, leading to the OE. In the case of hearing aids, the open-fitting decreases this "opposition" and thus the OE. In the case of earplug, an incomplete seal has a similar effect at frequencies lower than the Helmholtz resonance formed by the system: the neck of the resonator corresponding to the incomplete seal at the earplug/earcanal wall interface and the resonator cavity being the partially occluded earcanal (Hansen, 1998; Brummund, 2014; Sgard *et al.*, 2019). In the general case, the deep-fitting reduces the OE because the volume velocity imposed by the earcanal wall to the occluded earcanal cavity decreases since the surface as well as the vibration amplitude of the remaining earcanal wall diminish with the insertion depth (Zurbrügg *et al.*, 2014).

2.6 Conclusion

The physics of the OE has been thoroughly revisited at low frequencies using a 3D FE model of an outer ear in conjunction with an associated EA model. This study has analyzed and illustrated the earcanal wall vibration, the transfer of volume velocity imposed by the earcanal wall, the "opposition" of the earcanal cavity to this transfer, the acoustic pressure generated in reaction and the associated acoustic power flow in the earcanal cavity open and occluded by an infinite impedance. In particular, the distribution of the earcanal wall vibration is shown to influence the acoustic mass of the open earcanal cavity seen by its vibrating wall.

The earcanal wall vibration distribution has been characterized by its curvilinear centroid position which has also been assumed as the location of the volume velocity source in the EA model. This assumption has been successfully evaluated for several earcanal wall vibration patterns induced by various sets of loading and boundary conditions applied to the FE model. In harmonic regime, the volume velocity is alternatively transferred in the earcanal cavity through the "path" of least "opposition" (*i.e.*, acoustic impedance), between the source and the earcanal entrance in the open case, or between the source and the tympanic membrane in the occluded case. The increase of acoustic pressure is responsible for the increase of tympanic membrane volume velocity in the occluded case at low frequencies.

Common interpretations of the OE in terms of "leak" and "trap" have been shown to misrepresent the fundamental mechanism of the OE related to the earcanal impedance change. Interpretations based on this concept are considered more accurate. For example, the occlusion increases the "opposition" of the earcanal cavity to the volume velocity imposed by its wall and thus increases the acoustic pressure generated in reaction, leading to the OE. In this study, the distribution of the earcanal wall normal velocity has been shown to greatly influence the vibro-acoustic behavior of the open earcanal (and thus the OE) while that of the occluded earcanal is not affected due to the use of an acoustically rigid occlusion defined at the earcanal entrance. For future work, the intricate influence of the occlusion device, in conjunction with the earcanal wall vibration, on the OE, could be investigated.

2.7 Acknowledgments

The authors acknowledge the support of the Natural Sciences and Engineering Research Council of Canada (NSERC), [funding reference number RGPIN-2016-06795]. Also, the anonymous reviewers are gratefully thanked for their critical and wise comments.

CHAPTER 3

ON THE REMOVAL OF THE OPEN EARCANAL HIGH-PASS FILTER EFFECT DUE TO ITS OCCLUSION: A BONE-CONDUCTION OCCLUSION EFFECT THEORY

Kévin Carillo[a] , Olivier Doutres[a] , Franck Sgard[b]

[a] Department of Mechanical Engineering, École de technologie supérieure,
1100 Notre-Dame Ouest, Montréal, Québec, Canada H3C 1K3
[b] Direction Scientifique, Institut de recherche Robert-Sauvé en santé et en sécurité du travail,
505 Boulevard de Maisonneuve Ouest, Montréal, Québec, Canada H3A 3C2

Paper submitted for publication to *Acta Acustica*, March 2021 (first revision submitted in July 2021).

3.1 Abstract

The occlusion effect is commonly experienced by in-ear device wearers as an increased loudness sensation of bone-conducted low-frequency sounds. A widespread theory proposed by Tonndorf and based on a simplified electro-acoustic model describes the phenomenon as the removal of the open earcanal high-pass filter effect due to a perfect or partial occlusion. However, this filter has not been clearly defined and several ambiguities remain. Revisiting the model, a second order high-pass filter effect for the volume velocity transferred between the earcanal wall and the eardrum is highlighted. This filter remains for partial occlusion but vanishes for perfect occlusion. In the latter case, the volume velocity transferred from the earcanal cavity to the middle ear through the eardrum drastically increases, which explains the predominance of the occluded outer ear pathway on the hearing by bone-conduction at low frequencies.

3.2 Introduction

The occlusion effect (OE) is experienced as an increase of the auditory perception to bone-conducted sound when covering or blocking the earcanal (Berger, 2003). In everyday life, the OE is usually described as one's own voice perceived as "hollow" or "talking into a barrel" (Mueller

et al., 1996). This perception is the conjunction of the bone-conducted transmission increase and the air-conducted transmission decrease due to the occlusion device (Stenfelt & Reinfeldt, 2007). A common objective measurement of the OE is defined as the difference between sound pressure levels (SPLs) measured close to the tympanic membrane in occluded and open earcanal. This phenomenon is most prominent at low frequencies, typically below 1 kHz, and for shallow occlusions (Berger, 2003).

Since the first descriptions of experimental findings underlying the OE in the 1830s, several theories were developed to explain this phenomenon over the course of the next century. Historical reviews of these theories can be found in Huizing (1960); Tonndorf *et al.* (1966). In the 1960s, two explanations of the OE were developed. The first one, submitted by Huizing (1960), was based on the change in resonance properties of the earcanal due to its occlusion. A few years later, this concept was investigated experimentally by Tonndorf *et al.* (1966) and deemed valid only above 1 kHz. At low frequencies, Tonndorf rather suggested that the OE was a result of the removal of the open earcanal high-pass filter effect due to the occlusion (Tonndorf, 1964; Tonndorf *et al.*, 1966; Tonndorf, 1972). This theory relied on a simplified electro-acoustic (EA) model of the open and occluded earcanal. This model, involving acoustic mass and compliances, was the first model of the OE and has inspired several authors to date (Stenfelt & Reinfeldt, 2007; Carillo *et al.*, 2020). However, the open earcanal high-pass filter mentioned by Tonndorf has not been clearly defined and the simplified EA model has only been put forward to illustrate the concept, not to investigate the filter's parameters nor its removal due to a partial or perfect occlusion.

In the literature, the open earcanal filter effect has been mainly interpreted in terms of acoustic energy transfer (Stenfelt & Reinfeldt, 2007; Kuk, 1991; Fagelson & Martin, 1998; Small & Hu, 2011; Brummund *et al.*, 2014). Tonndorf himself related the open earcanal filter effect to the energy dissipated at the open earcanal entrance: "The open earcanal acts as a high-pass filter so that low-frequency sounds are dissipated through its external opening" (Tonndorf, 1972). However, since (i) these resistances are not required to model the OE at low frequencies (Carillo *et al.*, 2020) and (ii) Tonndorf's model itself did not include them to account for dissipation of

acoustic energy, the filter effect is not necessarily related to dissipation phenomena. Furthermore, the acoustic power dissipated through the earcanal opening is negligible at low frequencies in the open case compared to acoustic power dissipated in the earcanal cavity and at the tympanic membrane, and its reduction due to the occlusion cannot explain the OE (Carillo *et al.*, 2020). In the occluded case, Tonndorf explained that "the high-pass filter effect is eliminated, either partially or totally, depending upon the quality of the seal" (Tonndorf, 1972).

Tonndorf's theory has been widely quoted in the literature to explain the fundamentals of the OE at low frequencies until recently (*e.g.*, (Khanna *et al.*, 1976; Berger & Kerivan, 1983; Schroeter & Poesselt, 1986; Howell *et al.*, 1988; Kuk, 1991; Fagelson & Martin, 1998; Stenfelt *et al.*, 2003; Stenfelt & Goode, 2005; Reinfeldt *et al.*, 2007; Stenfelt & Reinfeldt, 2007; Lee, 2011; Small & Hu, 2011; Brummund *et al.*, 2014, 2015)). However, in the authors' opinion, this theory suffers from several ambiguities and remains unclear. To the authors' knowledge, no work has revisited in detail this widespread theory. The aim of the present paper is thus to investigate and clarify the open earcanal high-pass filter effect and how perfect and partial occlusions affect it. For this purpose, a revisited EA model inspired from Tonndorf's is presented. This work is believed to contribute to a better understanding of Tonndorf's theory and of the fundamental mechanism of the OE at low frequencies.

3.3 Models of the occlusion effect

3.3.1 Review of Tonndorf's model

Figure 3.1 presents the EA model of an open and occluded earcanal proposed by Tonndorf *et al.* (1966) for a bone-conducted stimulation at low frequencies. The source responsible for the acoustic pressure $\tilde{p}$ generated in the earcanal cavity is identified by Tonndorf to be the vibration of the earcanal wall. At that time, the mandibular condyle of the lower jaw was also believed to be a part of this source, but it has since then been shown to have little influence (Stenfelt *et al.*, 2003). In the open case (see Fig. 3.1(a)), the air within the earcanal cavity is accounted for using an acoustic compliance C_{EC} near the tympanic membrane and an acoustic mass L_{EC} near the

earcanal opening. In the occluded case (see Fig. 3.1(b)), the earcanal cavity is approximated by an acoustic compliance C_{EC}. In both cases, the tympanic membrane is approximated by an acoustic compliance C_{TM}.

The ambiguous points in Tonndorf's model are now highlighted. Firstly, the acoustic pressure generated in the earcanal cavity is identically referred to as $\tilde{p}$ in both open and occluded cases. It is certain that the acoustic pressure cannot be equal in both cases, or else the OE would be zero. In EA models subsequent to that of Tonndorf, the vibration of the earcanal wall has been represented as an equivalent and ideal source of volume velocity (Schroeter & Poesselt, 1986; Stenfelt & Reinfeldt, 2007; Zurbrügg *et al.*, 2014; Carillo *et al.*, 2020) which is not affected by the acoustic load. The acoustic pressure generated by the source then depends on the earcanal acoustic properties which differ when the earcanal is open or occluded. Secondly, the separation between the portion of air controlled by the acoustic mass L_{EC} and that controlled by the acoustic compliance C_{EC} in the open case has not been detailed. In a previous paper, the authors showed that the junction between both portions is defined by the location of the equivalent volume velocity source in the earcanal (Carillo *et al.*, 2020). In addition, the authors highlighted that the location of this source is not arbitrary but rather corresponds to the centroid position of the spatially distributed earcanal wall normal velocity. In the occluded case, the acoustic compliance C_{EC} only depends on the occluded earcanal residual volume. C_{EC} is thus not necessarily the same in both open and occluded cases, depending on the occlusion device insertion depth. Thirdly, the two compliances C_{TM} and C_{EC} in series in Tonndorf's model should be arranged in parallel since they share the same acoustic pressure, not the same volume velocity (Carillo *et al.*, 2020). Fourthly, the transfer function of the open earcanal, described by Tonndorf as a high-pass filter due to the acoustic mass L_{EC}, has not been explicitly defined (*i.e.*, physical nature of the input and output signals). In addition, this filter has been related to the earcanal opening acoustic "dissipation" while no acoustic resistance was accounted for in Tonndorf's model. Furthermore, the "removal" or "elimination" of this filter due to a partial or perfect occlusion of the earcanal opening has not been explicitly reported. Thus, Tonndorf's explanation of the OE remains unclear.

Since the first three ambiguous points have been clarified previously, we now focus on the fourth point related to the filter effect. As mentioned in the introduction, this clarification is important in the authors' opinion since the "removal of the open earcanal filter effect" is commonly used to explain the OE induced by perfect or partial occlusion.

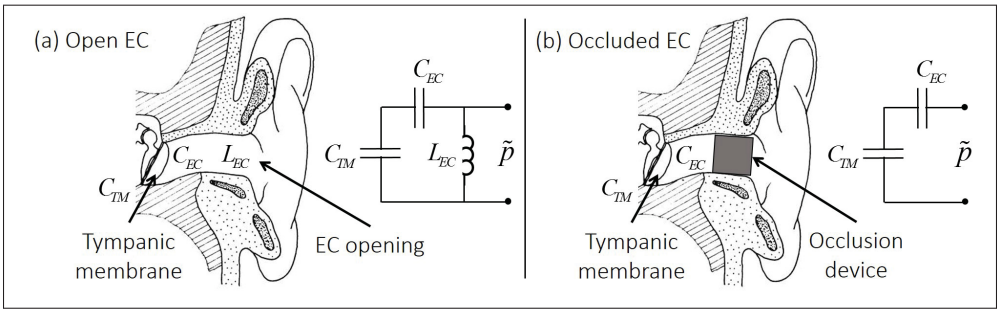

Figure 3.1 Tonndorf's EA model of (a) an open and (b) occluded earcanal. Adapted from Tonndorf (1964)

3.3.2 Revisited electro-acoustic model

3.3.2.1 Layout

In order to investigate the open earcanal filter effect mentioned by Tonndorf and its change due to a perfect and a partial occlusion, three configurations are modeled here using a revisited EA model illustrated in Fig. 3.2: (a) an open earcanal, (b) a perfectly occluded earcanal and (c) a partially occluded earcanal with a coaxial hole of radius $r_h = 0.9$ mm and length $l_h = 21$ mm (dimensions equivalent to those used by (Hansen, 1998) for comparison with experimental data in Sec. 3.3.3). Perfect and partial occlusions are defined at the earcanal entrance and correspond to an extreme case of shallow insertion. The volume velocity q_{wall} imposed by the earcanal wall represented by the source Q is thus equal in all cases. The earcanal is considered as a circular cross-sectional duct of curvilinear length $l_{EC} = 34.7$ mm and varying radius $r_{EC}(z)$, with z the earcanal curvilinear axis. The earcanal shape is taken from a realistic 3D finite element (FE) model of an outer ear (Carillo *et al.*, 2020) and displayed in Fig. 3.3. The volume velocity source Q is located at a distance $l_c = 23.6$ mm from the tympanic membrane. This distance corresponds

to the centroid position of the earcanal wall normal vibration and has been computed using the 3D FE model to which the current EA model is associated (Carillo *et al.*, 2020).

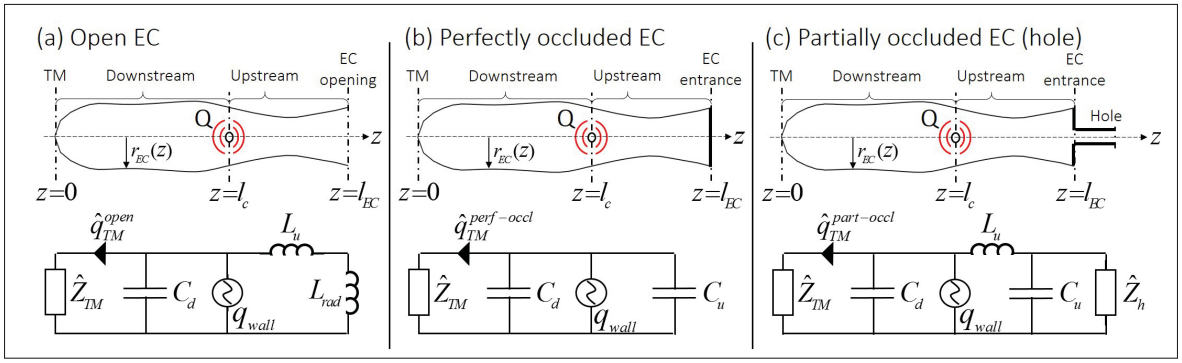

Figure 3.2 Revisited EA model of an (a) open, (b) perfectly occluded and (c) partially occluded earcanal

The source Q divides the earcanal into an upstream section and a downstream section (see Fig. 3.2). In all cases, the downstream section is dominated at low frequencies by its compressibility effect of acoustic compliance C_d. The downstream section is terminated by the tympanic membrane. The acoustic impedance $\hat{Z}_{TM}$ (complex-valued) of the tympanic membrane is defined by the model of Shaw & Stinson (1981) (see Appx. IV). In the open case, the upstream section is dominated by its inertia effect represented by the acoustic mass L_u. The radiation impedance of the earcanal opening is modeled by the acoustic impedance of a baffled circular piston of radius $r_{ent} = 2.8$ mm equal to that of the earcanal entrance (see Appx. V) and is governed at low frequencies by an acoustic mass L_{rad}. In the occluded case, the upstream section is dominated by the acoustic compliance C_u. The expressions of localized constants C_d, C_u, L_u, and L_{rad} derived from the 3D FE model are provided in Carillo *et al.* (2020) (see Table 2.1 in Sec. 2.3.2.1).

In the partially occluded case, the upstream section includes both the acoustic mass L_u and the acoustic compliance C_u since their respective importance depends on the hole impedance seen by the upstream section. The acoustic impedance of the hole is defined by $\hat{Z}_h = R_h + j\omega L_h^{eq}$. The equivalent acoustic mass of the hole $L_h^{eq} = L_h + L_{dis} + L_{rad}^h$ includes the hole acoustic mass L_h, the acoustic mass of discontinuity L_{dis} due to the sudden change of section at the

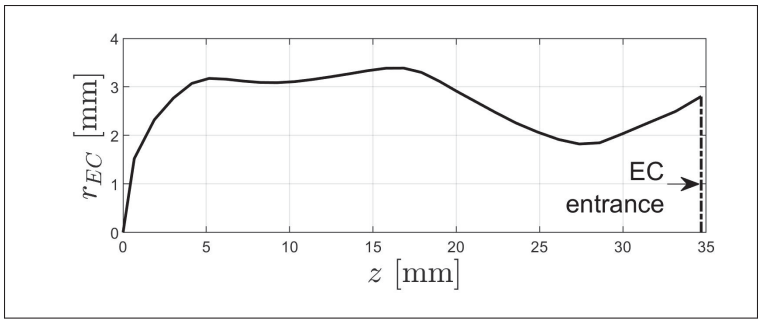

Figure 3.3 Earcanal radius $r_{EC}(z)$ as a function of the earcanal curvilinear axis z used in the EA model

earcanal entrance (Karal, 1953), and the acoustic mass of radiation L^h_{rad} in the surrounding environment. The equivalent acoustic mass is associated with viscous losses represented by the acoustic resistance R_h (Bruneau, 2013). Table 3.1 summarizes the calculation of R_h, L_h, L_{dis} and L^h_{rad}. It is noteworthy that the expressions of R_h and L_h are adapted for a "large" hole such that $\left|\hat{k}_{vi/th} r_h\right| > 10$ where $\hat{k}_{vi/th}$ represents either viscous or thermal wavenumbers (Bruneau, 2013).

Table 3.1 Calculation of the localized constants included in the hole impedance $\hat{Z}_h$. $\rho_0 = 1.2$ kg m^{-3} is the air density and $\mu = 1.8313 \times 10^{-5}$ Pa s is the air dynamic viscosity. $H(\alpha)$ represents the correction factor of the discontinuity mass L_{dis} as a function of α, the ratio of the hole and the earcanal entrance radius, and can be approximated by $H(\alpha) \approx 1 - 1.25\alpha$ for $\alpha \ll 1$ (Mechel, 2008)

$R_h = \frac{\sqrt{2\rho_0\omega\mu}}{\pi r_h^3} l_h$	$L_h = \frac{\rho_0 l_h}{\pi r_h^2}$	$L_{dis}(\alpha) = \frac{8\rho_0}{3\pi^2 r_h} H(\alpha)$	$L^h_{rad} = \frac{8\rho_0}{3\pi^2 r_h}$

3.3.2.2 Indicators

In order to clarify the filter effect described by Tonndorf and its role on the OE, a transfer function is sought between the source and the tympanic membrane. According to Fig. 3.2, the acoustic pressure at the tympanic membrane is equal to that generated by the source Q because

the earcanal downstream section is governed by its compressibility effect in all cases at low frequencies. The acoustic pressure generated by the source depends, however, on the acoustic impedance seen by the source, which differs between all cases. On the other hand, the volume velocity transferred to the tympanic membrane is not equal to that imposed by the source and can differ in each case. A transfer function in terms of volume velocity between the volume velocity imposed by the earcanal wall q_{wall} and that transferred to the tympanic membrane $\hat{q}_{TM}$ is computed as

$$\hat{T}_q^k = \frac{\hat{q}_{TM}^k}{q_{wall}}, \quad k \in \{open,\ perf-occl,\ part-occl\}\ . \tag{3.1}$$

In Eq. (3.1), the value of q_{wall} can be chosen arbitrarily since it is a transfer function whereas $\hat{q}_{TM}^k$ is computed using the EA model in each case and depends on all acoustic impedances and localized constants involved (see Fig. 3.2).

Simplified expressions of volume velocity transfer functions can be developed to help their interpretation and highlight the high-pass filter effect (see Sec. 3.3.3). To do so, the acoustic impedance at the tympanic membrane is first approximated to the compressibility effect of the middle ear cavity volume of acoustic compliance C_{TM}. This approximation is reasonable for frequencies below 500 Hz (Stepp & Voss, 2005; Carillo *et al.*, 2020). Secondly, the acoustic resistance R_h associated to viscous losses in the hole is omitted. Its influence is discussed in Sec. 3.3.3. Applied to Eq. (3.1), these approximations lead to the following straightforward expressions for the three cases of Fig. 3.2:

$$\hat{T}_q^{open} \approx \frac{-\omega^2 \left(L_u + L_{rad}\right) C_{TM}}{1 - \omega^2 \left(L_u + L_{rad}\right) \left(C_d + C_{TM}\right)}, \tag{3.2}$$

$$\hat{T}_q^{perf-occl} \approx \frac{C_{TM}}{C_u + C_d + C_{TM}}, \tag{3.3}$$

$$\hat{T}_q^{part-occl} \approx \frac{-\omega^2 \left(L_u + L_h^{eq}\right) C_{TM}}{1 - \omega^2 \left[L_h^{eq} C_u + \left(L_u + L_h^{eq}\right) \left(C_{TM} + C_d\right)\right]}. \tag{3.4}$$

The OE is defined in terms of tympanic membrane acoustic pressure $\hat{p}_{TM}$ by

$$OE_m = 20\log_{10}\left(\left|\frac{\hat{p}^m_{TM}}{\hat{p}^{open}_{TM}}\right|\right), \quad m \in \{perf-occl,\ part-occl\}\ . \tag{3.5}$$

Since the tympanic membrane acoustic pressure is related to the associated volume velocity by $\hat{p}^k_{TM} = \hat{Z}_{TM} \times \hat{q}^k_{TM}$, the OE can be rewritten in terms of volume velocity transfer functions $\hat{T}^k_q$ such as

$$OE_m = 20\log_{10}\left(\left|\frac{\hat{T}^m_q}{\hat{T}^{open}_q}\right|\right). \tag{3.6}$$

Compared to Eq. (3.5), Eq. (3.6) of the OE is strictly limited to occlusions (perfect or partial) performed at the earcanal entrance such that the volume velocity imposed by the earcanal wall is equal to the open case. If the occlusion occurs deeper in the earcanal, the OE computed using Eq. (3.6) would be weighted by the ratio of volume velocity imposed by the earcanal wall in occluded and open cases.

3.3.3 Results and discussions

The moduli of the volume velocity transfer function defined by Eq. (3.1) are displayed in Fig. 3.4 in dB for the open, occluded and partially occluded (hole) cases. Consider first the open case. The proportion of volume velocity transferred between the vibrating earcanal wall and the tympanic membrane is the lowest at 100 Hz (minimum frequency of interest) and increases up to 1 kHz (maximum frequency of interest). To interpret this result, Eq. (3.2) gives an approximation of the volume velocity transfer function. The latter exhibits a second order high-pass filter. As the frequency increases, the inertia effect of the earcanal upstream section $j\omega(L_u + L_{rad})$ imposes more "opposition" to the volume velocity transfer, unlike the compressibility effect of the earcanal downstream section $[j\omega(C_d + C_{TM})]^{-1}$, which diminishes with frequency. The conjunction of both phenomena is responsible for the increase of the volume velocity transferred between the earcanal wall and the tympanic membrane with frequency squared (+40 dB/decade, see Fig. 3.4). This transfer is maximum at the quarter-wavelength acoustic resonance of the open earcanal around 3 kHz (out of the frequency range of interest).

As suggested in introduction, the open earcanal high-pass filter effect is therefore not related to acoustic dissipation at the earcanal opening. Indeed, the acoustic resistance of radiation representing the acoustic dissipation at the earcanal opening can be neglected and the open earcanal high-pass filter effect is still there (see Eq. (3.2)). Therefore, the explanation of the high-pass filter effect provided by (Tonndorf, 1972) and the interpretations of the filter effect in terms of acoustic energy transfer seen in the literature are not accurate. Indeed, the open earcanal high-pass filter effect is caused by the acoustic radiation of the open earcanal entrance, which is governed at low frequencies by the acoustic mass of radiation L_{rad}. In practice, acoustic radiation include dissipative effect through an acoustic resistance associated with the acoustic mass of radiation. However, as mentioned above, this acoustic resistance has little influence on the acoustic pressure radiated by the earcanal wall in the earcanal cavity and can be neglected (Carillo *et al.*, 2020). The previous discussion clarifies and deepens the understanding of the high-pass filter effect presented by (Tonndorf *et al.*, 1966).

In the perfectly occluded case, the proportion of volume velocity transferred between the earcanal wall and the tympanic membrane is approximately constant with frequency (see Fig. 3.4). In this case, the earcanal upstream section is governed by its compressibility effect rather than its inertia effect. The high-pass filter effect thus vanishes (see Eq. (3.3)). From 100 Hz to 1 kHz, the volume velocity transferred through the eardrum is 55 to 10 dB greater in the occluded case compared to the open case. Hence, the volume velocity transferred through the middle ear (up to the cochlea) in addition to that transferred by bone-conduction *via* the ligaments connecting the ossicles to the tympanic cavity (not accounted for here), is significantly increased when the earcanal is occluded (Schroeter & Poesselt, 1986). As a result, while the outer ear pathway is of little influence on the hearing by bone-conduction when the earcanal is open (Stenfelt *et al.*, 2003; Stenfelt, 2016), it becomes predominant when the earcanal is occluded (Schroeter & Poesselt, 1986; Stenfelt *et al.*, 2003).

When the earcanal is partially occluded, Fig. 3.4 shows that the volume velocity transferred between the earcanal wall and the tympanic membrane increases with frequency by approximately +40 dB/decade (similar to the open case) until it reaches a maximum around approximately

450 Hz. This transfer is then almost constant with frequency (similar to the occluded case). The approximation given by Eq. (3.4) exhibits a second order high-pass filter, just like the open earcanal. The partially occluded earcanal, however, behaves as a Helmholtz resonator rather than a quarter-wavelength resonator. The Helmholtz resonance frequency is given by $f_0 = \left[4\pi^2 \left(L_h^{eq} C_u + \left(L_u + L_h^{eq}\right)\left(C_{TM} + C_d\right)\right)\right]^{-1/2}$. This resonance is mainly damped by the acoustic resistance of the tympanic membrane and to a lesser extent on the hole viscous resistance R_h, depending on the hole radius. These resistances are neglected in the approximation given by Eq. (3.4) which is not used in Fig. 3.4 for this reason. If the acoustic mass L_h^{eq} of the hole is significantly higher than that of the earcanal upstream section L_u (*e.g.*, hole radius small enough or length long enough), the hole corresponds to the neck of the Helmholtz resonator whereas the whole earcanal acts as the resonator cavity. On the contrary, if the length of the vent tends to zero and if its radius goes to that of the earcanal entrance, the partially occluded case tends to the open case (*i.e.*, Eq. (3.4) tends to Eq. (3.2)).

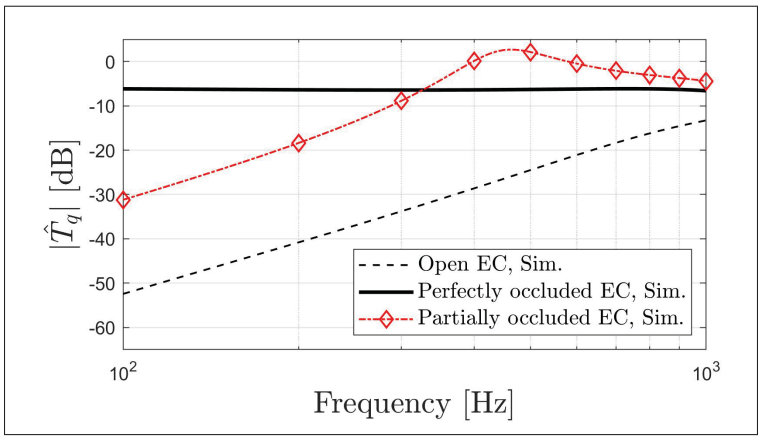

Figure 3.4 Level in dB (factor 20) of the volume velocity transfer function $\hat{T}_q$ defined between the earcanal wall and the tympanic membrane in open, perfectly occluded and partially occluded (with a hole) cases computed using Eq. (3.1)

The change in volume velocity transfer function between open and partially occluded cases is now investigated regarding the OE. Figure 3.5 displays the OE induced by the perfect and the partial occlusions of the earcanal entrance. In the perfect occlusion, the OE is maximum at

100 Hz and decreases with frequency by approximately −40 dB/decade. This slope is similar to literature data (Schroeter & Poesselt, 1986; Stenfelt & Reinfeldt, 2007; Brummund *et al.*, 2014) and results from the removal of the open earcanal high-pass filter effect. Tonndorf's model therefore included the minimum features to simulate the objective OE for a perfect occlusion. When the earcanal is partially occluded, the OE increases from 100 Hz to approximately 450 Hz and decreases above this frequency.

Figure 3.5 also displays the OE measured by Hansen (1998) on a human subject for a shallow partial occlusion. Simulation and experimental data exhibit similar slopes. The model approximately predicts the resonance frequency observed in experimental data around 450 Hz. However, the model overestimates the measured OE by approximately 6 dB in the whole frequency range of interest (100 Hz to 1 kHz). This difference in OE amplitude most likely comes from the difference in insertion depth between the current model (defined at the EC entrance) and the measurement (shallow insertion). Indeed, since the OE decreases with increasing insertion depth, the simulated OE is therefore higher than the measured OE. The influence of the insertion depth on the OE can be accounted for by adjusting the volume velocity imposed to the occluded EC cavity (Schroeter & Poesselt, 1986; Stenfelt & Reinfeldt, 2007; Zurbrügg *et al.*, 2014). When the occlusion device is deeply inserted, the OE is significantly reduced (Berger, 2003; Stenfelt & Reinfeldt, 2007).

The maximum of the OE induced by the partial occlusion occurs at the resonance frequency (around 450 Hz in Fig. 3.5) of the Helmholtz resonator formed by the hole and the earcanal cavity (Hansen, 1998; Brummund, 2014; Zurbrügg *et al.*, 2014). Below the Helmholtz resonance, the OE is significantly reduced compared to the perfect occlusion and approximately constant with frequency. The amplitude of the OE is given by the ratio between the acoustic mass of the hole and that of the open earcanal. The hole acts as a low acoustic impedance pathway for the volume velocity transfer. This phenomenon has inspired the use of vent in hearing aids to decrease the OE (Mueller *et al.*, 1996; Carle *et al.*, 2002; Winkler *et al.*, 2016). It is however associated with acoustic feedback which decreases the intelligibility provided by hearing aids. In the case of earplugs, an incomplete seal is generally avoided since it decreases their sound attenuation

(Viallet, Sgard, Laville & Nélisse, 2015). Fit testing methods have been developed to prevent this. In the simplest case, the perception of the OE can even be used as an estimate of the seal quality: the greater the perceived OE, the greater the seal (Berger, 2003).

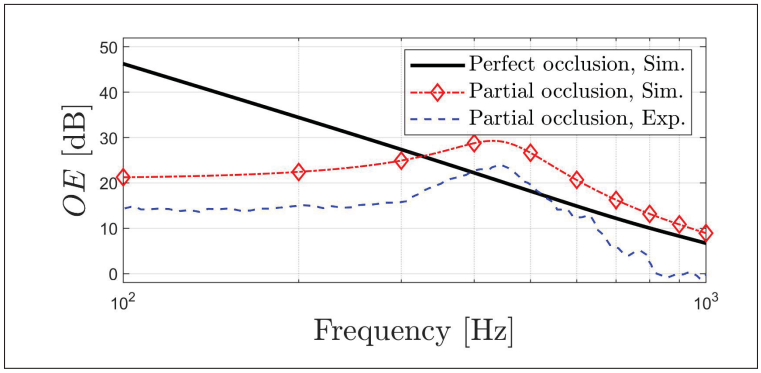

Figure 3.5 OE induced by a perfect and a partial (with a hole) occlusions (at the earcanal entrance) computed using Eq. (3.5) of the EA model. In addition, experimental data provided by Hansen (1998) are also displayed for a shallow partial occlusion

3.4 Conclusion

This paper has revisited and deepened the understanding of the high-pass filter effect mentioned by Tonndorf and how this filter is changed in occluded case (perfect or partial). The EA model proposed by Tonndorf has been clarified, and used to highlight a second order high-pass filter for the volume velocity transferred between the earcanal wall and the tympanic membrane in the open earcanal. The open earcanal high-pass filter effect is caused by the acoustic radiation of the earcanal opening which is governed at low frequencies by the acoustic mass of radiation whereas acoustic dissipation at the earcanal opening plays a negligible role and cannot explain the high-pass filter effect. The perfect occlusion replaces the open earcanal high-pass filter effect by a filter constant with frequency. On the contrary, the partial occlusion (hole) exhibits a high-pass filter effect just like the open earcanal but behaves as a Helmholtz resonator. For a perfect occlusion, the OE can be described as the removal of the open earcanal high-pass filter effect. In consequence, the volume velocity transferred from the earcanal cavity to the middle

ear through the tympanic membrane drastically increases, which explains the predominance of the occluded outer ear pathway on the hearing by bone-conduction at low frequencies. For a partial occlusion, however, the OE results from a change in properties of the open earcanal high-pass filter effect, which is not removed.

3.5 Acknowledgments

The authors acknowledge the support of the Natural Sciences and Engineering Research Council of Canada (NSERC), [funding reference number RGPIN-2016-06795]. Also, all reviewers are gratefully thanked for their critical and wise comments.

CHAPTER 4

PRINCIPLE OF AN ACOUSTICAL METHOD FOR ESTIMATING THE CENTROID POSITION OF THE EARCANAL WALL NORMAL VELOCITY INDUCED BY BONE-CONDUCTED STIMULATION: NUMERICAL EVALUATION

Kévin Carillo[a] , Olivier Doutres[a] , Franck Sgard[b]

[a] Department of Mechanical Engineering, École de technologie supérieure,
1100 Notre-Dame Ouest, Montréal, Québec, Canada H3C 1K3
[b] Direction Scientifique, Institut de recherche Robert-Sauvé en santé et en sécurité du travail,
505 Boulevard de Maisonneuve Ouest, Montréal, Québec, Canada H3A 3C2

Paper published in *Applied Acoustics*, June 2021.

4.1 Abstract

The occlusion effect is commonly experienced as the altered perception of one's own physiological noise when the earcanal entrance is blocked. Objectively, this phenomenon corresponds to an acoustic pressure increase in the occluded earcanal. The occlusion effect originates from the earcanal wall normal vibration and depends on the spatial distribution of the latter. At low frequencies, this spatial distribution can be characterized by the position of its centroid along the earcanal middle axis. This paper describes the principle of an acoustical method for estimating this centroid position at low frequencies. The proposed method consists in measuring the eardrum acoustic pressure transfer function between the earcanal open and occluded by an external capped duct coupled to the earcanal entrance of a subject submitted to a bone-conducted stimulation. The centroid position is then estimated at the antiresonance frequency of the coupled system using an associated electro-acoustic model. The proposed method is evaluated and investigated numerically using a 3D finite element model of an outer ear. The sensitivity of the method is shown to increase with frequency. To maximize the method accuracy, the radius of the coupling duct must be as large as possible (in the limits of the earcanal entrance dimension) and any incomplete seal between the duct and the earcanal entrance must be avoided. Also, the coupling position of the duct and its temperature must be known as precisely as possible.

On the contrary, the proposed method does not require the knowledge of the eardrum acoustic impedance.

4.2 Introduction

The occlusion effect (OE) is usually described as the increased perception of the bone-conducted part of one's own physiological noise (*e.g.*, one's own voice, chewing, heartbeat, etc.) when the earcanal entrance is covered or blocked. This phenomenon is most significant at low frequencies, typically below 1 kHz, and decreases above (Berger, 2003). The OE contributes to the lack of comfort associated with wearing hearing protection devices, in particular for earplugs whereas earmuffs are less concerned, and partly explains their non-use (Doutres *et al.*, 2019). Hearing aid users can also be affected by the OE (Kochkin, 2010), which is, however, greatly reduced by using vents or open-fit hearing aids (Winkler *et al.*, 2016). Bone-conducted sound propagates into the body from the excitation source (*e.g.*, vocal cords, bone-transducer, etc.) to the basilar membrane of the cochlea in the inner ear, which results in a hearing sensation. The hearing by bone-conduction has been extensively investigated since the past century and several sound transmission pathways have been highlighted through the outer ear, the middle ear and the inner ear itself (Bàràny, 1938; Békésy, 1948, 1949; Huizing, 1960; Tonndorf, 1964; Khanna *et al.*, 1976; Berger & Kerivan, 1983; Stenfelt *et al.*, 2003; Stenfelt & Goode, 2005; Dobrev *et al.*, 2017; Sohmer, 2017; Chordekar *et al.*, 2018; Zhao, Fridberger & Stenfelt, 2021). The occlusion of the earcanal entrance alters the contribution of the outer ear pathway to the hearing by bone-conduction (mainly at low frequencies below 1 kHz). This is due to the increased acoustic pressure generated by the earcanal wall when the earcanal entrance is occluded. The vibration of the earcanal wall constitutes the source of the OE.

This vibration is expected to be maximum in the cartilaginous part of the earcanal and minimum in the bony part (Stenfelt *et al.*, 2003). Most probably because of experimental difficulty, the spatial distribution of the earcanal wall normal vibration has never been directly measured. Indeed, direct measurement methods such as Doppler laser vibrometer or accelerometer could be intricate to perform in a human earcanal due to its small size, its tortuosity and the presence of hair

and wax. However, the spatial distribution of the earcanal wall normal vibration has significant influence on the vibro-acoustic behavior of the open earcanal (Carillo *et al.*, 2020). In addition, this distribution governs the reduction of the OE with insertion depth (Schroeter & Poesselt, 1986; Stenfelt & Reinfeldt, 2007). Furthermore, the earcanal wall normal vibration distribution could influence the contribution of earplugs to the OE (Hansen, 1998; Lee, 2011; Brummund *et al.*, 2015). Also, this distribution could be influenced by the bone-conducted stimulation which is known to influence the OE (Hansen, 1998; Reinfeldt *et al.*, 2013; Saint-Gaudens *et al.*, 2019) but remains unexplained. The earcanal wall normal vibration distribution is therefore of great interest to study the bone-conduction outer ear pathway and the OE.

Using a 3D finite element (FE) model of an outer ear, the authors have proposed to characterize the spatial distribution of the earcanal wall normal vibration by its centroid position (Carillo *et al.*, 2020). This centroid position represents the center of normal velocity distributed over the earcanal wall surface. Also, the authors have shown that the centroid position corresponds to the location of the equivalent volume velocity source representing the earcanal wall normal vibration in an associated electro-acoustic (EA) model of the open earcanal (Carillo *et al.*, 2020). Therefore, the centroid position could be used as a vibratory indicator of the earcanal wall normal vibration distribution to study its parameters of influence (*e.g.*, bone-conducted stimulation and position, anatomical differences, etc.). In addition, the knowledge of the centroid position could possibly guide to the optimal insertion depth of in-ear devices to reduce the OE without inserting them into the sensitive bony part of the earcanal.

In this paper, an indirect method is proposed to estimate this centroid position at low frequencies. This method is inspired from an experiment made by Huizing (1960). In order to highlight a standing wave pattern in the occluded earcanal, Huizing measured the objective OE (*i.e.*, sound pressure level (SPL) difference between occluded and open earcanal) induced by an external capped duct coupled to the earcanal entrance of a human subject submitted to a bone-conducted stimulation. Negative OEs were observed depending on the length of the coupling duct. Huizing (1960) interpreted these minima as acoustic resonances of the coupled system and assumed the occurence of an acoustic pressure node at the eardrum. In this paper, however, it is shown

that the acoustic pressure node does not occur at the eardrum but at the centroid position of the earcanal wall normal velocity induced by the bone-conducted stimulation. Using an EA model of the earcanal coupled to the external duct, the centroid position can be estimated from the lowest antiresonance frequency of the coupled system. This paper presents the experimental setup, the measurement procedure and the EA model associated with the indirect method. Then, the latter is evaluated and investigated numerically using a 3D FE model of an outer ear open and occluded by an external duct. Finally, the influence of several parameters of the coupled system on the estimation provided by the method is studied. The knowledge of parameters influencing the method is of great interest for a future experimental application on human subjects.

4.3 Principle of the method

To estimate the centroid position of the earcanal wall normal velocity, the proposed indirect method requires (i) the physical measurement of the acoustic pressure transfer function between the earcanal open and occluded by an external capped duct coupled at the earcanal entrance and (ii) analysis using an EA model of the earcanal coupled to the same duct. Section 4.3.1 describes the experimental setup and the measurement procedure of the proposed indirect method. Then, Sec. 4.3.2 details the EA model associated with the indirect method and used to estimate the centroid position of the earcanal wall normal velocity. Finally, Sec. 4.3.3 presents the methodology of the numerical evaluation and investigation of the proposed method using a 3D FE model of an outer ear. No measurements are performed in this work. The experimental investigation of the proposed method will be the subject of a future paper.

4.3.1 Experimental setup and measurement procedure

In both open and occluded ear, the acoustic pressure is measured close to the eardrum of a human subject submitted to a bone-conducted stimulation (*e.g.*, bone-transducer applied to the forehead or the mastoid (Reinfeldt *et al.*, 2013)). Figure 4.1 illustrates the corresponding experimental setup. In the occluded case (see Fig. 4.1(b)), a circular cross-section coupling duct is used. Its outer cross-sectional area must fit in the earcanal entrance plane. Since the earcanal

cross-sections (including the earcanal entrance) are generally not circular (Stinson & Lawton, 1989), the circular cross-section of the coupling duct is necessarily smaller than the earcanal entrance surface. The coupling duct is not inserted in the earcanal but rather held in position in the concha using a "duct holder." The duct holder could consist of an imprint of the concha up to the earcanal entrance plane and including a hole in which the coupling duct would be inserted. In practice, determining the position of the acoustic entrance of the earcanal is not trivial (Farmer-Fedor & Rabbitt, 2002; Hudde & Schmidt, 2009). Therefore, the earcanal entrance used in the proposed method could be chosen based on geometrical consideration (Voss, Horton, Fairbank, Xia, Tinglin & Girardin, 2020). In any case, however, the proposed method can only estimate the centroid position of the earcanal wall normal velocity between the chosen earcanal entrance plane and the eardrum as explained in the following.

The lowest antiresonance frequency of the coupled system is identified from the acoustic pressure transfer function and corresponds to the first local minimum associated to a sudden phase shift (see Sec. 4.4.1). An EA model of the coupled system (presented in next section) is then used to estimate the centroid position of the earcanal wall normal velocity. The estimation consists in minimizing the difference between the experimental and the simulated antiresonance frequency by varying both frequency and source position in the EA model. The latter requires the knowledge of the earcanal shape function between the eardrum and the coupling duct and the geometric dimensions (inner radius and length) of the coupling duct. The earcanal shape can be obtained from magnetic resonance images (Benacchio, Doutres, Varoquaux, Wagnac, Le Troter, Callot & Sgard, 2019), 3D scans (Lee, Yang, Jung, Bok, Kim, Kwon & You, 2018), earcanal imprint (Voss *et al.*, 2020) or estimated using indirect acoustic method (Hudde, 1983). In theory, the EA model also requires the tympanic membrane acoustic impedance.

4.3.2 Electro-acoustic model associated with the proposed method

This section presents the EA model used in the proposed indirect method to estimate the centroid position of the earcanal wall normal velocity. This model is illustrated in Fig. 4.2 and consists of the earcanal coupled to an external capped duct. This model is adapted from a previous

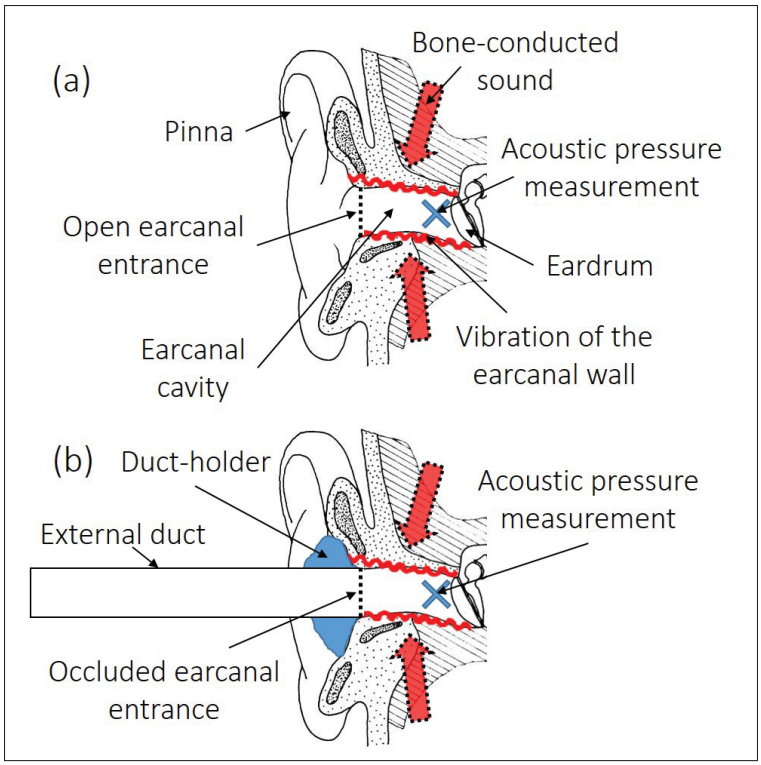

Figure 4.1 (a) Open and (b) occluded earcanal experimental setup associated with the indirect method proposed to estimate the centroid position of the earcanal wall normal velocity induced by a bone-conducted stimulation

model developed by the authors (Carillo *et al.*, 2020). The earcanal is considered as a circular cross-sectional duct of curvilinear length l_{EC} and radius $r_{EC}(z)$ where z is the earcanal middle axis. These parameters are calculated from the measured earcanal shape (Stinson & Lawton, 1989). The equivalent acoustic source Q represents the vibrating earcanal wall and is located at a position l_c which corresponds to the centroid position of the earcanal wall normal velocity (Carillo *et al.*, 2020). The earcanal downstream section goes from the eardrum to the source while the upstream section goes from the source to the earcanal entrance. An acoustic impedance $\hat{Z}_{TM}$ is defined at the eardrum. At low frequencies, the downstream section is governed by its compressibility effect of acoustic compliance C_d, associated with acoustic resistance R_d. The vibro-acoustic behavior of the earcanal upstream section depends on its inertia and

compressibility effects through the acoustic mass L_u and acoustic compliance C_u and their associated resistances $R_{u,vi}$ and $R_{u,th}$. Calculation of these constants is detailed in Carillo *et al.* (2020) (see Table 2.1 in Sec. 2.3.2.1). The vibro-acoustic behavior of the open earcanal upstream section also depends on the acoustic impedance $\hat{Z}_{duct}$ of the coupling duct seen from the earcanal. This acoustic impedance is given by $\hat{Z}_{duct} = -j\hat{Z}_{eq}^{duct} \cot\left(\hat{k}_{eq}^{duct} l_{duct}\right) \Big/ \left(\pi r_{duct}^2\right)$ with the duct length l_{duct}, its radius r_{duct}, the imaginary number j, and the equivalent wavenumber $\hat{k}_{eq}^{duct}$ and characteristic impedance $\hat{Z}_{eq}^{duct}$ accounting for visco-thermal losses in the duct, calculated using a low reduced frequency model detailed in Appx. VI. Since the duct inner cross-section is smaller than the earcanal entrance area, a discontinuity occurs at the earcanal entrance and implies an inertia effect at the medial aperture of the coupling duct. The acoustic mass of discontinuity is given by $L_{dis} = 8\rho_0 H(\alpha) \big/ \left(3\pi^2 r_{duct}\right)$ (Karal, 1953). $H(\alpha)$ corresponds to the correction factor of discontinuity as a function of α, the ratio between the duct and the equivalent earcanal entrance radius, and can be approximated by $H(\alpha) = 1 - 1.25\alpha$ for large discontinuities (Mechel, 2008) and to zero for negligible discontinuities.

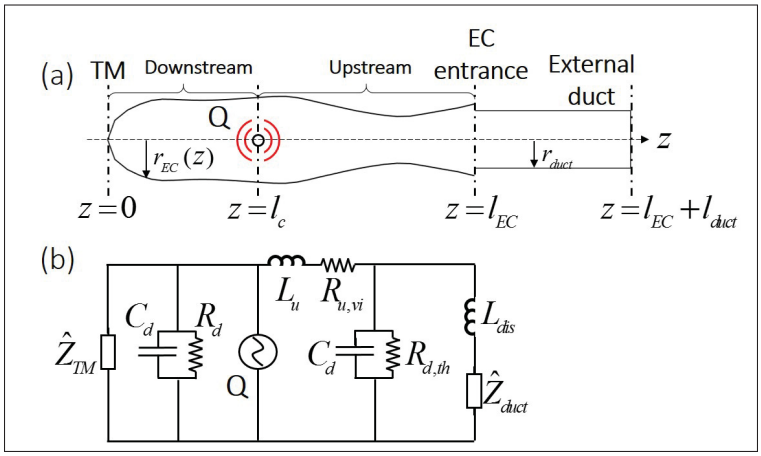

Figure 4.2 (a) Geometry of the earcanal coupled to the external capped duct and (b) its corresponding EA model. The tympanic membrane is indicated at $z = 0$

4.3.3 Numerical investigation of the indirect method

In this paper, the proposed indirect method is numerically investigated using an acousto-mechanical 3D FE model of the outer ear open and occluded by an external capped duct. Also, an associated purely acoustical 3D FE model is presented. This model considerably decreases the computational time and is therefore practical to study the influence of several parameters of the coupled system which could influence the accuracy of the method.

4.3.3.1 Acousto-mechanical model

The acousto-mechanical 3D FE model of an outer ear open and occluded by the external duct is presented here. This outer ear model has been constructed by Brummund *et al.* (2014) from cryosection images of a female cadaver from the Visible Human Project®. Recently, this model has been improved by the authors (Carillo *et al.*, 2020). The latter model is illustrated in Fig. 4.3(a) in the open case. The shape of the earcanal is also displayed in Fig. 4.4 assuming circular cross-sections. In the occluded case, the model is adapted here to include the external duct (see Fig. 4.3(b)). The earcanal is surrounded by skin, cartilaginous and bony tissues and a particular set of equivalent mechanical loading (reproducing a bone-conducted stimulation) and boundary conditions is defined to reproduce a "plausible" vibration pattern of the earcanal wall (Carillo *et al.*, 2020). The middle and inner ears are accounted for using the acoustic impedance $\hat{Z}_{TM}$ applied at the tympanic membrane and defined by Shaw and Stinson's model detailed in Appx. IV. The vibration of the TM and the ossicles induced by the bone-conducted stimulation are thus not accounted for. However, the contribution of this vibration to the sound pressure level (SPL) generated in the earcanal is not expected to have significant influence, at least at low frequencies below the middle ear resonance (Schroeter & Poesselt, 1986; Stenfelt *et al.*, 2002, 2003). In the open case, the acoustic impedance $\hat{Z}_{rad}$ is defined at the earcanal entrance plane to account for the acoustic radiation in the surrounding environment. In the occluded case, the coupling duct is made of aluminum whereas the duct holder is made of silicone and fills a portion of the concha ahead of the earcanal entrance plane. The external duct is coupled to the earcanal entrance in the normal direction and with a perfect seal. The outer surface of the

external duct portion which is not inserted in the duct holder is free. However, if the duct is too long, it should be held in position at its lateral end. The influence of the boundary condition (either free or fixed) defined at the lateral end circumference of the coupling duct (see Fig. 4.3(b)) is studied in Sec. 4.4.1.

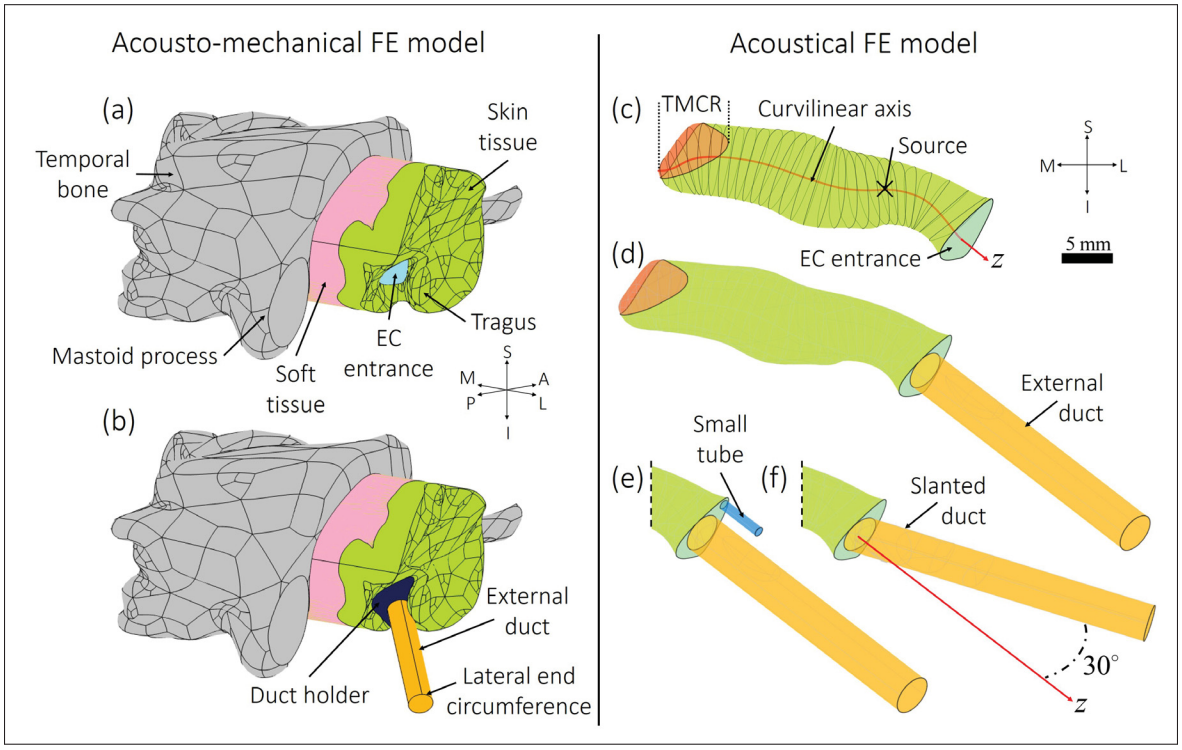

Figure 4.3 Acousto-mechanical FE model of the outer ear (a) open and (b) occluded by an external capped duct coupled to the earcanal entrance using a duct holder; purely acoustical FE model of the earcanal (c) open and (d) occluded by the external duct normal to earcanal entrance plane. In subplot (e), an incomplete seal between the earcanal cavity and the duct is accounted for as a small tube coupled to the earcanal entrance. In subplot (f), the orientation of the duct forms an angle of 30° with the normal to earcanal entrance plane. The coordinate system refers to superior (S), inferior (I), posterior (P), anterior (A), medial (M) and lateral (L)

4.3.3.2 Purely acoustical model

The purely acoustical 3D FE model of the earcanal open and occluded by the external capped duct is now presented (see Fig. 4.3(c) and (d)). The accuracy of the acoustical model is

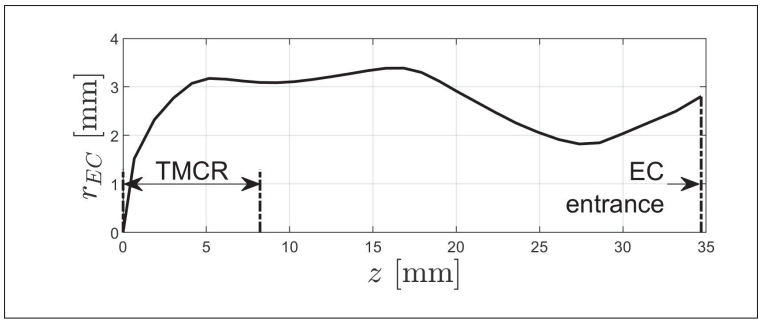

Figure 4.4 Earcanal radius $r_{EC}(z)$ of the 3D FE model assuming circular cross-section and displayed as a function of the earcanal middle axis z. The eardrum coupling region and the earcanal entrance are indicated

assessed against the acousto-mechanical model in Sec. 4.4.1. In the purely acoustical model, the earcanal and the coupling duct are rigidly walled (except the eardrum boundary where the acoustic impedance $\hat{Z}_{TM}$ is defined). The earcanal wall normal vibration is accounted for as an equivalent volume velocity source Q located on the earcanal middle axis at a curvilinear position $l_c^{FE} = 23.6$ mm. This location corresponds to the curvilinear position of the earcanal wall normal velocity centroid computed using the acousto-mechanical 3D FE model (Carillo *et al.*, 2020).

In practice, an incomplete seal could occur at the earcanal entrance since it is a common issue in hearing protection for example. The geometry of an incomplete seal is generally unknown and is expected to be intricate (Hansen, 1998). It can be made of several interconnected pathways (Macrae & McAlister, 1989). Here, this incomplete seal is modeled as a small tube of radius r_t and length l_t coupled to the earcanal entrance, in parallel with the external duct (see Fig. 4.3(e)). At the lateral end of the small tube, a radiation acoustic impedance of a circular baffled piston accounts for the coupling with the external environment. Furthermore, the external duct could be coupled in a direction that differs from the normal direction to the earcanal entrance cross-section (see Fig. 4.3(f)). The influence of the incomplete seal and the duct orientation is investigated in Secs. 4.4.2.5 and 4.4.2.3.

4.3.3.3 Finite element modeling and computation of indicators

In the acousto-mechanical 3D FE model, the sound propagation in solid domains is governed by the linear elasto-dynamics equation relating the linearized displacement field $\underline{\hat{u}}$, strain tensor $\underline{\underline{\hat{\xi}}}$, and stress tensor $\underline{\underline{\hat{\sigma}}}$ at all points of solid domains (Atalla & Sgard, 2015):

$$\underline{\nabla} \cdot \underline{\underline{\hat{\sigma}}} + \rho_s \omega^2 \underline{\hat{u}} = 0, \tag{4.1}$$

$$\underline{\underline{\hat{\sigma}}} = \underline{\underline{\underline{\underline{C}}}} : \underline{\underline{\hat{\xi}}}, \tag{4.2}$$

$$\underline{\underline{\hat{\xi}}} = \frac{1}{2}\left(\underline{\nabla}\,\underline{\hat{u}} + \left(\underline{\nabla}\,\underline{\hat{u}}\right)^T\right), \tag{4.3}$$

where ρ_s is the solid density, ω is the angular frequency, $\underline{\nabla}$ is the nabla operator and $\underline{\underline{\underline{\underline{C}}}}$ is the fourth-order stiffness (elasticity) tensor. In each solid domain, the structural damping is accounted for as a multiplier $(1 + j\eta_s)$ in the stiffness matrix where η_s corresponds here to the isotropic loss factor. Mechanical properties of skin, cartilaginous and bony tissues come from Brummund *et al.* (2014). Material properties of solid domains are summarized in Appx. II.

In both acousto-mechanical and purely acoustical 3D FE models, the sound propagation in acoustic domains is governed by Helmholtz equation:

$$\nabla^2 \hat{p} + \hat{k}_{eq}^2 \hat{p} = 0, \tag{4.4}$$

where $\hat{p}$ denotes the sound pressure and $\hat{k}_{eq}$ is the complex wavenumber accounting for viscous and thermal losses using a low reduced frequency model (see Appx. VI). Air properties used here are given in Appx. II.

At the interface between mechanical and acoustical domains, the continuity of stress is written as $\underline{\underline{\hat{\sigma}}}\,\underline{n} = -\hat{p}\,\underline{n}$, where $\underline{n}$ is the normal vector at the interface, whereas the continuity of normal displacements is given by $\frac{1}{\rho_0 \omega^2} \partial \hat{p} \Big/ \partial n = \underline{\hat{u}} \cdot \underline{n}$.

In the acousto-mechanical FE model, a standard ($\hat{\underline{u}}$, $\hat{p}$) formulation is used to solve for both displacements in solids and pressures in the fluid (Atalla & Sgard, 2015). In the purely acoustical FE model, the problem is only solved for pressures.

The geometry is meshed according to a criterion of at least six 10-noded (quadratic) tetrahedral elements per wavelength at 1 kHz (maximum frequency of interest). The wavelength, referred to as λ, is defined by $\lambda = c/f$ with c the sound speed and f the frequency. To minimize the size of the mesh in solid structures of the acousto-mechanical FE model, the minimum sound speed is taken between the compression and the shear wave speed defined respectively by

$$c_L = \sqrt{\frac{E(1-\nu)}{\rho(1+\nu)(1-2\nu)}}, \tag{4.5}$$

and

$$c_T = \sqrt{\frac{G}{\rho}}, \tag{4.6}$$

with E, ρ, ν and G the Young's modulus, density, Poisson's ratio and shear modulus respectively.

Figure 4.5 shows the mesh of both the acousto-mechanical FE model and the purely acoustical FE model using the mesh criteria previously detailed. It is noteworthy that the size of the mesh is also constrained to capture the geometry of each domain. A convergence study has been performed on both FE models to ensure the accuracy of simulation results presented in this paper. The current FE models have been solved using COMSOL Multiphysics® (Sweden).

The surface averaged acoustic pressure computed at the tympanic membrane is referred to as $\left\langle \hat{p}_{TM}^{k} \right\rangle$, where $k \in \{open, occl\}$. Using the acousto-mechanical 3D FE model only, the centroid position vector is computed by (Carillo *et al.*, 2020)

$$\underline{x}_c = \frac{\int\limits_{S_{wall}} \underline{x} \left| \hat{v}_{n,wall}(\underline{x}) \right| \mathrm{d}S}{\int\limits_{S_{wall}} \left| \hat{v}_{n,wall}(\underline{x}) \right| \mathrm{d}S}. \tag{4.7}$$

where $\underline{x}$ is the position vector in 3D space, S_{wall} is the earcanal wall surface and $\hat{v}_{n,wall}(\underline{x})$ is the complex-valued earcanal wall normal velocity. From Eq. (4.7), the curvilinear position l_c^{FE} of the centroid position is obtained by the normal projection of $\underline{x}_c$ on the earcanal middle axis and it is used in the purely acoustical 3D FE model as mentioned previously.

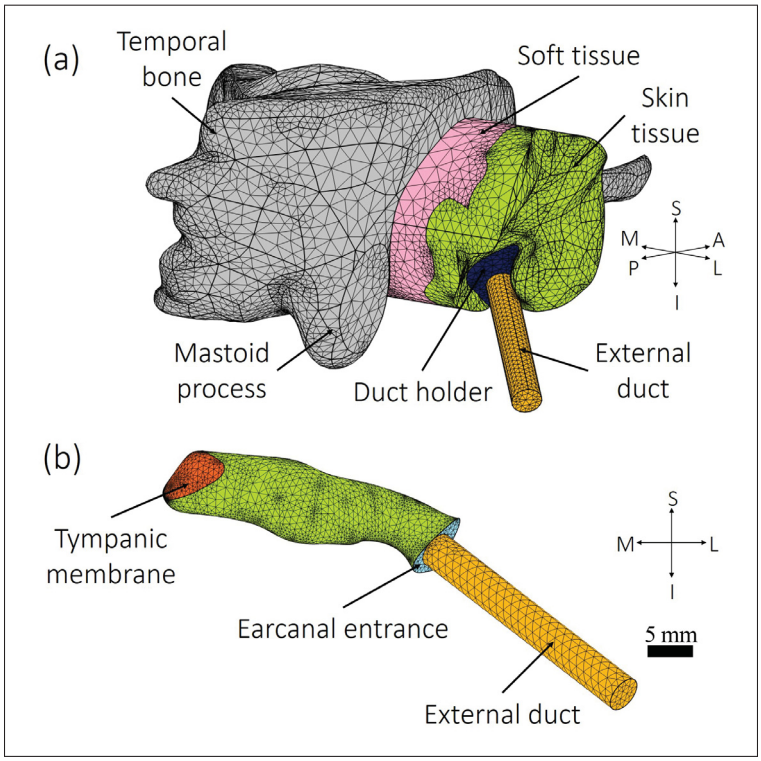

Figure 4.5 Mesh of (a) the acousto-mechanical and (b) purely acoustical 3D FE model of the outer ear occluded by the external duct. The coordinate system refers to superior (S), inferior (I), posterior (P), anterior (A), medial (M) and lateral (L)

4.4 Results and discussions

This section is organized as follows. In Sec. 4.4.1, the centroid position of the earcanal wall normal velocity is estimated using the inverse method proposed in this paper. In Sec. 4.4.2, the influence of several parameters of the coupling system is numerically investigated. Finally, Sec. 4.4.3 briefly discusses the main limitations of the work presented herein.

4.4.1 Estimation of the centroid position from acoustic pressure transfer function

In this section, the experimental setup (see Sec. 4.3.1) of the proposed method is simulated using both 3D FE models (see Sec. 4.3.3). The aim is to verify the accuracy of the purely acoustical FE model compared to the acousto-mechanical FE model taken as reference. Then, the centroid position of the virtual outer ear of interest is estimated using the associated EA model (see Sec. 4.3.2) and compared to the centroid position directly computed using the acousto-mechanical 3D FE model in order to validate the indirect method.

Figure 4.6(a) and (b) display respectively the level in dB and the phase of the tympanic membrane acoustic pressure transfer function between the earcanal open and occluded by an external capped duct computed as a function of frequency using the acousto-mechanical 3D FE model. Simulations considering both free (red squares) and fixed (blue stars) boundary conditions of the lateral end of the coupling duct are presented. The coupling duct has a length of 150 mm, an inner radius of 2 mm and a wall thickness of 0.2 mm and is normally coupled to the earcanal entrance with a perfect seal. Note that the level in dB (factor 20) of the tympanic membrane acoustic pressure transfer function corresponds to the objective OE. According to Fig. 4.6(a), the transfer function amplitude reaches a local minimum and a local maximum. Figure 4.6 also displays the results computed using the purely acoustical 3D FE model in which the earcanal wall normal vibration is modeled as an equivalent ideal source of volume velocity located at the centroid position of the corresponding vibration (see solid black line). This model gives the same results as the acousto-mechanical FE model (including both boundary conditions of the coupling duct), at least up to the transfer function local minimum frequency. Above this frequency, slight discrepancies are observed between both FE models due to the elastic modes of deformation of the coupling duct (not accounted for in the purely acoustical FE model). In the acousto-mechanical FE model, the boundary condition defined at the lateral end of the coupling duct (either free or fixed) is shown to have little influence on the results displayed in Fig. 4.6. According to Fig. 4.6(a) and (b), local extrema of the transfer function amplitude are associated with sudden phase shifts which characterize the occurrence of acoustic antiresonance (local

minimum at 516 Hz) and acoustic resonance (local maximum at 725 Hz) in the earcanal coupled to the duct.

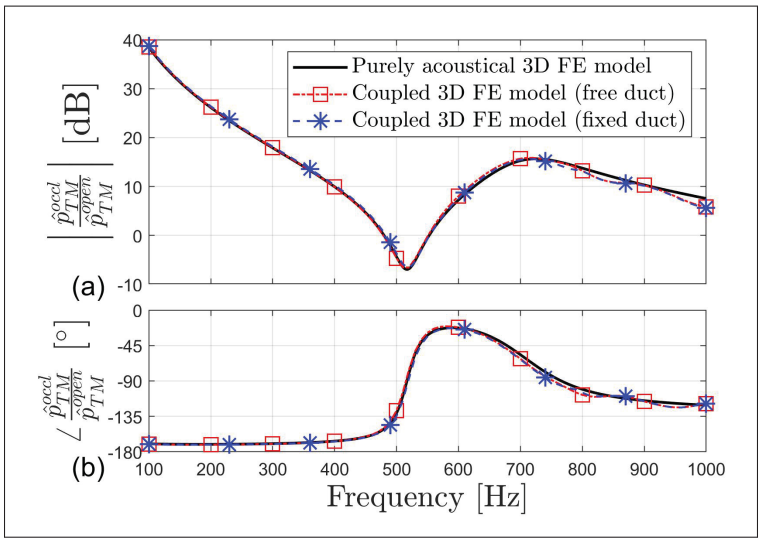

Figure 4.6 (a) Level in dB (factor 20) and (b) phase of the tympanic membrane acoustic pressure ratio between the occluded and the open earcanal computed using the acousto-mechanical and the purely acoustical 3D FE models. The occlusion is ensured by a capped duct coupled at the earcanal entrance of 150 mm length, 2 mm inner radius, and, in the acousto-mechanical model only, 0.2 mm wall thickness. In the acousto-mechanical model, the boundary condition at the external end of the duct is free or fixed

To illustrate these acoustic phenomena, Fig. 4.7 displays the acoustic pressure field (in dB) in the coupled system in (a) antiresonance and (b) resonance states computed using the purely 3D FE model. In Fig. 4.7(a), the acoustic pressure level is minimum in the region between the eardrum and the centroid position of the earcanal wall normal velocity and gradually increases to reach a maximum value at the capped lateral end of the duct. A quarter-wavelength acoustic resonance occurs in the earcanal upstream section (from the centroid position to the earcanal entrance) coupled to the external duct and corresponds to an antiresonance seen by the earcanal wall normal vibration which encounters a pronounced acoustic pressure dip at its centroid

position. The acoustic pressure is also approximately minimum up to the eardrum because the vibro-acoustic behavior of the earcanal downstream section (from the centroid position to the eardrum) is governed by its compressibility effect (Carillo *et al.*, 2020). In Fig. 4.7(b), the acoustic pressure level is maximum at both the eardrum and the capped lateral end of the coupling duct and minimum in between. This standing wave pattern is characteristic of a half-wavelength acoustic resonance of the whole coupled system excited by the earcanal wall normal vibration. Unlike resonance, antiresonance depends on the location of the source which corresponds to the centroid position of the earcanal wall normal vibration. Therefore, acoustic antiresonance can be used to estimate the centroid position.

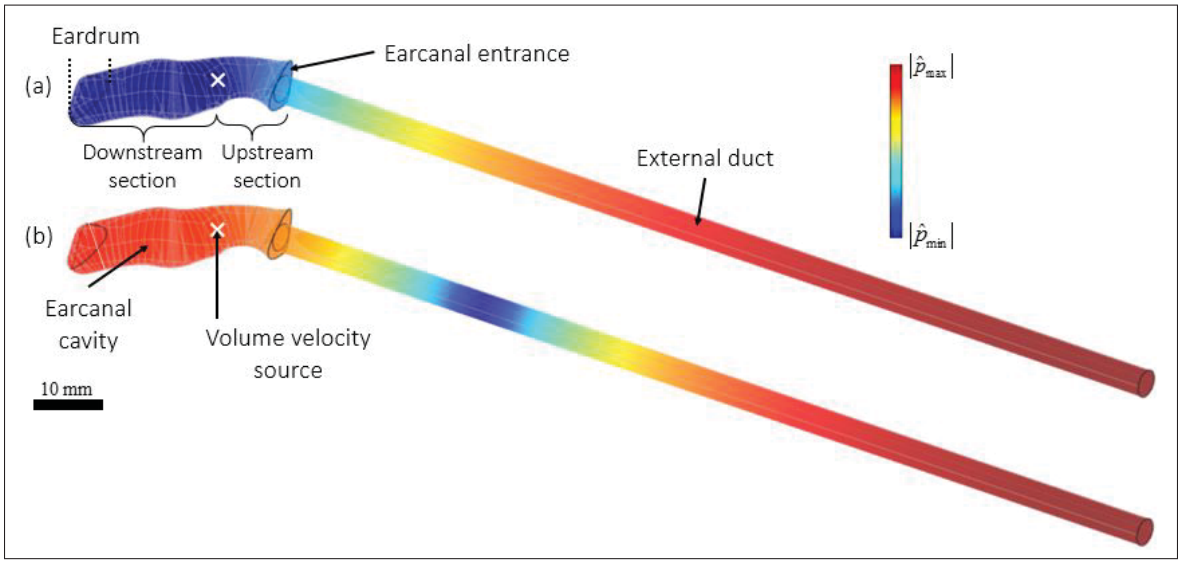

Figure 4.7 Acoustic pressure field in dB (factor 20) in the earcanal coupled to an external capped duct of length 150 mm and inner radius 2 mm in (a) antiresonance (516 Hz) and (b) resonance (725 Hz) states computed using the acoustical 3D FE model

To the authors' knowledge, no experimental data of the transfer function displayed in Fig. 4.6 exist in the literature. Huizing (1960), however, measured the objective OE induced by an external capped duct on a human subject for several duct lengths for a bone-conducted stimulation at a frequency 1 kHz. Huizing conducted this experiment to highlight a standing wave pattern in the earcanal. In Appx. IX, Huizing's experiment is simulated using the purely acoustical 3D FE model and both simulated and measured objective OE are shown to be in relatively

good agreement. Huizing interpreted OE minima as acoustic resonances with an acoustic pressure node at the eardrum. Several years after Huizing, Tonndorf (1964) reproduced this experiment and obtained similar results which were interpreted in the same way, assuming a low enough acoustic impedance of the tympanic membrane. However, as previously explained, OE minima rather come from acoustic antiresonances with an acoustic node at the centroid position of the earcanal wall normal velocity (see Fig. 4.7(a)). At antiresonance frequencies, the acoustic pressure is also minimum at the eardrum for the reason explained above (*i.e.*, earcanal downstream section governed by its compressibility effect).

The antiresonance frequency of the coupled system is then determined from the transfer function of Fig. 4.6 and corresponds to the amplitude minimum which is also associated with the sudden phase shift. For the 150 mm duct considered here, the antiresonance frequency is equal to 516 Hz. It is noteworthy that the antiresonance frequency could be determined directly from the acoustic pressure measured in the occluded earcanal. The use of the OE, however, has the advantage to avoid the influence of variations of the earcanal wall normal vibration (amplitude and phase) with frequency on the antiresonance frequency determination (not shown here).

From the antiresonance frequency determined using the 3D FE models (both models provide the same antiresonance frequency), the centroid position is estimated using the EA model. For this purpose, the antiresonance frequency of the coupled system is computed using the EA model as a function of the source position included between the tympanic membrane coupling region and the earcanal entrance. Then, the centroid position is obtained by minimizing the difference between the antiresonance frequency determined from the 3D FE model and that computed by the EA model as a function of the source position. In the configuration of interest, the EA model estimates the centroid position of the earcanal wall normal vibration with a difference of 0.3 mm compared to the 3D FE model. This difference does not come from a lack of convergence of the method (this has been checked but not shown here for conciseness), but is more likely due to the planar waves assumption used by the EA model. This assumption could be debatable mainly in the coupling region between the earcanal and the external duct and to a lesser extent in the tympanic membrane coupling region.

Regarding in particular the coupling region between the earcanal and the duct, the cross-sectional discontinuity is accounted for, in the EA model, as an inertia effect of acoustic mass L_{dis} added to the input acoustic impedance $\hat{Z}_{duct}$ of the duct (see Sec. 4.3.2). The acoustic mass is calculated from Karal's formula (Karal, 1953) developed for the coupling between two cylindrical ducts of constant radius. In the 3D FE model, however, the cross-section of the earcanal is not circular and its shape varies along the earcanal middle axis (see Fig. 4.4). Schmidt & Hudde (2009) underlined that the mass of discontinuity is critically dependent on the shape of the earcanal entrance region. Therefore, the EA model cannot exactly account for the influence of the earcanal entrance discontinuity and, in consequence, it cannot provide an exact estimation of the centroid position. A difference lower than 0.5 mm is however considered acceptable.

4.4.2 Influence of several parameters of the coupled system

This section investigates the influence of several parameters of the coupled system on the estimation of the centroid position using the proposed method. These parameters are the length of the duct, its radius, the duct orientation, the coupling position of the duct in the earcanal, the presence of an incomplete seal between the coupling duct and the earcanal entrance, the earcanal shape, the temperature in the coupled system and the earcanal downstream section and tympanic membrane acoustic impedance. In this section, the purely acoustical FE model is used instead of the acousto-mechanical FE model since it requires significantly less computational resources.

4.4.2.1 Length of the coupling duct and sensitivity of the indirect method

In the acousto-mechanical 3D FE model, the centroid position of the earcanal wall normal velocity does not significantly vary between 100 Hz and 1 kHz (Carillo *et al.*, 2020). In practice, however, it could be possible that the centroid position varies in the low-frequency range of interest. Since the proposed method estimates the centroid position at the antiresonance frequency of the coupled system, different duct lengths must be used to cover the frequency range (100 Hz to 1 kHz). Here, in addition to the 150 mm duct used in Sec. 4.4.1, two additional duct lengths are used: 750 and 75 mm. In the case of a 750 mm duct, several antiresonances

occur between 100 Hz and 1 kHz but only the lowest frequency is considered here. Table 4.1 presents the first antiresonance frequency $f_{antires}^{FE}$ of the earcanal coupled to these three external ducts and computed using the acoustical 3D FE model. The longer the coupling duct, the lower the first antiresonance frequency of the coupled system. The EA model is now used to estimate the centroid position from the antiresonance frequencies $f_{antires}^{FE}$. Table 4.1 presents the difference Δl_c between the centroid position l_c^{EA} estimated by the EA model and the effective centroid position l_c^{FE} used in the acoustical 3D FE model. According to Table 4.1, this difference is maximum for the longest duct (+1.2 mm) and minimum for the shortest (-0.1 mm). As discussed in Sec. 4.4.1, the error of estimation of the EA model mainly comes from the way the discontinuity at the earcanal entrance is accounted for between the earcanal and the coupling duct. The reason why this error increases with the length of the coupling duct is however related to the sensitivity of the method which is now investigated depending on the duct length.

Table 4.1 Antiresonance frequency of the coupled system depending on the external duct length computed using the 3D FE models. The centroid position estimated using the EA model is also presented in each case (relative to the effective position computed using the 3D FE model)

l_{duct} **[mm]**	$f_{antires}^{FE}$ **[Hz], FE model**	$\Delta l_c = l_c^{EA} - l_c^{FE}$ **[mm]**
750	104	+1.2
150	516	+0.3
75	980	−0.1

In order to illustrate the calculation of the method sensitivity, Fig. 4.8 displays the antiresonance frequency of the coupled system as a function of the source position l_c computed using the EA model for the three duct lengths (750, 150 and 75 mm). In practice, the centroid position is not expected to lie in the eardrum coupling region so this region is excluded from the variation range of the source. For each duct, the antiresonance frequency increases with l_c because the distance between the source and the capped lateral end of the duct decreases. More importantly, Fig. 4.8 shows that the range of variation of the antiresonance frequency is minimum for the longest duct and maximum for the shortest duct. The antiresonance frequency of the coupled system is

more sensitive to a variation of the centroid position when the coupling duct is short and vice versa. The mean sensitivity of the method, referred to as $\bar{\sigma}$ and expressed in Hz mm^{-1}, can be computed as the ratio between the antiresonance frequency interval and the source position interval. For the 750 mm duct, $\bar{\sigma} = (105 - 103)/(34.7 - 8) \approx 0.1$ Hz mm^{-1}. For the 150 mm, the mean sensitivity of the method is equal to approximately 2 Hz mm^{-1} and to about 8 Hz mm^{-1} for the 75 mm duct. It is not yet certain with which precision the centroid position should be estimated. It surely depends on the use of this position (*e.g.*, input of an EA model, validation of a FE model, study of the influence of a bone-conducted source to the earcanal wall vibration distribution). It is certain, however, that the antiresonance frequency cannot be identified from experimental data with an accuracy of 0.1 Hz. In fact, it would be probably tricky to obtain the antiresonance frequency with an accuracy of 1 Hz. In this condition, it could not be possible to accurately estimate the centroid position with the proposed method below approximately 500 Hz (*i.e.*, for a coupling duct longer than 150 mm). In the following, the 750 mm duct is therefore not considered anymore.

4.4.2.2 Inner radius of the coupling duct

In previous simulations, the inner radius of the duct has been chosen equal to 2 mm and corresponds to the largest admissible duct radius for the earcanal entrance considered here. In this section, the influence of the duct radius on the mean sensitivity of the method is investigated. Figure 4.9 displays the mean sensitivity of the method as a function of the duct radius computed using the EA model for two lengths of the coupling duct (150 and 75 mm). The duct radius r_{duct} decreases from the equivalent radius r_{EC} (l_{EC}) = 2.8 mm of the earcanal entrance (assuming circular cross-section) to almost 0.5 mm. For each duct radius, the mean sensitivity of the method is higher for the 75 mm duct compared to the 150 mm duct for the reason explained in Sec. 4.4.2.1. For both ducts, the mean sensitivity of the method would be maximum if the duct could have the same radius as the earcanal entrance (assuming circular cross-section). The mean sensitivity tends to zero when the duct radius diminishes. Indeed, when the radius of the coupling duct decreases, the modulus of its acoustic impedance $\hat{Z}_{duct}$ seen from the earcanal entrance increases,

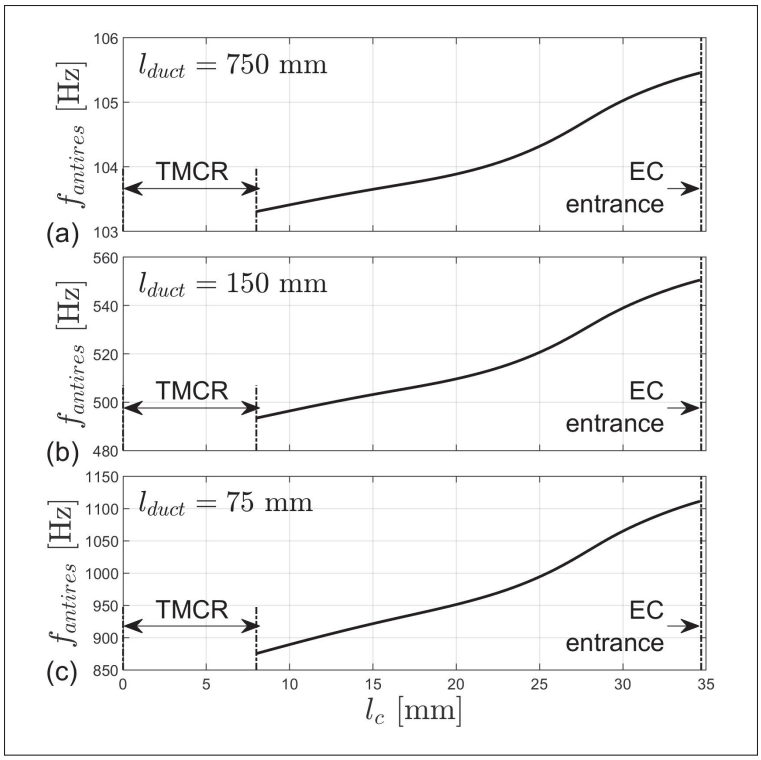

Figure 4.8 Antiresonance frequency computed as a function of the source position comprised between the eardrum coupling region and the earcanal entrance using the EA model for three duct lengths. In each case, the duct inner radius is equal to 2 mm

mainly due to (i) the sudden change in section between the earcanal entrance and the duct and (ii) the augmentation of visco-thermal losses in the coupling duct. In consequence, the earcanal upstream section gradually shifts from a mass-controlled vibro-acoustic behavior governed by the acoustic mass L_u to a compliance-controlled vibro-acoustic behavior dominated by the acoustic compliance C_u (see Fig. 4.2(b)). The antiresonance frequency of the coupled system thus tends to the quarter-wavelength resonance of the external duct and becomes independent from the centroid position. Since the influence of the centroid position on the antiresonance frequency of the coupled system vanishes when the duct radius decreases, the mean sensitivity of the method tends to zero (see Fig. 4.9). For small enough duct radius (below approximately 0.5 mm), the antiresonance phenomenon itself vanishes in the low-frequency range of interest

because there is no more wave propagation in the coupling duct due to visco-thermal damping and the earcanal coupled to the duct behaves as if the earcanal were occluded at its entrance (no coupling duct). To perform the method and maximize its accuracy, the outer radius of the coupling duct must be chosen as large as possible (in the limit, however, of the size of the earcanal entrance) whereas the thickness of its wall should be minimum.

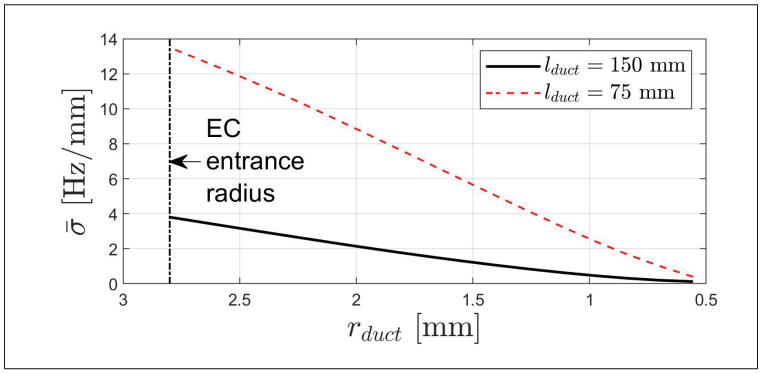

Figure 4.9 Mean sensitivity of the indirect method computed using the EA model as a function of the duct radius for two lengths of the external duct (150 and 75 mm)

4.4.2.3 Orientation of the coupling duct

In previous simulations, the direction of the coupling duct has been assumed normal to the plane of the earcanal entrance. In practice, however, when the contemplated physical measurements are made, the direction of the duct is constrained by the pinna and the tragus. Therefore, it would be certainly difficult, if not impossible, to ensure the coupling in the exact normal direction of the earcanal entrance plane. In this section, the influence of a variation of the duct direction on the accuracy of the method is studied for the two duct lengths 150 and 75 mm. For this purpose, the duct orientation is changed by 30° from the earcanal entrance normal direction (see Fig. 4.3(f)). Similarly to what proposed Schmidt & Hudde (2009), the rotation of the coupling duct is performed around a fixed point corresponding to the intersection of the earcanal middle axis and the earcanal entrance plane where the duct is coupled. Therefore, the

curvilinear length of the earcanal remains untouched, as well as the length of the coupling duct. The change in orientation increases, however, the area of the coupling between the earcanal entrance and the duct. Table 4.2 presents the corresponding change in antiresonance frequency computed using the 3D FE model. The coupling angle slightly increases the antiresonance frequency of the coupled system. Indeed, due to the increase of the coupling area, the associated acoustic mass of discontinuity decreases and therefore the apparent length of the coupled system also diminishes. Table 4.2 also presents the variation Δl_c of the centroid position induced by the change in orientation of the duct and estimated using the EA model from antiresonance frequencies predicted by the FE model. According to Table 4.2, Δl_c is close to 0.3 mm for each duct. The method proposed here to estimate the centroid position of the earcanal wall normal velocity is thus little influenced by the duct orientation in the range of variation considered here.

Table 4.2 Influence of the duct orientation on the antiresonance frequency computed using the 3D FE model. The influence on the centroid position estimated using the EA model is also presented

l_{duct} **[mm]**	$f^{FE}_{antires}$ **[Hz], normal direction**	$f^{FE}_{antires}$ **[Hz], 30° slanted**	Δl_c **[mm]**
150	516	516.5	+0.3
75	980	982	+0.3

4.4.2.4 Coupling position of the external duct

In previous simulations, the external capped duct has been exactly coupled to the earcanal entrance plane. In practice, however, the coupling position of the duct could be slightly more inside or outside the earcanal compared to the chosen position of the earcanal entrance plane used in the EA model involved in the indirect method. This section thus investigates the influence of this uncertainty on the estimated centroid position. Table 4.3 presents the change in antiresonance frequency of the coupled system computed using the EA model due to a shift in the coupling position from +3 mm (outward the earcanal entrance plane) to −3 mm (inward the earcanal entrance plane). Two lengths of coupling duct are considered (150 and 75 mm). In each case, the inner radius of the duct is equal to 2 mm. For both ducts, the antiresonance frequency

is the highest when the coupling position is the farthest inside the earcanal (see Table 4.3). This is explained by the reduction of the distance between the centroid position and the lateral capped end of the duct. Table 4.3 also presents the variation Δl_c of the estimated centroid position due to an error in the coupling position. The estimation is performed using the EA model assuming that the external duct is exactly coupled to the earcanal entrance plane (*i.e.*, a coupling position variation of 0 mm). When the effective coupling position is shifted outside the earcanal, the centroid position is estimated further in the earcanal, and vice versa (see Table 4.3). Also, the error in the estimated centroid position is lower than the coupling position shift (in absolute value). This error, however, depends on the earcanal shape and tends to be equal to the coupling position shift when the earcanal shape is straight (not shown in Table 4.3). The maximum error in the estimated centroid position is thus bounded by the coupling position shift.

Table 4.3 Influence of the coupling position (relative to the earcanal entrance position) on the antiresonance frequency computed using the EA model. The influence on the centroid position estimated using the EA model is also presented

l_{duct} **[mm]**	**Coupling position [mm]**	$f^{EA}_{antires}$ **[Hz]**	Δl_c **[mm]**
150	+3	513	−1.9
	+1.5	514	−0.8
	0	517	0
	−1.5	520	+0.9
	−3	523	+2.3
75	+3	962	−2.2
	+1.5	970	−1.2
	0	979	0
	−1.5	991	+0.9
	−3	1 005	+2.3

4.4.2.5 Incomplete seal at the earcanal/duct junction

In previous simulations, a perfect seal has been assumed between the coupling duct and the earcanal wall at the earcanal entrance. In this section, the influence of an incomplete seal on the accuracy of the method is investigated using the 3D FE model for two duct lengths 150 and

75 mm. The incomplete seal is modeled as a small cylindrical tube of radius r_t and length l_t coupled at the earcanal entrance in parallel with the external coupling duct (see Fig. 4.3(e)). Two "plausible" values of radius (0.4 and 0.6 mm) and length (5 and 10 mm) are chosen to illustrate the influence of an incomplete seal. Table 4.4 presents the change in antiresonance frequency computed using the 3D FE model. Table 4.4 also presents the variation Δl_c of the centroid position induced by incomplete seals and estimated using the EA model from antiresonance frequencies predicted by the FE model. According to Table 4.4, the influence of the incomplete seal on the estimated centroid position is similar for each coupling duct. In addition, this influence decreases when the length of the incomplete seal increases and when its radius decreases. This phenomenon is due to the augmentation of both the acoustic mass and the acoustic resistance of the incomplete seal which increases its acoustic impedance and thus decreases the volume velocity transfer through it. The influence of an incomplete seal on the acoustic pressure field of the coupled system is small around the antiresonance frequency because the acoustic pressure is already minimum in the earcanal (see Fig. 4.7(a)). The influence of an incomplete seal is rather of significant importance when the acoustic pressure is maximum in the earcanal (*e.g.*, at low frequencies for an occlusion ensured at the earcanal entrance (Hansen, 1998)). However, in order to maximize the accuracy of the proposed method, an incomplete seal must be avoided as much as possible. The quality of the seal could be assessed using fit-testing method developed for hearing protection (Voix & Hager, 2009; Trompette, Kusy & Ducourneau, 2015).

4.4.2.6 Straight cylindrical earcanal versus 3D earcanal shape

In previous simulations, the shape of the earcanal was perfectly known. If the 3D shape could not be measured, could the earcanal be assumed to a straight cylinder? This section investigates the error of estimation of the centroid position associated with this assumption. For this purpose, a straight earcanal of constant radius 2.8 mm and length 34.7 mm is used. The radius corresponds to the equivalent radius of the 3D earcanal entrance (assuming circular cross-section) whereas the length is equal to the curvilinear length of the 3D earcanal. Table 4.5 presents the antiresonance

Table 4.4 Influence of an incomplete seal between the duct and the earcanal entrance on the antiresonance frequency computed using the 3D FE model. The incomplete seal is modeled as a small tube of radius r_t and length l_t connected to the earcanal entrance in parallel with the coupling duct. The influence on the centroid position estimated using the EA model is also presented

l_{duct} **[mm]**	$f^{FE}_{antires}$ **[Hz], perfect seal**	$f^{FE}_{antires}$ **[Hz], incomplete seal**	Δl_c **[mm]**
150	516	518	+0.9
		517	+0.5
		520	+1.8
75	980	986	+0.7
		983	+0.4
		992	+1.4

frequency of the coupled system using the 3D earcanal shape and the straight earcanal for two duct lengths (150 and 75 mm). For both coupling ducts, higher antiresonance frequencies are obtained with the straight earcanal compared to the real 3D earcanal shape. Due to the absence of constriction close to the earcanal entrance in the straight earcanal compared to the 3D earcanal shape (see Fig. 4.4), the acoustic mass of the earcanal upstream section is smaller in the former than the latter earcanal. In consequence, the effective length of the earcanal upstream section appears smaller in the straight earcanal than in the 3D earcanal shape, explaining the antiresonance frequencies difference between both.

Table 4.5 also presents the influence of the earcanal shape on the estimated centroid position. The estimation is performed from antiresonance frequencies of the 3D earcanal shape coupled to the external ducts using the EA model which assumes a straight earcanal. According to Table 4.5, neglecting the 3D earcanal shape induces significant errors in the estimation of the centroid position (around 8 mm towards the eardrum) and, therefore, cannot be neglected. The magnitude of this error, however, depends on the individual earcanal shape and how the latter differs from a cylindrical shape.

Table 4.5 Influence of the earcanal shape on the antiresonance frequency computed using the EA model. The influence on the centroid position estimated using the EA model is also presented

l_{duct} **[mm]**	$f^{EA}_{antires}$ **[Hz], 3D earcanal shape**	$f^{EA}_{antires}$ **[Hz], straight earcanal**	Δl_c **[mm]**
150	517	543	−8.5
75	979	1 083	−7.4

4.4.2.7 Temperature in the coupled system

Air properties used in previous simulations approximately correspond to ambient temperature 19°C, atmospheric pressure 1013 hPa and relative humidity 20%. Appendix. X details the calculation of air properties from temperature, atmospheric pressure and relative humidity. These values can be easily measured during the experiment. An uncertainty exists, however, regarding the temperature in the earcanal occluded by the coupling duct. Indeed, assuming that the temperature of the earcanal wall is close to 37°C while the ambient temperature is equal to 19°C, a gradient of temperature occurs between the earcanal and the coupling duct. Also, this gradient could change during the measurement, depending on the measurement duration, due to heat transfer by convection.

In this section, the effect of the temperature is investigated. For this purpose, two additional configurations are proposed: (i) the temperature in the earcanal is equal to T_{EC} = 37°C whereas the temperature in the coupling duct is equal to T_{duct} = 19°C and (ii) the temperature in the coupled system is homogenous and equal to 37°C. Table 4.6 presents the change in antiresonance frequency of the coupled system computed using the EA model due to the variation in temperature. The augmentation of the temperature in the earcanal only or in the entire coupled system increases the antiresonance frequency. This is mainly explained by the increase of sound speed with temperature from 343 to 354 m s^{-1}. Table 4.6 also presents the variation Δl_c of the estimated centroid position induced by the change in antiresonance frequency due to the temperature. The estimation is performed using the EA model and assuming a homogeneous temperature of 19°C in the entire coupled system as reference. According to Table 4.6, an error

in temperature of the earcanal only has little effect on the estimation of the centroid position (Δl_c = 0.6 mm for both coupling ducts). However, the same error in temperature in the entire coupled system has more influence (Δl_c = 4.8 mm for the 150 mm duct and Δl_c = 2.7 mm for the 75 mm duct). The knowledge of the temperature in the earcanal is thus of lesser importance than that in the coupling duct.

Table 4.6 Influence of the temperature on the antiresonance frequency of the coupled system computed using the EA model. The influence on the centroid position estimated using the EA model is also presented

l_{duct} **[mm]**	**Temperature [°C]**	$f^{EA}_{antires}$ **[Hz]**	Δl_c **[mm]**
150	$T_{EC} = T_{duct} = 19$	517	0
	$T_{EC} = 37, T_{duct} = 19$	518	+0.6
	$T_{EC} = T_{duct} = 37$	533	+4.8
75	$T_{EC} = T_{duct} = 19$	979	0
	$T_{EC} = 37, T_{duct} = 19$	986	+0.6
	$T_{EC} = T_{duct} = 37$	1 010	+2.7

4.4.2.8 Earcanal downstream section and eardrum acoustic impedance

In previous sections, the EA model used to estimate the centroid position has accounted for both downstream and upstream sections of the earcanal. Since the acoustic antiresonance occurs in the earcanal upstream section coupled to the external duct, one may wonder if it is necessary to account for the earcanal downstream section and the acoustic impedance associated with the eardrum. Table 4.7 presents the change in centroid position estimated by the EA model when the eardrum only or the whole earcanal downstream section is assumed acoustically rigid. It is shown that using an infinite impedance instead of the tympanic membrane acoustic impedance implies an error of estimation in the centroid position lower than 0.2 mm for the 150 mm duct and negligible for the 75 mm duct. Neglecting the entire earcanal downstream section (*i.e.*, replacing its acoustic impedance by an infinite impedance) has also little influence on the centroid position estimation. Therefore, this method does not require the knowledge of the tympanic membrane acoustic impedance (for an intact ear). This is good to know since the latter can be difficult to

obtain with accuracy (Schmidt & Hudde, 2009). In addition, the EA model does not require the shape of the earcanal downstream section to estimate the centroid position. However, since the centroid position is *a priori* unknown before its estimation, the earcanal shape must be known at least up to the tympanic membrane coupling region.

Table 4.7 Influence of the earcanal downstream section and tympanic membrance acoustic impedance on the centroid position estimated by the EA model

l_{duct} **[mm]**	**Configuration**	Δl_c **[mm]**
150	Rigid eardrum	−0.2
	Rigid earcanal downstream section	−0.4
75	Rigid eardrum	−0.04
	Rigid earcanal downstream section	−0.1

4.4.3 Limitations

The indirect method proposed in this paper has been evaluated and investigated using a 3D FE model of a single outer ear open and occluded by an external capped duct. The FE model has been used (i) to simulate the measurement and compute the antiresonance frequency from which the EA model estimates the centroid position and (ii) as a reference to compare the theoretical and the centroid position estimated using the EA model. The acousto-mechanical 3D FE model accounts for the surrounding tissues of the earcanal, the external capped duct and its duct holder, and also the bone-conducted stimulation. However, this model is still a simplification of a real outer ear submitted by bone-conduction. In particular, this model is truncated so the influence of the whole head vibration has not been accounted for in this study. Also, it is certain that the determination of the acoustic antiresonance of the coupled system will be more difficult due to the presence of noise in measurement data and to the post-treatment process, contrary to FE simulations. In addition, several sources of uncertainty have been highlighted here and will affect to some extent the accuracy of the method in practice. Furthermore, a stimulation by bone-transducer has been assumed here. However, the method could be used to study the influence of the type of bone-conducted stimulation on the outer ear pathway and, in particular,

on the OE. Therefore, stimulation by chewing or speech could be required. However, lower jaw movement implies large deformation of the earcanal (Darkner, Larsen & Paulsen, 2007; Bouchard-Roy, Delnavaz & Voix, 2020). In consequence, the position of both the coupling duct (compared to the chosen earcanal entrance plane) and the centroid of the earcanal wall normal vibration could vary during the measurement. In addition, incomplete seal could occur due to lower jaw movement and therefore affect the accuracy of the method. Furthermore, since the same bone-conducted stimulation could not be exactly obtained between open and occluded measurements for chewing or speech, the acoustic pressure should be simultaneously measured in one ear open and in the other occluded by the coupling duct, such as in the "real-time" OE measurement (Saint-Gaudens *et al.*, 2019). This method, however, assumes a symmetry between ears (with respect to the sagittal plane) in terms of geometry and bone-conducted propagation whereas differences could be expected.

4.5 Conclusion

In this paper, the principle of an indirect method has been proposed to estimate the centroid position of the human earcanal wall normal velocity induced by a bone-conducted stimulation at low frequencies (100 Hz – 1 kHz). The centroid position can be used as an indicator of the earcanal wall normal vibration distribution to study the influence of the bone-conduction stimulation on the outer ear pathway and on the OE. Firstly, the indirect method consists in determining the frequency of the lowest local minima of the eardrum acoustic pressure transfer function between the earcanal open and occluded by an external capped duct coupled to the earcanal entrance. These local minima correspond to acoustic antiresonances occurring in the earcanal coupled to the duct and are associated with sudden phase shift. Secondly, the centroid position is estimated at the lowest antiresonance frequency using an EA model associated to the coupled system *in situ*. The estimation consists in minimizing the difference between the antiresonance frequency measured and that estimated using the EA model. In this paper, the method has been evaluated and investigated numerically using an acousto-mechanical 3D FE model of the earcanal open and occluded by the external capped duct. The sensitivity of the

method has been shown to increase with frequency and could be sufficient, in practice, to estimate the centroid position above 500 Hz. To maximize the accuracy of the method, the radius of the coupling duct must be as large as possible (in the limits of the earcanal entrance dimension) and any incomplete seal between the duct and the earcanal should be avoided. Also, the earcanal shape, the coupling position between the earcanal and the duct and the temperature in the coupling duct must be known as precisely as possible. On the contrary, the tympanic membrane acoustic impedance is not required to estimate the centroid position in an intact ear. While this study has presented the principle of the method and its numerical investigation, a future work will be dedicated to its experimental application on artificial ears and human subjects.

4.6 Acknowledgments

The authors acknowledge the support of the Natural Sciences and Engineering Research Council of Canada (NSERC), [funding reference number RGPIN-2016-06795]. Also, the authors want to thank gratefully Elliott Berger for his wise comments.

CHAPTER 5

NUMERICAL INVESTIGATION OF THE EARPLUG CONTRIBUTION TO THE LOW-FREQUENCY OBJECTIVE OCCLUSION EFFECT INDUCED BY BONE-CONDUCTED STIMULATION

Kévin Carillo[a] , Olivier Doutres[a] , Franck Sgard[b]

[a] Department of Mechanical Engineering, École de technologie supérieure,
1100 Notre-Dame Ouest, Montréal, Québec, Canada H3C 1K3
[b] Direction Scientifique, Institut de recherche Robert-Sauvé en santé et en sécurité du travail,
505 Boulevard de Maisonneuve Ouest, Montréal, Québec, Canada H3A 3C2

Paper submitted for publication to *Journal of the Acoustical Society of America*, December 2020
(second revision submitted in July 2021).

5.1 Abstract

The use of earplugs is commonly associated with an increased perception of the bone-conducted part of one's own physiological noise. This phenomenon is referred to as the occlusion effect and is most prominent at low frequencies. Several factors influence the occlusion effect such as the ear anatomy, the bone-conducted stimulation and the type of occlusion device, its fit, insertion depth and material properties. The latter factor is of great interest in order to potentially reduce the occlusion effect of passive earplugs. This paper investigates the mechanism(s) of contribution of earplugs to the objective occlusion effect. A 2D axi-symmetric finite element model of the outer ear is used and investigated in an electro-acoustic framework. Simulation results are shown to compare reasonably well with measurement data, which qualifies the model to study the influence of earplugs on the occlusion effect. Two mechanisms are highlighted: (i) a Poisson effect induced by the normal component of the earcanal wall vibration and (ii) a longitudinal motion caused by the tangential component of the earcanal wall vibration. By varying the geometry of the surrounding tissues, the spatial distribution of the earcanal wall vibration is shown to influence the contribution of the earplug to the occlusion effect.

5.2 Introduction

The use of earplugs is commonly accompanied by an increased perception of the bone-conducted part of one's own physiological noise (*e.g.*, one's own voice, chewing, heartbeat, etc.), a phenomenon called occlusion effect (OE) (Berger, 2003). This phenomenon is most significant at low frequencies (<1 kHz) for shallow occlusion and is deemed to be a notable source of discomfort, especially to workers wearing earplugs (Doutres *et al.*, 2019). As a consequence, these hearing protection devices may not be worn consistently and/or correctly (Doutres *et al.*, 2019). The name "OE" encompasses several descriptions of the phenomenon: (i) objective OE defined as the sound pressure level (SPL) difference measured by placing a microphone at or near the eardrum between occluded and open configurations (Bàràny, 1938; Huizing, 1960; Stenfelt & Reinfeldt, 2007; Reinfeldt *et al.*, 2013; Brummund *et al.*, 2015), (ii) subjective OE defined as the difference between the open and occluded hearing thresholds (Huizing, 1960; Berger & Kerivan, 1983; Stenfelt & Reinfeldt, 2007; Reinfeldt *et al.*, 2013), and (iii) perceptive OE related to the discomfort induced by the phenomenon and commonly quantified using questionnaires (Brown-Rothwell, 1986; Conrad & Rout, 2013). The perceptive OE is certainly the most important to reduce since it is directly related to the acoustical comfort dimension of earplugs' wearers. Both subjective and perceptive OE involve all bone-conduction pathways whereas the objective OE only involves the outer ear pathway. Since (i) this study focuses on the alteration of the outer ear pathway, and (ii) the outer ear pathway dominates the hearing by bone-conduction when the earcanal is occluded (Stenfelt *et al.*, 2003), this paper only deals with the objective OE, hereafter simply referred to as the OE for the sake of conciseness.

At low frequencies, the fundamental mechanism of the OE induced by an acoustically rigid occlusion of the earcanal entrance is explained by the acoustic impedance increase from the mass-controlled open earcanal to the compliance-controlled occluded earcanal. This impedance increase is responsible for the augmentation of the sound pressure radiated by the vibrating earcanal wall in the occluded case compared to the open one (Stenfelt & Reinfeldt, 2007; Berger & Kerivan, 1983; Carillo *et al.*, 2020; Hansen, 1998; Zurbrügg *et al.*, 2014). Several factors are known or are *a priori* expected to influence the OE and to explain its large variability

documented in the literature: (i) the ear anatomy (*e.g.*, the earcanal geometry (Zurbrügg *et al.*, 2014), the distribution and properties of the tissues surrounding the earcanal (Stenfelt *et al.*, 2003; Carillo *et al.*, 2019), (ii) the position (Reinfeldt *et al.*, 2013) and nature (Hansen, 1998) of the bone-conducted stimulation, and (iii) the type of occlusion device (Schroeter & Poesselt, 1986; Stenfelt & Reinfeldt, 2007), its fit (Hansen, 1998; Sgard *et al.*, 2019), insertion depth (Stenfelt & Reinfeldt, 2007; Brummund *et al.*, 2014), and material properties (Hansen, 1998; Lee, 2011; Brummund *et al.*, 2015). While the two first groups of factors are intrinsic to the wearer of earplugs and cannot be changed in practice, the third set of factors related to the contribution of the earplug on the OE is of great interest in order to reduce this phenomenon and increase the acoustic comfort of earplugs.

To the authors' knowledge, Bàràny (1938) was the first to suggest, in 1938, that the sound pressure generated in the earcanal occluded by an earplug could be caused by its vibration in the earcanal cavity, rather than generated only by the normal vibration of the "free" earcanal wall (*i.e.*, the portion not covered by the earplug (Békésy, 1932, 1960). Since then, few studies have been dedicated to understanding the earplug influence on the OE (Hansen, 1998; Lee, 2011; Lee & Casali, 2011; Brummund *et al.*, 2015; Sgard *et al.*, 2019). These studies are now discussed.

Hansen (1998) carried out OE experimental measurements on human subjects using a continuous speech, nasal sound and chewing stimulation for both foam and custom acrylic earplug at medium insertion. The OE was found 5 to 15 dB lower for the foam compared to the acrylic earplug at low frequencies. In order to explain the phenomenon, Hansen developed a lumped element model of the occluded earcanal. As a first step, the acoustical effect of the earplug on the earcanal SPL was modeled as an acoustic impedance, assuming that the sound pressure was solely generated by the "free" earcanal wall surrounding the occluded earcanal cavity. By measuring the acoustic impedance of a foam earplug, Hansen showed that its medial surface was seen as an acoustically rigid surface from the occluded earcanal cavity. Hansen concluded that if a foam earplug has an infinite impedance, then so does a silicone earplug. Hence, the OE difference between both earplugs cannot be explained by the acoustic impedance of their medial surface. Hansen then

hypothesized two other mechanisms of contribution of the earplug to the occluded earcanal SPL. In the first mechanism, Hansen (1998) assumed that the earplug vibrates as a rigid body (at least at low frequencies) in the longitudinal direction (*i.e.*, earcanal central axis) depending on its mass (similar to what was suggested by Bàràny (1938)) and on the elasticity of the earcanal wall surrounding tissues covered by the earplug. However, Hansen's model predicted a decrease of the occluded earcanal SPL when the earplug mass increased whereas the opposite was observed experimentally (the acrylic earplug was heavier than the foam earplug but generated the greatest OE). Hansen concluded that the vibration of the medial earplug surface did not contribute to the occluded earcanal SPL. However, the influence of other earplug mechanical properties was not investigated since the earplug was considered to be rigid. In the second mechanism, while considering that the whole (open or occluded) earcanal wall vibration acted as an ideal source of volume velocity, Hansen proposed that the mass of the earplug decreased the vibration of the portion of the earcanal wall coupled to the earplug, thus increasing the vibration of the "free" earcanal wall (not coupled to the earplug). By this mechanism, Hansen's model predicted that a heavy earplug caused a higher OE compared to a light earplug, such as a silicone earplug compared to a foam earplug. The role of the earplug mass attributed by Hansen to the OE is, however, in contradiction with an experimental work provided by Watson & Gales (1943) who showed that there is no direct relation between the earplug mass and the resulting OE. Also, the assumption proposed by Hansen (1998) considering that the whole earcanal wall vibration acts as an ideal volume velocity source seems debatable when the earcanal wall is coupled to the earplug. The presence of the earplug could rather be expected to decrease the vibration of the whole earcanal wall.

In an attempt to understand the influence of the earplug on the OE, Brummund *et al.* (2015) investigated the difference in OE between a foam and a silicone earplug at medium insertion, both experimentally and numerically using a 2D axi-symmetric FE model of the outer ear which accounts for anatomical tissues surrounding the earcanal cavity. Simulations showed that most of the acoustic power dissipated at the eardrum was injected by the medial earplug surface rather than the "free" earcanal wall surface, especially for the silicone earplug compared to the foam

earplug. Brummund *et al.* concluded that the contribution of the "free" earcanal wall was of secondary importance compared to the contribution of the medial earplug surface, at least for medium insertion, contrary to what Hansen (1998) proposed. However, Brummund *et al.* did not explain how the earplug contributed to the OE.

Lee & Casali (2011) carried out an experimental study to examine the influence of the earplug type on the OE for shallow and medium insertions. Experimental results showed that the influence of the earplug type significantly increased with insertion depth. These results demonstrated that the relative contribution between the "free" earcanal wall and the medial earplug surface depends on the insertion depth of the earplug. Sgard *et al.* (2019) observed the increase of the earplug influence on the OE with insertion depth using the FE model developed by Brummund *et al.* (2015). In the limits of the model (discussed along this paper), FE simulations showed that the earplug did not significantly influence the vibration of the "free" earcanal wall. This emphasized that the influence of the earplug on the OE is directly driven by radiation of the medial earplug surface in the occluded earcanal cavity. However, the vibro-acoustic behavior was investigated and interpreted in terms of acoustic power flow in the occluded earcanal cavity. This approach revealed intricate acoustic power exchanges, in particular between the medial earplug surface and the "free" earcanal wall, but did not explain the mechanism(s) of contribution of the earplug.

This paper is a continuation of previous studies (Brummund *et al.*, 2015; Sgard *et al.*, 2019) and focuses on the understanding of the influence of the earplug on the OE in order to ultimately be able to modify earplug designs to reduce the magnitude of the phenomenon. In particular, this study aims at explaining the difference in OE highlighted in experimental studies (Hansen, 1998; Lee & Casali, 2011; Brummund *et al.*, 2015) between a foam and a silicone earplug and its dependence on the insertion depth (Lee & Casali, 2011). For this purpose, a improved model of the 2D axi-symmetric FE model initially developed by Brummund *et al.* (2015) is proposed. The use of a 2D axi-symmetric truncated model of the outer ear considerably decreases the computation time compared to a realistic 3D truncated model (Brummund *et al.*, 2014) and even more in comparison with a whole head model (Chang *et al.*, 2016; Xu *et al.*, 2019). In

addition, the simplified geometry of the current 2D axi-symmetric model greatly facilitates the examination of the role of the earplug on the objective OE.

To analyze and interpret the FE results, an electro-acoustic (EA) framework of the open and occluded earcanal is developed. The conjunction of both FE model and EA framework allows for a straightforward interpretation of the complex phenomena involved in the vibro-acoustic behavior of such an occluded outer ear excited by bone-conducted stimulation (Carillo *et al.*, 2020). Compared to past EA approaches (Tonndorf *et al.*, 1966; Schroeter & Poesselt, 1986; Hansen, 1998; Stenfelt & Reinfeldt, 2007; Zurbrügg *et al.*, 2014; Carillo *et al.*, 2020), the medial earplug surface is here accounted for as an ideal source of volume velocity which is distinct from the source representing the "free" earcanal wall surrounding the occluded earcanal cavity. Hence, FE simulations are investigated in terms of volume velocity imposed by the "free" earcanal wall and the medial earplug surface to the occluded earcanal cavity. The influence of the earplug mechanical properties is studied using a design of experiment for shallow, medium and deep insertion depths. In addition, the influence of the earcanal wall vibration distribution on the OE is investigated in conjunction with the earplug insertion depth by varying the geometry of the earcanal surrounding tissues. Simulations of the OE are compared to experimental data available in the literature. By examining in detail the vibro-acoustic behavior of the earplug using the FE model, this research provides insight about its mechanism(s) of contribution to the objective OE.

5.3 Finite element model of the outer ear

5.3.1 Geometry

The 3D geometry of the open ear, initially developed by Brummund *et al.* (2015) from literature data, is illustrated in Fig. 5.1(a). Since the problem is considered axi-symmetric, only a cross-sectional cut through the $(r,\ z)$ plane is depicted in Fig. 5.1(b). The outer ear consists of a cylindrical earcanal of length l_{EC} and radius r_{EC} surrounded by soft (cartilage and skin) and bony tissues. The anatomical landmarks of the pinna are not accounted for in the current model, mainly to preserve the axi-symmetry of the problem. The geometry of the earcanal entrance

region is thus simplified to a 2 mm protrusion from $z = 0$ made of cartilaginous and skin tissues. The eardrum is assumed to mark the end of the cylindrical earcanal perpendicular to its central axis.

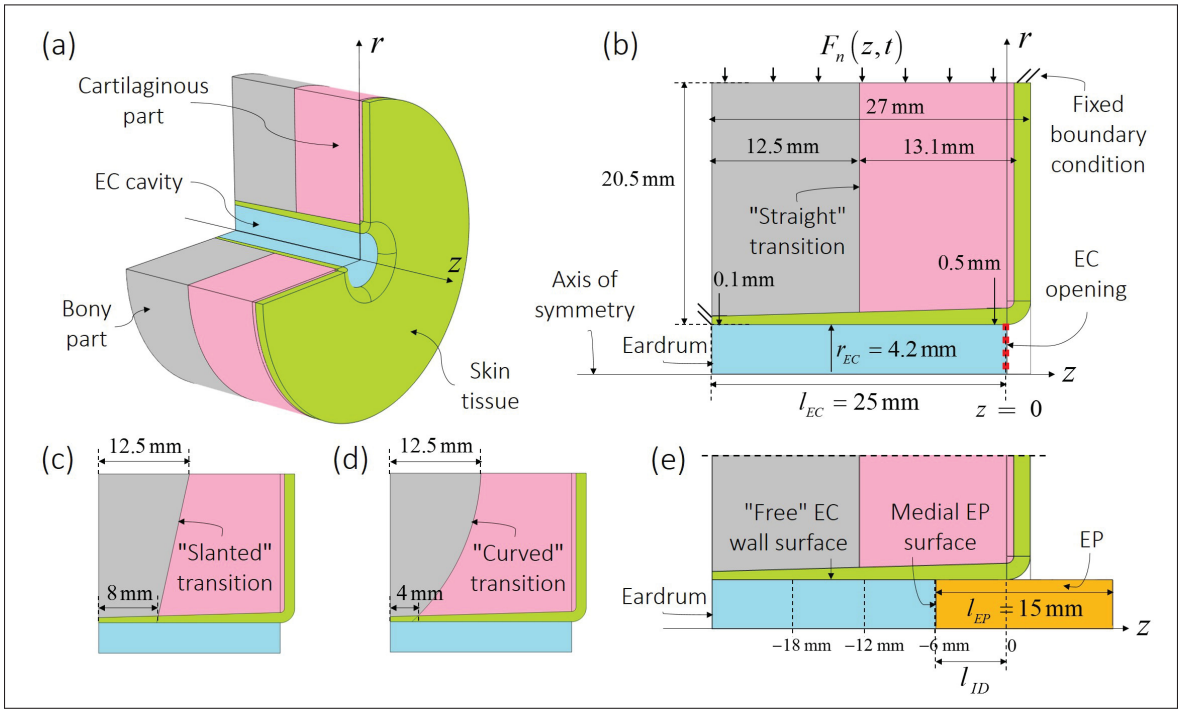

Figure 5.1 (a) 3D view of the axi-symmetric FE model of an outer ear, 2D view in the $(r,\ z)$ plane of the (b) open earcanal with (c, d) different transitions between cartilaginous and bony tissues, and (e) 2D view of the occluded earcanal. In subplot (b), the red dashed line at $z = 0$ indicates the earcanal opening, the red arrows at the top of the model indicate where the normal force $F_n(z,\ t)$ is exerted and the double slash indicate fixed constraint. In subplot (e), the drawing of the model has been cut along the z-axis (see the dashed black line) in order to limit the size of the figure

Compared to the original model developed by Brummund *et al.* (2015), the thickness of the skin surrounding the earcanal cavity varies linearly from the eardrum to the earcanal entrance instead of changing abruptly at the bony part/cartilaginous part transition. In addition, the edge of the skin and cartilaginous tissues at the earcanal entrance has been radiused in order to not couple the earplug with the protruding extension representing the pinna in the occluded case. In a real ear, the transition between soft and bony tissues along the earcanal is not clear and

varies gradually around the 3D earcanal cavity from the earcanal entrance to the eardrum. This transition is estimated to occur approximately at the second bend of the earcanal, close to its half-length (Alvord & Farmer, 1997; Oliveira & Hoeker, 2003). In the current model, a "straight" transition of the underlying tissues is assumed at the earcanal half-length. In addition, in order to study the influence of a variation of the earcanal wall vibration distribution on the contribution of the earplug to the OE, two other simplified anatomical geometries ("slanted" and "curved", see Fig. 5.1(c) and (d) respectively) of the earcanal surrounding tissues including gradual transitions along both radial and longitudinal axis are also used (see Sec. 5.4.3). These additional transitions have been determined from a 3D anatomical model constructed by Brummund *et al.* (2014) based on cryosection images of a human female cadaver from the Visible Human Project®. Figure 5.2 displays the 3D anatomical model developed by Brummund *et al.* (2014) in subplot (a), the "slanted" transition in subplot (b) and both "straight" and "curved" transition in subplot (c). An example of cryosection image superimposed on a sectional view of the 3D model is shown in Fig. 5.2(d). Figure 5.2 illustrates the geometrical complexity of the anatomical tissues surrounding the earcanal. In the current 2D FE model, this complexity is simplified due to the axi-symmetrical assumption.

The axi-symmetric geometrical representation of the earcanal occluded by an earplug is depicted in Fig. 5.1(e). Two earplugs are considered: foam and silicone. Their length is equal to 15 mm which is in between a push-to-fit foam earplug (about 10 mm length) and a roll-down foam earplug (19 mm length). The silicone earplug represents a custom molded earplug. This selection of two identical earplugs except for their composition, allowed for studying the influence of the earplug material properties on the OE. Furthermore, the diameter of each earplug is identical and selected to match exactly the inside diameter of the earcanal. Therefore, no deformation of the earcanal surrounding tissues due to the presence of the earplug is taken into account. In the case of the roll-down foam earplug, its insertion in the earcanal induces a radial deformation which is accounted for by using equivalent mechanical properties (see Sec. 5.3.2). In the case of the custom molded earplug, it is assumed here to not deform. In practice, however, custom molded earplugs are slightly larger than the earcanal imprints from which they are made in order

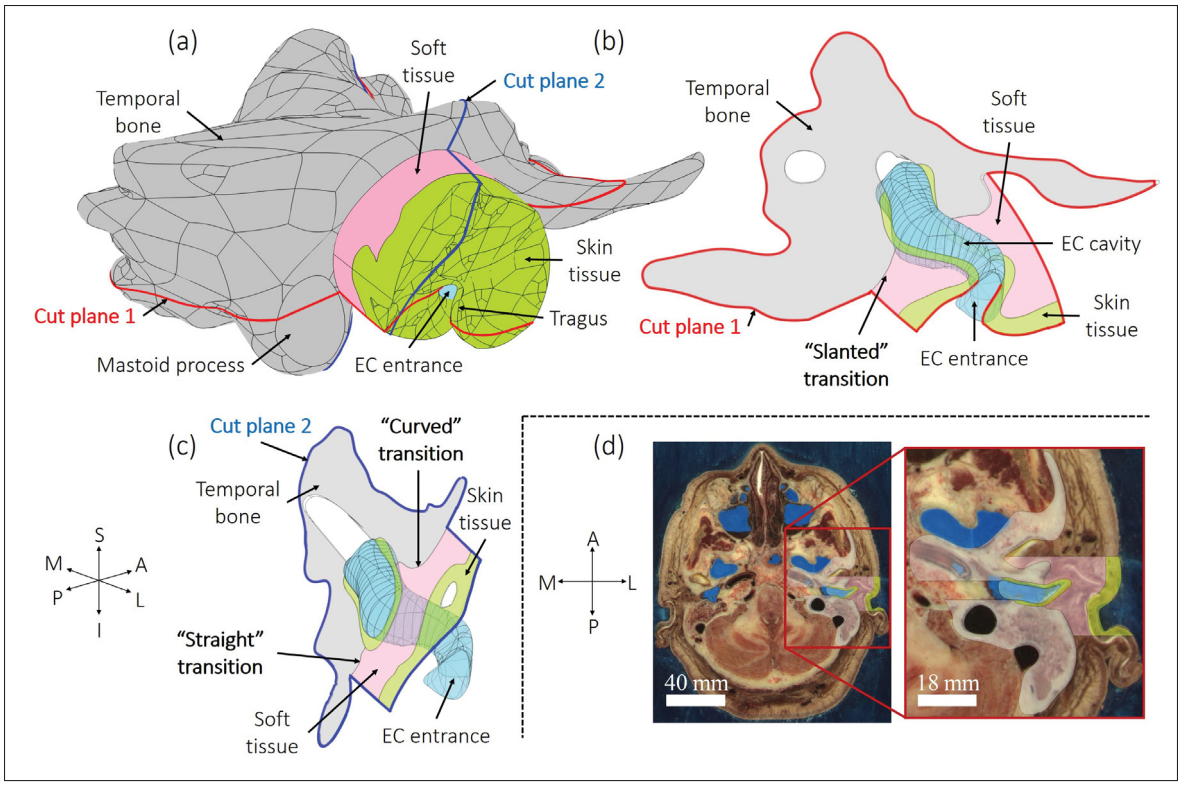

Figure 5.2 (a) 3D anatomical model of a human outer ear developed by Brummund et al. (2014), sectional view of the model in (b) cut plane 1, and (c) cut plane 2, and (d) example of a cryosection image from the Visible Human Project® used to reconstruct the 3D anatomical model. Cut planes 1 and 2 are perpendicular to a same earcanal cross-sectional plane located close to the second bend of the earcanal. Subplot (b) shows a "slanted" transition between bony and cartilaginous tissues whereas subplot (c) shows "straight" and "curved" transitions. The coordinate system refers to superior (S), inferior (I), posterior (P), anterior (A), medial (M), and lateral (L)

to fit tightly and seal the earcanal. This is likely to deform the earcanal surrounding tissues of a certain amount (Benacchio *et al.*, 2019) but this phenomenon is not accounted here due to the lack of knowledge of the deformation and the prestress material properties of the earcanal surrounding tissues.

Three insertion depths, defined from the earcanal entrance to the medial earplug surface, are considered here: shallow (6 mm), medium (12 mm) and deep (18 mm). These insertion depths are consistent with the literature. Berger & Kerivan (1983) used partial (shallow) insertion at

about 5 mm, standard (medium) insertion at about 10 mm and deep insertion at about 19 mm. Stenfelt & Reinfeldt (2007) and Brummund *et al.* (2014) used slightly longer insertion depths (*i.e.*, a 7 mm shallow insertion and a 22 mm deep insertion). For the E·A·R® Classic® earplug of 19 mm length, Berger (2013) defined the partial (shallow) insertion for about 15-20% of the earplug inserted in the earcanal, the standard (medium) insertion for about 50-60% of the earplug in the earcanal, and the deep insertion when about 80-100% of the earplug is inserted in the earcanal. Considering the shorter length of the earplug considered here, the resulting insertion depths are equivalent in this study.

5.3.2 Materials

Modeling the OE using the FE method requires the knowledge of the effective material properties of the earcanal surrounding tissues, which are difficult to assess experimentally, and that of the earplug. Similar to other FE models of the outer ear (Brummund *et al.*, 2014; Chang *et al.*, 2016; Xu *et al.*, 2019), solid domains are assumed to exhibit linear elastic isotropic material behavior with constant structural loss factor. Material properties come from previously published experimental data detailed by Brummund *et al.* (2015, 2014) (except for structural loss factors which were assumed) and are summarized in Table-A II-1 (see Appx. II). In practice, the earcanal surrounding tissues are more likely to be nonlinear, viscoelastic and anisotropic materials. However, as mentioned previously, the lack of experimental knowledge about human tissues' mechanical properties limits the accuracy of the earcanal surrounding tissues modeling. Also, the effective material properties of soft tissues could be influenced by the deformation of the earcanal wall induced by the coupling with the earplug in the occluded case, depending on the earplug type (Benacchio *et al.*, 2019), but soft tissues' deformation is not accounted for in the current model as can be be understood from discussion in the prior section.

Foam material properties depend on the earplug radial strain (James, 2006). Considering the small EAR Classic® (diameter around 12.3 mm), its insertion in the current earcanal (diameter of 8.4 mm) leads to a radial strain of the earplug around 31%. James (2006) determined the equivalent (*i.e.*, effective) Young's modulus, density and Poisson's ratio of a foam earplug for

several radial strains: 6%, 18% and 30%. Here, material properties of the foam earplug were therefore taken to correspond to the 30% radial strain to account for its prestress in the earcanal. In addition, the isotropic structural loss factor of the foam earplug (small EAR Classic®) has been measured in the laboratory using a quasi-static mechanical analyzer (Anonymous, 2011) for a longitudinal compression rate equal to 30%. The material properties of the silicone earplug are taken from experimental data used by Sgard, Nélisse, Boutin, Laville, Voix & Gaudreau (2009). In the frequency range of interest, both Young's modulus and loss factor do not significantly vary with frequency and are thus taken as constant (Sgard, Nélisse, Gaudreau, Boutin, Voix & Laville, 2010). Material properties of foam and silicone earplugs are summarized in Table-A II-1 (see Appx. II).

The air within the earcanal cavity is assumed to be a perfect compressible fluid of density $\rho_0 = 1.2$ kg m^{-3} and sound speed $c_0 = 343$ m s^{-1}. These values are also used in the EA model presented in Sec. **??**. Viscous and thermal losses at the fluid/structure boundary are not accounted for since they do not significantly influence the acoustic pressure nor the volume velocity transfer in the earcanal cavity between 100 Hz and 1 kHz (Carillo *et al.*, 2020).

5.3.3 Boundary and loading conditions

The coupling between the earcanal cavity of the open ear and the surrounding environment is modeled as a locally reacting acoustic impedance boundary condition defined at the earcanal entrance, similarly to other models (Schroeter & Poesselt, 1986; Stenfelt & Reinfeldt, 2007; Brummund *et al.*, 2014, 2015; Carillo *et al.*, 2020). The acoustic radiation impedance of the earcanal entrance depends on the geometry of the pinna, on the size of the earcanal entrance and on scattering effects induced by the head and the body. This impedance is here assumed equal to the radiation impedance $\hat{Z}_{rad}$ (the caret symbol represents a complex-value) of a baffled circular piston of the same area as the earcanal entrance (see Appx. V). At low frequencies, this assumption provides a reasonable approximation of the measured acoustic radiation impedance of the earcanal entrance (Hudde & Engel, 1998a). The sound radiation of the external tissue in the open earcanal is however neglected. This effect can be accounted for by modeling the

external air environment surrounded by a perfectly matched layer (simulating the Sommerfeld radiation condition) (Sgard *et al.*, 2019) but has little influence on the open earcanal SPL in the current model (simulation not shown here).

The middle and inner ears are accounted for as a locally reacting acoustic impedance $\hat{Z}_{TM}$ boundary condition specified at the eardrum and defined by the model of Shaw & Stinson (1983) (see Appx. IV). This impedance compares well to measurement data at low frequencies (Hudde & Engel, 1998a). This assumption is, however, a simplification in regard to the sound radiation that stems from the inertial movement of the ossicles in the middle ear. However, the SPL generated in open and occluded earcanals is not expected to be significantly influenced by the acoustic radiation of the tympanic membrane induced by the vibration of the middle ear ossicles excited *via* their ligaments by the bone-conducted sound propagation, at least at low frequencies below the middle ear resonance (Stenfelt *et al.*, 2003; Schroeter & Poesselt, 1986; Stenfelt *et al.*, 2002). Another argument supporting this assumption is that the OE would not decrease with insertion depth if the tympanic membrane was a significant source for the SPL generated in the earcanal (Hansen, 1998). The bone-conducted pathway through the middle ear rather influences the vibration transmitted to the cochlea and therefore influences the subjective OE (Huizing, 1960; Stenfelt & Reinfeldt, 2007; Schroeter & Poesselt, 1986). This paper, however, only focuses on the objective OE (*i.e.*, difference in SPL generated in occluded and open cases), and in particular on the contribution of earplugs on the SPL generated in the occluded earcanal. Finally, fixed boundary conditions applied to solid domains are indicated by double slash in Fig. 5.1(b) whereas remaining solid boundaries are free.

The structure-borne mechanical boundary load is introduced as a uniform normal force field $F_n(z, t) = \Re\left[A(z)\, e^{j\omega t}\right]$ applied to the cartilaginous and bony tissues circumferential boundary where $A(z) = 1$ N $(-l_{EC} \leq z \leq 0)$, j is the imaginary number, ω is the circular frequency such that $\omega = 2\pi f$ with f the frequency and t represents the time. It should be noted that this loading is an idealization of the real stress vectors which act on the human tissues and likely vary in terms of amplitude, phase and direction along the tissue boundaries. The resulting vibration of the earcanal wall is thus analyzed in Sec. 5.4.2.

5.3.4 Finite element modeling

A temporal dependency $e^{j\omega t}$ for all fields is assumed henceforth. The sound propagation in solid domains is governed by the classic linear elasto-dynamic equation (Atalla & Sgard, 2015). Continuity of stress vectors and displacements is assumed between solid domains. The sound propagation within the air-filled earcanal cavity is governed by the homogeneous Helmholtz equation $\nabla^2\hat{p} + k_0^2\hat{p} = 0$, where $k_0 = \omega/c_0$ is the lossless wavenumber. The coupling at the earcanal wall/earcanal cavity boundary is achieved by the continuity of normal component velocity vectors and normal component stress vectors. Finally, the coupled FE model is meshed according to a criterion of at least six 6-noded quadratic triangular elements per wavelength $\lambda = c/f$ at 1 kHz. In a solid, both compression waves and shear waves can propagate. The shortest wavelength has to be taken at the highest frequency of interest (*i.e.*, 1 kHz) to determine the size of elements allowing for achieving convergence. Sound speeds associated with compression and shear waves are respectively defined in 2D by $c_L = \sqrt{E/[2\rho\,(1-\nu)]}$ and $c_T = \sqrt{E/[2\rho\,(1+\nu)]}$, with the Young's modulus E, the density ρ and the Poisson's ratio ν of a given solid domain. The less stiff domains, such as skin tissue are thus the most finely meshed. The mesh of the whole model approximately consists of 4 500 elements depending on the configuration and allows for convergence of the solution. This coupled elasto-acoustic FE model is solved using COMSOL Multiphysics 5.5 (COMSOL®, Sweden). Displacement fields in the tissues and acoustic pressure field in the earcanal cavity are computed at each node of the mesh.

5.3.5 Vibro-acoustic indicators and framework of interpretation

The OE is computed from the acoustic pressure $\left\langle \hat{p}_{TM}^{k} \right\rangle$, where $k \in \{open,\ occl\}$, calculated at the tympanic membrane (surface averaged) in open and occluded case such as

$$OE = 20\log_{10}\left(\left|\frac{\left\langle \hat{p}_{TM}^{occl} \right\rangle}{\left\langle \hat{p}_{TM}^{open} \right\rangle}\right|\right). \tag{5.1}$$

Brummund *et al.* (2015) proposed to investigate the OE computed using FE models based on an acoustic power balance approach. However, acoustic power exchanges can be intricate to investigate (i) the relative contribution between the "free" EC wall and the medial earplug surface and (ii) the influence of the earplug material on the OE. Hence, in the current paper, a framework of investigation based on EA analogy is provided to dissect and interpret the OE computed using the FE model.

According to the EA framework, when the earcanal is open, the vibration of the earcanal wall acts as an ideal source of volume velocity $\hat{q}_{wall}^{open}$ defined by

$$\hat{q}_{wall}^{open} = \left\langle \hat{v}_{n,wall}^{open} \right\rangle S_{wall}^{open}, \tag{5.2}$$

with $\left\langle \hat{v}_{n,wall}^{open} \right\rangle$ the surface averaged earcanal wall normal vibration computed using the FE model and S_{wall}^{open} the whole earcanal wall area. The acoustic pressure generated at the tympanic membrane by the earcanal wall vibration is then given by

$$\hat{p}_{TM,EA}^{open} = \hat{Z}_{EC}^{open} \times \hat{q}_{wall}^{open}. \tag{5.3}$$

where $\hat{Z}_{EC}^{open}$ is the acoustic impedance of the open earcanal cavity seen by the volume velocity source representing the earcanal wall vibration. The acoustic impedance $\hat{Z}_{EC}^{open}$ can be approximated at low frequencies (Carillo *et al.*, 2020) by

$$\hat{Z}_{EC}^{open} \approx j\omega \left(L_{EC}^{open} + L_{rad} \right), \tag{5.4}$$

with $L_{EC}^{open} = -\rho_0 l_{c,n} \Big/ \left(\pi r_{EC}^2 \right)$ the acoustic mass of the open earcanal cavity and $L_{rad} = 8\rho_0 \Big/ \left(3\pi^2 r_{EC} \right)$ the acoustic radiation mass of the earcanal opening considered as a baffled circular piston. The open earcanal acoustic mass L_{EC}^{open} depends on the centroid position $l_{c,n}$ of the earcanal wall normal velocity (Carillo *et al.*, 2020). In Appx. XI, this dependence is

mathematically justified. In the FE model, the centroid position $l_{c,n}$ is computed by

$$l_{c,n} = \frac{\int_{-l_{EC}}^{0} z \left| \hat{v}_{n,wall}^{open}(z) \right| \mathrm{d}z}{\int_{-l_{EC}}^{0} \left| \hat{v}_{n,wall}^{open}(z) \right| \mathrm{d}z}. \tag{5.5}$$

where the z-axis represents the earcanal curvilinear axis in the current 2D axi-symmetric FE model. In the current paper, a centroid position $l_{c,t}$ is similarly defined by Eq. (5.5) but uses the tangential component $\hat{v}_{t,wall}^{open}$ of the earcanal wall velocity instead of the normal component $\hat{v}_{n,wall}^{open}$.

When the earcanal is occluded, the "free" earcanal wall (portion of the earcanal not covered by the earplug) and the medial earplug surface impose to the earcanal cavity the volume velocities $\hat{q}_{wall}^{occl}$ and $\hat{q}_{EP}$ respectively. The volume velocity imposed by the "free" earcanal wall is defined by

$$\hat{q}_{wall}^{occl} = \left\langle \hat{v}_{n,wall}^{occl} \right\rangle S_{wall}^{occl}, \tag{5.6}$$

with $\left\langle \hat{v}_{n,wall}^{occl} \right\rangle$ the surface averaged earcanal wall normal vibration computed using the FE model in the occluded case and S_{wall}^{occl} the "free" earcanal wall area. The volume velocity imposed by the medial earplug surface is defined by

$$\hat{q}_{EP} = \left\langle \hat{v}_{n,EP} \right\rangle S_{EP}, \tag{5.7}$$

with $\left\langle \hat{v}_{n,EP} \right\rangle$ the surface averaged normal vibration of the medial earplug surface and S_{EP} the medial earplug surface area. Using the superposition principle, the acoustic pressure at the tympanic membrane in the occluded case is then given by

$$\hat{p}_{TM,EA}^{occl} = \hat{Z}_{EC}^{occl} \times \left(\hat{q}_{wall}^{occl} + \hat{q}_{EP} \right). \tag{5.8}$$

where $\hat{Z}_{EC}^{occl}$ is the acoustic impedance of the occluded earcanal cavity. The acoustic impedance $\hat{Z}_{EC}^{occl}$ can be approximated at low frequencies (Carillo *et al.*, 2020) by

$$\hat{Z}_{EC}^{occl} \approx \left[j\omega \left(C_{EC}^{occl} + C_{TM} \right) \right]^{-1}, \tag{5.9}$$

where $C_{EC}^{occl} = \pi r_{EC}^2 \left(l_{EC} - l_{ID} \right) \Big/ \left(\rho_0 c_0^2 \right)$ represents the acoustic compliance of the occluded earcanal cavity which depends on the insertion depth l_{ID} and C_{TM} represents the acoustic compliance of the tympanic cavity volume equal here to 0.78 cm^3 (Carillo *et al.*, 2020). It is noteworthy that the simplification of the eardrum acoustic impedance to the acoustic compliance C_{TM} is accurate below approximately 500 Hz (Carillo *et al.*, 2020).

Finally, by substituting Eqs. (5.3) and (5.8) into Eq. (5.1), the OE computed using the FE model can be approximated in the EA framework by

$$OE \approx 20\log_{10} \left(\frac{\hat{Z}_{EC}^{occl} \times \left(\hat{q}_{wall}^{occl} + \hat{q}_{EP} \right)}{\hat{Z}_{EC}^{open} \times \hat{q}_{wall}^{open}} \right). \tag{5.10}$$

5.4 Results and discussions

This section is organized as follows. In Sec. 5.4.1, the simulations of OE computed using the FE model are compared to corresponding experimental measurements on human subjects available in the literature in order to assess the realism of the model. In Sec. 5.4.2, the contribution of earplugs to the OE is analyzed as a function of its insertion depth and its material properties. In Sec. 5.4.3, the influence of the distribution of the earcanal wall vibration on the OE and in particular on the contribution of earplugs is studied. Finally, Sec. 5.4.4 discusses the limits of the current study.

5.4.1 Evaluation of the finite element simulations with respect to experimental data

Figure 5.3 displays FE simulations of the OE paired with experimental data taken from the literature. Figure 5.3(a) shows the OEs of the shallowly (6 mm) and deeply (18 mm) inserted foam earplug computed using the FE model as a function of frequency (third octave bands) in comparison with the median values of experimental data measured by Stenfelt & Reinfeldt (2007) on 20 human subjects. Means and associated standard deviations were not available in (Stenfelt & Reinfeldt, 2007). In the measurements, the bone-conducted stimulation was ensured by a bone-transducer applied at the center of the forehead. The OE was computed as the difference in SPL measured in the occluded and open earcanal using a probe tube microphone. The shallow and deep insertion of the foam earplug corresponded respectively to 7 and 22 mm from the earcanal entrance. According to Fig. 5.3(a), the greatest experimental OE is observed for shallow insertion, and begins close to 35 dB at 125 Hz and then decreases to 9 dB at 1 kHz. For deep insertion, the mean of experimental OE is 15 dB lower than for shallow insertion for the whole frequency range. The model overestimates by 4 to 15 dB the median experimental OE for shallow insertion while both simulated and median experimental OEs are in good agreement for deep insertion.

In complement to Fig. 5.3(a), Fig. 5.3(b) shows the OE induced by the foam earplug at medium insertion (12 mm) computed using the FE model as a function of frequency (third octave bands) and compared to experimental data (means and associated standard deviations) obtained by Reinfeldt *et al.* (2013) on 20 human subjects. In the measurements, three positions for the bone-transducer were considered: (i) at the center of the forehead (similar to Stenfelt & Reinfeldt (2007)), (ii) at the contralateral mastoid, and (iii) at the ipsilateral mastoid. The OE was measured using a probe tube microphone inserted close to the eardrum. The occlusion was ensured by a foam earplug inserted 10 mm relative to the earcanal opening. The current FE model could account for the influence of the stimulation position by using another set of mechanical boundary conditions and loading than the set defined in Sec. 5.3.3. However, the present work focuses on the influence of EP material on the OE. Hence, the influence of the stimulation position is not of primary importance here. Furthermore, according to Fig. 5.3(b), the simulated OE lies within

one standard deviation associated with the mean experimental data for all stimulation positions above 200 Hz. Below this frequency, the model overestimates the mean experimental OEs by 10 dB (forehead stimulation) to 19 dB (ipsilateral stimulation) at 125 Hz.

Finally, Fig. 5.3(c) shows the OEs provided by the medium insertion (12 mm) of the foam and the silicone earplugs computed using the FE model as a function of frequency (third octave bands) in comparison with experimental data (means and associated standard deviations) measured by Brummund *et al.* (2015) in a group of 37 participants. In the measurement, the bone transducer was placed on the mastoid process for ipsilateral stimulation and the SPL was measured in open and occluded earcanal using miniature microphone. Foam and custom molded silicone earplug were respectively inserted into the earcanal at 11 ± 3 mm and 12 ± 1 mm from the earcanal entrance of participants. According to Fig. 5.3(c), the greatest experimental OE is observed for the silicone earplug, and begins close to 35 dB at 125 Hz and then decreases to 15 dB at 1 kHz. The mean experimental OE induced by the foam earplug is 8 dB lower than the silicone earplug for the whole frequency range. For a similar insertion depth, Lee & Casali (2011) found the same difference in OE between a foam earplug and a medical balloon-based earplug (made of silicone and inflated after insertion) measured on 6 human subjects at 500 Hz (third octave band). For both earplugs, the variability of experimental data decreases with frequencies above 250 Hz (see Fig. 5.3(c)). The model overestimates the mean experimental OEs induced by foam and silicone earplugs by around 9 dB at 125 Hz and 5 dB at 250 Hz. However, the simulated OEs lie within one standard deviation of the mean of the experimental data. The discrepancy between simulated and mean experimental OEs then vanishes at 500 Hz and 1 kHz.

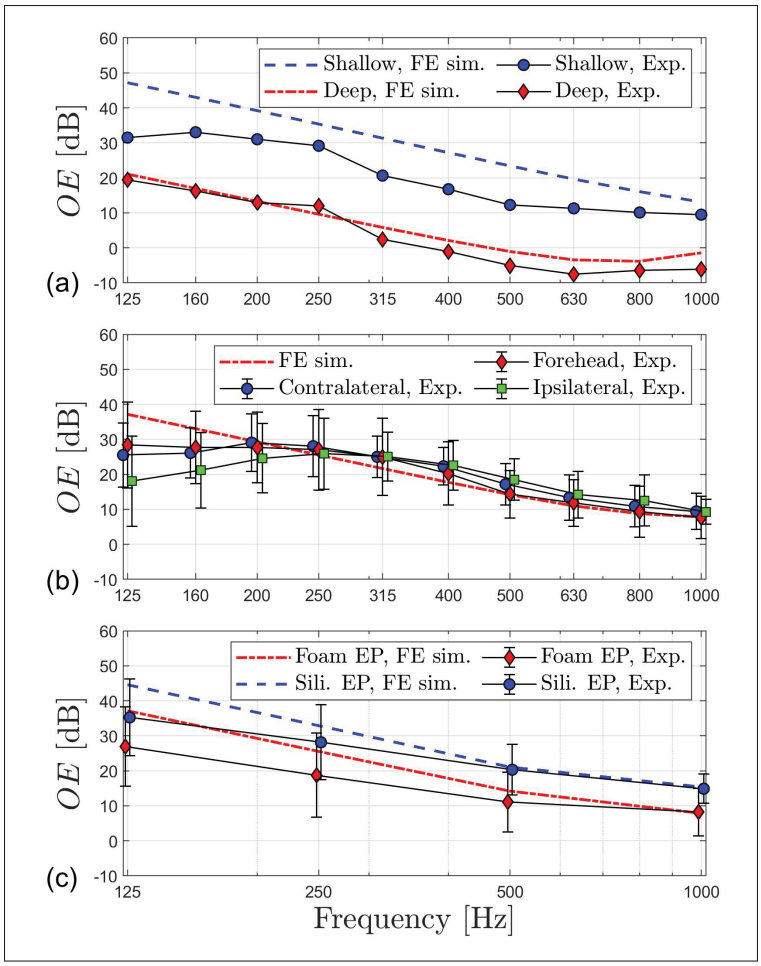

Figure 5.3 Comparison of predicted and measured objective OE for various conditions. (a) OEs induced by a foam earplug at shallow (6 mm) and deep (18 mm) insertion computed using the FE model versus experimental data (median value only) measured on human subjects by Stenfelt & Reinfeldt (2007) in third octave bands. (b) OEs induced by a foam earplug at medium insertion (12 mm) computed using the FE model versus experimental data (mean and associated standard deviation) measured on human subjects by Reinfeldt *et al.* (2013) for contralateral, ipsilateral and forehead stimulation in third octave bands. (c) OEs induced by a foam earplug and a silicone earplug at medium insertion (12 mm) computed using the FE model versus experimental data (mean and associated standard deviation) measured by Brummund *et al.* (2015) in third octave bands

The decrease with frequency of the OE (see Fig. 5.3) is explained by the change in the character of the acoustic impedance between the open earcanal, controlled by its acoustic mass (see Eq. (5.4)), and the occluded earcanal, controlled by its compliance (Stenfelt & Reinfeldt, 2007; Hansen, 1998; Carillo *et al.*, 2020) (see Eq. (5.9)). The FE simulations provide this characteristic slope of the OE but tend to overestimate the OE below 250 Hz, particularly for shallow (see Fig. 5.3(a)) and medium insertion (see Fig. 5.3(b) and (c)). This overestimation could be explained by an incomplete seal between the earplug and the earcanal wall during OE measurements (Hansen, 1998; Brummund *et al.*, 2014). An incomplete seal is indeed more likely to occur when the earplug is not deeply inserted in the earcanal. The effect of an incomplete seal is not accounted for in this work but has been also investigated by the authors (Sgard *et al.*, 2019) and corroborates the previous observation that it could be responsible for a reduction of the OE below 250 Hz.

Also, the simplifications of the current model in terms of geometry, boundary conditions and loading could explain the difference in OE between simulations and experimental data below 250 Hz. First, the current model does not account for the acoustic radiation of external tissues which could influence the SPL in the open earcanal (Brummund, 2014). This phenomenon could be accounted for using a whole head model surrounded by the external air environment and bounded by a perfectly matched layer (Sgard *et al.*, 2019). Second, the current model does not differentiate stimulation positions (*e.g.*, forehead, contralateral mastoid and ipsilateral mastoid) due to its truncation whereas this factor is shown to influence the experimental OE mainly below 250 Hz (see Fig. 5.3(b)). Whole head models (Chang *et al.*, 2016; Xu *et al.*, 2019) could be great candidate to account for the influence of both the acoustic pathway through the open earcanal entrance and the stimulation position, which are not studied here. The most important discrepancy between simulation and measurement occurs for the shallowly inserted foam earplug (see Fig. 5.3(a)). In this case, the FE model overestimates by 15 dB the median value of experimental data but fits between the extrema of measured OEs (Stenfelt & Reinfeldt, 2007), not presented here. The model does not necessarily represent the median subject of experimental data but rather a particular subject. In other cases, the FE model compares well with measurements (above 250 Hz). In particular, the FE model accurately predicts the difference

in OE between a foam and a silicone earplug (see Fig. 5.3(c)) which makes it possible to use this model to investigate the role of the earplug on the OE.

5.4.2 Contribution of the earplug to the occlusion effect

Figure 5.4 displays the OE induced by a foam earplug and a silicone earplug at (a) shallow (6 mm), (b) medium (12 mm) and (c) deep (18 mm) insertions computed using the FE model. It is noteworthy that part of the FE simulations displayed in Fig. 5.4 in narrow band have already been presented in third octave bands in Fig. 5.3.

In Fig. 5.4, the OE induced by the infinite impedance represents a reference case in which the contribution of the "EP" in terms of volume velocity to the OE is zero. This configuration is used to quantify the OE only induced by the vibration of the "free" earcanal wall. It is important to note that the differences in OE across the various insertion depths and impedances observed in Fig. 5.4 are solely due to the vibro-acoustic response of the occluded earcanal because the open earcanal is the same for all simulations of the OE. These differences in OE depend on the insertion depth of the occlusion, investigated in Sec. 5.4.2.1, and on the type of occlusion (infinite impedance, foam or silicone earplug), studied in Sec. 5.4.2.2. In the following, FE simulations of the OE displayed in Fig. 5.4 are investigated and interpreted in the EA framework (presented in Sec. 5.3.5). For this purpose, the accuracy of the EA framework to approximate FE simulations of the objective OE is verified in Appx. **??**.

5.4.2.1 Influence of the earplug insertion depth

According to Fig. 5.4, the OE decreases with the insertion depth for all occlusions (infinite impedance, foam earplug and silicone earplug). In the EA framework, Eq. (5.10) indicates that the OE depends on the volume velocity imposed by the "free" earcanal wall ($\hat{q}_{wall}^{occl}$) and the medial earplug surface ($\hat{q}_{EP}$) and on the acoustic impedance of the occluded earcanal cavity ($\hat{Z}_{EC}^{occl}$). Since the acoustic impedance $\hat{Z}_{EC}^{occl}$ tends to increase when the volume of the occluded earcanal cavity diminishes (*i.e.*, the cavity becomes stiffer, see Eq. (5.9)), the decrease of the OE

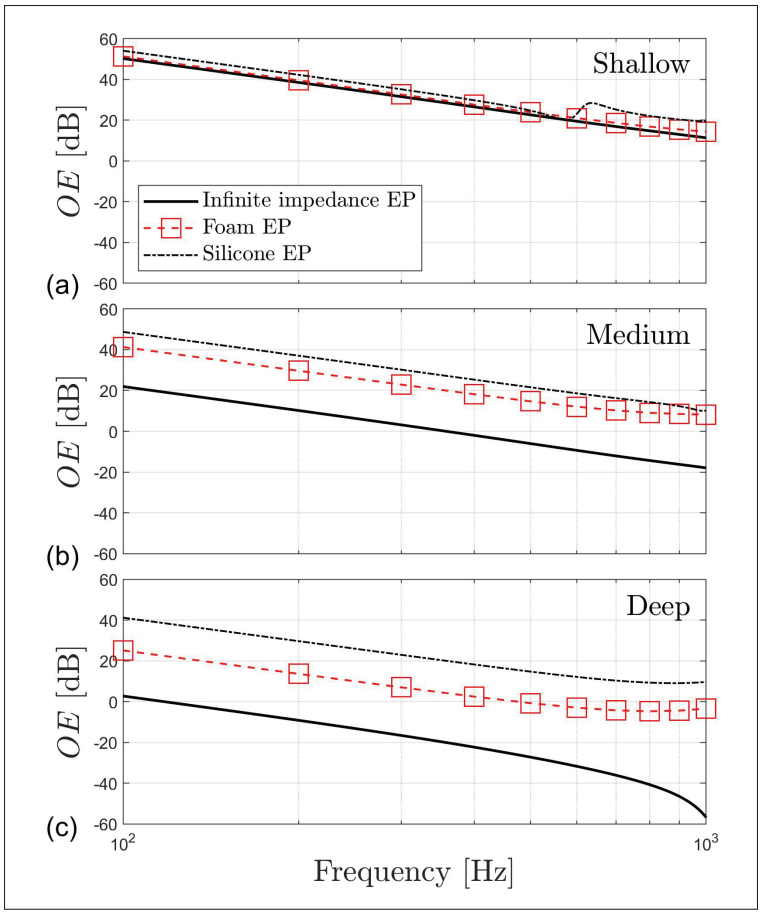

Figure 5.4 Predicted objective OE induced by an infinite impedance, a foam earplug and a silicone earplug at (a) shallow (6 mm), (b) medium (12 mm) and (c) deep (18 mm) insertion computed using the FE model

with insertion depth is necessarily explained by the reduction of the volume velocity imposed on the occluded earcanal cavity (Hansen, 1998; Zurbrügg *et al.*, 2014). According to Eq. (5.10), a sufficiently low volume velocity imposed to the occluded earcanal cavity compared to that imposed in the open case leads to a negative OE (see Fig. 5.4(b) for the infinite impedance occlusion and Fig. 5.4(c) for both the infinite impedance occlusion and the foam earplug occlusion) despite the increase of the acoustic impedance of the earcanal cavity in the occluded case compared to the open one (Carillo *et al.*, 2020).

When the occlusion is created by an infinite impedance earplug, the resulting OE is solely due to the volume velocity imposed by the "free" earcanal wall. This volume velocity $\hat{q}_{wall}^{occl}$ depends on the surface averaged normal velocity field (*i.e.*, causing compression and rarefaction in the earcanal cavity) and its vibrating area (see Eq. (5.6)). In this case (*i.e.*, infinite impedance earplug), the OE is observed to decrease by 28 dB from shallow to medium insertion and by 19 to 40 dB (depending on the frequency) from medium to deep insertion (see Fig. 5.4).

Figure 5.5 displays the volume velocity imposed by the "free" earcanal wall $\hat{q}_{wall}^{occl}$ (for the case of infinite impedance earplug but similar for foam and silicone earplugs occlusion) and the medial earplug surface $\hat{q}_{EP}$ at (a) shallow, (b) medium, and (c) deep insertion and normalized by the volume velocity imposed by the whole earcanal wall in the open case. The normalization of volume velocities imposed to the occluded earcanal by that imposed to the open earcanal is justified by Eq. (5.10) of the OE computed by the EA model in which $\hat{q}_{wall}^{occl}$ and $\hat{q}_{EP}$ are divided by $\hat{q}_{wall}^{open}$. All normalized volume velocities displayed in Fig. 5.5 are lower than 0 dB, meaning that volume velocities imposed by the "free" earcanal wall and the medial earplug surface are always lower than the volume velocity imposed by the whole earcanal wall in the open case.

Figure 5.5 shows that the volume velocity $\hat{q}_{wall}^{occl}$ imposed by the "free" earcanal wall drastically decreases with insertion depth, as expected (Stenfelt & Reinfeldt, 2007; Schroeter & Poesselt, 1986). According to Eq. (5.6), $\hat{q}_{wall}^{occl}$ is computed as the product of the surface average "free" earcanal wall normal velocity times the "free" earcanal wall area. If the earcanal wall normal velocity field amplitude were equally distributed over the earcanal wall surface, the reduction of the volume velocity $\hat{q}_{wall}^{occl}$ imposed by the "free" earcanal wall from the medium insertion case to the deep insertion case would only be of 3 dB (since the "free" earcanal wall surface would be reduced by a factor 2), which is negligible compared to the 20 dB decrease observed in Fig. 5.5 at 100 Hz. The reduction of $\hat{q}_{wall}^{occl}$ with insertion depth seen in Fig. 5.5 is therefore mainly due to the decrease of the surface average "free" earcanal wall normal velocity with insertion depth whereas the reduction of its vibrating area has little effect. To illustrate the reduction of the earcanal wall normal velocity with insertion depth, Fig. 5.7(a) displays the radial component (r-direction, normal to the earcanal wall surface) of the structural velocity field of

the earcanal surrounding tissues (*i.e.*, skin, cartilage and bone) computed for the silicone earplug occlusion using the FE model at 100 Hz. The amplitude of the earcanal wall normal velocity is maximal at the earcanal entrance, where the soft tissues are located, and suddenly decreases in the bony part, where the tissues are much less able to deform at low-frequency as mentioned by Berger & Kerivan (1983). The minimum normal velocity does not exactly occur at the tympanic membrane but rather a few millimeters ahead (see the blue region). The centroid position $l_{c,n}$ (see the red "X" in Fig. 5.7(a)) of the earcanal wall normal velocity distribution is located at 4.2 mm from the earcanal entrance, in the cartilaginous part. This centroid position does not significantly vary with frequency due to the absence of structural modes at low frequencies in the present FE model. The current vibration pattern cannot be directly compared to measurement due to the absence of experimental data. This is mainly explained by the difficulty to assess the distribution of the earcanal wall vibration (discussed in Sec. 5.4.4). However, this pattern is in qualitative agreement with experimental findings which suggest that the cartilaginous part of the earcanal vibrates the most (Bàràny, 1938; Stenfelt *et al.*, 2003).

When the earplug is considered, Fig. 5.4 shows that the associated OE is higher than that induced by the infinite impedance, depending on the earplug type and its insertion depth. At shallow insertion (see Fig. 5.4(a)), the OE induced by the foam earplug is almost equal to that of the infinite impedance while the OE of the silicone earplug is 4 to 7 dB higher. At medium insertion (see Fig. 5.4(b)), the foam earplug induces an OE 20 dB higher (28 dB for the silicone earplug) than the infinite impedance. At deep insertion (see Fig. 5.4(c)), the gap widens since the OE of the foam earplug is 23 to 53 dB higher (39 to 66 dB for the silicone earplug) than that of the infinite impedance. The increase with insertion depth of the difference in OE between the infinite impedance, the foam, and the silicone earplugs is clearly noticeable in Fig. 5.6 which shows the predicted objective OE computed at 500 Hz as a function of the insertion depth using the FE model.

Contrary to what Hansen (1998) proposed, the presence of the earplug does not significantly influence the volume velocity imposed by the "free" earcanal wall in the current model (Sgard *et al.*, 2019) (not shown here). The use of a truncated FE model of small size and the application

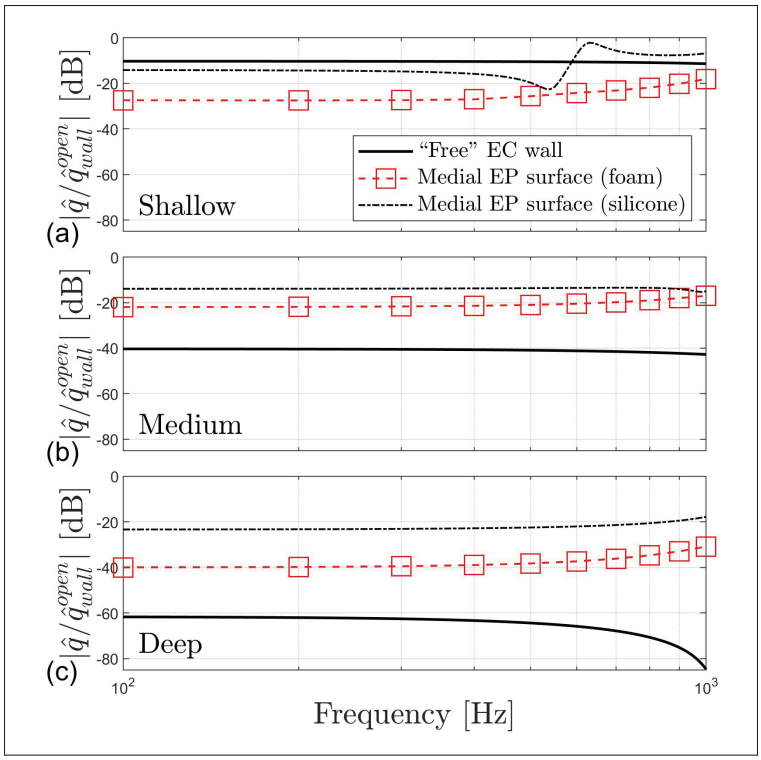

Figure 5.5 Amplitude in dB (factor 20, ref. 1) of the volume velocity imposed to the occluded earcanal cavity by the "free" earcanal wall and the medial earplug surface (foam and silicone) divided by the volume velocity imposed to the open earcanal cavity by the whole earcanal wall at (a) shallow (6 mm), (b) medium (12 mm) and (c) deep (18 mm) insertion computed using the FE model as a function of frequency

of current boundary and loading conditions (see Sec. 5.3.3) might lead to a structure stiffer than a real ear. Therefore, the volume velocity imposed by the "free" earcanal wall could be less influenced by the coupling with the earplug in the present model than in reality. Also, this influence could be greater if the earcanal surrounding tissues were prestressed. In this study, prestress of earcanal surrounding tissues by earplugs has been neglected (see Sec. 5.3.1). Indeed, accounting for prestress could be challenging due to the modeling complexity associated with nonlinear deformation and the lack of knowledge related to constitutive relations governing the mechanical behavior of prestressed earcanal surrounding tissues. However, the volume velocity

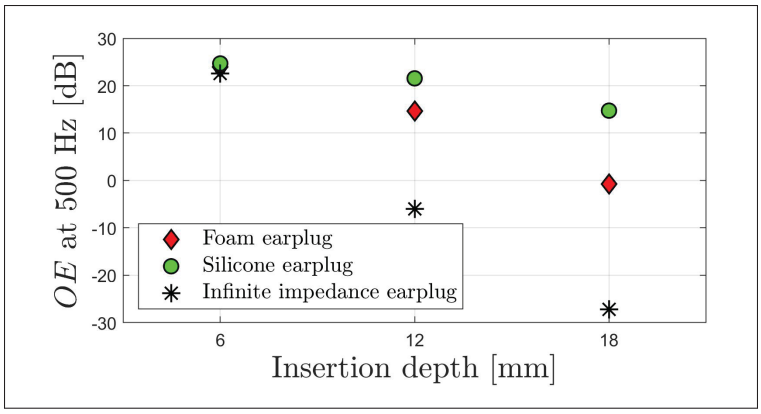

Figure 5.6 Predicted objective OE induced by an infinite impedance, a foam earplug and a silicone earplug at (a) shallow (6 mm), (b) medium (12 mm) and (c) deep (18 mm) insertion computed at 500 Hz using the FE model

imposed by the "free" earcanal wall is negligible in the current model compared to that imposed by the earplug medial surface at medium and deep insertion (see Fig. 5.5(b) and (c)). Therefore, the hypothetical influence of the earplug on the "free" earcanal wall vibration is not of primary importance since it could not explain the influence of the earplug on the OE at medium and deep insertion (see Fig. 5.4(b) and (c)).

As suggested by Brummund *et al.* (2015), the influence of the earplug on the OE is rather directly due to the normal vibration of its medial surface. The latter imposes a volume velocity $\hat{q}_{EP}$ to the occluded earcanal cavity which is displayed in dB (normalized by the volume velocity imposed by the whole earcanal wall in the open case) in Fig. 5.5 at each insertion depth and for both earplug types. At a given insertion depth, the higher the volume velocity imposed by the medial earplug surface (see Fig. 5.5), the higher the associated OE (see Fig. 5.4). According to Fig. 5.5, the volume velocity imposed by earplugs does not significantly vary between shallow and medium insertion, but it decreases by 10 to 15 dB at deep insertion. To illustrate this aspect, Fig. 5.7 illustrates the structural velocity field (r and z-directions) in the outer ear occluded by the silicone earplug at shallow (c, d), medium (e, f) and deep (g, h) insertion computed at

100 Hz using the FE model. In Fig. 5.7, a scale factor is applied to the deformed structures in order to highlight the total deformation of the system. Hence, the color maps are seen to exceed the nominal geometrical dimensions of the extent of the earcanal and earplug in the drawings. It is noteworthy that similar structural vibration patterns are obtained with the foam earplug and are thus not presented.

According to Fig. 5.7(d), (f) and (h), the amplitude of the normal velocity (z-direction) of the medial earplug surface decreases by approximately 10 dB when the silicone earplug is inserted in the bony part of the earcanal (deep insertion) since this portion vibrates much less than the cartilaginous part. It should be noted that volume velocities imposed by the "free" earcanal wall and medial earplug surfaces are in-phase in the whole frequency range of interest for each earplug and insertion (not presented for the sake of conciseness), except around 600 Hz for the shallowly inserted silicone earplug. Indeed, in the latter case, the normal velocity of the earcanal wall ir oriented inwards the earcanal cavity (see Fig. 5.7(i)) whereas the normal velocity of the medial earplug surface is oriented outwards the earcanal cavity (see Fig. 5.7(j)). Around this frequency, the silicone earplug imposes a volume velocity in phase quadrature with the "free" earcanal wall due to a structural resonance of the earplug coupled to the earcanal wall. The structural velocity field of the system associated to this frequency is illustrated in Fig. 5.7(i, j). The silicone earplug is driven by a longitudinal motion in which its medial and lateral surfaces vibrate in-phase (see Fig. 5.7(j)). In addition, the medial earplug surface is seen to not vibrate in-phase with the "free" earcanal wall surface normal vibration (see Fig. 5.7(i)). This resonance is responsible for a 2 dB decrease of the OE of the silicone earplug at 600 Hz due to the phase difference between the vibration of the medial earplug surface and that of the "free" earcanal wall. A similar phenomenon was expected by Berger & Kerivan (1983) to explain a local minimum in the subjective OE measured on human subjects around 500 Hz using a deep inserted foam earplug. In the current model, such a phenomenon cannot appear in deep insertion because volume velocities imposed by the medial earplug surface and the "free" earcanal wall are not of the same order of magnitude (see Fig. 5.5(c)). As observed in Fig. 5.5, the volume velocity imposed by the medial earplug surface becomes of major importance compared to the volume

velocity imposed by the "free" earcanal wall when the insertion depth of the earplug increases. At shallow insertion, the contribution of the earplug can be approximately neglected, except above 600 Hz for the silicone earplug (see Fig. 5.4(a)). This approximation is, however, not valid anymore when the earplug insertion depth increases to medium and deep (see Fig. 5.4(b) and (c)) because the contribution of the earplug in terms of volume velocity (depending on the earplug type) dominates that of the "free" earcanal wall and thus cannot be neglected (see Fig. 5.5(b) and (c)).

At medium and deep insertion, these results give support to the suggestion proposed by Bàràny Bàràny (1938) that the vibration of the medial earplug surface was of primary importance for the OE. Hence, these results differ from the common assumption that the main source of volume velocity was assumed to be the "free" earcanal wall (even in the occluded case) and which originates from the early work of Békésy (1932, 1960). However, these results explain the experimental observation made by Lee & Casali (2011) that the influence of the earplug type on the OE is little at shallow insertion and increases with insertion depth (see Fig. 5.4). Indeed, for the earplug's influence on the OE to vary according to its material properties, the earplug has to be the main source of volume velocity in the occluded earcanal. In past EA models (Schroeter & Poesselt, 1986; Hansen, 1998; Stenfelt & Reinfeldt, 2007; Zurbrügg *et al.*, 2014), the contribution of the earplug in terms of volume velocity was thus generally neglected or hidden into the volume velocity source representing the "free" earcanal wall vibration, mainly due to the difficulty to account for the earplug's vibro-acoustic behavior (Hansen, 1998).

5.4.2.2 Influence of the earplug material properties

In the previous section, the silicone earplug has been shown to impose a volume velocity $\hat{q}_{EP}$ higher than the foam earplug for each insertion depth (see Fig. 5.5), resulting in a higher OE induced by the silicone earplug compared to the foam earplug (see Fig. 5.4). In order to investigate the influence of the earplug material properties (*e.g.*, complex Young's modulus including the structural loss factor, density and Poisson's ratio) on the volume velocity imposed to the occluded earcanal cavity by the medial earplug surface, a 2^3 full factorial design of

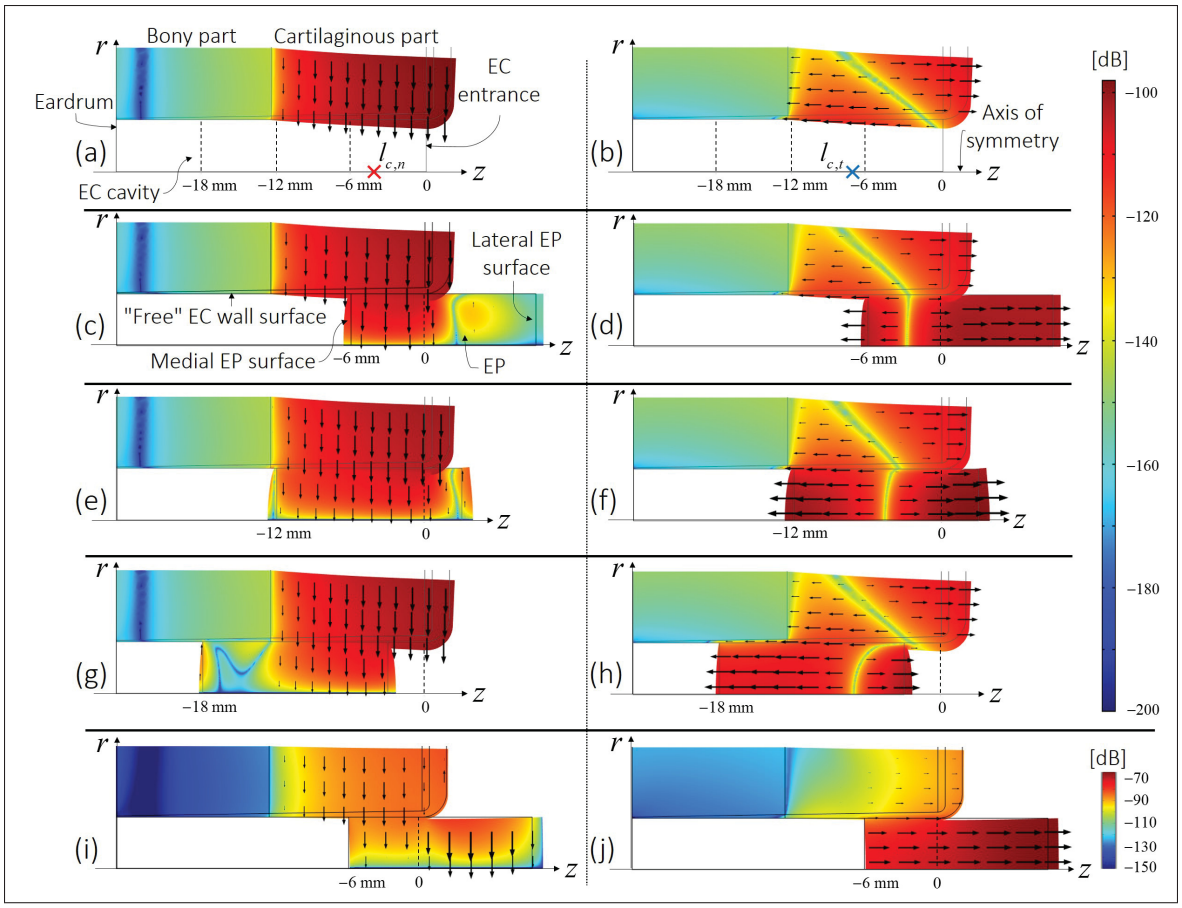

Figure 5.7 Amplitude in dB (factor 20, ref. 1 m s^{-1} for the colorbar) of the radial (r-direction, left side) and longitudinal (z-direction, right side) structural velocity components of the system computed at 100 Hz ($t = T/8$, where $T = 1/f$ is the period) using the FE model. Black arrows represent structural velocity vectors (the longer the arrow, the larger the velocity amplitude). The earcanal is (a, b) open and occluded by the silicone earplug in (c, d) shallow, (e, f) medium, and (g, h) deep insertion. Similar results are presented for the shallowly inserted silicone earplug at 600 Hz in subplot (i, j). In subplot (a, b), the red and blue "X" indicates the centroid position of the earcanal wall vibration respectively in normal and tangential directions. In all subplots, label on the z-axis indicates the earcanal entrance ($z = 0$ mm) and the three different insertion depths of the medial earplug surface ($z \in \{-6\text{ mm},\ -12\text{ mm},\ -18\text{ mm}\}$). A scale factor has been applied in all subplots to highlight the total deformation of the system in the $(r,\ z)$ plane and this is evidenced by the appearance of the color maps exceeding the actual dimensions of the extent of the earcanal and earplug in the drawings. Each drawing of the model has been cut in the r-direction along the z-axis to limit the size of the figure

experiment has been performed using the FE model. This design of experiment makes it possible to assess the main effect of each parameters as well as the interactions between parameters. The lower level of each material property comes from the foam earplug while the upper level comes from the silicone earplug (see Table-A II-1 in Appx. II).

Results of the design of experiment are shown in detail in Appx. XIII while the main conclusions are presented here. For all insertion depths, the design of experiment reveals that, compared to the Poisson's ratio, the Young's modulus and the density of the earplug are of minor influence on the volume velocity imposed by the medial earplug surface (for the range of variation considered here). The difference in terms of volume velocity imposed by the medial earplug surface between the foam and the silicone earplug seen in Fig. 5.5 is thus explained by Poisson's effect. The sensitivity analysis of the OE to the Poisson's ratio displayed in Fig. XIII-2 (see Appx. XIII) shows a gradual increase of the OE with Poisson's ratio, in particular above a value of 0.2. The Poisson's effect corresponds to the medial and lateral expansion of the earplug induced by the radial compression imposed by the normal vibration of the earcanal wall, depending on the value of the Poisson's ratio of the earplug material. However, there is no simple relation between the normal vibration applied by the earcanal wall to the circumferential surface of the earplug and the vibration of the medial earplug surface mainly because the vibration field of the earcanal wall is not spatially uniform but significantly varies along the earplug surface, depending on its insertion depth (see Fig. 5.7(c), (e) and (g)). Figure 5.8 displays the OE imposed by the "foam" and "silicone" earplugs by presuming a Poisson's ratio equal to zero for (a) shallow, (b) medium and (c) deep insertion. For the comparison, the OE induced by the infinite impedance, the foam and the silicone earplugs (with Poisson's effect) are also displayed. The simulated OE obtained presuming zero Poisson's ratio has been computed in narrow band but displayed at selected frequencies only to increase the readability of Fig. 5.8. For each insertion depth, there is no significant difference in OE between the foam and the silicone earplug when neglecting Poisson's effect: Poisson's effect explains the difference in OE between the two earplugs. For each insertion depth, the OE of the foam earplug is influenced much less by the Poisson's effect

than that to the silicone earplug. This is due to the much lower Poisson's ratio of the foam material ($\nu = 0.1$) compared to the silicone material ($\nu = 0.48$), almost incompressible.

For the medium and deep insertions (see Fig. 5.8(b) and (c)), the OE induced by both earplugs without considering Poisson's effect is approximately 20 dB higher than the OE induced by the infinite impedance. This difference is explained by a second mechanism of contribution of the earplug which corresponds to a longitudinal motion of the earplug induced by the tangential component of the earcanal wall vibration along the z-direction. Figure 5.7(b) displays the longitudinal component (z-direction) of the structural velocity field of the earcanal surrounding tissues in the open earcanal. The amplitude of the earcanal wall tangential velocity (parallel to the earcanal longitudinal z-direction) is at a minimum at the earcanal entrance where the longitudinal velocity changes sign (see the green diagonal region in Fig. 5.7(b)), then increases up to the mid-length of the cartilaginous part and finally drastically decreases in the bony part. According to Fig. 5.7(b), the centroid position $l_{c,t}$ (see the blue "X") of the earcanal wall tangential velocity distribution is located at 7.3 mm from the earcanal entrance, farther than $l_{c,n}$. This second mechanism (*i.e.*, longitudinal body motion of the earplug) does not depend on the material properties of the earplugs in the range of variation considered here and at low frequencies. This mechanism is however decreased with a rigid or heavy earplug (not shown here). In the current model, both mechanisms (*i.e.*, Poisson's effect and the longitudinal body motion) of contribution of the earplug in terms of volume velocity imposed to the earcanal cavity, act in-phase because the tangential component of the earcanal wall vibration is oriented towards the eardrum (see Fig. 5.7(b)) when the normal component is oriented radially inwards within the earcanal cavity (see Fig. 5.7(a)). Also, both mechanisms could be expected to influence each other. For example, by causing the earplug to expand and contract longitudinally, the Poisson's effect of the earplug influences the spatial distribution of the tangential velocity of the earcanal wall, depending on the earplug insertion depth (see Fig. 5.7(d), (f), (h)). In consequence, a change of the earcanal wall tangential velocity could result in a change in the earplug longitudinal body motion. The influence of the Poisson's effect on the longitudinal body motion is, however, intricate to distinguish in the volume velocity imposed by the earplug to the earcanal cavity.

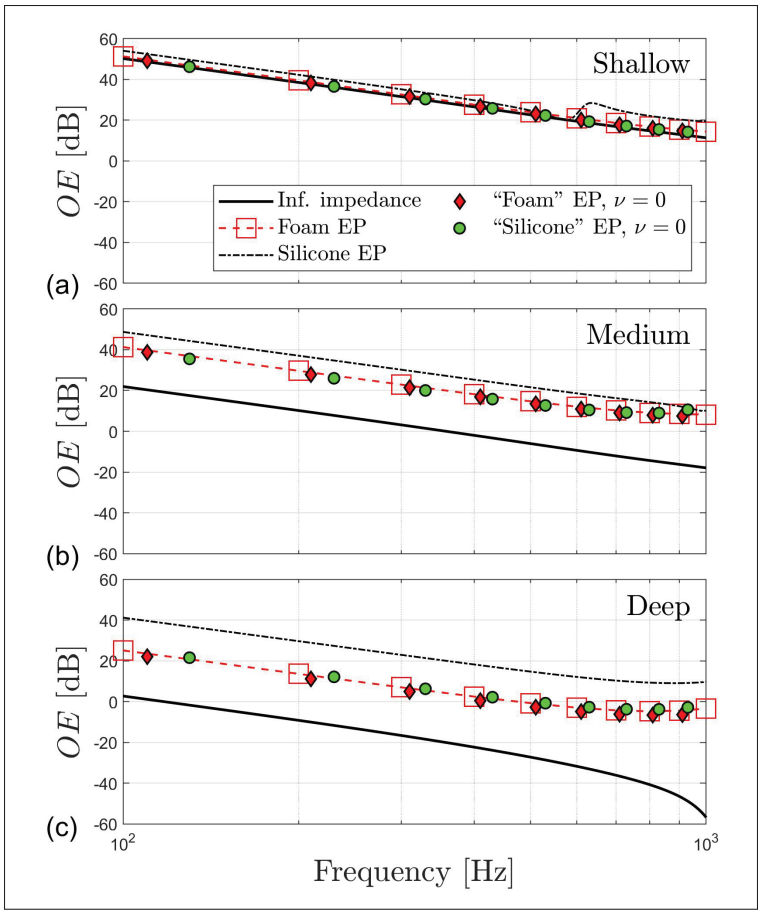

Figure 5.8 Predicted objective OE induced a "foam" and a "silicone" earplug presuming zero Poisson's ratio ($\nu = 0$) at (a) shallow (6 mm), (b) medium (12 mm) and (c) deep (18 mm) insertion computed using the FE model (in narrow band but displayed at selected frequencies only). For comparison, OE induced by an infinite impedance, a foam and a silicone earplug computed using the FE model and presented in Fig. 5.4

5.4.3 Influence of the earcanal wall vibration distribution on the occlusion effect

In the previous section, two mechanisms of contribution of the earplug to the OE have been highlighted: (i) Poisson's effect induced by the normal component of the earcanal wall vibration and (ii) the longitudinal motion governed by the tangential component of the earcanal wall vibration. Both mechanisms depend on the vibration of the surrounding earcanal wall. The

influence of the distribution of this vibration is now studied. In Carillo *et al.* (2020), the distribution of the earcanal wall vibration was varied by applying different sets of loading and boundary conditions while the geometry was fixed. In this study, however, the influence of a geometric parameter on this distribution and consequently on the OE is examined. A geometric parameter that has not been studied in previous work is the transition between the cartilaginous and bony tissues surrounding the earcanal cavity. This transition is expected to approximately occur at the mid-length of the earcanal (Stenfelt & Reinfeldt, 2007) but the geometry of the transition varies significantly around the earcanal cavity, as exposed in Sec. 5.3.1. Here, three anatomically different geometries of the transition between cartilaginous and bony tissues have been constructed using the 2D FE model from an anatomical model of a 3D human outer ear (see Fig. 5.2). These 2D geometries have been presented in Sec. 5.3.1 (see Fig. 5.1(b), (c) and (d)) and only differ by their transitions between the cartilaginous and bony tissues.

Figure 5.9 illustrates the structural vibration of the earcanal wall surrounding tissues computed using the FE model at 100 Hz for the three transitions: (a) "straight", (b) "slanted" and (c) "curved." It is noteworthy that each drawing of the model has been cut in the r-direction along the z-axis in order to limit the size of the figure. Due to this cut, the full geometry of each transition between cartilaginous and bony part is not visible in Fig. 5.9 but can be seen in Fig. 5.1(b), (c) and (d). The first case (see Fig. 5.9(a)) corresponds to the standard configuration of the FE model used in previous sections. For each transition, the amplitude of the earcanal wall vibration decreases from the earcanal entrance to the eardrum and is significantly lower in the bony part compared to the cartilaginous part. Distributions of the normal and tangential vibrations of the earcanal wall are characterized by their centroid positions $l_{c,n}$ and $l_{c,t}$ defined from the earcanal entrance. As shown in Fig. 5.9, when the transition between cartilaginous and bony tissues moves towards the eardrum, both centroid positions move too: $l_{c,n}$ decreases from -4.5 mm to -6.2 mm and $l_{c,t}$ decreases from -7.3 mm to -10.6 mm. For the same reasons exposed in Sec. 5.4.2.1, vibration patterns exhibited here by the two additional anatomical models of the outer ear (see Fig. 5.9(b) and (c)) cannot be compared to experimental data.

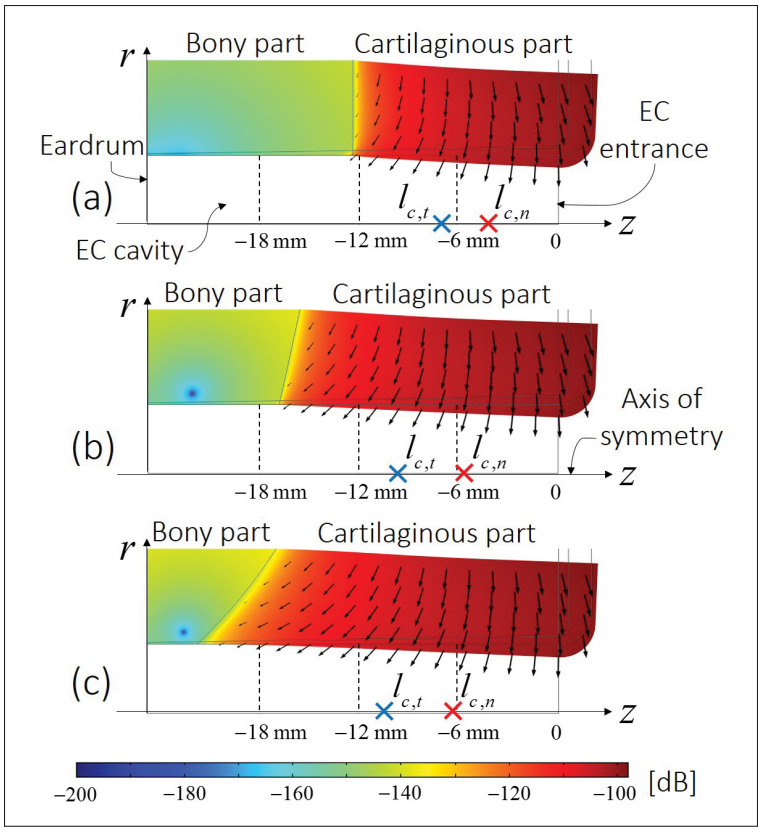

Figure 5.9 Amplitude in dB (factor 20, ref. 1 m s^{-1}) of the structural velocity of the earcanal surrounding tissues computed using the FE model at 100 Hz ($t = T/8$) for the three different transitions between cartilaginous and bony tissues of the outer ear: (a) "straight", (b) "slanted" and (c) "curved." Black arrows represent velocity vectors. A scale factor has been applied in all subplot to highlight the total deformation of the system in the (r, z) plane. Each drawing of the model has been cut in the r-direction along the z-axis to limit the size of the figure

Figure 5.10 displays the OE induced by the infinite impedance, the foam earplug and the silicone earplug computed at 100 Hz as a function of insertion depth (from 6 to 18 mm) using the FE model for the three anatomical geometries characterized by their different transitions between cartilaginous and bony tissues of the outer ear: (a) "straight", (b) "slanted" and (c) "curved." At shallow insertion (6 mm), there is no significant difference in OE between the three different

anatomical models. In each case, the OE induced by the infinite impedance is equal to the OE of the foam earplug (*i.e.*, negligible longitudinal motion of the earplug) and almost equal to the OE of the silicone earplug (*i.e.*, little influence of the earplug Poisson's effect). This means that the volume velocity imposed by the "free" earcanal wall governs the OE while the contribution of the earplug has little influence.

However, substantial variations in OE occur between the three anatomical models when the insertion depth increases. Firstly, the OE induced by the infinite impedance increases between the three cases, in particular from medium to deep insertion. At deep insertion (18 mm), the OE induced by the infinite impedance increases from 3 dB in the "straight" transition (see Fig. 5.10(a)) to 25 dB in the "curved" transition (see Fig. 5.10(c)). This is explained by the fact that the medial surface of the earplug does not enter the portion of the earcanal wall which is directly backed by bony tissue in the "curved" transition. The augmentation of the OE induced by the infinite impedance from the "straight" transition to the "curved" transition (in particular at medium and deep insertions) reveals an increase of the contribution of the "free" earcanal wall in terms of volume velocity to the OE. This increase is explained by the variation of the earcanal wall normal vibration distribution which moves towards the eardrum (*i.e.*, the centroid position $l_{c,n}$ diminishes from -4.5 mm in the "straight" transition to -6.2 mm in the "curved" transition). Secondly, due to the increase of the "free" earcanal wall contribution between the three cases, the reduction of the OE with insertion depth decreases. Indeed, the reduction with insertion depth (from 6 mm to 18 mm) of the OE induced by the foam earplug decreases from 26 dB (see Fig. 5.10(a)) to 13 dB (see Fig. 5.10(c)) and from 13 dB (see Fig. 5.10(a)) to 8 dB (see Fig. 5.10(c)) for the silicone earplug. Thirdly, in consequence to the increase of the "free" earcanal wall contribution between the three cases, the influence of the earplug contribution decreases. The difference in OE between the foam and the silicone earplug decreases between the three cases (from 22 dB to 14 dB at 18 mm, see Fig. 5.10(a) and (c)). The influence of Poisson's effect of the earplug on the OE thus diminishes. In addition, the difference in OE between the foam earplug and the infinite impedance also decreases (from 22 dB to 14 dB at

18 mm, see Fig. 5.10(b) and (c)). The influence of the longitudinal motion of the earplug on the OE thus also diminishes.

It should be noted that the variation of the earcanal wall normal vibration distribution not only influences the vibro-acoustic behavior of the occluded earcanal but also that of the open earcanal since its acoustic mass is defined between the earcanal entrance and the centroid position $l_{c,n}$ (see Eq. (5.4) of the EA model and the proof given in Appx. XI). However, the variation of $l_{c,n}$ from -4.5 mm to -6.2 mm between the "straight" and the "curved" configurations (see Fig. 5.9(a) and (c)) has little influence here (<2 dB) on the open earcanal cavity acoustic impedance.

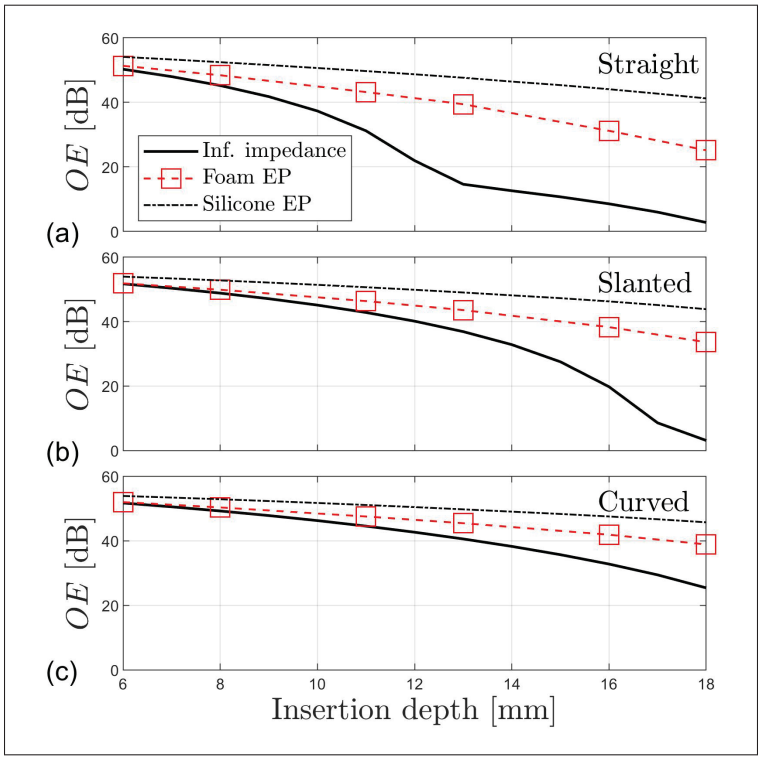

Figure 5.10 Predicted objective OEs induced by an infinite impedance, a foam earplug and a silicone earplug computed at 100 Hz as a function of the insertion depth using the FE model for the three different transitions between cartilaginous and bony tissues of the outer ear: (a) "straight", (b) "slanted" and (c) "curved"

5.4.4 Main limitations and perspectives of the study

A 2D axi-symmetric FE model initially developed by Brummund *et al.* (2015) and slightly modified here has been used to predict and investigate the objective OE induced by an earplug depending on its material properties and its insertion depth. Since this study focuses on the objective OE, the FE model that was developed only accounts for the outer ear while other pathways such as the middle and inner ears have been neglected. If the subjective OE were to be investigated, the bone-conducted transmission through the middle and inner ears could not be neglected because the outer ear pathway does not dominate the hearing by bone-conduction when the earcanal is open, as mentioned in the introduction. As a consequence, the subjective OE is generally 5 to 10 dB lower than the objective OE, mainly below 500 Hz, due to the difference in bone-conduction pathways (Huizing, 1960; Stenfelt & Reinfeldt, 2007; Reinfeldt *et al.*, 2007). However, the current study only aimed at investigating the mechanisms of contribution of earplugs on the SPL generated in the occluded earcanal cavity and particularly exploring and explaining the difference in OEs induced by a foam and a silicone earplug. Therefore, the perception of this difference and its influence on the acoustic comfort of earplugs' wearers was not investigated in this work.

The present model includes the earcanal cavity (from its entrance to the tympanic membrane) surrounded by a portion of human tissues (*e.g.*, skin, cartilage, bone). For the purpose of the current study, the FE model presents several simplifications, particularly in terms of geometry, boundary conditions and loading. A whole head model could alleviate these limitations but loses the main advantage of the current FE model (*i.e.*, few computational resources and parametric geometrical model). In particular, a whole head model could account for the influence of the stimulation position seen in experimental data below 250 Hz (see Sec. 5.4.1). Another limitation of the 2D FE model was to assume negligible the prestress in the earcanal surrounding tissues due to the insertion of the earplug. This limitation mainly comes from the lack of knowledge regarding the tissues mechanical properties under prestress (see Sec. 5.3.2). Accounting for prestress could influence the respective contribution of each mechanism highlighted here. Also, prestress could lead to a stiffer system which could result in lower vibration of the medial

earplug surface and the "free" earcanal wall and therefore a lower OE than what was obtained here. However, in the authors' opinion, the effect of prestress is not expected to invalidate the mechanisms of contribution of earplugs highlighted in this paper. The effect of prestress in earplugs and earcanal surrounding tissues should be accounted for when more knowledge about their mechanical behavior will be obtained experimentally.

It is noteworthy to recall that the main purpose of the additional anatomical geometries was to study the influence of the earcanal wall vibration distribution on the OE. Indeed, while the three geometrical transitions between cartilaginous and bony tissues have been derived from a realistic anatomical model of a human outer ear, they represent simplified cases since the geometry of the model is axi-symmetric. This distribution would also be expected to vary with different stimulus types and locations. Such variation might explain the variation in OE with stimulator position (Reinfeldt *et al.*, 2013) and could also contribute to the OE inter-individual difference (Stenfelt & Reinfeldt, 2007) observed in Sec. 5.4.1 (see Fig. 5.3(b) and (c)). In the case of chewing or speaking, the mandibular movement (Darkner *et al.*, 2007) could affect the influence of the earplug to the OE. In addition, the contribution of the earplug could also be influenced by the shape of the earcanal while ear hairs and wax could influence its coupling with the earcanal wall. Due to the complexity associated to their modeling, these phenomena have not been accounted for in this study.

Although the model compares reasonably well with experimental data of the OE (see Fig. 5.3), the knowledge of the spatial distribution of the earcanal wall vibration in the normal and the tangential directions as well as the vibration of the earplug is necessary to confirm the two mechanisms of the earplug contribution exposed in this paper (see Sec. 5.4.2). The main reason there is a lack of experimental data related to the vibration of the earcanal wall and the medial earplug surface in human subject is due to the remarkable difficulty to perform such measurements. Indeed, the small size of the earcanal as well as its tortuosity make it difficult to assess in a direct way the 3D spatially distributed earcanal wall vibration using common measurement methods such as a laser Doppler vibrometer (Vogel, Zahnert, Hofmann & Huettenbrink, 1996; Stenfelt *et al.*, 2003) or an accelerometer. Hansen has proposed a method to estimate the volume velocity imposed to the

occluded earcanal cavity based on the measure of the acoustic pressure in the occluded earcanal cavity and the knowledge of its acoustic impedance (Hansen & Stinson, 1998). However, this method does not make it possible to distinguish the contribution of the medial earplug surface from that of the "free" earcanal wall. The understanding highlighted in the current paper on the mechanisms of contribution of earplugs to the OE will be helpful to ultimately measure them.

Finally, as a perspective of this work which focused on investigating and explaining the difference in objective OE between foam and silicone earplugs, an existing concept of material used in other application fields which could theoretically be used to design earplugs mitigating the OE is suggested. Since the Poisson's ratio governs the difference in OE between foam and silicone earplugs, auxetic metamaterial (negative Poisson's ratio) could make it possible to generate destructive interference between the volume velocity imposed by the "free" earcanal wall ($\hat{q}_{wall}^{occl}$) and that imposed in phase opposition by the medial surface ($\hat{q}_{EP}$) of the auxetic EP (*i.e.*, $\hat{q}_{wall}^{occl} = -\hat{q}_{EP}$ in Eq. (5.10)). For this solution to reduce the OE to zero, both volume velocities should have an equal magnitude (*i.e.*, $\left|\hat{q}_{wall}^{occl}\right| = |\hat{q}_{EP}|$). In practice, the design of auxetic earplugs to reduce the OE would be a difficult task since it would require the knowledge of the earcanal wall velocity field in both normal and tangential directions, which is likely to differ between individuals and to vary from one bone-conducted excitation to another.

5.5 Conclusion

This paper has investigated the mechanisms of contribution of earplugs to the OE. For this purpose, a 2D axi-symmetric FE model of an outer ear has been used. Simulation results of the OE have been compared successfully to existing data taken from the literature. Finite element simulations have been investigated and interpreted using the "framework" of an EA model associated with the FE model. Using a design of experiment performed on the earplug material properties, the difference in OE between a silicone and a foam earplug has been attributed to a higher Poisson's effect for the latter compared to the former, which increases the OE. This Poisson's effect is induced by the normal component of the earcanal wall vibration. The increase of the earplug influence on the OE with insertion depth has been explained by the augmentation

of the relative contribution of the medial earplug surface in terms of volume velocity compared to that of the "free" earcanal wall coupled to the occluded earcanal cavity. In conjunction to Poisson's effect, a longitudinal motion of the earplug induced by the tangential component of the earcanal wall vibration has been highlighted. Results have shown that this mechanism is independent from the earplug material properties in the range of variation considered here (foam or silicone). Both mechanisms depend on the earcanal wall vibration and its spatial distribution in terms of direction and amplitude. This study has underlined the lack of experimental data related to the vibration of the earcanal wall and the earplug, mainly due to the complexity of such measurements. In the authors' opinion, further work should focus on this experimental aspect. In addition, the current study could be continued using a whole head model in order to include a realistic vibratory behavior of the human head. Also, a whole head model could include the middle and inner ears which would allow to study the subjective OE in addition to the objective OE.

5.6 Acknowledgments

The authors acknowledge the support of the Natural Sciences and Engineering Research Council of Canada (NSERC), [funding reference number RGPIN-2016-06795]. Also, all reviewers are gratefully thanked for their critical and wise comments.

CHAPTER 6

CONCLUSION

In conclusion, this chapter presents a synthesis of the research problem and the results obtained in this thesis (see Sec. 6.1) and then discusses the main limitations of this work and provides future perspectives (see Sec. 6.2).

6.1 Synthesis

6.1.1 Research problem

Hearing protection devices (*i.e.*, earplugs, earmuffs) are frequently used to avoid noise-induced hearing loss. The use of hearing protectors, however, is associated with discomfort issues. Therefore, these protection devices are not always consistently and/or correctly worn during the exposure time. The occlusion effect (OE) is one acoustical discomfort that mostly affects wearers of earplugs. This phenomenon also decreases the acoustic comfort of hearing aids' users. The term "OE" usually describes an increased auditory perception of bone-conducted sound that results from occluding the earcanal entrance and which is mainly perceived at low frequencies, typically below 1 kHz. In everyday life, bone-conducted sounds correspond to physiological noise such as one's own voice, breathing, chewing or heartbeat. The research presented in this thesis aims at improving the understanding of the OE induced by in-ear devices in order to ultimately develop new concepts that mitigate the phenomenon using their own passive vibro-acoustic behavior.

In this work, an objective description of the OE was used, which corresponded to the difference in sound pressure levels (SPLs) between the occluded and the open earcanal. This research was divided into three specific objectives. The first objective consisted to revisit the fundamental mechanism of the OE and to clarify its multiple interpretations. The second objective was to investigate the influence and characteristics of the earcanal wall vibration from which the OE originates and to propose experimental method to measure them. Finally, the third objective was

to highlight the mechanisms of contribution of in-ear devices to the OE. Results obtained during this research project were presented in four papers published in or submitted to peer-reviewed journals and are summarized in next sections.

6.1.2 Fundamental mechanism of the objective occlusion effect

In this work, the fundamental mechanism of the objective OE induced by a bone-conducted stimulation was thoroughly revisited at low frequencies (100 Hz – 1 kHz) using an existing 3D finite element (FE) model of a "realistic" outer ear including the skin, cartilaginous and bony tissues surrounding the earcanal. The model was constructed by Brummund *et al.* (2014) based on cross-sectional cryosection images of a female cadaver from the Visible Human Project® and improved in this work to exhibit a "plausible" vibration pattern of the earcanal wall. The vibration of the earcanal wall, the transfer of volume velocity imposed by the earcanal wall to the earcanal cavity, the "opposition" of the earcanal cavity to this transfer, the acoustic pressure generated in reaction and the acoustic power flow associated to wave propagation were analyzed and illustrated in open and occluded cases. In the latter case, the occlusion was simplified to an infinite impedance defined at the earcanal entrance in order to focus on the fundamental mechanism of the OE.

In conjunction with the 3D FE model, an associated electro-acoustic (EA) model was proposed to clarify and interpret in a simplified way physical phenomena involved in open and occluded earcanals. Compared to past EA models, the proposed one used the curvilinear shape function of the 3D earcanal and the parameters of its ideal volume velocity source representing the earcanal wall normal velocity (*i.e.*, complex-valued amplitude and curvilinear position) were related to the earcanal wall vibration pattern of the 3D FE model. The complex-valued amplitude of the source was computed as the surface averaged earcanal wall normal velocity times the earcanal wall surface. In addition, the location of the source was shown to correspond to the centroid position of the spatially distributed earcanal wall normal velocity. This assumption was successfully evaluated for several earcanal wall vibration patterns induced by various sets

of loading and boundary conditions applied to the 3D FE model. In addition, a proof of this assumption was provided in the case of a cylindrical earcanal shape.

The fundamental mechanism of the OE has been detailed as follows. In harmonic regime, the volume velocity imposed by the earcanal wall is alternatively transferred in the earcanal cavity through the "path" of least "opposition", *i.e.*, mainly between the earcanal wall and the earcanal entrance in the open case, and mainly between the earcanal wall and the eardrum when the earcanal is occluded by an infinite impedance. The greater opposition of the occluded earcanal compared to the open earcanal is responsible for the acoustic pressure increase in the former case. The increase of acoustic pressure is responsible for the increase of volume velocity at the eardrum in the occluded case. The opposition of the earcanal to the volume velocity transfer is represented by the concept of acoustic impedance. In the open case, the acoustic impedance of the earcanal seen by its wall is governed by the inertia effect of the portion of air comprised between the earcanal entrance and the centroid position of the earcanal wall normal vibration. In the occluded case, the earcanal acoustic impedance is rather governed by the compressibility effect of the whole earcanal volume and the tympanic cavity volume of the middle ear. Due to the gradient of acoustic pressure in the open earcanal, the surface averaged acoustic impedance seen by the earcanal wall is lower than the acoustic impedance seen by the ideal volume velocity source representing the vibrating earcanal wall. This difference depends on the centroid position of the earcanal wall normal vibration. In the occluded case, the earcanal wall and its corresponding source see the same acoustic impedance since the acoustic pressure is uniform at low frequencies. The objective OE (*i.e.*, SPL difference at the eardrum between occluded and open cases) is strictly equal to the difference in acoustic impedance level seen by the equivalent source representing the earcanal wall normal vibration located at its centroid position.

In complement to the previous investigation, a commonly accepted theory of the objective OE proposed by Tonndorf (1964) and known as the removal of the open earcanal high-pass filter effect due to the occlusion was revisited. In particular, the focus was put on the definition of the open earcanal high-pass filter and how this filter would be changed in partial and perfect

occlusions. For this purpose, the EA model proposed by Tonndorf to support his theory was revisited in detail and its ambiguities were resolved. Then, using a revisited EA model, a second order high-pass filter for the volume velocity transferred between the earcanal wall and the eardrum was highlighted in the open case. A perfect occlusion was shown to replace the open earcanal high-pass filter effect by a filter constant with frequency. For a partial occlusion, a high-pass filter effect was demonstrated just like in the open earcanal. The partially occluded earcanal, however, was shown to behave as a Helmholtz resonator. In consequence, the OE which Tonndorf considered to be the removal of the open earcanal high-pass filter effect for a perfect occlusion instead was determined to result from a change in high-pass filter effect properties for a partial occlusion. The definition of the OE in terms of volume velocity transfer function was proved to be equal to the OE expressed in terms of earcanal acoustic impedance seen by its wall.

Finally, common interpretations of the OE in terms of “leak” and “trap” were shown to misrepresent the fundamental mechanism of the phenomenon related to the earcanal acoustic impedance change. Interpretations based on impedance changes were therefore considered more accurate. For example, the occlusion increases the “opposition” of the earcanal cavity to the volume velocity imposed by its wall and thus increases the acoustic pressure generated in reaction, leading to the OE.

6.1.3 Vibration of the earcanal wall

In this work, the spatial distribution of the earcanal wall normal vibration was shown to significantly influence the vibro-acoustic behavior of the open earcanal, which subsequently affected the objective OE. Indeed, in conjunction with the earcanal shape, the centroid position of the earcanal wall normal vibration distribution was shown to govern the inertia effect of the open earcanal seen by its wall. In the occluded case, the spatial distribution governed both the reduction of the OE with insertion depth, and the contribution of in-ear devices to the OE through the volume velocity imposed to the earcanal cavity by their medial surface. In particular,

this study highlighted the dependence of contributing mechanisms of in-ear devices such as earplugs on both normal and tangential components of the earcanal wall vibration.

In this work, the principle of an indirect method was proposed to estimate the centroid position of the human earcanal wall normal velocity induced by a bone-conducted stimulation at low frequencies (100 Hz – 1 kHz). The centroid position was used as an indicator of the earcanal wall normal vibration distribution to study the influence of the latter on the bone-conduction outer ear pathway and therefore on the OE. The method consisted in measuring the OE induced by an external capped duct coupled to the earcanal entrance. The centroid position was then estimated at the acoustic antiresonance frequency that occured in the coupled system using an EA model of the earcanal occluded by the external capped duct. The estimation consisted in minimizing the difference between the experimental antiresonance frequency and that computed using the EA model as a function of the centroid position. This EA model required the knowledge of the earcanal shape function and the dimension of the coupling duct. The proposed method was investigated using the 3D FE model improved by the authors from (Brummund *et al.*, 2014) and adapted to the occlusion by an external capped duct. Several parameters was shown to influence the accuracy of the method such as the radius and length of the coupling duct, the presence of an incomplete seal between the duct and the earcanal entrance and finally the knowledge of the earcanal shape as well as the temperature in the duct. On the contrary, the acoustic impedance of the eardrum was shown of little influence on the method accuracy.

6.1.4 Mechanisms of contribution of in-ear devices to the occlusion effect

In this work, the mechanisms of contribution of in-ear devices such as earplugs to the occlusion effect were investigated at low frequencies (100 Hz – 1 kHz) using an existing 2D axi-symmetric FE model of a simplified outer ear. The model was originally developed by Brummund *et al.* (2015) using geometry and material properties taken from literature data and slightly improved in this study to better compare to literature data of the objective OE. In particular, the model was used to study the influence of earplug material properties in conjunction with both the earplug insertion depth and the earcanal wall vibration distribution.

An EA model associated to the 2D FE model was proposed to facilitate the interpretation of FE simulations. Compared to past EA models, the vibration of the medial earplug surface coupled to the earcanal cavity was included as an ideal volume velocity source distinct from the source representing the vibration of the uncovered portion of the earcanal wall coupled to the earcanal cavity. This distinction was facilitated by the fact that inputs of the EA model were derived from the FE model. Using a design of experiment performed on the earplug material properties, the greater OE induced by a silicone earplug compared to a foam earplug was attributed to the difference in Poisson's effect, higher for the former than the latter. The Poisson's effect originated from the normal component of the earcanal wall vibration induced by the bone-conducted stimulation. The decrease of the OE with insertion depth was mainly explained by the reduction of the earcanal wall normal velocity with insertion depth whereas the reduction of its vibrating area had little effect. The increase of the earplug influence on the OE with insertion depth was explained by the augmentation of the relative contribution of the medial earplug surface in terms of volume velocity imposed to the occluded earcanal cavity compared to that of the uncovered earcanal wall. In conjunction to Poisson's effect, a longitudinal motion of the earplug induced by the tangential component of the earcanal wall vibration was highlighted. Results showed that this mechanism was independent from the earplug material properties in the range of variation considered (*i.e.*, between foam and silicone earplugs). Both mechanisms depended on the earcanal wall vibration and its spatial distribution in terms of direction and amplitude.

6.2 Limitations and perspectives

The investigation of the objective OE caused by in-ear devices due to a bone-conducted stimulation was mainly based on the use of 3D and 2D axi-symmetrical FE models. These models, however, are limited in several ways in terms of geometry, material properties, boundary conditions and loading. In both models, the geometry was truncated in order to reduce the computation time. These models only included tissues surrounding the earcanal rather than the entire head. Therefore, they required a set of equivalent boundary conditions and loading in

order to provide simulation results comparable to OE experimental data. In addition, truncated models cannot account for the modal behavior of the whole head, which could however influence the vibro-acoustic behavior of both open and occluded earcanals.

Using the approach proposed by Chang *et al.* (2016) and also Xu *et al.* (2019) to model the entire head, the influence of the truncation of models on OE simulations could be investigated in the future. In particular, the approach of Xu *et al.* (2019) is interesting since the head model comes from a living human subject. This makes it possible to validate their models instead of just compare its simulation results to literature data as it has been done previously and in the current study. Also, full head models could be of great interest in order to exhibit, *a priori*, more realistic earcanal wall vibration patterns and to account for the dependence of vibro-acoustic phenomena on the bone-conducted stimulation. Furthermore, full head models could be used to study the subjective OE by including the middle ear components (Homma *et al.*, 2009; O'Connor, Cai & Puria, 2017) and the inner ear.

Another limitation of FE models used here is the simplification of surrounding tissues. Indeed, these models distinguished the skin (including the fat) from other soft tissues (including cartilage and muscle) whereas more recent studies rather separated cartilage from soft tissues (including skin, fat and muscle) (Chang *et al.*, 2016; Benacchio *et al.*, 2018; Xu *et al.*, 2019). In addition, tissues were considered isotropic linear elastic solids whereas they are more likely to be anisotropic, nonlinear and visco-elastic in practice. Also, the different layers and sublayers of the skin (Li, Li, Xue & Tian, 2018; Joodaki & Panzer, 2018) were not distinguished. However, this could influence the mechanical coupling of in-ear devices in the earcanal, therefore affecting their contribution to the OE.

Another limitation of the current study comes from the lack of experimental data regarding the vibration, in normal and tangential directions, of the earcanal wall. Therefore, FE simulations were been compared to OE data. Also, the indirect method proposed in this study to estimate the centroid position of the earcanal wall normal vibration was not investigated experimentally and, for the moment, cannot be compared to other measurement methods. In addition, the

centroid position only provides a particular characteristic of the earcanal wall normal vibration pattern, not its spatial distribution. Furthermore, the centroid position is not unique and could be shared by several spatial distributions of the earcanal wall normal vibration. It is certain that the measure of the earcanal wall vibration distribution, in normal and tangential directions, would be intricate to perform using direct methods but is *a priori* necessary in order to confirm the mechanisms of contribution of in-ear devices highlighted here with FE models. Experimental investigations of the earcanal wall vibration should be the subject of future studies.

Finally, this thesis ends at the beginning of the development of new passive concepts of in-ear devices that could mitigate the OE using their own vibro-acoustic behavior while achieving their main purpose (*e.g.*, sound attenuation for earplugs, sound amplifier for hearing aids). On the basis of the scientific results obtained in this thesis, a variety of concepts have been elaborated but not presented here due to their early stage of development. Continuing this development will be of primary importance in order to increase the acoustical comfort of users wearing earplugs or hearing aids. For this purpose, the relation between the objective OE and its perception should be better understand. Furthermore, other dimensions of users' comfort should be considered too during the design process of new concepts.

APPENDIX I

ACADEMIC ACHIEVEMENTS

This section summarizes the academic achievements that I obtained during my doctorate (from September 2017 to July 2021), including prizes, papers published in scientific journals, communications presented in scientific conferences and declaration of invention.

The prizes that I obtained include:

1. Grants *Substance ÉTS* for dissemination of research obtained in 2020 (amount $1 000).
2. ÉTS internal scholarships intended to support deserving students obtained in 2020 (amount $7 500).
3. Financial support for the dissemination and promotion of research work attributed by ÉTS in 2019 (amount $1 000).
4. ÉTS internal scholarships intended to support deserving students obtained in 2019 (amount $5 000).
5. Student conference award attributed by the *National Hearing Conservation Association* in 2018 (amount $800).
6. Financial support for the dissemination and promotion of research work attributed by ÉTS in 2017 (amount $1 000).
7. Second prize in the scientific poster competition organized by the *Association Québécoise pour l'Hygiène, la Santé et la Sécurité du Travail* in 2017 (amount $250).

The papers that I published in scientific journals are:

1. Carillo, K., Sgard, F., Xu, H., Guilloteau, A., Benacchio, S., Poissenot-Arrigoni, B., & Doutres, O. (2021). On the modeling of the objective occlusion effect induced by earplugs: Recent advances, challenges and perspectives. *Spectrum*, 38(2), 16-23.
2. Carillo, K., Doutres, O., & Sgard, F. (2021). Principle of an acoustical method for estimating the centroid position of the earcanal wall normal velocity induced by bone-conducted stimulation: Numerical evaluation. *Applied Acoustics*, 182, 108245.

3. Carillo, K., Doutres, O., & Sgard, F. (2020). Theoretical investigation of the low frequency fundamental mechanism of the objective occlusion effect induced by bone-conducted stimulation. *The Journal of the Acoustical Society of America*, 147(5), 3476-3489.
4. Carillo, K., Doutres, O., & Sgard, F. (2020). When hearing our own voice is disturbing: The occlusion effect. *Substance ÉTS*.
5. Carillo, K., Sgard, F., & Doutres, O. (2018). Numerical study of the broadband vibro-acoustic response of an earmuff. *Applied Acoustics*, 134, 25-33.
6. Bonfiglio, P., Pompoli, F., Horoshenkov, K. V., Rahim, M. I. B. S. A., Jaouen, L., Rodenas, J., Bécot, F. X., Gourdon, E., Jaeger, D., Kursch, V., Tarello, M., Roozen, N. B., Glorieux, C., Ferrian, F., Leroy, P., Vangosa, F. B., Dauchez, N., Foucart, F., Lei, L., Carillo, K., Doutres, O., Sgard, F., Panneton, R., Verdiere, K., Bertolini, C., Bär, R., Groby, J. P., Geslain, A., Poulain, N., Rouleau, L., Guinault, A., Ahmadi, H., & Forge, C. (2018). How reproducible are methods to measure the dynamic viscoelastic properties of poroelastic media?. *Journal of Sound and Vibration*, 428, 26-43.

The communications that I presented (or contributed to) in scientific conferences are:

1. Carillo, K., Doutres, O., & Sgard, F. (2020). A finite element model to study the earplug contribution to the objective occlusion effect. *The Journal of the Acoustical Society of America*, 148(4), 2781-2781.
2. Xu, H., Sgard, F., Carillo, K., Wagnac, E., & De Guise, J. (2020). A three-dimensional finite-element model of a human head for predicting the objective occlusion effect induced by earplugs. *The Journal of the Acoustical Society of America*, 148(4), 2780-2780.
3. Sgard, F., Carillo, K., & Doutres, O. (2019). A 2D axisymmetric finite element model to assess the contribution of in-ear hearing protection devices to the objective occlusion effect. *48^{th} International Congress and Exhibition on Noise Control Engineering (Internoise)*, Madrid, Spain.
4. Carillo, K., Doutres, O., & Sgard, F. (2019). Numerical investigation of the fundamental low frequency mechanism of the objective occlusion effect: Focus on the earcanal wall vibration. *26^{th} International Congress on Sound and Vibration (ICSV)*, Montréal, Canada.

5. Voix, J., Carillo, K., Bouchard-Roy, J., Saint-Gaudens, H., Crétot-Richert, G., & Bouserhal, R. (2019). Classe techno "Bruit": Acoustic workshop for high school students at Université du Québec (ÉTS). *26th International Congress on Sound and Vibration (ICSV)*, Montréal, Canada.
6. Carillo, K., Doutres, O., & Sgard, F. (2019). Fundamental mechanisms of the objective occlusion effect revisited using a finite element model of the outer ear. *43rd Annual conference of the National Hearing Conservation Association (NHCA)*, Grapevine, Texas.
7. Carillo, K., Doutres, O., & Sgard, F. (2018). Experimental evaluation of an impedance tube measurement method for assessing earplugs insertion loss. *42nd Annual conference of the National Hearing Conservation Association (NHCA)*, Orlando, Florida.
8. Sgard, F., Benacchio, S., Luan, Y., Xu, H., Carillo, K., Doutres, O., Nelisse, H., Wagnac, E., & De Guise, J. (2018). Vibroacoustic modeling of an in vivo human head wearing a hearing protection device using the finite element method. *11th European Congress and Exposition on Noise Control Engineering (Euronoise)*, Heraklion, Crete.
9. Carillo, K., Sgard, F., & Doutres, O. (2017). Numerical prediction of the broadband sound attenuation of a commercial earmuff: Impact of the cushion modeling. *173rd Meeting of the Acoustical Society of America (ASA)*, Boston, Massachusetts.
10. Bonfiglio, P., Pompoli, F., Horoshenkov, K. V., Rahim, M. I. B. S. A., Jaouen, L., Rodenas, J., Bécot, F. X., Gourdon, E., Jaeger, D., Kursch, V., Tarello, M., Roozen, N. B., Glorieux, C., Ferrian, F., Leroy, P., Vangosa, F. B., Dauchez, N., Foucart, F., Lei, L., Carillo, K., Doutres, O., Sgard, F., Panneton, R., Verdiere, K., Bertolini, C., Bär, R., Groby, J. P., Geslain, A., Poulain, N., Rouleau, L., Guinault, A., Ahmadi, H., & Forge, C. (2017). Round Robin test on elastic properties of poro-and viscoelastic materials for vibro-acoustic applications. *5th Symposium on the Acoustics of Poro-Elastic Materials (SAPEM)*, Le Mans, France.
11. Carillo, K., Doutres, O., & Sgard, F. (2017). Simulation numérique de l'atténuation sonore d'un projecteur auditif de type casque anti-bruit. *39^{e} Congrès de l'Association québécoise pour l'hygiène, la santé et la sécurité du travail (AQHSST)*, Victoriaville, Canada.

Finally, the declaration of invention that I submitted to ÉTS is:

1. Carillo, K., Doutres, O., & Sgard, F. (2021). Methods and devices for mitigating the occlusion effect of in-ear devices.

APPENDIX II

DOMAINS' PROPERTIES

Solid domain properties used in FE models are summarized in Table-A II-1. Air properties used in both FE and EA models are given in Table-A II-2. The molecular dissipation is negligible in the earcanal cavity so the bulk viscosity μ_B is here zero but could be estimated by $\mu_B = 0.6\mu$ (Pierce, 1994). Also, air properties can be calculated from temperature, atmospheric pressure and relative humidity (see Appx. X).

Table-A II-1 Density ρ, Young's modulus E, Poisson's ratio ν and structural loss factor η of solid domains

Tissue	ρ **[kg m^{-3}]**	E **[MPa]**	ν **[1]**	η **[1]**
Skin	1 100	0.5	0.4	0.1
Soft	1 080	7.2	0.26	0.05
Bone	1 714	11 316	0.3	0.01
Foam earplug	220	0.1	0.1	0.5
Silicone earplug	1 050	0.85	0.48	0.1
External duct	2 700	70 000	0.33	0.01
Duct holder	1 050	0.85	0.48	0.1

Table-A II-2 Air density ρ_0, sound speed c_0, dynamic viscosity μ, thermal conductivity coefficient κ, ratio of specific heats γ and heat capacity at constant pressure C_p

Property	**Value**	**Property**	**Value**
ρ_0 [kg m^{-3}]	1.2	κ [W m^{-1} K^{-1}]	0.025
c_0 [m s^{-1}]	343	γ [1]	1.4
μ [Pa s]	1.8313×10^{-5}	C_p [J kg^{-1} K^{-1}]	1.0025×10^{3}

APPENDIX III

VARIOUS SETS OF LOADING AND BOUNDARY CONDITIONS OF THE 3D FINITE ELEMENT MODEL

Various sets of loading and boundary conditions applied to the 3D FE model are summarized in Fig.-A III-1. These sets are used to vary the distribution of the earcanal wall normal velocity characterized by the corresponding curvilinear centroid position l_c defined from the tympanic membrane. Configurations (j) and (k) are similar to those used by Brummund *et al.* (2014). In these cases, switching from fixed (blue surface) to free (gray surface) boundary conditions has little influence on the OE (Brummund *et al.*, 2014) because the earcanal wall vibration distribution is also little influenced (l_c decreases from 17.9 to 16.9 mm).

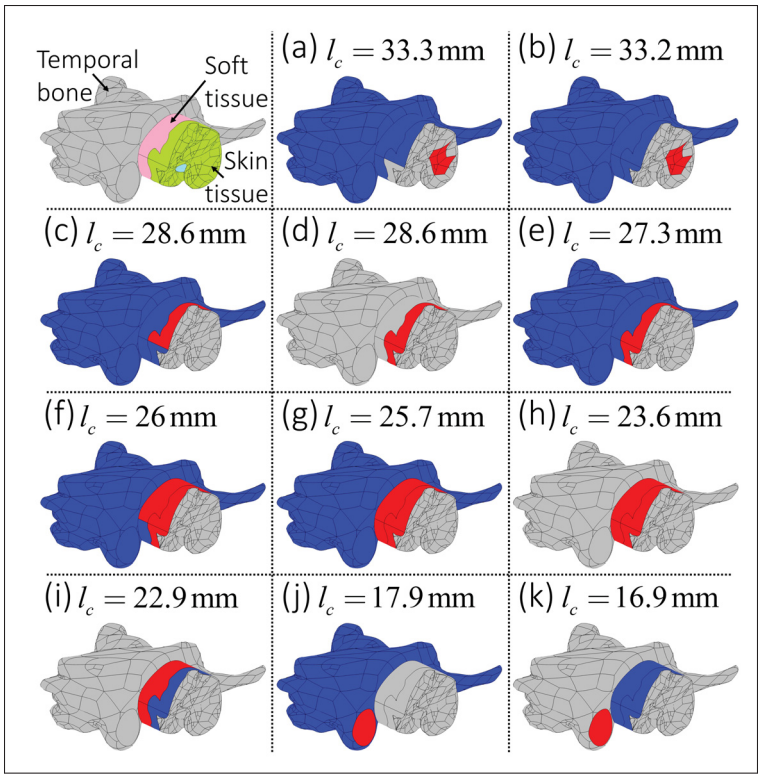

Figure-A III-1 Various sets of mechanical loading and boundary conditions applied to the 3D FE model. Free surface is indicated in gray, fixed surface in blue and excitation surface in red. The curvilinear position l_c (from the tympanic membrane) of the induced earcanal wall normal velocity centroid is also indicated

APPENDIX IV

ACOUSTIC IMPEDANCE DEFINED AT THE TYMPANIC MEMBRANE

This section presents the lumped element model of the middle ear developed by Shaw & Stinson (1981) (see detail in (Shaw & Stinson, 1983) and (Schroeter & Poesselt, 1986)) and illustrated in Fig.-A IV-1. This model is here used to compute the acoustic impedance $\hat{Z}_{TM}$ defined at the eardrum. The localized constants involved in the model are now described. The acoustic compliance C_t represents the compressibility effect of the tympanic cavity. The acoustic resistance R_m accounts for the energy dissipation in the ligaments coupled to the ossicular chain. The acoustic compliance C_p, the acoustic mass L_a and the acoustic resistance R_a correspond respectively to the compressibility effect, the inertia effect and the energy dissipation of the mastoid antrum (a large cavity connected to the tympanic cavity). The mechanical compliance C_{do} and the mechanical resistance R_{do} represent a spring-damper system corresponding to the coupling between the tympanic membrane and the ossicular chain. The mechanical inductance L_d, compliance C_d and resistance R_d correspond to a mass-spring-damper system representing the coupling of the tympanic membrane to ligaments in the tympanic cavity. The ideal transformer of ratio $m = 1/9$ represents the acousto-mechanical coupling between the tympanic membrane and the ossicular chain and transforms the acoustical energy into a mechanical energy. The mechanical inductance L_o, compliance C_o and resistance R_o correspond to a mass-spring-damper system representing the coupling between the malleus and the incus of the ossicular chain. The mechanical compliance C_s and resistance R_s represents the coupling between the incus and the stapes of the ossicular chain. Finally, the mechanical inductance L_c, compliance C_c and resistance R_c correspond to a mass-spring-damper system representing the coupling between the stapes and the oval window of the cochlea. Table-A IV-1 summarizes the value of aforementioned localized constants. Figure-A IV-2 displays the resulting acoustic impedance $\hat{Z}_{TM}$ at the tympanic membrane in dB as well as its low-frequency approximation. In this approximation, the equivalent acoustic compliance includes the compressibility effect of the tympanic cavity and the stiffness of the ossicular chain coupled to the eardrum (*i.e.*, $C_{TM} = C_t + C_{do}$).

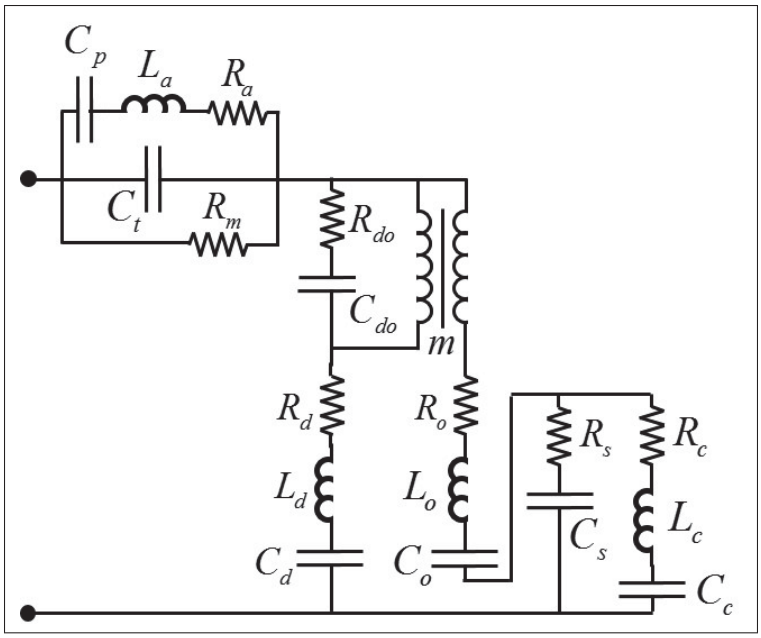

Figure-A IV-1 Lumped element model of the middle ear reproduced from Shaw & Stinson (1981)

Table-A IV-1 Value of localized constants involved in the middle ear model taken from Shaw & Stinson (1981)

Inductance [N s^2 m^{-5}]	**Capacity [m^5 N]**	**Resistance [N s m^{-5}]**
	$C_t = 3.5 \times 10^{-12}$	$R_m = 2 \times 10^7$
$L_a = 2 \times 10^3$	$C_p = 5.1 \times 10^{-11}$	$R_a = 10^6$
	$C_{do} = 2 \times 10^{-12}$	$R_{do} = 1.7 \times 10^7$
$L_d = 1.2 \times 10^3$	$C_d = 3 \times 10^{-11}$	$R_d = 10^6$
$L_o = 3$	$C_o = 1.5 \times 10^{-15}$	$R_o = 9 \times 10^8$
	$C_s = 2.7 \times 10^{-14}$	$R_s = 3 \times 10^{10}$
$L_c = 2$	$C_c = 5 \times 10^{-14}$	$R_c = 6 \times 10^4$

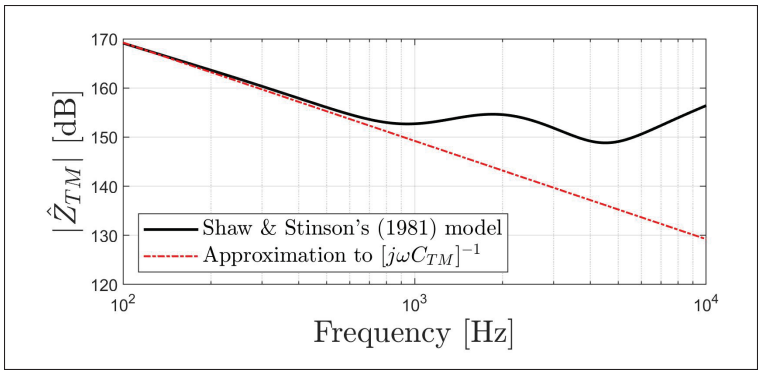

Figure-A IV-2 Level in dB (factor 20, ref. 1 N s m^{-5}) of the tympanic membrane acoustic impedance and its low-frequency approximation based on the lumped element model of the middle ear developed by Shaw & Stinson (1981)

APPENDIX V

RADIATION ACOUSTIC IMPEDANCE DEFINED AT THE EARCANAL OPENING

The radiation acoustic impedance $\hat{Z}_{rad}$ defined at the earcanal opening is equal to that of a baffled circular piston of radius $r_{ent} = r_{EC}(l_{EC})$ coupled to a semi-infinite acoustic domain and is given by (Bruneau, 2013)

$$\hat{Z}_{rad} = \frac{\rho_0 c_0}{\pi r_{ent}^2}\left(1 - \frac{J_1\left(2k_0 r_{ent}\right)}{k_0 r_{ent}} - j\frac{H_1\left(2k_0 r_{ent}\right)}{k_0 r_{ent}}\right), \tag{A V-1}$$

where J_1 and H_1 are the first order Bessel and Struve functions respectively and $k_0 = \omega/c_0$ is the lossless wavenumber.

APPENDIX VI

LOW REDUCED FREQUENCY MODEL

The low reduced frequency model is used to account for viscous and thermal losses that exist in tubes (Kampinga, 2010). Compared to a visco-thermal acoustic model, the low reduced frequency model requires significantly less computational resources. The low reduced frequency model is valid when the acoustic wavelength is much larger than both the tube cross-section and the boundary layer thickness. In a domain i, the equivalent wavenumber $\hat{k}_{eq}^{i}$ and the equivalent characteristic impedance $\hat{Z}_{eq}^{i}$ are given by

$$\hat{k}_{eq}^{i} = k_0 \left[\frac{\gamma - (\gamma - 1)\, \psi_{th}^{i}}{\psi_{vi}^{i}} \right]^{1/2}, \tag{A VI-1}$$

$$\hat{Z}_{eq}^{i} = Z_0 \left[\psi_{vi}^{i} \left(\gamma - (\gamma - 1)\, \psi_{th}^{i} \right) \right]^{-1/2}. \tag{A VI-2}$$

In Eqs. (A VI-1) and (A VI-2), $k_0 = \omega / c_0$ and $Z_0 = \rho_0 c_0$ represent respectively the free space wavenumber and characteristic impedance, ρ_0 and c_0 are respectively the air density and the sound speed, and γ corresponds to the ratio of specific heats. In addition, ψ_{vi}^{i} and ψ_{th}^{i} correspond to geometry and material dependent functions associated to viscous and thermal effects and defined by

$$\psi_{vi}^{i} = -\frac{J_2 (k_{vi} r_i)}{J_0 (k_{vi} r_i)}, \tag{A VI-3}$$

$$\psi_{th}^{i} = -\frac{J_2 (k_{th} r_i)}{J_0 (k_{th} r_i)}. \tag{A VI-4}$$

In Eqs. (A VI-3) and (A VI-4), J_α is the first order Bessel function for integer α. In addition, $k_{vi} = \sqrt{-j\omega\rho_0/\mu}$ and $k_{th} = \sqrt{-j\omega\rho_0 C_p/\kappa}$ are the viscous and thermal wavenumbers while μ, C_p and κ represent respectively the dynamic viscosity, the heat capacity at constant pressure and the thermal conductivity coefficient.

APPENDIX VII

ACOUSTIC POWER BALANCE COMPUTED USING THE 3D FINITE ELEMENT MODEL

This section details the various contributions of the acoustic power balance in open and occluded cases computed using the low reduced frequency 3D FE model. In the open case, the visco-thermal dissipation represents approximately 99% at 100 Hz of the injected acoustic power and decreases with frequency to approximately 11% at 1 kHz. This dissipation mainly occurs in the earcanal wall upstream section boundary layer where the fluid experiences friction due to its viscosity and the gradient of tangential acoustic particle velocity. It should be noted that the damping factor in a real open earcanal has been estimated to be approximately 3 times higher than that computed in an earcanal with smooth wall (Hudde & Engel, 1998b). The acoustic power radiated through the earcanal opening only represents a fraction of the injected acoustic power at low frequencies (<3%). This proportion was greatly overestimated by Brummund *et al.* (2014) since they neglected the visco-thermal dissipation. The remaining proportion of the acoustic power injected to the open earcanal cavity by its wall is dissipated at the tympanic membrane and increases with frequency. In the occluded case, the acoustic power dissipated at the tympanic membrane represents approximately 85% at 100 Hz of the injected acoustic power and increases with frequency to approximately 99.9% at 1 kHz. The remaining acoustic power injected in the occluded earcanal is mainly dissipated by thermal effect in the earcanal wall boundary layer.

APPENDIX VIII

OCCLUSION EFFECT EXPRESSED IN TERMS OF ACOUSTIC POWER

This section details the expression of the OE in terms of time-averaged acoustic power dissipated at the tympanic membrane $\bar{W}_{TM}^{k}$. From Eq. (2.5), the time-averaged tympanic membrane acoustic power can be computed by

$$\bar{W}_{TM}^{k} = \frac{1}{2}\Re\left[\int_{S_{TM}} \frac{\left|\hat{p}_{TM}^{k}\right|^2}{\hat{Z}_{TM}^{*}}\,\mathrm{d}S\right]. \tag{A VIII-1}$$

Consider now the difference in acoustic power level dissipated at the tympanic membrane between the occluded and the open earcanals:

$$10\log_{10}\left(\frac{\bar{W}_{TM}^{occl}}{W_{ref}}\right) - 10\log_{10}\left(\frac{\bar{W}_{TM}^{open}}{W_{ref}}\right) = 10\log_{10}\left(\frac{\frac{1}{2}\Re\left[\int_{S_{TM}} \frac{\left|\hat{p}_{TM}^{occl}\right|^2}{\hat{Z}_{TM}^{*}}\,\mathrm{d}S\right]}{\frac{1}{2}\Re\left[\int_{S_{TM}} \frac{\left|\hat{p}_{TM}^{open}\right|^2}{\hat{Z}_{TM}^{*}}\,\mathrm{d}S\right]}\right). \tag{A VIII-2}$$

At low frequencies, the acoustic pressure is spatially homogeneous over the tympanic membrane surface in both open and occluded cases (see Fig. 2.4(c)) such that $\hat{p}_{TM}^{k} = \left\langle \hat{p}_{TM}^{k} \right\rangle$. Using this assumption, Eq. (A VIII-2) can be rewritten such as

$$10\log_{10}\left(\frac{\left|\left\langle \hat{p}_{TM}^{occl}\right\rangle\right|^2 \Re\left[\frac{1}{\hat{Z}_{TM}^{*}}\right]}{\left|\left\langle \hat{p}_{TM}^{open}\right\rangle\right|^2 \Re\left[\frac{1}{\hat{Z}_{TM}^{*}}\right]}\right) = 10\log_{10}\left(\frac{\left|\left\langle \hat{p}_{TM}^{occl}\right\rangle\right|^2}{\left|\left\langle \hat{p}_{TM}^{open}\right\rangle\right|^2}\right) = 20\log_{10}\left(\left|\frac{\left\langle \hat{p}_{TM}^{occl}\right\rangle}{\left\langle \hat{p}_{TM}^{open}\right\rangle}\right|\right) = OE, \tag{A VIII-3}$$

which is equal to the OE defined by Eq. (2.4).

The computation of OE_{leak} is now detailed. Starting from the OE computed in terms of time-averaged acoustic power dissipated at the tympanic membrane in open and occluded earcanals (see Eq. (A VIII-3)) and using the acoustic power balance in both cases (see Sec. 2.3.1.4), the

OE can be written as

$$OE = 10\log_{10}\left(\frac{\bar{W}_{TM}^{occl}}{\bar{W}_{TM}^{open}}\right) = 10\log_{10}\left(\frac{\bar{W}_{wall}^{occl} - \bar{W}_{diss}^{occl}}{\bar{W}_{wall}^{open} - \bar{W}_{diss}^{open} - \bar{W}_{ent}^{open}}\right), \quad \text{(A VIII-4)}$$

which is equivalent to

$$OE = 10\log_{10}\left(\frac{\bar{W}_{wall}^{occl} - \bar{W}_{diss}^{occl}}{\bar{W}_{wall}^{open} - \bar{W}_{diss}^{open}}\right) + 10\log_{10}\left(\frac{\bar{W}_{wall}^{open} - \bar{W}_{diss}^{open}}{\bar{W}_{wall}^{open} - \bar{W}_{diss}^{open} - \bar{W}_{ent}^{open}}\right). \quad \text{(A VIII-5)}$$

In Eq. (A VIII-5), the left term of the product can be interpreted as an equivalent OE, referred to as OE_{leak}, representing the reduction to 0 of the acoustic power $\bar{W}_{ent}^{open}$ radiated at the earcanal opening due to its occlusion by an infinite impedance. In this case, the acoustic power that was radiated at the earcanal opening in the open case is rather dissipated at the tympanic membrane in the occluded case. From Eq. (A VIII-5), OE_{leak} can be rewritten as

$$OE_{leak} = 10\log_{10}\left(\frac{1}{1 - \frac{\bar{W}_{ent}^{open}}{\bar{W}_{wall}^{open} - \bar{W}_{diss}^{open}}}\right) = 10\log_{10}\left(1 + \frac{\bar{W}_{ent}^{open}}{\bar{W}_{wall}^{open}}\right). \quad \text{(A VIII-6)}$$

From Eq. (A VIII-5), the right term of the product can also be interpreted as an equivalent OE computed such that no acoustic power is radiated at the earcanal opening in the open case. The acoustic power that would be radiated at the earcanal opening is rather dissipated at the tympanic membrane in the open case.

APPENDIX IX

OCCLUSION EFFECT INDUCED BY AN EXTERNAL CAPPED DUCT: SIMULATION VERSUS EXPERIMENTAL DATA

This section provides a comparison between experimental data and simulation of the objective OE induced by an external capped duct coupled to the earcanal entrance. Experimental data were measured by Huizing (1960) on a human subject as a function of the duct length while the bone-conducted stimulation was fixed at 1 kHz. Huizing used a copper duct of 500 mm length which was occluded at 12 different positions along its length. The radius of the duct was chosen "equal" to that of the earcanal entrance, which is *a priori* not circular. The seal between the earcanal entrance and the duct was not detailed. The bone-conducted stimulation was ensured by a bone-transducer located at the ipsilateral mastoid. The acoustic pressure was measured close to the tympanic membrane. In this work, Huizing's experiment is numerically reproduced using the purely acoustical 3D FE model in order to assess the model's validity. The radius of the coupling duct is equal to the equivalent radius of the earcanal entrance assuming circular cross-section. Measured and simulated OEs induced by an external capped duct are displayed in Fig.-A IX-1 as a function of the duct length l_{duct} (added to the earcanal length l_{EC} and normalized by the lossless wavelength calculated at 1 kHz). According to Fig.-A IX-1, experimental and simulated OEs are in relative agreement and present similar slopes which periodically decrease and increase with the length of the coupling duct.

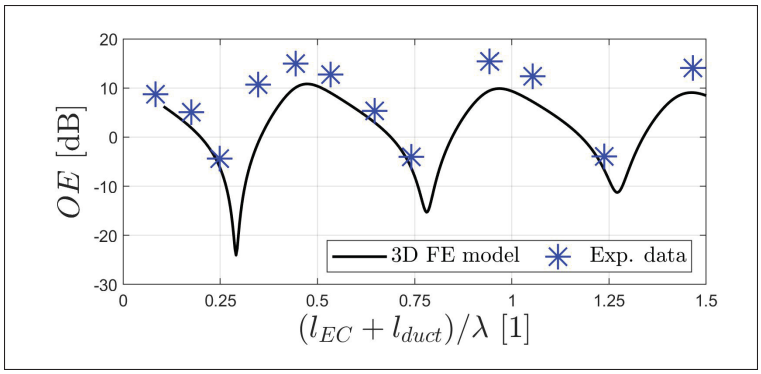

Figure-A IX-1 OE induced by an external capped duct coupled at the earcanal entrance computed at 1 kHz as a function of the duct length using the purely acoustical 3D FE model versus experimental data measured on a human subject by Huizing (1960)

APPENDIX X

CALCULATION OF AIR PROPERTIES FROM TEMPERATURE, ATMOSPHERIC PRESSURE AND RELATIVE HUMIDITY

This section details the computation of density ρ_0, sound speed c_0, dynamic viscosity μ, heat capacity at constant pressure C_p and ratio of specific heats γ of air from the knowledge of the temperature T (in Kelvin, 1°C is equal to 273.15 K), atmospheric pressure P_{atm} (in Pascal) and relative humidity $H_{\%}$ (in percentage). The thermal conductivity κ, however, can be assumed constant within the usual range of variation of these parameters and equal to 0.025 W m^{-1} K^{-1}.

The density of humid air is given by

$$\rho_0 = \frac{P_{atm}}{R_d T} - \left(\frac{1}{R_d} - \frac{1}{R_v}\right) \frac{H_{\%}}{100} \times \frac{P_{sat}}{T}, \tag{A X-1}$$

where $R_d = 287.031$ J kg^{-1} K^{-1} and $R_v = 461.521$ J kg^{-1} K^{-1} are the specific gas constants for dry air and for water vapor respectively whereas P_{sat} is the saturation water vapor pressure estimated as a function of the temperature by (Pierce, 1994)

$$P_{sat} = 0.0658 \times T^3 - 53.7558 \times T^2 + 14\,703.8127 \times T - 1\,345\,485.0465. \tag{A X-2}$$

The specific heat at constant pressure can also be estimated as a function of temperature by (Touloukian & Makita, 1970)

$$C_p = 4168.8 \times (0.249679 - 7.55179 \times 10^{-5} \times T + 1.69194 \times 10^{-7} \times T^2 - 6.46128 \times 10^{-11} \times T^3). \tag{A X-3}$$

The ratio of specific heat is then given by

$$\gamma = \frac{C_p}{C_p - R_d}. \tag{A X-4}$$

Under the ideal gas assumption, the isentropic sound speed is then calculated by

$$c_0 = \left[\frac{\gamma P_{atm}}{\rho_0}\right]^{1/2}. \qquad \text{(A X-5)}$$

Finally, the dynamic viscosity can be estimated as a function of the temperature by (Lide & Kehiaian, 1994)

$$\mu = 7.72488 \times 10^{-8} \times T - 5.95238 \times 10^{-11} \times T^2 + 2.71368 \times 10^{-14} \times T^3. \qquad \text{(A X-6)}$$

APPENDIX XI

LOCATION OF THE EQUIVALENT IDEAL VOLUME VELOCITY SOURCE IN A CYLINDRICAL EARCANAL

This section provides more details on the location of the equivalent ideal volume velocity source Q representing the whole earcanal wall normal vibration at the corresponding centroid position using an EA model of the open earcanal. The case of a cylindrical earcanal of constant radius r_{EC} and length l_{EC} is considered. The earcanal axis is referred to as z. The eardrum is defined at $z = -l_{EC}$ whereas the earcanal entrance is defined at $z = 0$. The normal vibration of the surrounding earcanal wall is accounted for as a distribution of an infinite number of ideal volume velocity sources along the earcanal axis. Each source Q_i represents an infinitesimal portion of length δ_{EC} of the earcanal and imposes a volume velocity $\hat{q}_i$ ($i \in \mathbb{N}^*$) such that the sum of all volume velocities is equal to the volume velocity $\hat{q}_{wall}^{open}$ imposed by the whole earcanal wall (*i.e.*, $\hat{q}_{wall}^{open} = \sum_{i=1}^{\infty} \hat{q}_i$). In addition, each source is located at a position $z = -l_i$ ($-l_{EC} \leq -l_i \leq 0$) corresponding to the position of the infinitesimal portion of earcanal and neglecting its infinitesimal length δ_{EC}. Applying the principle of superposition (linear system), the acoustic pressure at the eardrum ($z = -l_{EC}$) is given by

$$\hat{p}_{TM}^{open} = \sum_{i=1}^{\infty} \hat{p}_{TM,i}^{open}, \tag{A XI-1}$$

where $\hat{p}_{TM,i}^{open}$ is the acoustic pressure generated by a source Q_i and defined by

$$\hat{p}_{TM,i}^{open} = \hat{Z}_{EC/Q,i}^{open} \times \hat{q}_i, \tag{A XI-2}$$

where $\hat{Z}_{EC/Q,i}^{open}$ represents the acoustic impedance of the open earcanal cavity seen by a source Q_i. In first approximation, this acoustic impedance can be simplified to

$$\hat{Z}_{EC/Q,i}^{open} \approx j\omega \left(L_{rad} + L_u^i \right), \tag{A XI-3}$$

where L_{rad} represents the acoustic mass of radiation at the earcanal entrance and L_u^i the acoustic mass of the earcanal upstream section. The latter is defined by $L_u^i = -\rho_0 l_i / S_{EC}$ with the air density ρ_0 and the earcanal cross-section area $S_{EC} = \pi r_{EC}^2$. Substituting Eqs. (A XI-2) and (A XI-3) into Eq. (A XI-1), the acoustic pressure at the eardrum can be rewritten as

$$\begin{aligned}
\hat{p}_{TM}^{open} &= \sum_{i=1}^{\infty} j\omega \left(L_{rad} + L_u^i\right) \times \hat{q}_i \\
&= \sum_{i=1}^{\infty} j\omega L_{rad} \times \hat{q}_i + \sum_{i=1}^{\infty} j\omega L_u^i \times \hat{q}_i \\
&= j\omega L_{rad} \times \hat{q}_{wall}^{open} + \frac{j\omega\rho_0}{S_{EC}} \sum_{i=1}^{\infty} -l_i \times \hat{q}_i \\
&= j\omega L_{rad} \times \hat{q}_{wall}^{open} + \frac{j\omega\rho_0}{S_{EC}} \left(\sum_{i=1}^{\infty} \frac{-l_i \times \hat{q}_i}{\hat{q}_{wall}^{open}} \right) \times \hat{q}_{wall}^{open}. \qquad \text{(A XI-4)}
\end{aligned}$$

From the latter equation, one can recognize an expression of the centroid position l_c of the earcanal wall normal vibration given by $l_c = \sum_{i=1}^{\infty} \frac{-l_i \times \hat{q}_i}{\hat{q}_{wall}^{open}}$.

APPENDIX XII

VERIFICATION OF THE ACCURACY OF THE ELECTRO-ACOUSTIC FRAMEWORK ASSOCIATED WITH THE 2D FINITE ELEMENT MODEL

To investigate and interpret FE simulations in the EA framework, the latter must provide accurate approximations of the former. In Fig.-A XII-1, the OE computed using Eq. (5.10) of the EA framework is displayed, superimposed with OE computed using the FE model. It is noteworthy that EA simulations are displayed at selected frequency points rather than in narrow band in order to increase the readability of Fig.-A XII-1. As expected, approximations of the OE obtained using the EA model are in good agreement with FE simulations in all cases (foam, silicone and infinite impedance earplugs) and at all insertion depths. This verifies the accuracy of the EA framework, despite its simplifications and assumptions (see Sec. 5.3.5).

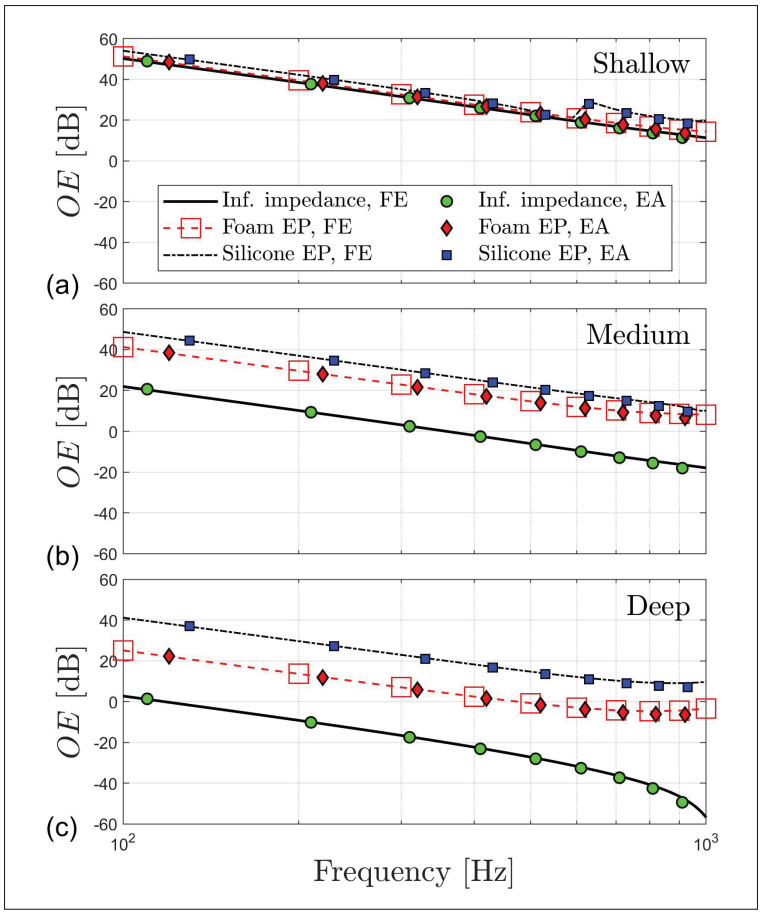

Figure-A XII-1 Predicted objective OE induced by an infinite impedance, a foam earplug and a silicone earplug at (a) shallow (6 mm), (b) medium (12 mm) and (c) deep (18 mm) insertion computed using both FE model and EA model (in narrow band but displayed at selected frequencies only)

APPENDIX XIII

RESULTS OF THE DESIGN OF EXPERIMENT PERFORMED ON THE EARPLUG PROPERTIES USING THE 2D FINITE ELEMENT MODEL

Figure-A XIII-1 displays the influence of the earplug material properties on the volume velocity $\hat{q}_{EP}$ imposed by its medial surface and computed using the 2D FE model for (a) shallow, (b) medium and (c) deep insertion. Results are presented in terms of variation $\Delta\hat{q}_{EP}$ in dB from the mean value (0 dB) of the volume velocity imposed by the medial earplug surface computed from the $2^3 = 8$ configurations of the design of experiment. A positive variation means that the parameter (or the couple of parameters) tends to increase the volume velocity imposed by the earplug on the occluded earcanal cavity whereas negative variation means the opposite. Most important effects only are presented in Fig.-A XIII-1. For all insertion depths, the Young's modulus and the density of the earplug are seen to be of minor influence on the volume velocity imposed by the medial earplug surface compared to the Poisson's ratio. Indeed, Poisson's effect is the only one that substantially moves the curves from the 0 dB line, by from 10 to 17 dB across conditions depending upon frequency. Poisson's effect thus governs the difference in contribution between a foam and a silicone earplug. Both the Young's modulus (main effect) and the interaction between the Young's modulus and the Poisson's ratio (interaction effect) tend to decrease the volume velocity imposed by the medial earplug surface. This is explained by the bulk modulus of the earplug defined in 2D by $K = E/[2\,(1-\nu)]$ which measures the resistance of the earplug to compression. The bulk modulus of the earplug increases with both Young's modulus and Poisson's ratio which in consequence constrains the normal vibration of the earcanal wall portion coupled to the earplug and therefore reduces the volume velocity imposed by the medial earplug surface by Poisson's effect. The effect solely due to Poisson's ratio accounts for the influence of the bulk modulus and Poisson's effect, both of which act in opposition to each other on $\hat{q}_{EP}$. However, since the effect due to Poisson's ratio is positive and significantly greater, it is concluded that the Poisson's effect largely dominates the effect of the bulk modulus in the design of experiment.

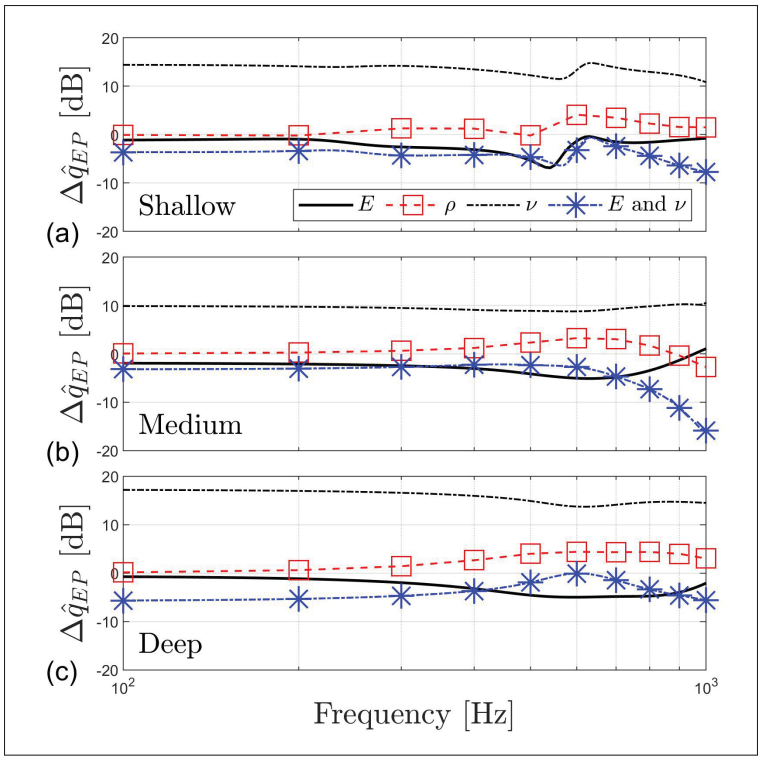

Figure-A XIII-1 Variation in dB (factor 20, ref. 1 m^3 s^{-1}) from the mean value of the volume velocity $\hat{q}_{EP}$ imposed by the medial earplug surface as computed using the 2D FE model. The results derive from the design of experiment performed on the earplug material properties at (a) shallow (6 mm), (b) medium (12 mm) and (c) deep (18 mm) insertion as a function of frequency

In complement to Fig.-A XIII-1, Fig.-A XIII-2 displays the OE induced for several Poisson's ratios for a silicone earplug. For all insertion depths, the overall amplitude of the OE is seen to increase with Poisson's ratio, confirming the preponderant role of the Poisson's effect in the difference in OE between a foam ($\nu = 0.1$) and a silicone ($\nu = 0.48$) earplug. The increase of the Poisson's ratio from 0 to 0.2 increases the OE by approximately 3 dB for all insertion depths. The increase of Poisson's ratio from 0.2 to 0.48 increases the OE by approximately 6 dB (above the resonance frequency around 600 Hz), 8 dB, and 12 dB for shallow, medium, and deep insertion respectively. Hence, the influence of the Poisson's ratio is not linear and increases with insertion depth.

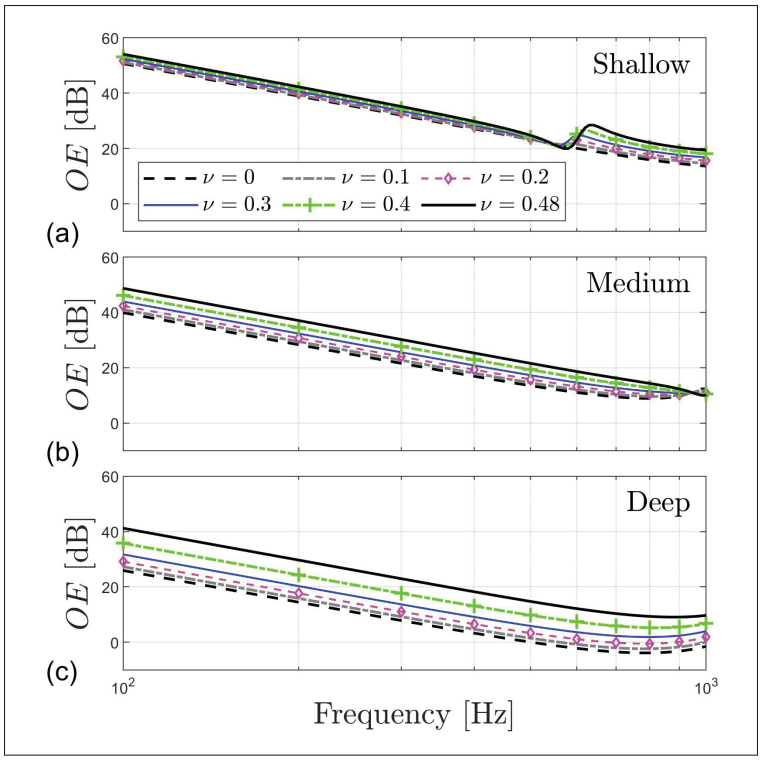

Figure-A XIII-2 Predicted objective OE induced for several Poisson's ratios for a silicone earplug at (a) shallow (6 mm), (b) medium (12 mm) and (c) deep (18 mm) insertion as a function of frequency

LIST OF REFERENCES

Alvord, L. S. & Farmer, B. L. (1997). Anatomy and orientation of the human external ear. *Journal of the American Academy of Audiology*, 8, 383–390.

Anonymous. (2011). *ISO 18437-5:2011 Mechanical vibration and shock — Characterization of the dynamic mechanical properties of visco-elastic materials — Part 5: Poisson ratio based on comparison between measurements and finite element analysis*.

Atalla, N. & Sgard, F. (2015). *Finite element and boundary methods in structural acoustics and vibration*. CRC Press.

Ballachanda, B. (2013). *The human ear canal*. Plural Publishing.

Basner, M., Babisch, W., Davis, A., Brink, M., Clark, C., Janssen, S. & Stansfeld, S. (2014). Auditory and non-auditory effects of noise on health. *The Lancet*, 383(9925), 1325–1332.

Benacchio, S., Doutres, O., Le Troter, A., Varoquaux, A., Wagnac, E., Callot, V. & Sgard, F. (2018). Estimation of the ear canal displacement field due to in-ear device insertion using a registration method on a human-like artificial ear. *Hearing Research*, 365, 16–27.

Benacchio, S., Doutres, O., Varoquaux, A., Wagnac, E., Le Troter, A., Callot, V. & Sgard, F. (2019). Use of magnetic resonance image registration to estimate displacement in the human earcanal due to the insertion of in-ear devices. *The Journal of the Acoustical Society of America*, 146(4), 2452–2465.

Berger, E. H. (2003). Hearing protection devices. In *The noise manual* (ed. Revised Fifth edition). Fairfax, VA: AIHA Press.

Berger, E. H. (2013). "Calibrating" the insertion depth of roll-down foam earplugs. *Proceedings of Meetings on Acoustics ICA2013*, 19.

Berger, E. H. & Kerivan, J. E. (1983). Influence of physiological noise and the occlusion effect on the measurement of real-ear attenuation at threshold. *The Journal of the Acoustical Society of America*, 74(1), 81–94.

Berger, E. H., Kieper, R. W. & Gauger, D. (2003). Hearing protection: Surpassing the limits to attenuation imposed by the bone-conduction pathways. *The Journal of the Acoustical Society of America*, 114(4), 1955–1967.

Bernier, A. (2013). *Towards an active hearing protection device for musicians*. (Master's thesis, École de technologie supérieure, Montréal).

Békésy, G. (1932). Zur theorie des hörens bei der schallaufnahme durch knochenleitung. *Ann. Physik*, 13, 111–136.

Békésy, G. (1960). *Experiments in Hearing*. New York, USA: McGraw-Hill.

Békésy, G. (1948). Vibration of the head in a sound field and its role in hearing by bone conduction. *The Journal of the Acoustical Society of America*, 20(6), 749–760.

Békésy, G. (1949). The structure of the middle ear and the hearing of one's own voice by bone conduction. *The Journal of the Acoustical Society of America*, 21(3), 217–232.

Blau, M., Sankowsky, T., Stirnemann, A., Oberdanner, H. & Schmitt, N. (2008). Acoustics of open fittings. *The Journal of the Acoustical Society of America*, 123(5), 3011–3011.

Borges, R. C., Costa, M. H., Naylor, P. A. & Ferreira, A. A. (2014). Impact of the vent size in the feedback-path and occlusion-effect in hearing aids. *Biomedical Circuits and Systems Conference (BioCAS) Proceedings*, pp. 25–28.

Bouchard-Roy, J., Delnavaz, A. & Voix, J. (2020). In-ear energy harvesting: Evaluation of the power capability of the temporomandibular joint. *IEEE Sensors Journal*, 20(12), 6338–6345.

Branda, E. (2012). Deep canal fittings: Advantages, challenges, and a new approach. *Hearing Review*, 19, 24–27.

Bàràny, E. (1938). A contribution to the physiology of bone conduction. *Acta Oto-Laryngologica*, 26(Suppl.26), 1–223.

Brown-Rothwell, D. (1986). *The comfort of earplugs: basis for a descriptive model*. (Master's thesis, University of Southampton, England).

Brummund, M. (2014). *Study of the occlusion effect induced by an earplug: Numerical modelling and experimental validation*. (Ph. D. thesis, École de technologie supérieure, Canada).

Brummund, M., Sgard, F., Petit, Y. & Laville, F. (2014). Three-dimensional finite element modeling of the human external ear: Simulation study of the bone conduction occlusion effect. *The Journal of the Acoustical Society of America*, 135(3), 1433–1444.

Brummund, M., Sgard, F., Petit, Y., Laville, F. & Nélisse, H. (2015). An axisymmetric finite element model to study the earplug contribution to the bone conduction occlusion effect. *Acta Acustica United with Acustica*, 101(4), 775–788.

Bruneau, M. (2013). *Fundamentals of acoustics* (ed. John Wiley \& Sons). New York.

Carillo, K., Doutres, O. & Sgard, F. (2019). Numerical investigation of the fundamental low frequency frequency mechanism of the objective occlusion effect: Focus on the earcanal wall vibration. *Proceedings of the 26th International Congress on Sound and Vibration (ICSV26)*, pp. 1–8.

Carillo, K., Doutres, O. & Sgard, F. (2020). Theoretical investigation of the low frequency fundamental mechanism of the objective occlusion effect induced by bone-conducted stimulation. *The Journal of the Acoustical Society of America*, 147(5), 3476–3489.

Carle, R., Laugesen, S. & Nielsen, C. (2002). Observations on the relations among occlusion effect, compliance, and vent size. *Journal of the American Academy of Audiology*, 13(1), 25–37.

Chang, Y., Kim, N. & Stenfelt, S. (2016). The development of a whole-head human finite-element model for simulation of the transmission of bone-conducted sound. *The Journal of the Acoustical Society of America*, 140(3), 1635–1651.

Chordekar, S., Perez, R., Adelman, C., Sohmer, H. & Kishon-Rabin, L. (2018). Does hearing in response to soft-tissue stimulation involve skull vibrations? A within-subject comparison between skull vibration magnitudes and hearing thresholds. *Hearing Research*, 364, 59–67.

Chung, K. (2004). Challenges and recent developments in hearing aids: Part II. Feedback and occlusion effect reduction strategies, laser shell manufacturing processes, and other signal processing technologies. *Trends in Amplification*, 8(4), 125–164.

Conrad, S. & Rout, A. (2013). Perceived occlusion and comfort in receiver-in-the-ear hearing aids. *American Journal of Audiology*, 22(2), 283–290.

Darkner, S., Larsen, R. & Paulsen, R. R. (2007). Analysis of deformation of the human ear and canal caused by mandibular movement. *International Conference on Medical Image Computing and Computer-Assisted Intervention*, 10, 801–808.

Dobrev, I., Sim, J. H., Stenfelt, S., Ihrle, S., Gerig, R., Pfiffner, F., Eiber, A., Huber, A. M. & Röösli, C. (2017). Sound wave propagation on the human skull surface with bone conduction stimulation. *Hearing Research*, 355, 1–13.

Dobrev, I., Farahmandi, T. S., Sim, J. H., Pfiffner, F., Huber, A. M. & Röösli, C. (2020). Dependence of skull surface wave propagation on stimulation sites and direction under bone conduction. *The Journal of the Acoustical Society of America*, 147(3), 1985–2001.

Doutres, O., Sgard, F., Terroir, J., Perrin, N., Jolly, C., Gauvin, C. & Negrini, A. (2019). A critical review of the literature on comfort of hearing protection devices: Definition of

comfort and identification of its main attributes for earplug types. *International journal of audiology*, 58(12), 824–833.

Doutres, O., Sgard, F., Terroir, J., Perrin, N., Jolly, C., Gauvin, C. & Negrini, A. (2020). A critical review of the literature on comfort of hearing protection devices: Analysis of the comfort measurement variability. *International Journal of Occupational Safety and Ergonomics*, 1–36.

Fagelson, M. A. & Martin, F. N. (1998). The occlusion effect and ear canal sound pressure level. *American Journal of Audiology*, 7(2), 50–54.

Farmer-Fedor, B. L. & Rabbitt, R. D. (2002). Acoustic intensity, impedance and reflection coefficient in the human ear canal. *The Journal of the Acoustical Society of America*, 112(2), 600–620.

Gelfand, S. A. (2009). *Hearing: an introduction to psychological and physiological acoustics* (ed. 5. ed). New York: Informa Healthcare.

Goldstein, D. P. & Hayes, C. S. (1965). The occlusion effect in bone conduction hearing. *Journal of speech and hearing research*, 8(2), 137–148.

Guild, S. (1936). Hearing by bone conduction: the pathways of transmission of sound. *Ann. Otol. Rhinol. Lar.*, (45), 736–754. 00035.

Hansen, M. O. (1998). *Occlusion effects, Part II: A study of the occlusion effect mechanism and the influence of the earmould properties*. (Ph. D. thesis, Department of Acoustic Technology, Technical University of Denmark, Denmark).

Hansen, M. O. & Stinson, M. R. (1998). Air conducted and body conducted sound produced by own voice. *Canadian Acoustics*, 26(2), 11–19.

Homma, K., Du, Y. & Puria, S. (2009). Ossicular resonance modes of the human middle ear for bone and air conduction. *The Journal of the Acoustical Society of America*, 2(125), 968–979.

Homma, K., Shimizu, Y., Kim, N., Du, Y. & Puria, S. (2010). Effects of ear-canal pressurization on middle-ear bone- and air-conduction responses. *Hearing Research*, 263(1), 204–215.

Howell, P., Williams, M. & Dix, H. (1988). Assessment of sound in the ear canal caused by movement of the jaw relative to the skull. *Scandinavian audiology*, 17(2), 93–98.

Hudde, H. & Engel, A. (1998a). Measuring and modeling basic properties of the human middle ear and ear canal. Part III: Eardrum impedances, transfer functions and model

calculations. *Acta Acustica united with Acustica*, 84(6), 1091–1109.

Hudde, H. & Engel, A. (1998b). Measuring and modeling basic properties of the human middle ear and ear canal. Part II: Ear canal, middle ear cavities, eardrum, and ossicles. *Acta Acustica united with Acustica*, 84(5), 894–913.

Hudde, H. & Schmidt, S. (2009). Sound fields in generally shaped curved ear canals. *The Journal of the Acoustical Society of America*, 125(5), 3146–3157.

Hudde, H. (1983). Estimation of the area function of human ear canals by sound pressure measurements. *The Journal of the Acoustical Society of America*, 73(1), 24–31.

Huizing, E. H. (1960). Bone conduction-the influence of the middle ear. *Acta Oto-Laryngol.*, Suppl. 155, 1–99.

James, C. (2006). *Finite Element Modeling and Exploration of Double Hearing Protection Systems*. (Master's thesis, Virginia Polytechnic Institute and State University, Blacksburg, Virginia).

Joodaki, H. & Panzer, M. B. (2018). Skin mechanical properties and modeling: A review. *Proceedings of the Institution of Mechanical Engineers, Part H: Journal of Engineering in Medicine*, 232(4), 323–343.

Kampinga, W. R., Wijnant, Y. H. & de Boer, A. (2010). Performance of several viscothermal acoustic finite elements. *Acta Acustica united with Acustica*, 96(1), 115–124.

Kampinga, W. (2010). *Viscothermal acoustics using finite elements: analysis tools for engineers*. (Ph. D. thesis, University of Twente, Enschede).

Karal, F. C. (1953). The analogous acoustical impedance for discontinuities and constrictions of circular cross section. *The Journal of the Acoustical Society of America*, 25(2), 327–334.

Keefe, D. H., Bulen, J. C., Campbell, S. L. & Burns, E. M. (1994). Pressure transfer function and absorption cross section from the diffuse field to the human infant ear canal. *The Journal of the Acoustical Society of America*, 95(1), 355–371.

Keidser, G., Carter, L., Chalupper, J. & Dillon, H. (2007). Effect of low-frequency gain and venting effects on the benefit derived from directionality and noise reduction in hearing aids. *International Journal of Audiology*, 46(10), 554–568.

Khanna, S. M., Tonndorf, J. & Queller, J. E. (1976). Mechanical parameters of hearing by bone conduction. *The Journal of the Acoustical Society of America*, 60(1), 139–154.

Kiessling, J., Brenner, B., Jespersen, C. T., Groth, J. & Jensen, O. D. (2005). Occlusion effect of earmolds with different venting systems. *Journal of the American Academy of Audiology*, 16(4), 237–249.

Killion, M., Wilber, L. & Gudmundsen, G. (1988). Zwislocki was right. *Hearing Instruments*, 39(1), 14–18.

Kochkin, S. (2010). MarkeTrak VIII: Consumer satisfaction with hearing aids is slowly increasing. *The Hearing Journal*, 63(1), 19–20.

Kuk, F. K. (1991). Perceptual consequence of vents in hearing aids. *British Journal of Audiology*, 25(3), 163–169.

Lebeau, M. (2014). Maladies professionnelles : impact économique au Québec.

Lee, K. (2011). *Effects of earplug material, insertion depth, and measurement technique on hearing occlusion effect*. (Ph. D. thesis, Virginia Polytechnic Institute and State University, Blacksburg, Virginia).

Lee, K. & Casali, J. G. (2011). Investigation of the Auditory Occlusion Effect with Implications for Hearing Protection and Hearing Aid Design. *Proceedings of the Human Factors and Ergonomics Society Annual Meeting*, 55(1), 1783 –1787.

Lee, W., Yang, X., Jung, H., Bok, I., Kim, C., Kwon, O. & You, H. (2018). Anthropometric analysis of 3D ear scans of Koreans and Caucasians for ear product design. *Ergonomics*, 61(11), 1480–1495.

Légis-Québec. (2020). Règlement sur la santé et la sécurité du travail. Consulted at http://www.legisquebec.gouv.qc.ca/fr/showdoc/cr/S-2.1,%20r.%2013?langCont=fr#ga:l_xv-h1.

Li, X., Li, C., Xue, Z. & Tian, X. (2018). Analytical study of transient thermo-mechanical responses of dual-layer skin tissue with variable thermal material properties. *International Journal of Thermal Sciences*, 124, 459–466.

Lide, D. R. & Kehiaian, H. V. (1994). *CRC handbook of thermophysical and thermochemical data*. CRC Press.

Mach, E. (1863). Zur Theorie des Gehörorgans. *Sber. Akad. Wiss. Wien, math-naturw. Kl., Abh. II*, (48), 283–300.

MacKenzie, D. J. (2006). Open-canal fittings and the hearing aid occlusion effect. *The Hearing Journal*, 59(11), 50–52.

Macmillan-Dictionary. (2020). Leak (verb) definition and synonyms. Consulted at https://www.macmillandictionary.com/dictionary/british/leak_1.

Macrae, J. & McAlister, P. (1989). A mathematical model of acoustic leakage through air pathways past earmoulds. *Australian Journal of Audiology*, 11(2), 89–100.

Makous, J. C. & Middlebrooks, J. C. (1990). Two-dimensional sound localization by human listeners. *The Journal of the Acoustical Society of America*, 87(5), 2188–2200.

Mechel, F. P. (Ed.). (2008). *Formulas of acoustics* (ed. 2nd ed). Berlin ; New York: Springer.

Mueller, H., Bright, K. & Northern, J. (1996). Studies of the hearing aid occlusion effect. *Seminars in Hearing*, 17(1), 21–31.

Mueller, H. G. (1994). CIC hearing aids: What is their impact on the occlusion effect? *The Hearing Journal*, 47(11), 29–30.

Nelson, P., Kohnert, K., Sabur, S. & Shaw, D. (2005). Classroom noise and children learning through a second language: Double jeopardy? *Language, Speech, and Hearing Services in Schools*, 36(3), 219–229.

Nielsen, C. & Darkner, S. (2011). The cartilage bone junction and its implication for deep canal hearing instrument fittings. *The Hearing Journal*, 64(3), 35–36.

O'Connor, K. N., Cai, H. & Puria, S. (2017). The effects of varying tympanic-membrane material properties on human middle-ear sound transmission in a three-dimensional finite-element model. *The Journal of the Acoustical Society of America*, 142(5), 2836–2853.

Oliveira, R. J. & Hoeker, G. (2003). Ear Canal Anatomy and Activity. *Seminars in hearing*, 24(4), 265–276.

Otis. (2002). Tirade du scribe. In *Astérix et Obélix : Mission Cléopâtre*.

Pierce, A. D. (1994). *Acoustics: an introduction to its physical principles and applications*. Woodbury, N.Y.: Published by the Acoustical Society of America through the American Institute of Physics.

Ravicz, M. E., Cheng, J. T. & Rosowski, J. J. (2019). Sound pressure distribution within human ear canals: II. Reverse mechanical stimulation. *The Journal of the Acoustical Society of America*, 145(3), 1569–1583.

Reinfeldt, S., Stenfelt, S. & Håkansson, B. (2013). Estimation of bone conduction skull transmission by hearing thresholds and ear-canal sound pressure. *Hearing Research*,

299, 19–28. doi: 10.1016/j.heares.2013.01.023.

Reinfeldt, S., Stenfelt, S., Good, T. & Håkansson, B. (2007). Examination of bone-conducted transmission from sound field excitation measured by thresholds, ear-canal sound pressure, and skull vibrations. *The Journal of the Acoustical Society of America*, 121(3), 1576–1587.

Ruggero, M. A. & Temchin, A. N. (2002). The roles of the external, middle, and inner ears in determining the bandwidth of hearing. *Proceedings of the National Academy of Sciences*, 99(20), 13206–13210.

Ryan, J. G., Rule, B. & Armstrong, S. W. (2006). Reducing the occlusion effect with active noise control. *The Journal of the Acoustical Society of America*, 119(5), 3385–3385.

Saint-Gaudens, H., Nélisse, H., Sgard, F., Laville, F. & Doutres, O. (2019). Comparison of different excitations to assess the objective occlusion effect measured on human subjects. *Proceedings of the 26th International Congress on Sound and Vibration (ICSV26)*, pp. 1–8.

Schmidt, S. & Hudde, H. (2009). Accuracy of acoustic ear canal impedances: Finite element simulation of measurement methods using a coupling tube. *The Journal of the Acoustical Society of America*, 125(6), 3819–3827.

Schroeter, J. & Poesselt, C. (1986). The use of acoustical test fixtures for the measurement of hearing protector attenuation. Part II : Modeling the external ear, simulating bone conduction, and comparing test fixture and real-ear data. *The Journal of the Acoustical Society of America*, 80(2), 505–527.

Sgard, F., Nélisse, H., Boutin, J., Laville, F., Voix, J. & Gaudreau, M. A. (2009). Finite element modeling for the evaluation of sound attenuation of hearing protectors. *Proceedings of Euronoise 2009*, pp. 1–9.

Sgard, F., Carillo, K. & Doutres, O. (2019). A 2D axisymmetric finite element model to assess the contribution of in-ear hearing protection devices to the objective occlusion effect. *Proceedings of Internoise*, 259, 2494–2505.

Sgard, F., Nélisse, H., Gaudreau, M.-A., Boutin, J., Voix, J. & Laville, F. (2010). *Étude de la transmission sonore à travers les protecteurs auditifs et application d'une méthode pour évaluer leur efficacité effective en milieu de travail - Partie 2 : Étude préliminaire d'une modélisation des protecteurs auditifs par éléments finis*.

Shaw, E. a. G. & Stinson, M. R. (1981). Network concepts and energy flow in the human middle-ear. *Acoustical Society of America*, 69(S1), S43–S43.

Shaw, E. & Stinson, M. R. (1983). The human external and middle ear: Models and concepts. In *Mechanics of hearing* (ed. University Press, pp. 3–10). Delft: E. de Boer and M.A Viergever.

Small, S. A. & Hu, N. (2011). Maturation of the occlusion effect: A bone conduction auditory steady state response study in infants and adults with normal hearing. *Ear and Hearing*, 32(6), 708–719.

Sohmer, H. (2017). Soft tissue conduction: Review, mechanisms, and implications. *Trends in Hearing*, 21, 1–8.

Staab, W., Dennis, M. J., Schweitzer, H. C. & Weber, J. E. (2004). Measuring the occlusion effect in a deep-fitting hearing device. *Hearing Review*, 11(13), 44–50.

Staab, W. J. (1996). Introduction to deep canal principles. *Seminars in Hearing*, 17, 3–19.

Stenfelt, S. & Reinfeldt, S. (2007). A model of the occlusion effect with bone-conducted stimulation. *International Journal of Audiology*, 46(10), 595–608. doi: 10.1080/14992020701545880.

Stenfelt, S., Wild, T., Hato, N. & Goode, R. (2003). Factors contributing to bone conduction: The outer ear. *The Journal of the Acoustical Society of America*, 113(2), 902–913. doi: doi: 10.1121/1.1534606.

Stenfelt, S. (2016). Model predictions for bone conduction perception in the human. *Hearing Research*, 340, 135–143.

Stenfelt, S. & Goode, R. L. (2005). Bone-conducted sound: Physiological and clinical aspects. *Otology \& Neurotology*, 26(6), 1245–1261.

Stenfelt, S., Hato, N. & Goode, R. L. (2002). Factors contributing to bone conduction: The middle ear. *The Journal of the Acoustical Society of America*, 111(2), 947–959. Cited by 0053.

Stepp, C. E. & Voss, S. E. (2005). Acoustics of the human middle-ear air space. *The Journal of the Acoustical Society of America*, 118(2), 861–871.

Stinson, M. R. & Daigle, G. A. (2005). Comparison of an analytic horn equation approach and a boundary element method for the calculation of sound fields in the human ear canal. *The Journal of the Acoustical Society of America*, 118(4), 2405–2411.

Stinson, M. R. & Lawton, B. W. (1989). Specification of the geometry of the human ear canal for the prediction of sound-pressure level distribution. *The Journal of the Acoustical*

Society of America, 85(6), 2492–2503.

Sunohara, M., Osawa, M., Hashiura, T. & Tateno, M. (2015). Occlusion reduction system for hearing aids with an improved transducer and an associated algorithm. *2015 23rd European Signal Processing Conference (EUSIPCO)*, pp. 285–289.

Suter, A. H. (2002). Construction noise: Exposure, effects, and the potential for remediation; a review and analysis. *AIHA Journal*, 63(6), 768–789.

Tonndorf, J. (1964). Animal experiments in bone conduction: Clinical conclusions. *Transactions of the American Otological Society*, 52, 22–41. doi: 10.1177/000348946407300308.

Tonndorf, J. (1972). Bone Conduction. In Tobias, J. V. (Ed.), *Foundations of Modern Auditory Theory* (vol. 2, pp. 195–237). New York: Academic Press.

Tonndorf, J., Greenfield, E. C. & Kaufman, R. S. (1966). The occlusion of the external ear canal: Its effect upon bone conduction in cats. *Acta Oto-Laryngologica*, 61(Suppl. 213), 80–104.

Tortual. (1827). Die sirme des menschen und die wechsel. *Beziehungen ihres phys. u. agan. Lebens etc.*

Touloukian, Y. S. & Makita, T. (1970). *Thermophysical properties of matter-the TPRC data series. volume 6. specific heat-nonmetallic liquids and gases*.

Trompette, N., Kusy, A. & Ducourneau, J. (2015). Suitability of commercial systems for earplug individual fit testing. *Applied Acoustics*, 90, 88–94.

Vasil, K. A. & Cienkowski, K. M. (2006). Subjective and objective measures of the occlusion effect for open-fit hearing aids. *Journal of the Academy of Rehabilitative Audiology*, 39, 69–82.

Viallet, G., Sgard, F., Laville, F. & Nélisse, H. (2015). Investigation of the variability in earplugs sound attenuation measurements using a finite element model. *Applied Acoustics*, 89, 333–344.

Vogel, U., Zahnert, T., Hofmann, G. & Huettenbrink, K.-B. (1996). Approach to evidence of middle ear occlusion effect by laser vibrometry. *Proc. SPIE 2927, Optical and Imaging Techniques for Biomonitoring II*, 2927, 1–8.

Voix, J. & Hager, L. D. (2009). Individual fit testing of hearing protection devices. *International Journal of Occupational Safety and Ergonomics*, 15(2), 211–219.

Voss, S. E., Horton, N. J., Fairbank, K. E., Xia, L., Tinglin, L. R. K. & Girardin, K. D. (2020). Measurements of ear-canal cross-sectional areas from live human ears with implications for wideband acoustic immittance measurements. *The Journal of the Acoustical Society of America*, 148(5), 3042–3051.

Watson, N. & Gales, R. (1943). Bone-conduction threshold measurements: Effects of occlusion, enclosures, and masking devices. *The Journal of the Acoustical Society of America*, 14(4), 207–215.

Wheatstone, C. (1827). Experiments on audition. *Quarterly Journal of Science, Literature and Art*, 67–72.

WHO. (2020). Deafness and hearing loss. Consulted at https://www.who.int/news-room/fact-sheets/detail/deafness-and-hearing-loss.

Wightman, F. L. & Kistler, D. J. (1989). Headphone simulation of free-field listening. I: Stimulus synthesis. *The Journal of the Acoustical Society of America*, 85(2), 858–867.

Winkler, A., Latzel, M. & Holube, I. (2016). Open versus closed hearing-aid fittings: A literature review of both fitting approaches. *Trends in Hearing*, 20, 1–13.

Xu, H., Sgard, F., Wagnac, E. & De Guise, J. (2019). Development of an entire human head finite element model based on in-vivo medical images for investigation of sound transmission. *Proceedings of the 26th International Congress on Sound and Vibration (ICSV26)*, pp. 1–8.

Zhao, M., Fridberger, A. & Stenfelt, S. (2021). Vibration direction sensitivity of the cochlea with bone conduction stimulation in guinea pigs. *Scientific Reports*, 11(1), 1–13.

Zurbrügg, T., Stirnemannn, A., Kuster, M. & Lissek, H. (2014). Investigations on the physical factors influencing the ear canal occlusion effect caused by hearing aids. *Acta Acustica united with Acustica*, 100(3), 527–536.